IN-39,
51751

NASA CONTRACTOR REPORT 187621

p. 151

THERMOVISCOPLASTIC RESPONSE OF Ti-15-3 UNDER VARIOUS LOADING CONDITIONS

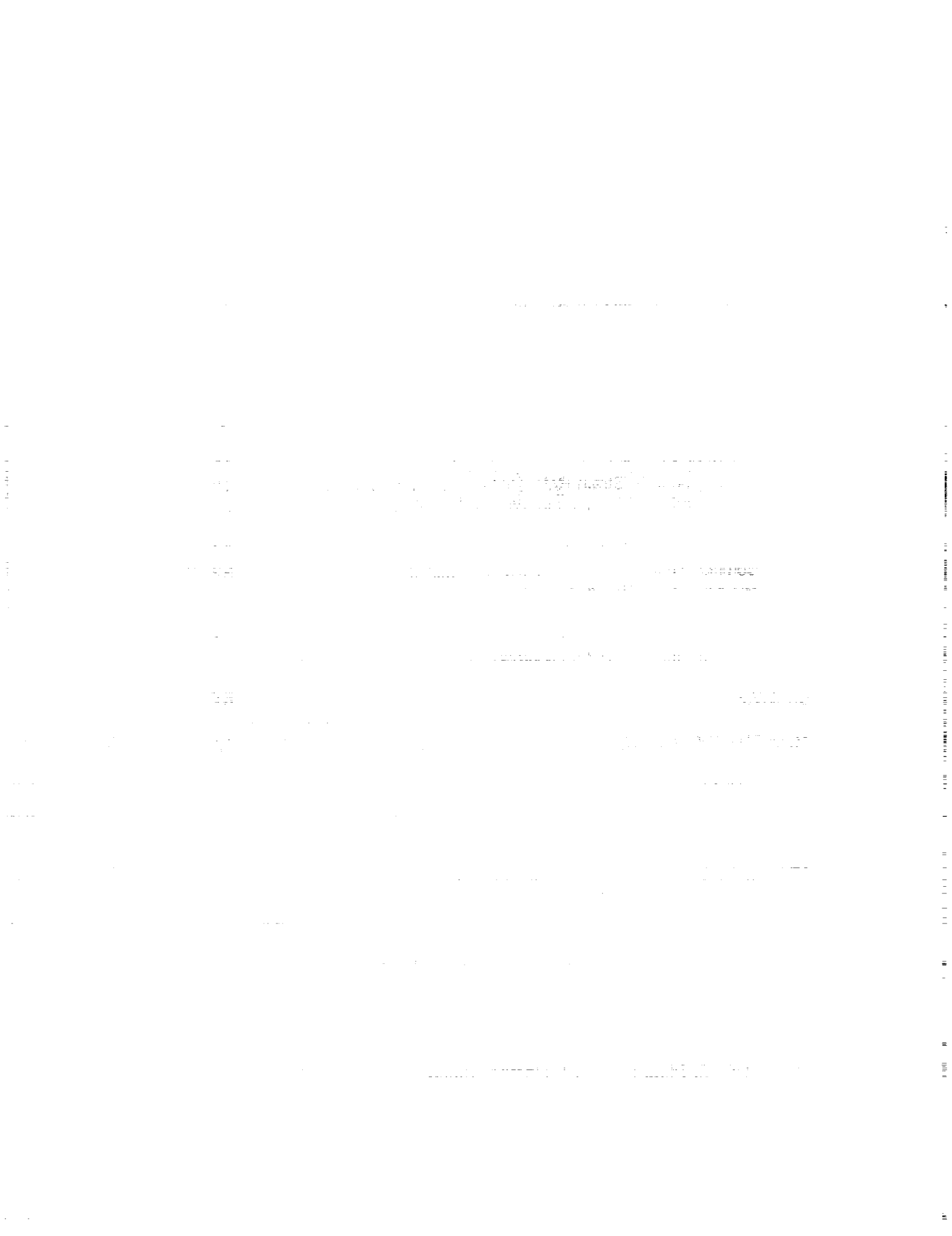## M. E. Tuttle and J. Rogacki

UNIVERSITY OF WASHINGTON
Seattle, Washington

NASA

National Aeronautics and
Space Administration

LANGLEY RESEARCH CENTER
Hampton, Virginia 23665-5225

TABLE OF CONTENTS

THERMOVISCOPLASTIC RESPONSE OF TI-15-3
UNDER VARIOUS LOADING CONDITIONS

M. Tuttle, Associate Professor

J. Rogacki, PhD Candidate

Department of Mechanical Engineering, FU-10
University of Washington
Seattle, WA 98195

INTRODUCTION

Metal matrix composites (MMCs) are candidate materials for use in high temperature, high loading applications. In particular, an MMC consisting of a titanium alloy reinforced with silicon-carbide fibers is being considered for use on the National Aerospace Plane (NASP). Compared to other metals and metallic alloys, titanium alloys retain relatively high stiffness, strength, and corrosion resistance at elevated temperatures. However, above roughly 316°C (600°F) titanium exhibits a significant thermoviscoplastic (i.e., "creep") response. Since the temperatures encountered in many regions of the NASP are expected to exceed 316°C, the potential thermoviscoplastic behavior of titanium-based MMC's at elevated temperatures must be thoroughly investigated.

The present study was initiated in February 1989 via a grant from the NASA-Langley Research Center (NAG-1-974). The long-term objective of the study is to develop a combined experimental-analytic methodology for predicting the thermoviscoplastic behavior of multi-angle MMC laminates [1,2]. Briefly, the approach is to first model the thermoviscoplastic behavior of the fiberless (i.e., unreinforced) titanium matrix. Once a constitutive model which adequately describes the behavior of titanium has been identified, the viscoplastic behavior of unidirectional composites will be predicted

through the use of the rule-of-mixtures. Then, the behavior of multi-angle laminates will be predicted by combining rule-of-mixtures-type relationships with lamination theory.

Perhaps the most crucial aspect of the study is selection of a constitutive model to describe the thermoviscoplastic behavior of titanium. Four constitutive models are currently being considered: the Bodner-Partom model [3-5], the Miller model [6-9], the Walker model [10], and the Eisenberg model [11,12]. The first three of these are categorized as "unified" (or "coupled") theories, so called because in these theories no distinction is made between "plastic" and "creep" strains and hence these theories do not involve a yield surface. The Eisenberg model does include a yield surface, and therefore belongs to the class of models referred to as "uncoupled" theories. Each of these models involve various material constants which must be measured experimentally. Hence, an extensive testing program has been undertaken to evaluate these material constants for a particular titanium alloy.

The thermoviscoplastic models will not be further discussed herein. Rather, the objective of this report is to describe an extensive data base which has been generated in support of the analysis. The stress-strain-time response of fiberless titanium specimens subjected to four distinct types of loading histories and at three different elevated temperatures has been measured. The data collected will eventually be used to deduce the material parameters associated with the four thermoviscoplastic constitutive models mentioned above. In addition to these material characterization tests, various "complex" tests have been performed. The complex tests will provide "benchmark" data. That is, once the material parameters associated with a constitutive model have been determined, the model will then be used to predict the behavior under the complex test conditions. The comparison between measurement and prediction will serve to indicate whether the model is suitable for use with the titanium-based MMC under consideration. Three types of specimens have been used during these complex tests: fiberless titanium specimens, unidirectional [0°] and [90°] SCS6/Ti composite specimens, and crossply [0°/90°]$_s$ SCS6/Ti composite specimens.

The data files collected during the study contain a large number of data points. The data were stored using a computer-controlled data acquisition system, and in some cases

contain 4000 - 5000 data scans. The data is presented in this report in the form of graphs and tables. If desired, a copy of the original data files on computer diskettes can also be obtained. The interested reader should contact the first listed author (Dr. M. E. Tuttle, University of Washington) for instructions on obtaining a copy of the data on computer diskettes.

In addition to mechanical testing, a limited number of specimens have been inspected using optical and scanning electron microscopy. The objective of this inspection was to determine if any gross changes in the crystalline microstructure of Ti-15-3 occur during thermomechanical loading. Results of this inspection will also be presented in this report.

TECHNICAL APPROACH

The Ti-15-3 Alloy

The specific titanium alloy being investigated is the Ti-15V-3Cr-3Al-3Sn alloy, commonly referred to as "Ti-15-3." Ti-15-3 is a metastable beta strip alloy, used where cold formability and high strength are desired. The alloy is weldable, ageable to high strength, and relatively insensitive to corrosive environments. Ti-15-3 also provides cost advantages when compared to other titanium alloys [13]. Because Ti-15-3 is readily available in the form of thin sheets, it may be an ideal matrix for titanium-based composites.

The metastable beta phase undergoes a rapid phase transformation to the more stable (and brittle) alpha phase when subjected to elevated temperatures. This change in microstructure may be accompanied by changes in the macroscopic behavior of the material (i.e., changes in stiffness, strength, creep rates, etc.). Therefore, in the present study all specimens were subjected to a heat treatment prior to testing, which was intended to stabilize the microstructure. The heat treatment consisted of exposure to 649°C (1200°F) for one hour, followed by an air quench. Transformation from the beta to alpha phase during the heat treatment was confirmed using optical and scanning electron microscopy, as will be discussed in a later section.

Description of the Test Matrix

The testing program involved tests at three different temperatures: 482°C, 566°C, and 649°C (900°F, 1050°F, and 1200°F). The following five types of tests were conducted, as described individually in subsequent sections: creep tests, constant strain rate (CSR) tests, cyclic constant strain rate (CCSR) tests, constant stress rate (CσR) tests, and "complex" tests. The test matrix is summarized in Tables 1 through 4. The creep tests were performed at the University of Washington in Seattle, WA, while the CSR, CCSR, and CσR tests were conducted at the NASA-Langley Research Center in Hampton, VA.

4

Creep Test Condition No.	Creep Stress (MPa)	Temperature (°C)	No. Repeated Tests (Test Numbers)
1	34.5	482	2 (U1, U2)
2	34.5	566	1 (U4)
3	34.5	649	2 (U5,U6)
4	68.9	482	2 (U7,U8)
5	68.9	566	2 (U9,U10)
6	68.9	649	2 (U11,U12)
7	103.4	482	2 (U13, U14)
8	103.4	566	2 (U15, U16)
9	103.4	649	2 (U17, U18)
10	138.0	482	2 (U19,U20)
11	138.0	566	2 (U21,U22)
12	138.0	649	2 (U23,U24)
13	172.4	482	1 (U26)
14	172.4	566	2 (U27, U28)
15	172.4	649	2 (U29, U30)

Table 1: Creep Tests conducted at the University of Washington.

Test No.	Type	Load Rate (N/sec)	Stress Rate (MPa/sec)	Temperature (°C)
L40	CσR	44.48	2.6	21
L41	CσR	88.96	5.2	21
L42	CσR	44.48	2.6	482
L43	CσR	44.48	2.6	649

Table 2: Constant Stress Rate tests conducted at the NASA-Langley Research Center

Test No.	Test Type	Strain Rate (m/m/sec)	Temp (°C)
L1	CSR	1×10^{-4}	482
L2	CSR	1×10^{-4}	566
L3	CSR	1×10^{-4}	649
L4	CSR	5×10^{-4}	482
L5	CSR	5×10^{-4}	566
L6	CSR	5×10^{-4}	649
L7	CSR	1×10^{-3}	482
L8	CSR	1×10^{-3}	566
L9	CSR	1×10^{-3}	649
L10	CSR	5×10^{-3}	482
L11	CSR	5×10^{-3}	566
L12	CSR	5×10^{-3}	649
L13	CSR	1×10^{-2}	482
L14	CSR	1×10^{-2}	566
L15	CSR	1×10^{-2}	649
L16	CCSR	1×10^{-4}	482
L17	CCSR	1×10^{-4}	566
L18	CCSR	1×10^{-4}	649
L19	CCSR	5×10^{-4}	482
L20	CCSR	5×10^{-4}	566
L21	CCSR	5×10^{-4}	649
L22	CCSR	1×10^{-3}	482
L23	CCSR	1×10^{-3}	566
L24	CCSR	1×10^{-3}	649
L25	CCSR	5×10^{-3}	482
L26	CCSR	5×10^{-3}	566
L27	CCSR	5×10^{-3}	649
L28	CCSR	1×10^{-2}	482
L29	CCSR	1×10^{-2}	566
L30	CCSR	1×10^{-2}	649

Table 3: Constant Strain Rate (CSR) and Cyclic Constant Strain Rate (CCSR) Tests conducted at NASA LaRC

Test Number	Specimen Type	Temp (°C)	Test Description
U31	Fiberless	482	Multi-step Creep (48 MPa/96 MPa)
U33	Fiberless	482	Multi-step Creep (48 MPa/96 MPa)
U34	Fiberless	566	Multi-step Creep (48 MPa/96 MPa)
U35	Fiberless	649	Multi-step Creep (48 MPa/96 MPa)
U36	Fiberless	649	Multi-step Creep (48 MPa/96 MPa)
U38	[0°]	566	Multi-step Creep (48 MPa/96 MPa)
U41	[90°]	566	Creep at 48 MPa (premature failure)
L33	[0°]	649	Multi-strain rate and stress relaxation
L34	[90°]	482	Multi-strain rate and stress relaxation
L35	[90°]	566	Multi-strain rate and stress relaxation
L36	[90°]	649	Multi-strain rate and stress relaxation
L37	[0°/90°]s	482	Constant strain rate (premature failure)
L38	[0°/90°]s	566	Const strain rate and stress relaxation
L39	[0°/90°]s	649	Const strain rate and stress relaxation

Table 4: "Complex" Tests (Tests Numbered "Uxx" Were Conducted at the University of Washington; Tests Numbered "Lxx" Were Conducted at the NASA-LaRC)

Mechanical Testing Equipment Used

Creep Tests. All creep tests were conducted at the University of Washington. The tests were performed using a SATEC Model G creep rupture tester, equipped with a high temperature furnace. The furnace can provide test temperatures up to 1093°C (2000°F). Axial strains were measured using a SATEC Model 200 high temperature extensometer, equipped with an ATS linear-variable-differential-transformer (LVDT). The LVDT was used to measure displacements and hence strains over a 5.08-cm (2-in) gage length. Displacement data was recorded automatically using an A/D board mounted within an IBM PC/AT. Temperature was monitored using three type K chromel-alumel thermocouples mounted along the gage length of each specimen.

CSR, CCSR, and CσR Tests: The constant strain rate, cyclic constant strain rate, and constant stress rate tests were all performed at the NASA-Langley Research Center. The tests were performed using one of two MTS Model 810 load frames. Both frames are capable of fully reversed, load- or strain-controlled loading, and are equipped with

Instron liquid-cooled hydraulically-activated grips. One load frame is equipped with an induction furnace which uses two infrared pyrometers for temperature control, while the second load frame is equipped with a quartz lamp heating system equipped with thermocouples to provide temperature control. Load and displacement (i.e., stress and strain) data were collected in both cases using a Nicolet XF-44 data acquisition system. A back-up analog record was also obtained using an X-Y plotter.

Specimen Preparation

Specimens used during the creep, CSR, and CσR tests were all machined from 13-ply "parent" panels of Ti-15-3. The parent panels were purchased from Textron Specialty Materials, Inc (Lowell, MA) and were produced by Textron using the "HIP" (Hot Isostatic Pressure) process. The HIP treatment consolidated 13 individual Ti-15-3 sheets, so as to form a "fiberless" composite.

Nominal machined specimen dimensions were 0.145 x 1.27 x 15.24 cm (0.057 x 0.50 x 6.0 in). The specimens were received in an annealed condition and were subsequently aged at 649°C (1200°F) for one hour prior to testing. As previously mentioned this thermal aging was intended to stabilize the microstructure.

Thicker specimens were required for the CCSR tests so as to avoid buckling during the reversed (i.e., compressive) loading portion of the test cycle. The CCSR test specimens were machined from a solid plate of Ti-15-3 to nominal dimensions of 0.76 x 0.76 x 12.7 cm (0.3 x 0.3 x 5 in). All of the specimens were received in an annealed condition and were subsequently aged at 649°C (1200°F) for one hour prior to testing.

RESULTS

Creep Tests

During the creep tests a constant tensile load was applied to the specimen using the lever-arm creep frame, and the resulting axial strain was monitored as a function of time. In most cases the creep test was continued until a steady-state (i.e., constant) creep rate was reached, although in a few cases (i.e., at the highest temperature and highest stress considered) specimen failure occurred prior to reaching steady-state creep.

As previously indicated in Table 1, creep tests were conducted at 482°C, 566°C, and 649°C and at five different stress levels ranging from 34.5 MPa to 172.4 MPa. Fifteen different creep test conditions were used. Two replicate tests were conducted at each test condition, with the exception of test conditions 2 and 13. The two data files obtained at a given test condition were combined into one data fiel and smoothed using a commercially-available software package called Passage II [14]. The data collected in this manner are presented in Appendix A. The creep response is presented at common temperatures of 482°C, 566°C, and 649°C in Figures A1-A3, respectively. This same data is replotted at common stress levels ranging from 34.5 to 172.4 MPa in Figures A4 through A8.

Creep compliance curves which correspond to the data shown in Appendix A are presented in Figures 1 through 3. Creep compliances at 482°C are presented in Figure 1. Curves for five distinct stress levels are shown. The compliance measured at 34.5 MPa was markedly higher than those measured at the other four stress levels, and hence it is suspected that the data collected during this test is in error. With the exception of the 34.5 MPa compliance curve, the remaining four curves show that the compliance is essentially independent of stress level at 482°C. This implies that the behavior of Ti-15-3 is linearly viscoplastic at temperatures at or below 482°C, at least over the time periods considered during this study. Conversely, the compliances measured at 566°C and 649°C are clearly stress-dependent, which indicates nonlinear viscoplastic behavior at these higher temperatures.

9
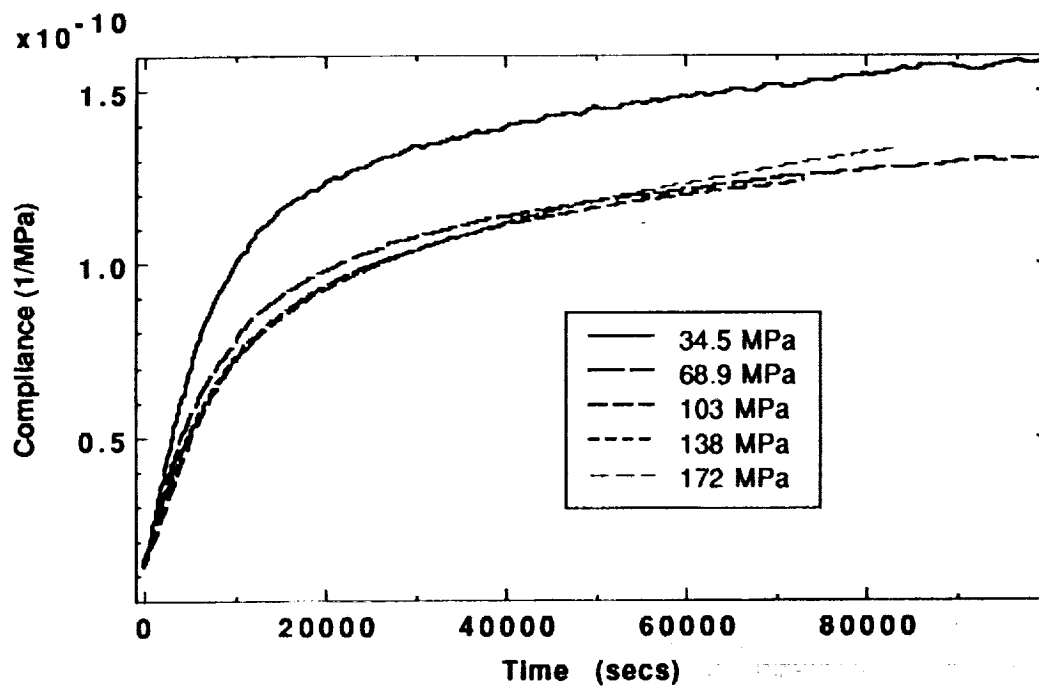
Figure1: Creep Compliances Measured at 482°C
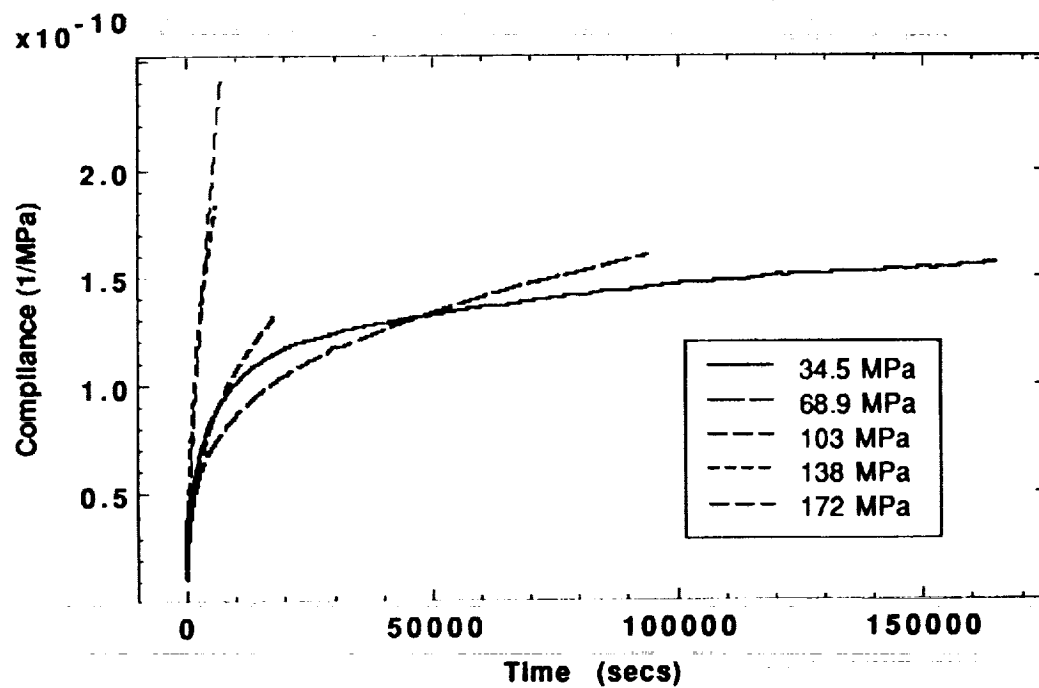
Figure 2: Creep Compliances Measured at 566°C
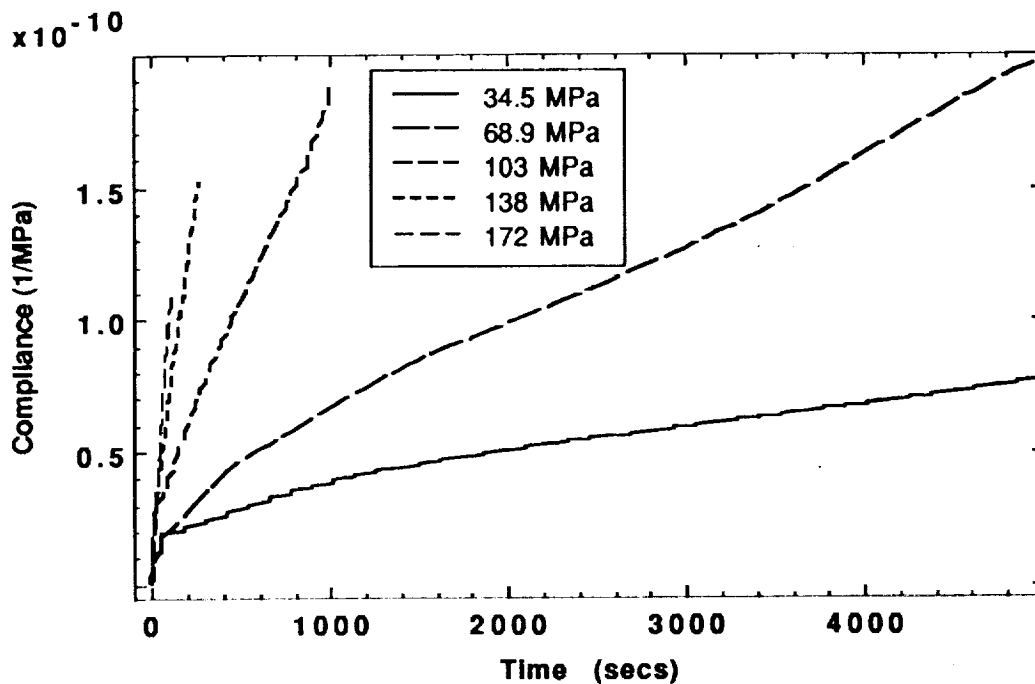
Figure 3: Creep Compliances Measured at 649°C

From these results it is readily apparent that the thermoviscoplastic response of Ti-15-3 is pronounced at all test temperatures considered. Creep rates increased with increasing temperature and increasing stress, as would be expected. A very rapid increase in viscoplastic behavior begins at stress levels above about 103.4 MPa and/or at temperatures above about 566°C.

Constant Strain Rate Tests

In the constant strain rate (CSR) tests a variable tensile load was applied such that a constant strain rate was induced in the specimen. Typical data sets are shown in Figures 4 and 5. As indicated, strain was increased from zero to some maximum value (typically 7 percent strain) at a constant rate, while the associated stress level varied as

dictated by the material response. Five different constant strain rates were imposed, ranging from a relatively low strain rate (100 μm/m/sec) to a relatively high strain rate (10,000 μm/m/sec).

Stress-strain data recorded during all CSR tests are presented in Appendix B. The CSR response is presented at common temperatures of 482°C, 566°C, and 649°C in Figures B1-B3, respectively. This same data is replotted in Figures B4 through B8, where the CSR response is presented at common strain rates ranging from 100 to 10,000 μm/m/sec. Two interesting characteristics should be noted. First, the Ti-15-3 alloy exhibited strain softening at high strain levels during all CSR tests, i.e., at strain levels beyond yielding the slope of the stress-strain curve was always negative. Secondly, in many tests the Ti-15-3 specimens exhibited the "upper/lower yield point" phenomenon often observed in low-carbon steels (e.g., see Figure 5c). This phenomenon was also encountered during several of the cyclic constant strain rate (CCSR) tests, which will be described in a following section.

Three general characteristics of the CSR data were monitored in an attempt to identify overall trends. Namely, the initial modulus, the 0.2 percent offset stress, and the tensile strength. These variables were defined and measured as follows:

Initial Modulus: The initial modulus was defined as the slope of the stress-strain curve at relatively low stress values. In most cases there was a linear region in which the modulus was readily discernible. In a few cases the initial stress-strain response of the material was not linear (especially at 649°C and at the lower strain rates). In these cases an approximate modulus was determined by measuring the slope of a line connecting the stress/strain values near the point (σ,ε) = (0,0) withthe stress/strain values at a stress equal to approximately 50 percent of the maximum stress encountered during the individual test.

0.2 percent offset ("yield") stress: The 0.2 percent offset stress will be referred to as the "yield" stress in this report, and was defined in the same manner as the conventional offset yield stress. That is, it is defined by the point of intersection between the measured stress-strain response and a straight line with a slope equal

12

(a) Axial Strain vs Time

(b) Axial Stress vs Time

(c) Stress vs Strain
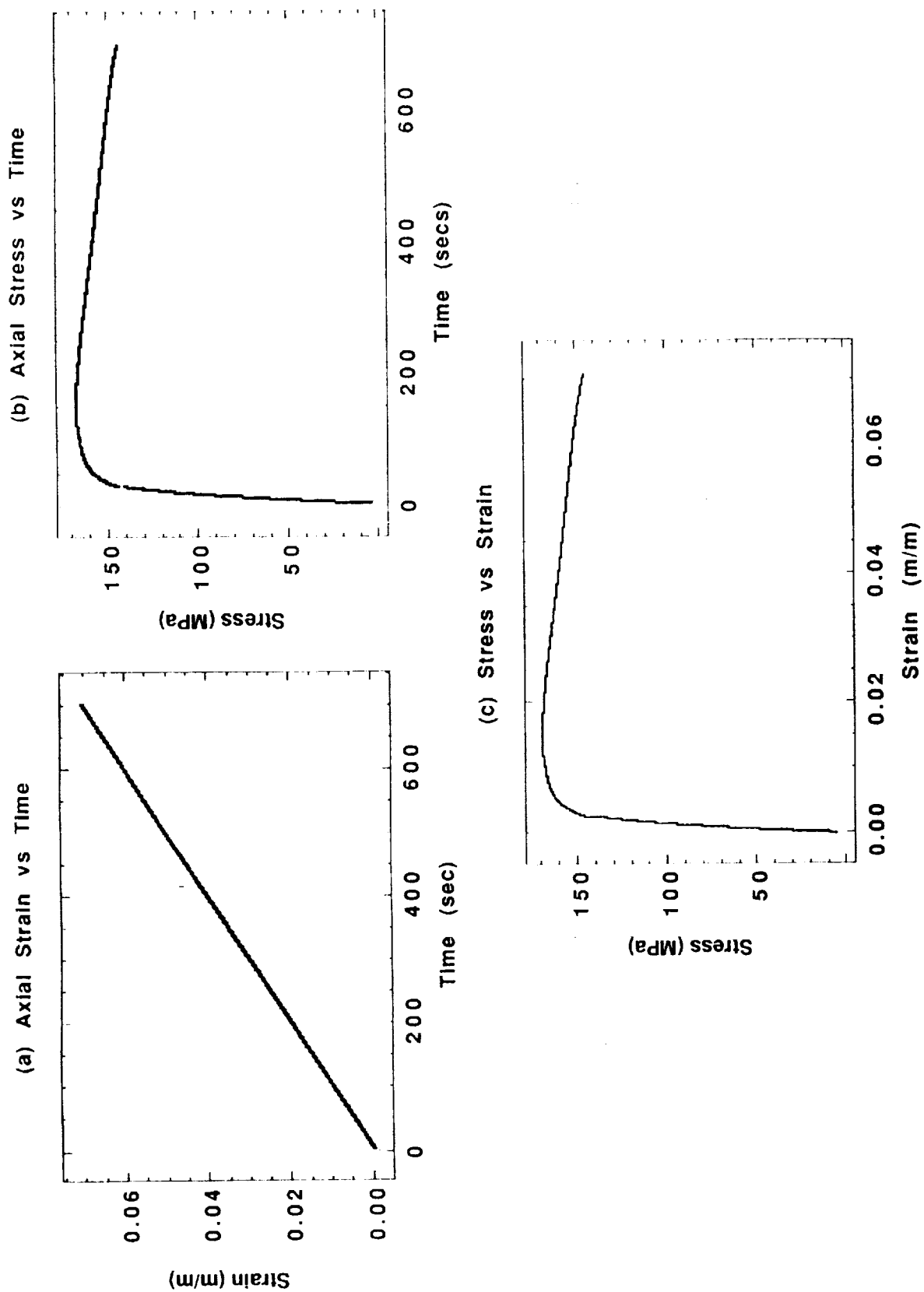
Figure 4: CSR Results Obtained During Test L3 (100 μm/m/sec, 649C)

a) Axial Strain vs Time

b) Axial Stress vs Time

c) Axial Stress vs Strain
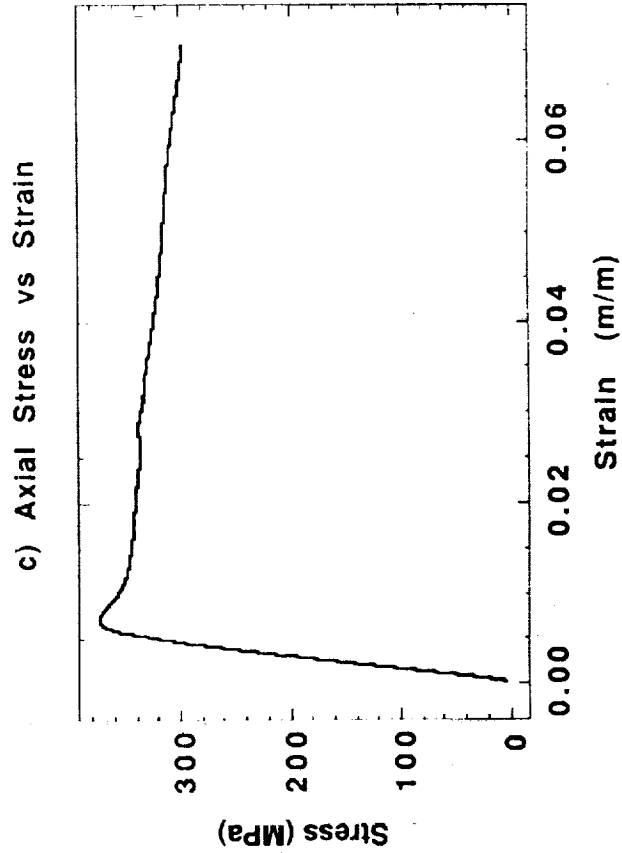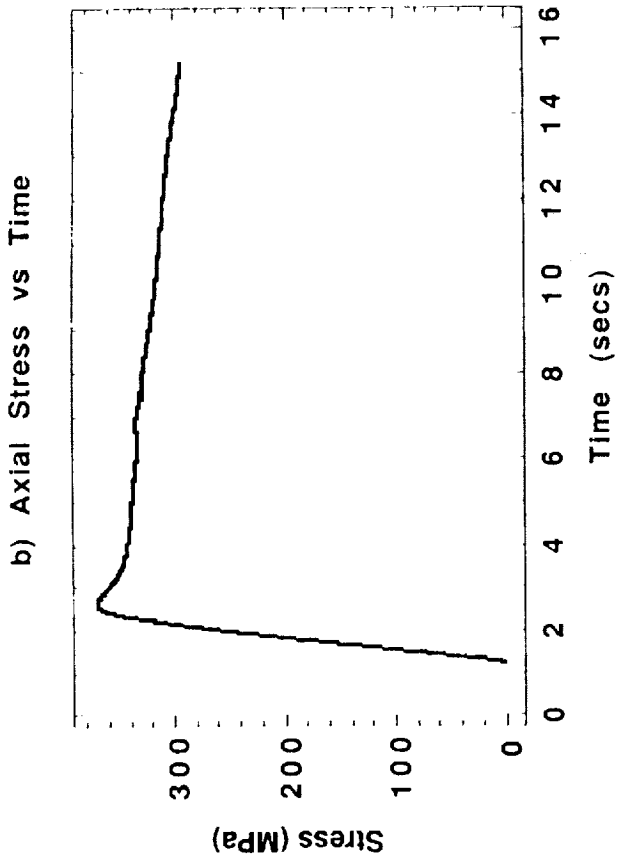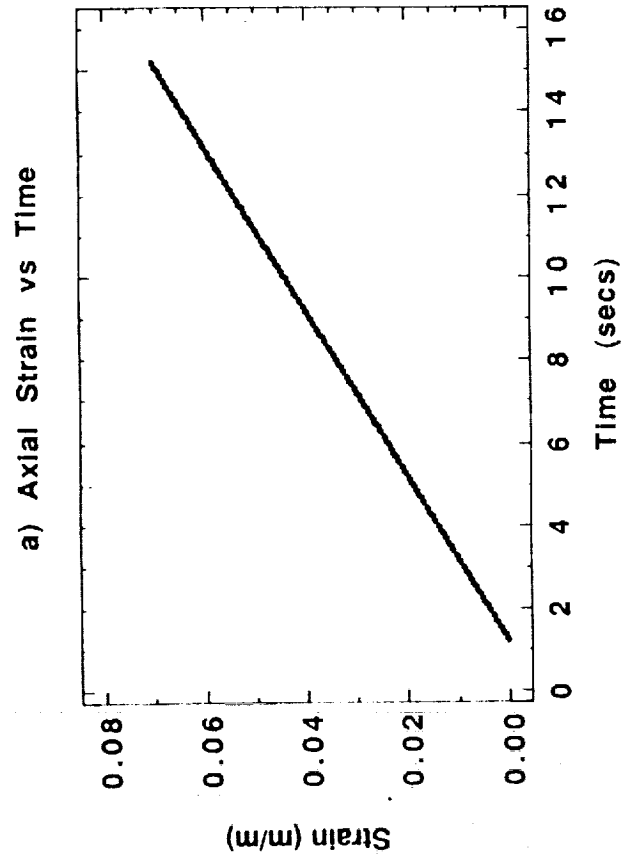
Figure 5: CSR Results Obtained During Test L9 (5000 µm/m/sec, 649C)

to the initial modulus, but with a strain offset of 0.2 percent. Note that since the Ti-15-3 alloy exhibited pronounced viscoplastic behavior at the temperatures considered during this study, the "yield stress" is not a material constant but rather varies with both strain rate and temperature.

tensile strength: This parameter was defined as the maximum stress measured during an individual CSR test for a particular temperature and strain rate.

The measured value of the initial modulus during all CSR tests is summarized in Table 5 and plotted in Figure 6. The initial modulus is seen to be relatively insensitive to strain rate, but generally decreases with increasing temperature over the temperature range considered. Average modulus values at 482°C, 566°C, and 649°C were 78.5 GPa (11.4 Msi), 75.7 GPa (11.0 Msi), and 70.7 GPa (10.3 Msi), respectively. Thus, the increase in temperature from 482°C to 649°C resulted in a 9.9 percent decrease in stiffness. Johnson et al. [15] have reported a room temperature value of 104.8 GPa (15.2 Msi). Hence, an increase from room temperature to 649°C (an increase of roughly 630°C) results in a decrease in stiffness of about 33 percent for the Ti-15-3 alloy.

In contrast, the yield stress was found to be highly sensitive to both temperature and strain rate. Measured yield strengths are presented in Table 6 and plotted in Figure 7. As indicated, the yield stress increases with an increase in strain rate, and decreases with an increase in temperature. It also appears that the yield stress may reach an asymptotic limit with an increase in strain rate. The yield stress at 482°C approaches a limiting value of about 600 MPa for strain rates greater than 5×10^{-4} m/m/sec. The experimental trend seems to indicate that this same asymptotic limit may apply at higher temperatures as well.

The tensile strength measured during each CSR test is shown in Table 7 and plotted in Figure 8. The tensile strength was found to be highly sensitive to both temperature and strain rate. As indicated, the tensile strength increased with an increase in strain rate, and decreased with an increase in temperature.

Test No.	Strain Rate (m/m/sec)	Temperature (°C)	Modulus (GPa)
L-1	10^{-4}	482	79.2
L-2	10^{-4}	566	75.6
L-3	10^{-4}	649	68.5
L-4	5×10^{-4}	482	78.5
L-5	5×10^{-4}	566	77.3
L-6	5×10^{-4}	649	71.5
L-7	10^{-3}	482	78.7
L-8	10^{-3}	566	76.5
L-9	10^{-3}	649	72.5
L-10	5×10^{-3}	482	79.2
L-11	5×10^{-3}	566	75.5
L-12	5×10^{-3}	649	71.4
L-13	10^{-2}	482	76.8
L-14	10^{-2}	566	73.6
L-15	10^{-2}	649	69.6

Table 5: Initial Modulus of Ti-15-3 at Various Temperatures and Strain Rates.
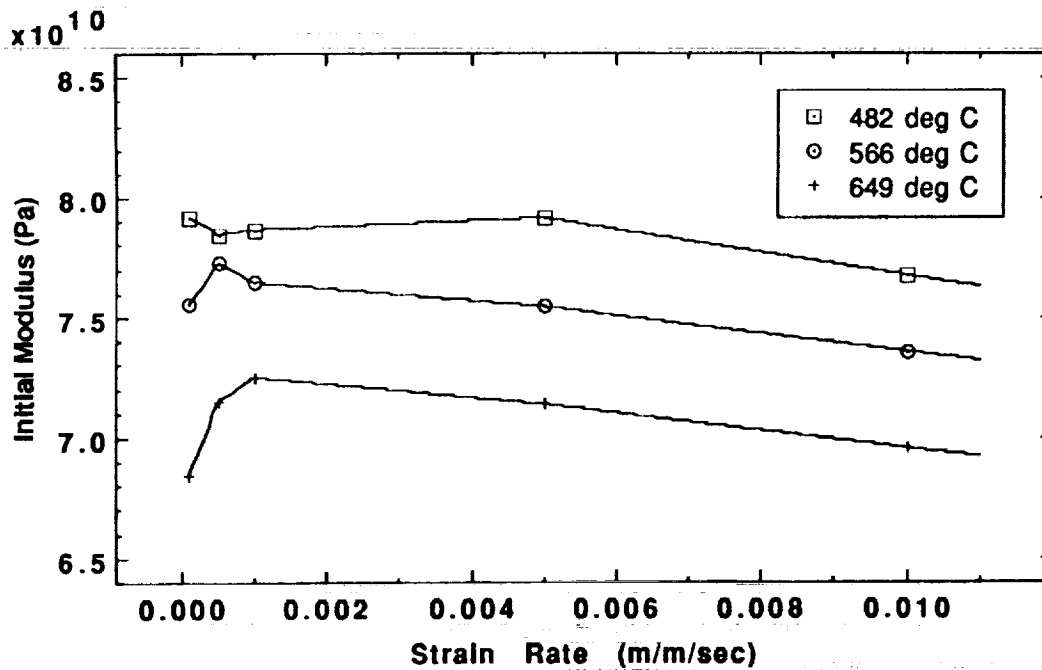
Figure 6: Initial Modulus as a Function of Temperature and Strain Rate

16

Test No.	Strain Rate (m/m/sec)	Temperature (°C)	Yield Stress (MPa)
L-1	10^{-4}	482	260
L-2	10^{-4}	566	142
L-3	10^{-4}	649	97
L-4	5×10^{-4}	482	400
L-5	5×10^{-4}	566	208
L-6	5×10^{-4}	649	153
L-7	10^{-3}	482	491
L-8	10^{-3}	566	278
L-9	10^{-3}	649	175
L-10	5×10^{-3}	482	553
L-11	5×10^{-3}	566	464
L-12	5×10^{-3}	649	267
L-13	10^{-2}	482	590
L-14	10^{-2}	566	555
L-15	10^{-2}	649	374

Table 6: Yield Stress of Ti-15-3 at Various Temperatures and Strain Rates.
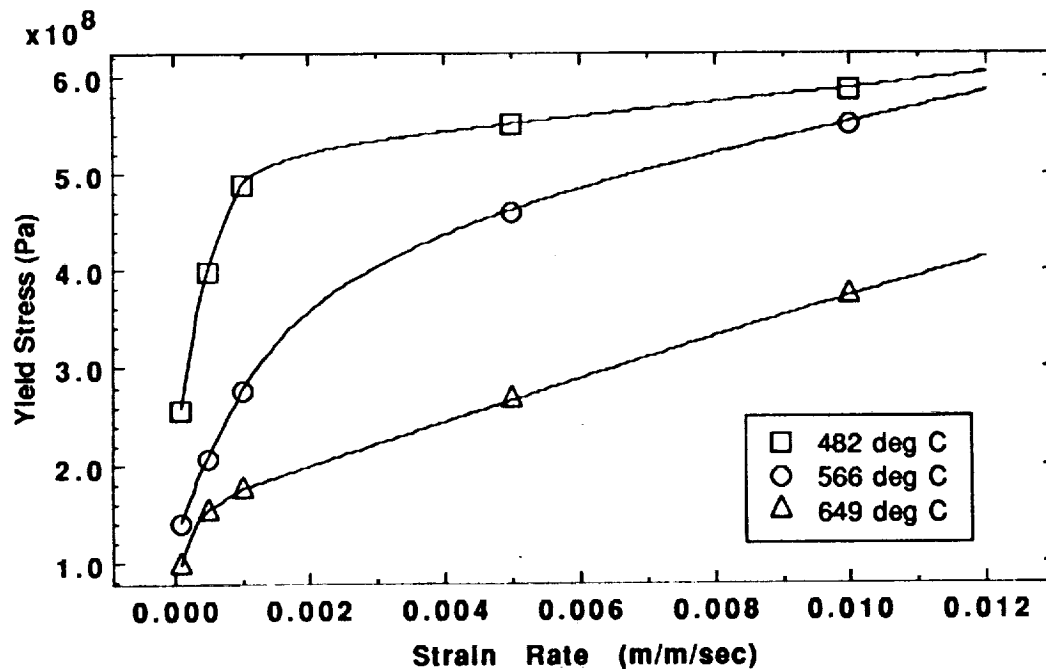
Figure 7: Yield Stress as a Function of Temperature and Strain Rate

17

Cyclic Constant Strain Rate Tests

In the cyclic constant strain rate (CCSR) tests a time-varying load was applied such that a cyclic constant strain rate was imposed. That is, strains were increased at a constant rate until a maximum tensile strain was reached (typically 1.0% strain). Loading was then reversed and strains were decreased at this same constant strain rate until a maximum compressive strain was reached (typically −1.0% strain). Typical measurements obtained during the first 3 cycles of CCSR test L18 are shown in Figure 9. This test was conducted at a temperature of 649°C, and strain was increased/decreased at a constant rate of 100 X 10^{-4} m/m/sec, as shown in Figure 9a. The associated stress vs time plot is shown in Figure 9b. Combining these data results in the hysteresis loop shown in Figure 9c. This loading profile was repeated until the cyclic stress vs. strain behavior of the material had stabilized.

The CCSR tests were difficult to accomplish. Several tests were clearly erroneous, so the data were discarded and the test repeated. Also, the data collected by the Nicolet XF-44 data acquisition was severely contaminated by electronic noise. Although the source of this noise has not been firmly established, it was almost certainly due to the inductance furnace used to heat the specimens. Where possible, the electronic noise has been removed from the data using a smoothing routine contained in a commercial software package.

The CCSR tests were conducted at the same five strain rates (100 to 10,000 μm/m/sec) and three temperatures (482, 566, and 649°C) as were used during the CSR tests. Strain levels were lower during the CCSR tests, however. The maximum strain levels imposed during most of the CCSR tests were approximately 1% (exceptions are described below), whereas the maximum strain levels imposed during the CSR tests were 7 - 8%.

Specially-modified CCSR test cycles are required in order to measure some of the material parameters associated with the Miller [7] and Walker [10] models. Therefore the loading history during six of the CCSR tests were specially modified to accommodate these requirements. Specifically, tests L22, L23, and L24 were modified to accommodate

18

Test No.	Strain Rate (m/m/sec)	Temperature (°C)	Tensile Strength (MPa)
L-1	10^{-4}	482	541
L-2	10^{-4}	566	262
L-3	10^{-4}	649	169
L-4	5×10^{-4}	482	660
L-5	5×10^{-4}	566	414
L-6	5×10^{-4}	649	229
L-7	10^{-3}	482	699
L-8	10^{-3}	566	462
L-9	10^{-3}	649	266
L-10	5×10^{-3}	482	730
L-11	5×10^{-3}	566	564
L-12	5×10^{-3}	649	374
L-13	10^{-2}	482	720
L-14	10^{-2}	566	605
L-15	10^{-2}	649	411

Table 7: Tensile strengths measured during constant strain rate tests of Ti-15-3 at various temperatures and strain rates.
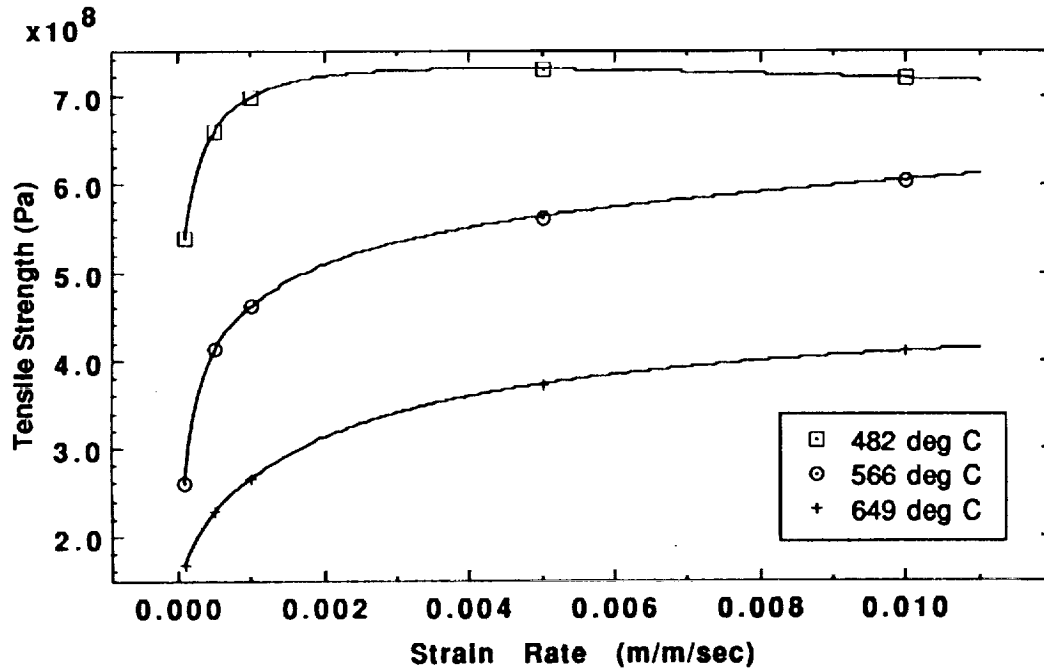
Figure 8: Tensile Strength as a Function of Temperature and Strain Rate

a) Strain vs Time During First Three Cycles
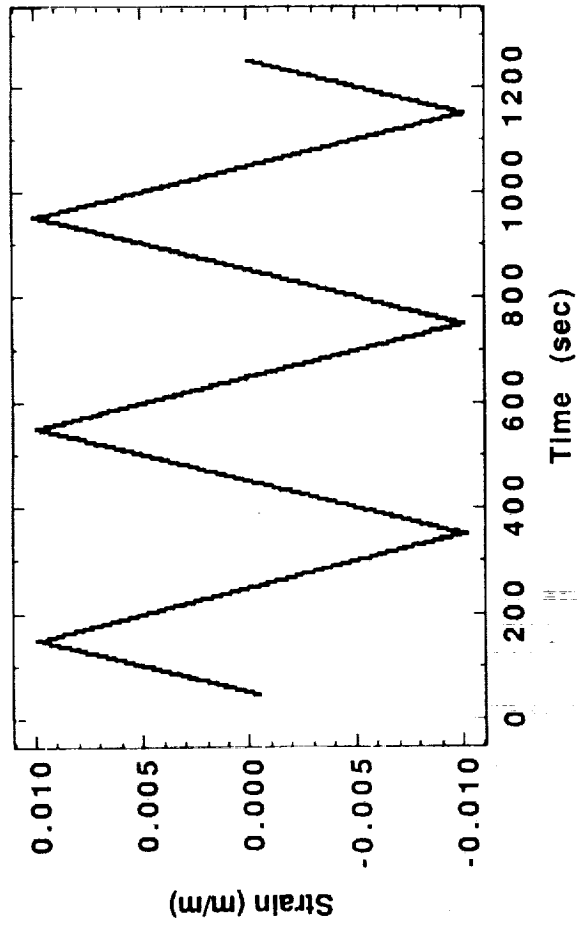
b) Stress vs Time During First Three Cycles
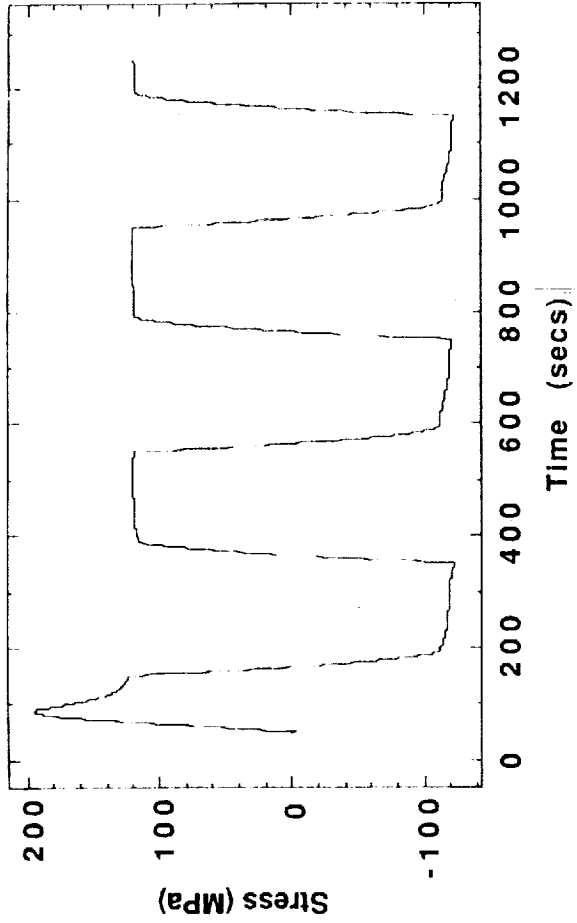
c) Stress Vs Strain During First Three Cycles
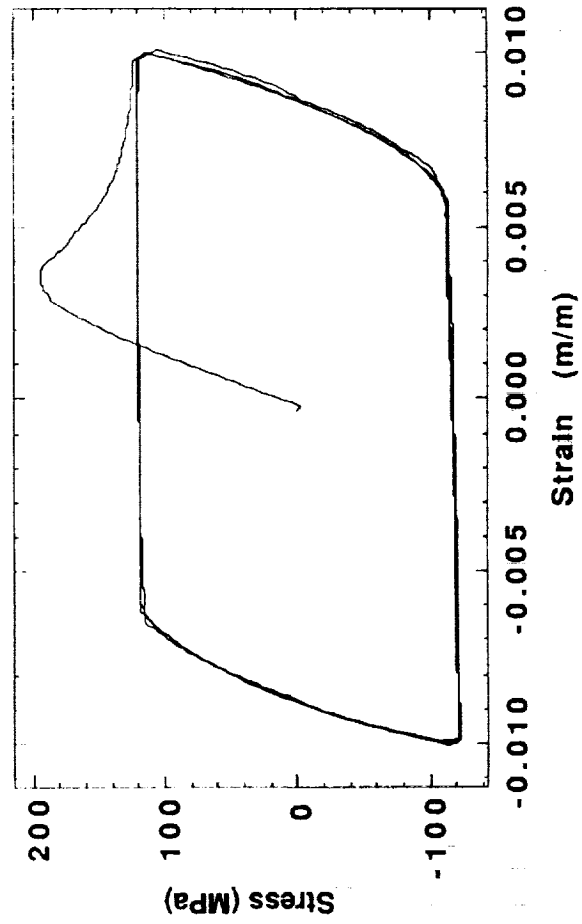
Figure 9: CCSR Measurements Obtained During First Three Cycles of Test L18

the Walker model, and tests L25, L26, and L27 were modified to accommodate the Miller model. These special variations in the CCSR load history will be described separately in later subsections.

The CCSR test results are presented in Figures C1 through C15, Appendix C. In general, the stress-strain curves exhibit the familiar hysteresis loops commonly seen in cyclic fatigue testing. The "shape" of the hysteresis loops changed with the number of loading cycles in two ways. First, the total range in loading required to impose the desired strain range varied as the number of loading cycles was increased. Secondly, the slopes of the loading and unloading portions of the hysteresis loops changed with loading cycles. The shape of the hysteresis loops generally stabilized after 15-30 cycles.

Three general characteristics of the CCSR data were monitored in an attempt to identify overall trends. Namely, the "hysteresis loop width ratio", the "average unloading modulus ratio", and the "stress ratio". These quantities were defined as:

Hysteresis Loop Width Ratio (HLWR)—The HLWR was defined as the hysteresis loop width on the fourteenth CCSR cycle (measured along the strain axis at zero stress) divided by the hysteresis loop width on the second cycle. Thus, an HLWR of 1.0 indicates that the hysteresis loop width during the fourteenth cycle was identical to that measured during the second cycle. This parameter, along with the "average unloading modulus ratio" (see below), indicates whether the material is becoming more stiff (width ratio greater than 1.0) as the number of loading cycles increases.

Average Unloading Modulus Ratio (AUMR): The "average unloading modulus" (AUM) was defined as the average of the slopes of the two lines connecting the (stress, strain) point at the maximum tensile and compressive strains with the residual stress value at zero strain for a given loading cycle. The AUM increases if the material becomes stiffer and/or exhibits less time-dependent behavior as the number of loading cycles increases. The "average unloading modulus ratio" (AUMR) was defined as the ratio of the AUM during the fourteenth and second loading cycles. An AUMR greater than 1.0 indicates that the material is stiffer and/or exhibits less time-dependent behavior on the fourteenth cycle than it did on the second cycle.

<u>Stress Ratio (SR):</u> The SR is defined as the sum of the absolute values of the tensile and compressive stresses at the strain extremes of the fourteenth cycle divided by the sum of the absolute values of the tensile and compressive stresses at the strain extremes of the second cycle. This parameter indicates whether the material is undergoing cyclic hardening (SR greater than 1.0) or cyclic softening (SR less than 1.0).

HLWRs are listed in Table 8 and plotted on Figures 10 and 11. In Figure 10 measured HLWR are plotted against test temperature, while in Figure 11 the HLWR are plotted against strain rate. Note that at 482°C the hysteresis loops became narrower as the tests progressed. At the higher temperatures hysteresis loop showed relatively little change with loading, although the greatest HLWR were measured during the 566°C tests. The HLWR increased with strain rate at all temperatures considered (see Figure 11).

Measured AUMR are listed in Table 9 and plotted against test temperature and strain rate in Figures 12 and 13, respectively. No major trends regarding the AUMR were identified.

Measured SRs are listed in Table 10 and plotted against test temperature and strain rate in Figures 14 and 15, respectively. The SR increased with number of loading cycles for all tests at the lowest temperature (482°C) and for all tests at the lowest strain rate (10^{-4}/s), indicating strain hardening. At 566°C and 649°C, however, strain softening occurred at the four fastest strain rates. SRs generally decreased with increasing strain rate at all three temperatures. That is, an increase in strain rate resulted in an increase strain softening behavior.

As previously mentioned, tests L22 through L27 were specially modified CCSR tests. Data obtained during the "normal" CCSR tests (i.e., during tests L16 through L21 and L28 through L30) are presented in Appendix C, Figures C1 through C6 and Figures C13 through C15, respectively. The specially modified CCSR tests will be discussed in the following two subsections.

22

Test No.	Strain Rate (m/m/sec)	Temperature (°C)	HLWR
L16	10^{-4}	482	.635
L17	10^{-4}	566	.930
L18	10^{-4}	649	.989
L19	5×10^{-4}	482	.704
L20	5×10^{-4}	566	1.046
L21	5×10^{-4}	649	.977
L22	10^{-3}	482	.792
L23	10^{-3}	566	1.082
L24	10^{-3}	649	.984
L25	5×10^{-3}	482	.753
L26	5×10^{-3}	566	1.036
L27	5×10^{-3}	649	1.024
L28	10^{-2}	482	.884
L29	10^{-2}	566	1.121
L30	10^{-2}	649	1.036

Table 8: Hysteresis Loop Width Ratio (HLWR) at various temperatures and strain rates
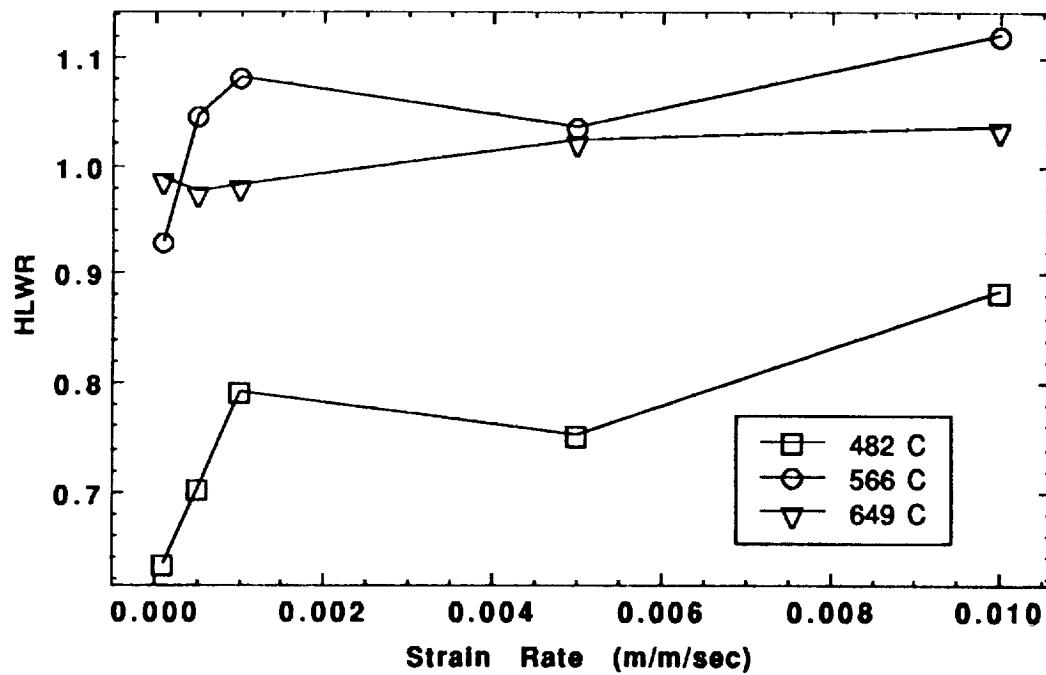
Figure 10: HLWR as a Function of Strain Rate

23
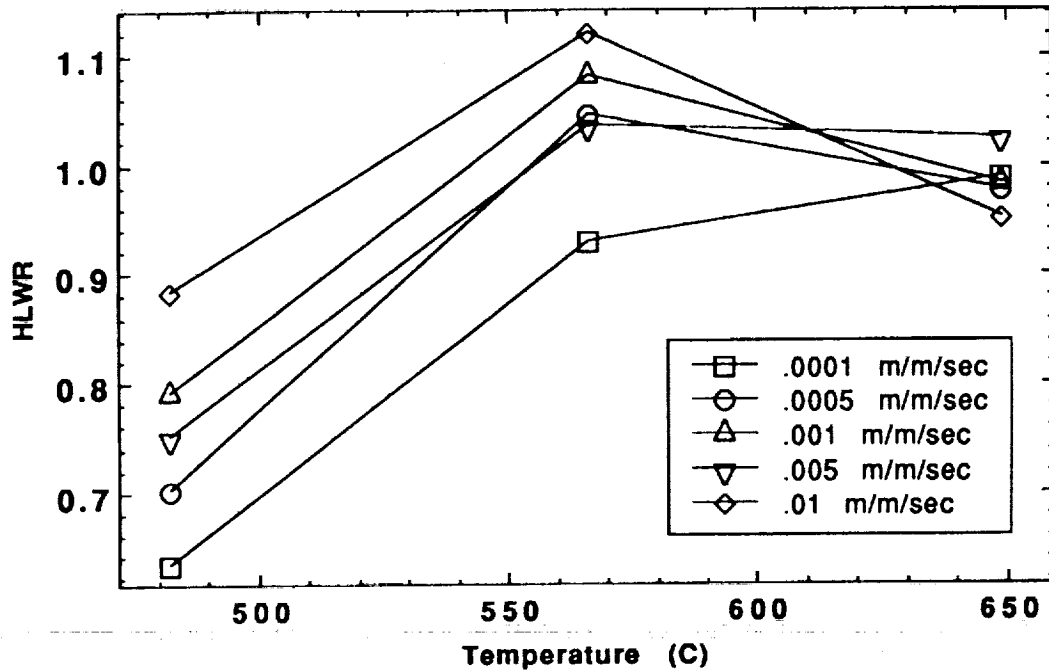
Figure 11: HLWR as a Function of Temperature

Test No.	Strain Rate (m/m/sec)	Temperature (°C)	AUMR
L-16	10^{-4}	482	.910
L-17	10^{-4}	566	1.031
L-18	10^{-4}	649	.945
L-19	5×10^{-4}	482	.967
L-20	5×10^{-4}	566	1.033
L-21	5×10^{-4}	649	1.027
L-22	10^{-3}	482	1.020
L-23	10^{-3}	566	1.022
L-24	10^{-3}	649	.942
L-25	5×10^{-3}	482	.980
L-26	5×10^{-3}	566	1.024
L-27	5×10^{-3}	649	1.003
L-28	10^{-2}	482	1.040
L-29	10^{-2}	566	.981
L-30	10^{-2}	649	.952

Table 9: Average Unloading Modulus Ratio (AUMR) at various temperatures and strain rates.
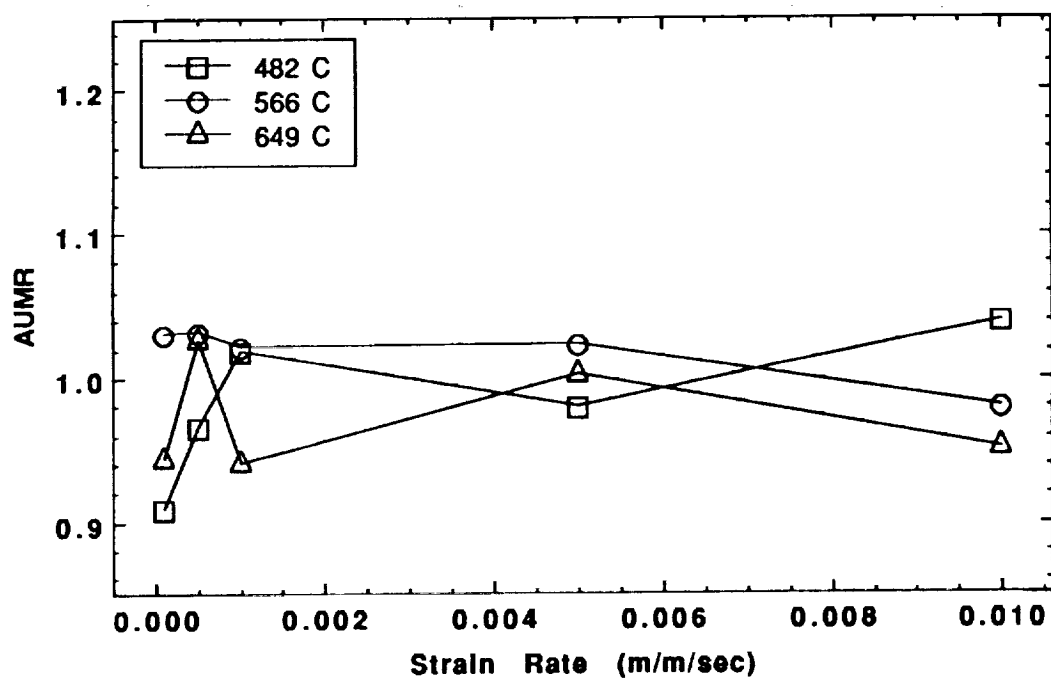
Figure 12: AUMR as a Function of Strain Rate
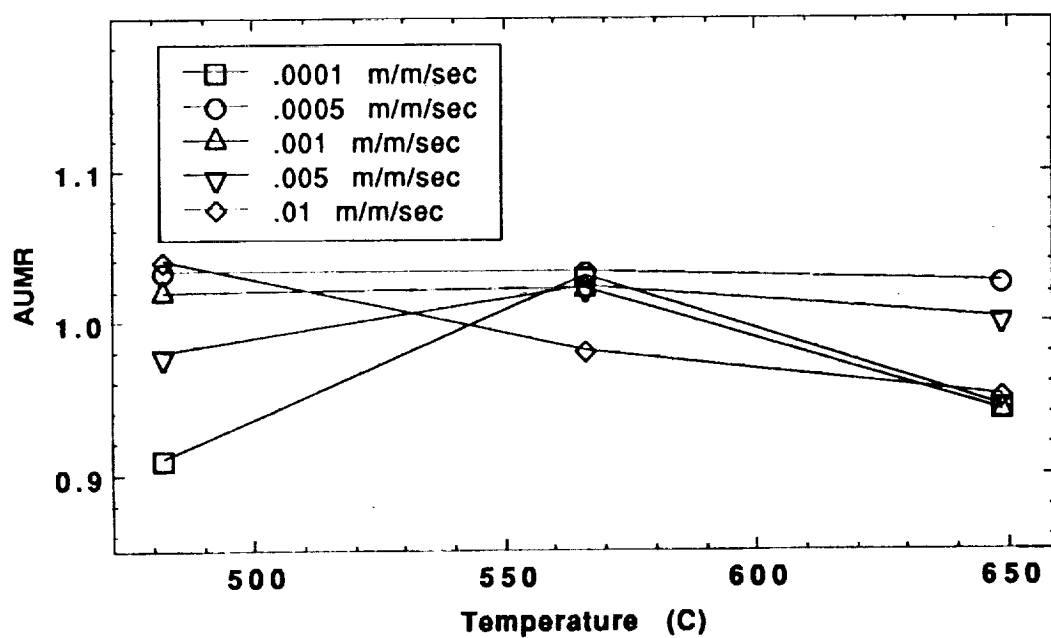
Figure 13: AUMR as a Function of Temperature

25

Test No.	Strain Rate (m/m/sec)	Temperature (°C)	Stress Ratio
L-16	10^{-4}	482	1.044
L-17	10^{-4}	566	1.240
L-18	10^{-4}	649	1.045
L-19	5×10^{-4}	482	1.061
L-20	5×10^{-4}	566	.936
L-21	5×10^{-4}	649	1.000
L-22	10^{-3}	482	1.061
L-23	10^{-3}	566	.939
L-24	10^{-3}	649	.970
L-25	5×10^{-3}	482	1.019
L-26	5×10^{-3}	566	.949
L-27	5×10^{-3}	649	.968
L-28	10^{-2}	482	1.001
L-29	10^{-2}	566	.982
L-30	10^{-2}	649	.946

Table 10: Stress Ratio (SR) at various temperatures and strain rates.
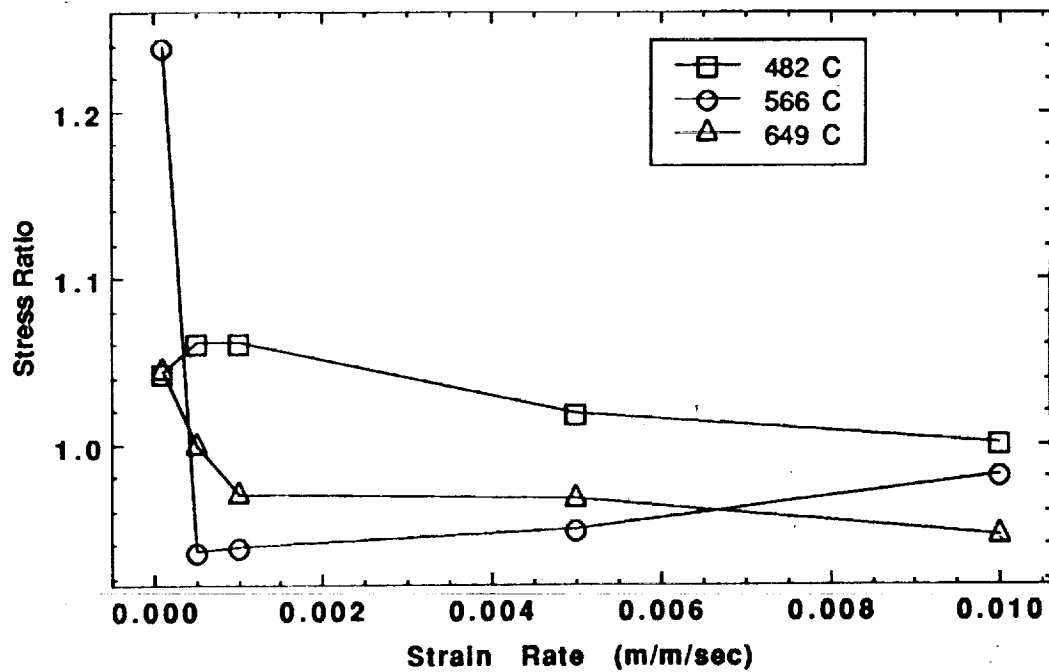
Figure 14: Stress Ratio as a Function of Strain Rate
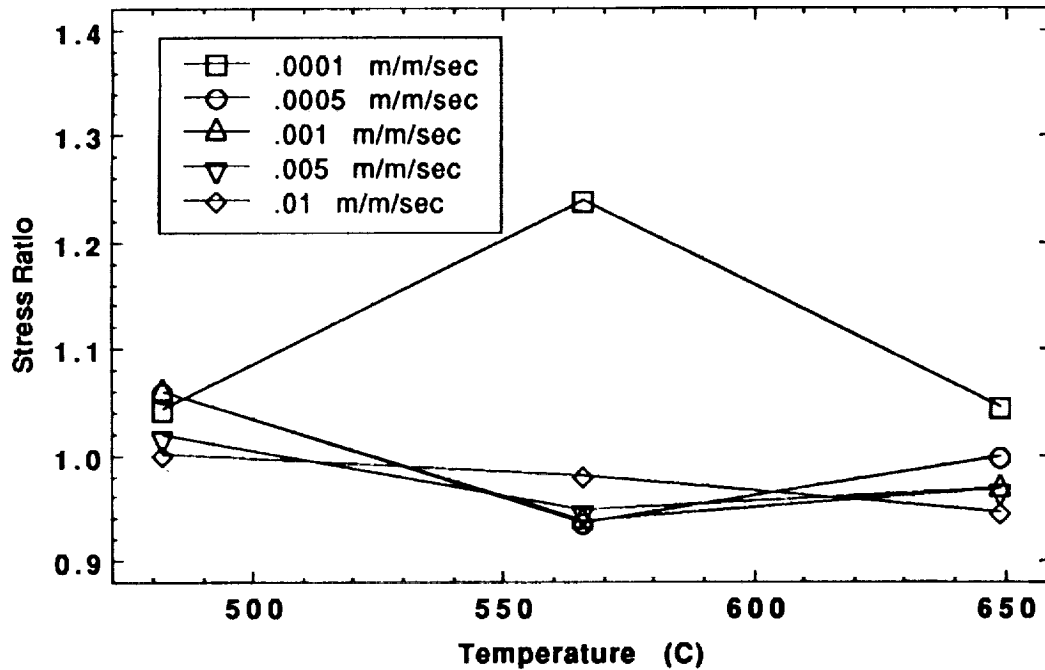
Figure 15: Stress Ratio as a Function of Temperature

Modifications for the Walker Model. Tests L22, L23, and L24 were specially modified to accommodate the Walker model. As described in Ref [10], the Walker model requires that stress relaxation behavior be measured at several distinct strain levels. Furthermore, it is required that these stress relaxation tests be initiated after the material response has been stabilized during CCSR loading cycles.

The strain histories imposed during tests L22 through L24 are summarized in Table 11. A typical loading sequence will be described using test L22 as an example. Test L22 began by subjecting the specimen to 30 "normal" CCSR cycles. The initial 30 cycles are referred to as "CCSR Cycle #1" in Table 11. The resulting 30-cycle stress-strain

27

hysteresis loop is plotted in Figure C7a, Appendix C. A stress relaxation test was then initiated during the tensile unloading portion of the 31st cycle. That is, during the unloading portion of the 31st cycle the crosshead of the MTS frame was suddenly stopped so as to impose and maintain a constant strain of 0.80%, and the load was allowed to increase or decrease as dictated by the specimen response. This portion of the test is referred to as "Stress Relaxation #1" in Table 11. The strain was held at 0.80% for 205 secs (3.4 min). A plot of the resulting stress vs time response is shown in Figure C7b. Initially a relatively high tensile stress of about 500 MPa was measured. The stress then steadily decreased; after 205 secs the stress had decreased to about 240 MPa.

After Stress Relaxation #1 was completed the specimen was subjected to an additional 20 CCSR cycles, referred to as "CCSR Cycle #2" in Table 11. The resulting hysteresis loop is shown as Figure C7c. Note that the specimen response almost immediately stabilized during CCSR Cycle # 2. Also, the stabilized hysteresis loop shown in Figure C7c is essentially identical to the corresponding hysteresis loop shown In Figure C7a. Stress Relaxation #2 was initiated during the tensile unloading portion of the 51st CCSR cycle. Strain was maintained at 0.70% for 205 secs, and the measured response is shown in Figure C7d. In this case the stress was initially about 440 MPa, and decreased to about 240 MPa after 205 secs. The specimen was subjected to a third set of 20 CCSR cycles (Figure C7e), and subsequently stress relaxation was measured at a strain level of 0.60% (Figure C7f). The stress was initially about 375 MPa and decreased to about 240 MPa after 210 secs. The specimen was subjected to a fourth set of 20 CCSR cycles (Figure C7g), and stress relaxation was measured at a strain level of 0.50% (Figure C7h). The stress was initially about 300 MPa and decreased to about 215 MPa after 205 secs. Finally, the specimen was subjected to a fifth set of CCSR cycles (Figure C7i), and stress relaxation was measured at a strain level of 0.40% (Figure C7j). The stress was initially about 230 MPa and decreased to about 165 MPa after 205 secs.

Tests L23 and L24 followed similar loading sequences. The data obtained during these tests are presented in Figures C8 and C9, respectively, in Appendix C.

Test No.	Temp (°C)	CCSR Cycle #1 No. CCSR Cycles	Stress Relaxation #1 Strain Level (%)	Time (secs)	CCSR Cycle #2 No. CCSR Cycles	Stress Relaxation #2 Strain Level (%)	Time (secs)	CCSR Cycle #3 No. CCSR Cycles	Stress Relaxation #3 Strain Level (%)	Time (secs)	CCSR Cycle #4 No. CCSR Cycles	Stress Relaxation #4 Strain Level (%)	Time (secs)	CCSR Cycle #5 No. CCSR Cycles	Stress Relaxation #5 Strain Level (%)	Time (secs)
L22	482	30	0.80	260	20	0.70	205	20	0.60	205	20	0.50	205	20	0.40	300
L23	566	30	0.80	205	20	0.70	205	20	0.60	210	20	0.50	205	20	0.40	200
L24	649	30	0.85	215	20	0.8	95	20	0.75	160	20	0.70	275	20	0.65	300

Table 11: Summary of strain histories imposed during the CCSR tests modified to accommodate the Walker model

Modifications for the Miller Model. As described in Ref [7], the Miller model requires that CCSR tests be conducted at progressively higher strain levels. Tests L25, L26, and L27 were specially modified to accommodate these requirements. The strain histories imposed during these tests will be described using Test L25 as an example.

Test L25 was conducted at 482°C. A cyclic constant strain rate of .005 m/m/sec was used throughout the test. A total of 60 loading cycles were recorded during the test. The test differed from "normal" CCSR tests in that three different maximum strain levels were imposed. During the first 20 cycles the maximum strain was ±0.6%, during the next 20 cycles the maximum strain was ±1.0%, and during the final 20 cycles the maximum strain was ±1.2%. The stress-strain data collected during each interval are presented in Figures C10a,b, and c. Unfortunately, data collected during these tests were badly distorted due to electronic noise. The noise is particularly severe at the lower strain levels (see Figure C10a, for example). The source of this electronic noise is assumed to be the inductance furnace used to heat the specimen.

Tests L26 and 27 were conducted at temperatures of 566°C and 649°C, respectively, and at a cyclic constant strain rate of .005 m/m/sec. Maximum strains of ±0.6%, ±1.0%, and ±1.2% were imposed during these tests as well. The data collected during these tests are presented in Figures C11(a-c) and C12(a-c), respectively.

Constant Stress Rate Tests

During the constant stress rate (CσR) tests a linearly increasing tensile load was applied to each specimen, resulting in a linearly increasing stress. The resulting strain rate was allowed to increase or decrease as dictated by the specimen response. Typical CσR test results are shown in Figure 16.

A total of four CσR tests were conducted, as summarized in Table 12. Two room temperature CσR tests were conducted using loading rates of 44.5 and 89.0 N/sec, which correspond to constant stress rates of 2.6 and 5.2 MPa/sec, respectively. In addition, two CσR tests were conducted at elevated temperatures of 482°C and 649°C using a loading rate of 44.5 N/s, i.e., a constant stress rate of 2.6 MPa/sec.

(b) Strain vs Time

(a) Stress vs Time

(c) Stress vs Strain
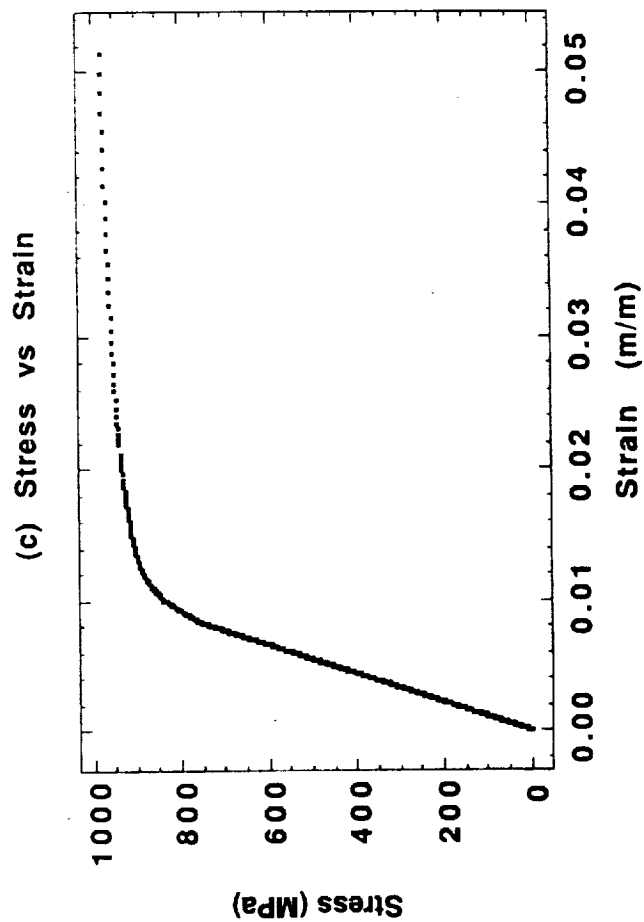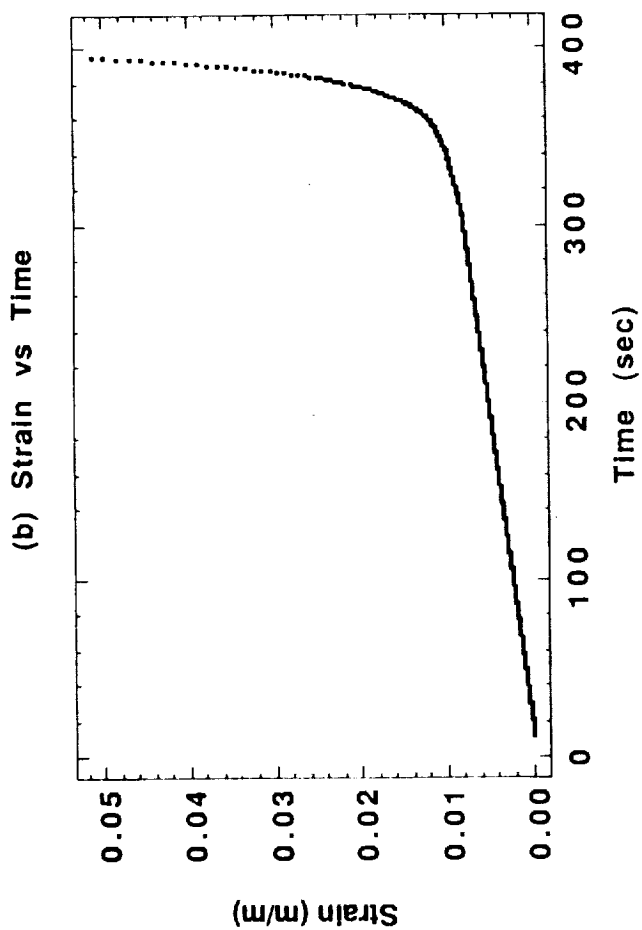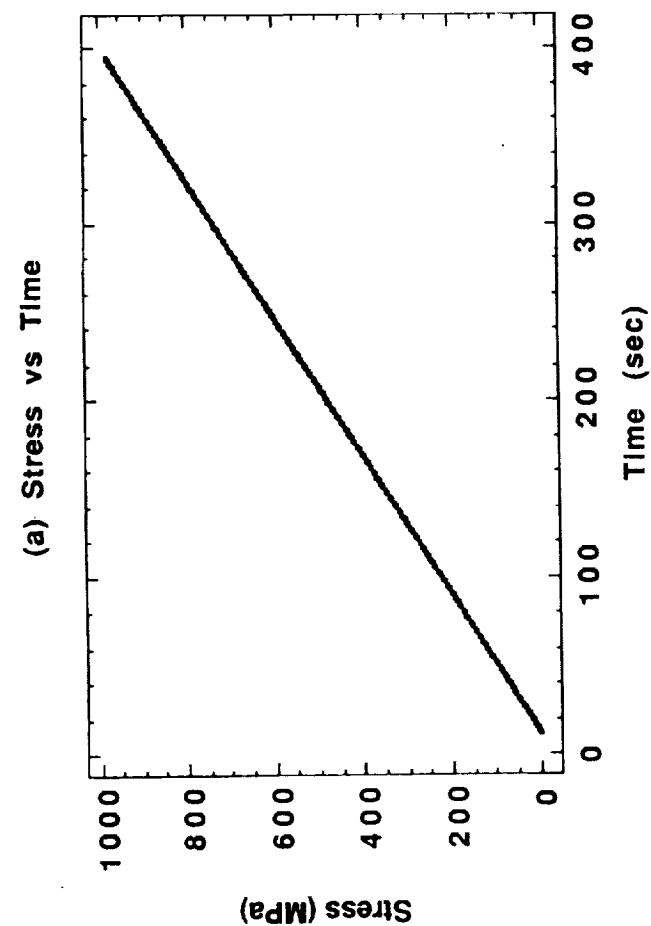
Figure 16: CσR Test Results Obtained During Test L40

The stress-strain data recorded during the CσR tests are presented in Appendix D, Figures D1 through D5. These data were collected during Tests L40 through L43. Some of the pertinent features of the data are summarized in Table 12. Note that during the initial (elastic) portion of these tests the constant stress rates imposed correspond to constant strain rates. For example, during test L-42 (conducted at 482°C) a constant stress rate of 2.6 MPa/sec was imposed, and an initial elastic modulus and yield strength of 66.8 GPa and 495 MPa, respectively, were measured. Therefore during the initial (elastic) portion of this test a constant strain rate of (2.6 MPa/sec)/(66.8 GPa) = 39 μm/m/sec was induced. This strain rate is lower than the lowest strain rate used during the constant strain rate (CSR) tests discussed in a preceding section. Based on the conclusions reached during the CSR tests, the elastic modulus and yield strength measured during the CσR tests should therefore be lower than those measured during the CSR tests at the same temperature. Comparing the data presented in Table 12 with that presented in Tables 4 and 5, it is seen that this is indeed the case. Therefore, the CσR data presented in Appendix D appears to be entirely consistent with the CSR and CSSR data previously discussed.

Test No.	Stress Rate (MPa/sec)	Temperature (°C)	Elastic Modulus (GPa)	0.2% Offset Yield Stress (MPa)
L-40	2.6	21	91.6	890
L-41	5.2	21	94.6	885
L-42	2.6	482	66.8	495
L-43	2.6	649	54.5	165

Table 12: Results of Constant Stress Rate tests conducted at the NASA Langley Research Center.

Complex Tests

The "complex" tests were performed so as to provide benchmark results. The tests have been previously listed in Table 4, and all data collected during these tests are presented in Appendix E. Multi-step creep tests were performed on the UW campus using the SATEC creep frame, and multi-rate tests were performed at NASA-LaRC using the MTS frames.

Seven multi-step creep tests were performed; five tests using fiberless Ti-15-3 specimens (Tests U31 and U33 through U36), one test using a [0°] unidirectional specimen (Test U38), and one test using a [90°] unidirectional specimen (Test U41). In a typical test a creep stress of 48.3 MPa (7 ksi) was applied and maintained for time t_1. At time t_1 the creep stress was doubled to 96.5 MPa (14 ksi) and maintained for an additional time t_2. Total test time was therefore ($t_1 + t_2$). Times t_1 and t_2 are listed for all multi-step creep tests in Table 13. The data are plotted in Appendix E, Figures E1 through E7.

Seven multi-rate tests were performed; one test using a [0°] unidirectional specimen (Test L33), three tests using a [90°] unidirectional composite specimen (Tests L34, L35, L36), and three tests using crossply [0°/90°]$_s$ composite specimens (Tests L37, L38, L39). The strain history imposed during tests L33 through L36 is shown schematically in Figure E8. As indicated, strain was increased from zero at a constant rate (nominally 0.0001 m/m/sec) over time increment t_1. At time t_1 the crosshead motion was reversed and strain was decreased at the same constant rate over time increment ($t_2 - t_1$). At time t_2 the crosshead motion was again reversed and strain was increased at a high constant rate (nominally 0.001 m/m/sec) for time increment ($t_3 - t_2$). At time t_3 the crosshead was stopped, and strain was maintained a constant value ε_3 for a time increment ($t_4 - t_3$). Numerical values for time and strains for tests L33 through L36 are listed in Table 14. The stress-strain responses induced by these strain histories are shown in Appendix E, Figures E9 through E12.

The strain history imposed during tests L37, L38, and L39 is shown schematically in Figure E13 (specimen failure occurred during test L37, so the strain history shown in Fig E13 was not completed for this test). Strain was increased from zero at a constant rate (nominally 1×10^{-4} m/m/sec) over time t_1. At time t_1 the crosshead was stopped, and strain was maintained a constant value ε_1 until time t_2. Numerical values for each test are listed in Table 15. The stress responses induced by these strain histories are shown in Appendix E, Figures E14 through E16.

Test Number	Specimen Type	Temp (°C)	Creep Time @ 48.3 MPa (t_1;secs)	Creep Time @ 96.5 MPa (t_2;secs)	Total Creep Test Time (secs)
U31	fiberless	482	66375	18168	84543
U33	fiberless	566	12499	9533	22032
U34	fiberless	566	5958	8151	14109
U35	fiberless	649	7386	989	8375
U36	fiberless	649	6547	868	7415
U38	[0°]	566	71890	17818	89708
U41	[90°]	566	7860	(failed)	7860

Table 13: Conditions for Creep Tests U31, U33 through U36, U38, and U41

Test No.	Spec Type	Temp (°C)	ε_1 (μm/m)	t_1 (secs)	ε_2 (μm/m)	t_2 (secs)	ε_3 (μm/m)	t_3 (secs)	t_4 (secs)
L33	0°	649	6540	66.2	2618	105.9	6488	110.1	180.4
L34	90°	482	5376	64.9	2340	104.8	7067	111.0	721.9
L35	90°	566	7013	68.7	2985	108.5	6570	112.1	723.7
L36	90°	649	6983	68.3	2977	108.2	5483	110.7	726.1

Table 14: Conditions for Multi-Rate Tests L33 through L36

Test No.	Specimen Type	Temp (°C)	ε_1 (μm/m)	t_1 (secs)	t_2 (secs)
L37	[0°/90°]s	482	8151	97.6	(spec. failure)
L38	[0°/90°]s	566	6875	74.5	644.5
L39	[0°/90°]s	649	6579	83.5	683.5

Table 15: Conditions for Multi-Rate Tests L37, L38 and L39.

34

Microstructural Changes

The crystalline microstructure of the Ti-15-3 specimens was inspected at magnifications ranging from 100 to 5,000X using optical and scanning electron microscopy. Inspections were completed for specimens in the as-received, annealed, and creep-tested conditions. The objective of this inspection was to determine if any gross changes in the crystalline microstructure had occurred during annealing and/or creep testing at elevated temperatures. As discussed in a preceding section, Ti-15-3 is a metastable beta-phase alloy. Of particular interest was whether the more stable (and brittle) alpha phase would precipitate during annealing and/or creep testing. Also, it was speculated that the uniaxial tensile creep loading might cause the grains to elongate in the direction of loading.

Specimen Preparation. The specimens were prepared in the following manner. First, three samples were machined from each tensile specimen, such that three orthogonal planes could be inspected, as defined in Figure 17. The three samples were mounted in phenolic resin and wet sanded in four stages, using 240, 320, 400 and 600 grit silicon carbide paper. Next, the specimens were polished in four stages, using progressively finer alumina powder (5/15, 1.0, 0.3 and 0.05 μm dia) suspended in distilled water. The specimens were cleaned in distilled water using an ultrasonic cleaner after each polishing stage. After polishing, all three surfaces of the specimen appeared completely smooth and featureless (at optical magnification levels). The specimens were then etched
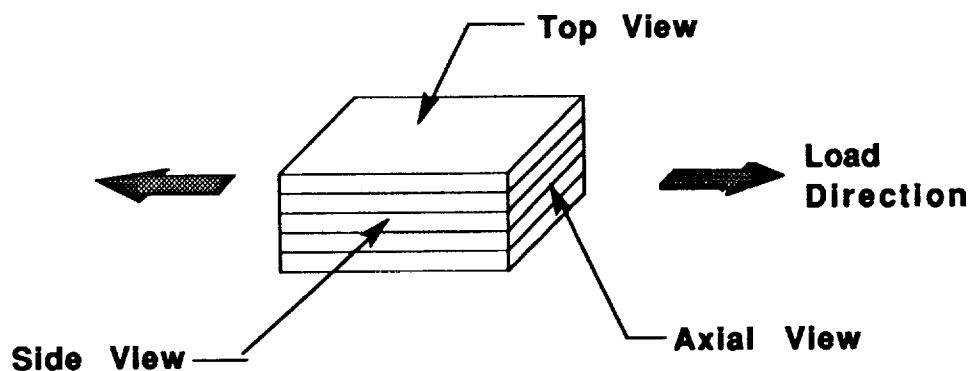
Figure 17: Surfaces Inspected Using Optical and Scanning Electron Microscopy

using Kroll's reagent (HF-7, HNO$_3$-18, H$_2$O-75) for three to five seconds. The Kroll's reagent selectively etched the alpha-phase, thereby highlighting the size and shape of the alpha grains while leaving the beta grains relatively intact. After etching, various features of the grain structure could be easily identified using either an optical microscope or an SEM.

Optical Microscopy. Inspections at magnification levels of 100 to 200X were accomplished using a Nikon Optiphot Metallurgical Microscope equipped with a G1F filter and Polaroid camera. Photographs of the "as-received" condition (i.e., neither heat treated nor creep tested) are shown in Figure 18. Figures 18(a,b) show the top surface at a magnification of 100X and 200X, respectively, while a side view is shown in Figure 18(c) at a magnification of 200X. The large beta grain structure is readily apparent at both 100X and 200X. At a magnification of 200X, dark "pebbles" embedded within the larger beta grains become apparent. These dark pebbles are believed to be regions of alpha phase, although they may also be contaminants and/or voids. Assuming they are alpha grains, they were apparently precipitated during the HIP process used to fabricate the laminated parent panel. Note that the original lamina interfaces are clearly visible in Figure 18(c), even though they were not visible prior to etching. Since in many places the beta grain boundaries extend across the original lamina interface, the specimen seems to have been very well consolidated during the HIP process. On the other hand, since the original interfacial regions are so readily apparent, the interfacial regions must be sites for preferential alpha precipitation, contaminants, and/or void formation.

Figures 19(a) through (c) are similar photographs of specimens which have been heat treated and subjected to creep testing. Figures 19(a,b) show the top and side views, respectively, of a specimen tested at 566°C and subjected to a two-step creep stress of 48 and 97 MPa, while Figure 19(c) shows a side view of a specimen tested at 34.5 MPa and 649°C. It is immediately apparent that exposure to elevated temperature has caused extensive precipitation of additional alpha grains. It was also originally speculated that the beta grain structure would become elongated (or otherwise distorted) during creep loading of the specimen. No such distortion is apparent, however. The original beta grain boundaries are still visible in Figure 19, and these boundaries are relatively undisturbed.
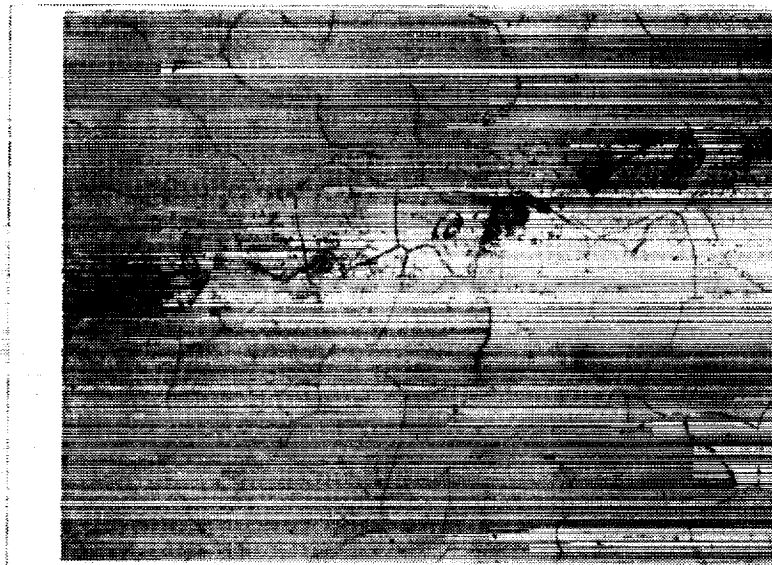
Figure 18a - Optical microscope photograph of as received 13 ply neat
Ti-15-3 laminate (top view, 100x).
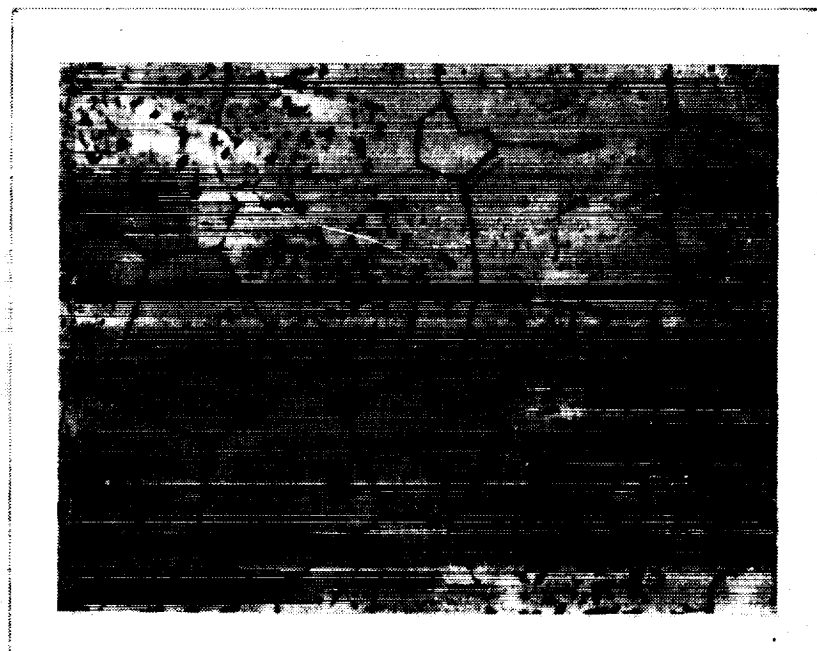
Figure 18b - Optical microscope photograph of as received 13 ply neat
Ti-15-3 laminate (top view, 200x).

37
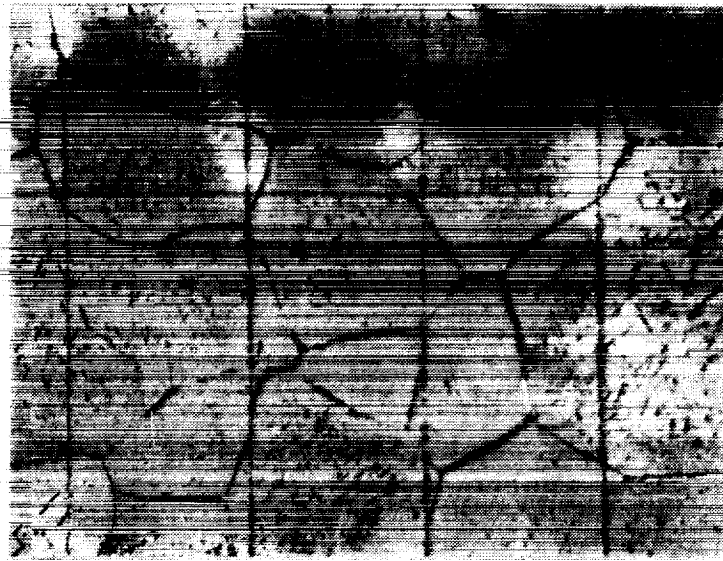
Figure 18c - Optical microscope photograph of as received 13 ply neat
Ti-15-3 laminate (side view, 200x).
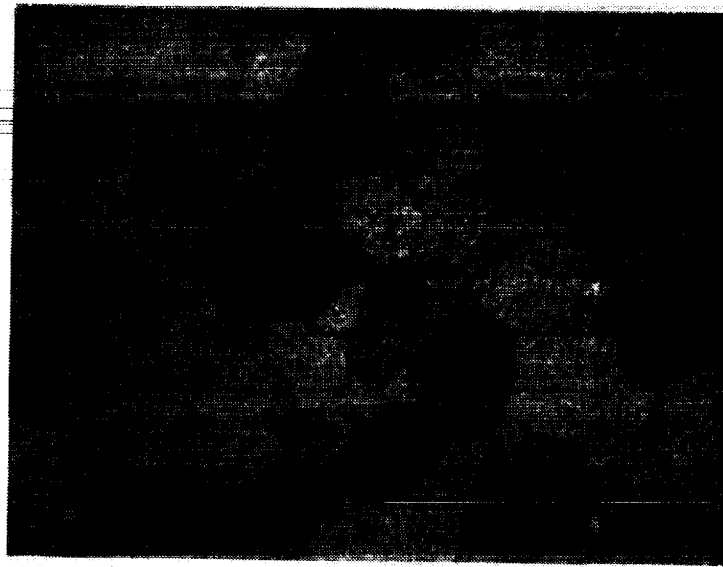
Figure 19a - Optical microscope photograph of heat treated 13 ply neat Ti-13-5 laminate after creep testing at 566 C and 48/97 Mpa (top view, 100x).

Figure 19b - Optical microscope photograph of heat treated 13 ply neat Ti-13-5 laminate after creep testing at 566 C and 48/97 Mpa (side view, 100x).
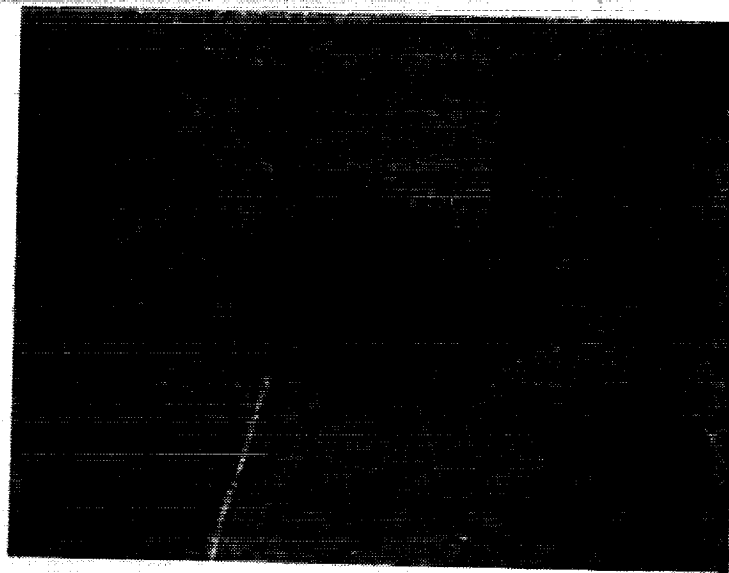
Figure 19c - Optical microscope photograph of heat treated 13 ply neat
Ti-13-5 laminate after creep testing at 649 C and 34.5 Mpa
(top view, 200x).

Figure No.	Stress (MPa)	Temperature (°C)	Test Duration (sec)	Total Strain (m/m)
20a	0	NA	NA	0
20b	0	NA	NA	0
20c	0	NA	NA	0
21a	0	538	4.32×10^4	0
21b	0	538	4.32×10^4	0
21c	0	538	4.32×10^4	0
22a	48/97	482	8.50×10^{-4}	.0070
22b	48/97	566	2.20×10^4	.0105
22c	48/97	649	8.50×10^3	.0255
23a	34.5	482	1.60×10^5	.0050
23b	34.5	649	7.50×10^4	.0260
23c	172.4	482	8.50×10^4	.0220
23d	172.4	649	105	.019

Table 16: Test Conditions for specimens shown in Figures. 20 through 23.

Scanning Electron Microscopy Photographs. A JEOL JSM-T330A Scanning Electron Microscope with Polaroid Type 55 film was used to obtain photographs at magnifications up to 5000X. A thin strip of colloidal graphite suspended in iso-propanol was painted on each specimen to improve the electrical contact between the Ti-15-3 sample and the SEM. An accelerating voltage of 15kV provided the best results. A series of SEM photographs were obtained for specimens tested under the conditions summarized in Table 16.

Figures 20(a, b, and c) show the same site on a specimen at magnifications of 200X, 1000X, and 5000X, respectively. The specimen is in the as-received condition, and the beta grain structure is clearly visible. The original lamina interface (the straight, lightly-colored lines) are readily discernible in these photographs . Small amounts of alpha are visible at the lamina interface, at beta grain boundaries, and at interior regions of the beta grains.

Figures 21(a) through (c) show three orthogonal views of a specimen that was heat treated at 538°C for 12 hours. Although the beta grain structure is still discernible, note the dramatic increase in the amount of alpha phase, compared to the as received specimen shown in Figure 20.

Figures 22(a,b,c) show specimens creep tested at 482, 566, and 649°C, respectively. All photos were taken at a magnification of 5000X. It is apparent that the increase in test temperature caused a decrease in the number of alpha grains but a corresponding increase in average alpha grain size.

Finally, Figures 23(a) through (d) are photographs of four specimens which were creep tested under various conditions as listed in Table 16. Figure 23 (a,b) show specimens tested at a common stress level of 34.5 MPa, and at temperatures of 482 and 649°C, respectively. Figure 23 (c,d) show specimens tested at a common stress level of 172.4 MPa, and at temperatures of 482 and 649°C, respectively. The two specimens tested at 482°C (Figures 23a and c) have a larger number of alpha grains than do the specimens tested at 649°C (Figures 23b and d), but the alpha grains are smaller at 482°C than at 649°C. The specimens stressed at 34.5 MPa (Figure 23a and b) have somewhat larger alpha grains than do those tested at 649°C (Fig. 23c and d), probably because of the longer test times used at the lower temperatures.

Figure 20a - SEM photograph of as received 13 ply neat Ti-15-3 laminate
(top view, 200x).
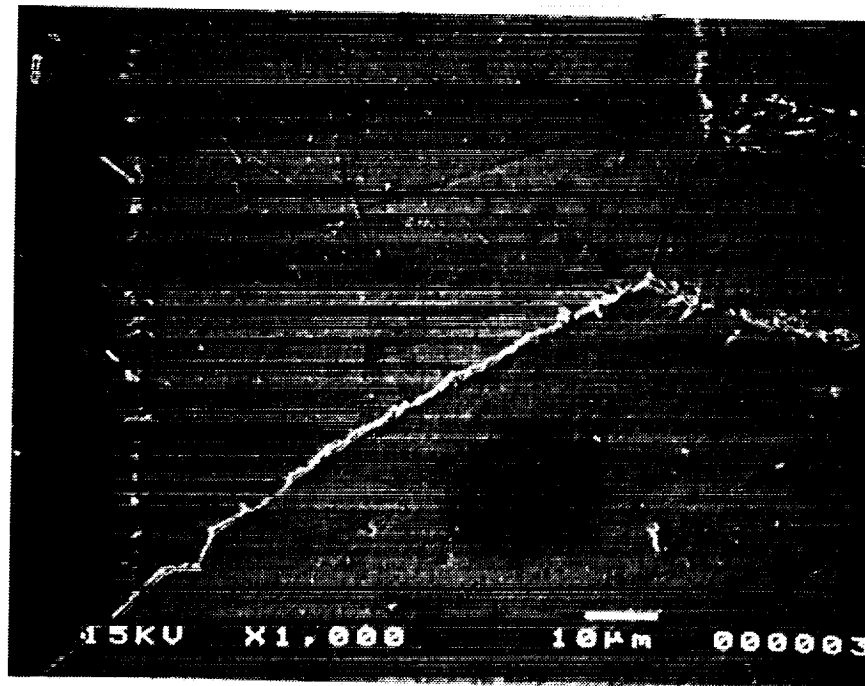
Figure 20b - SEM photograph of as received 13 ply neat Ti-15-3
laminate (top view, 1000x).

43
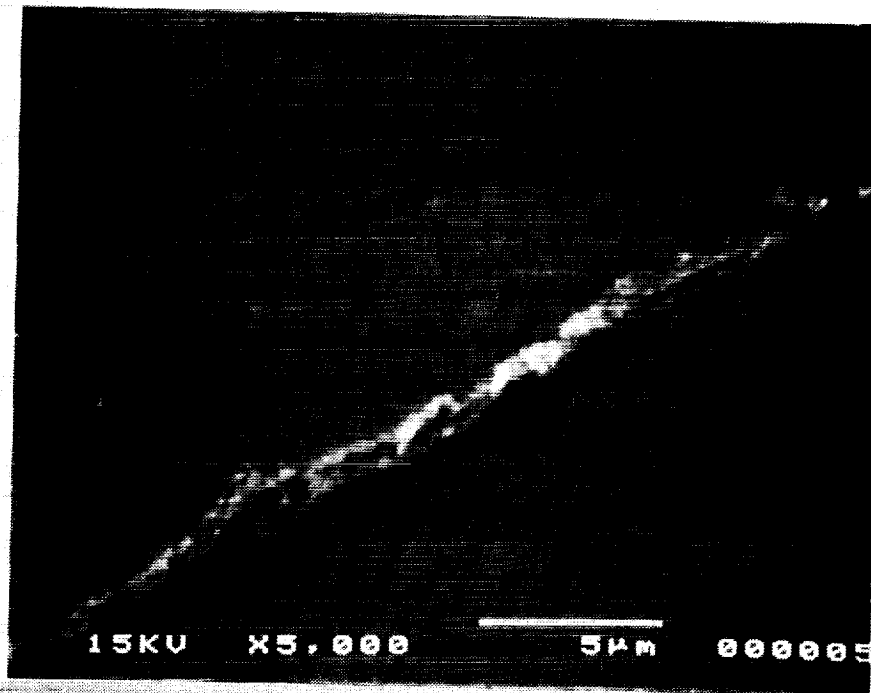
Figure 20c - SEM photograph of as received 13 ply neat Ti-15-3 laminate
(top view, 5000x)
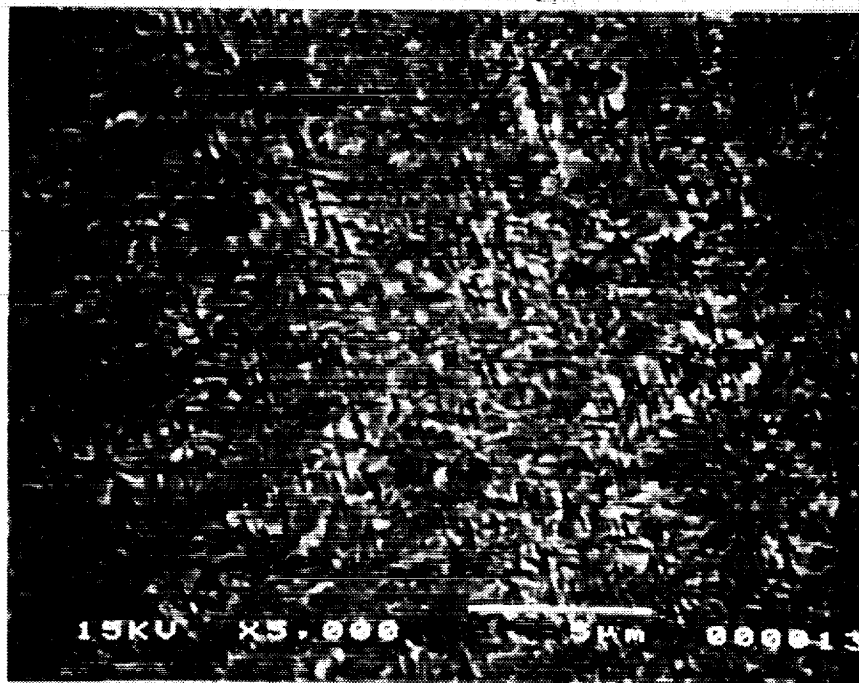
Figure 21a - SEM photograph of heat treated 13 ply neat Ti-15-3 laminate
(top view, 5000x).
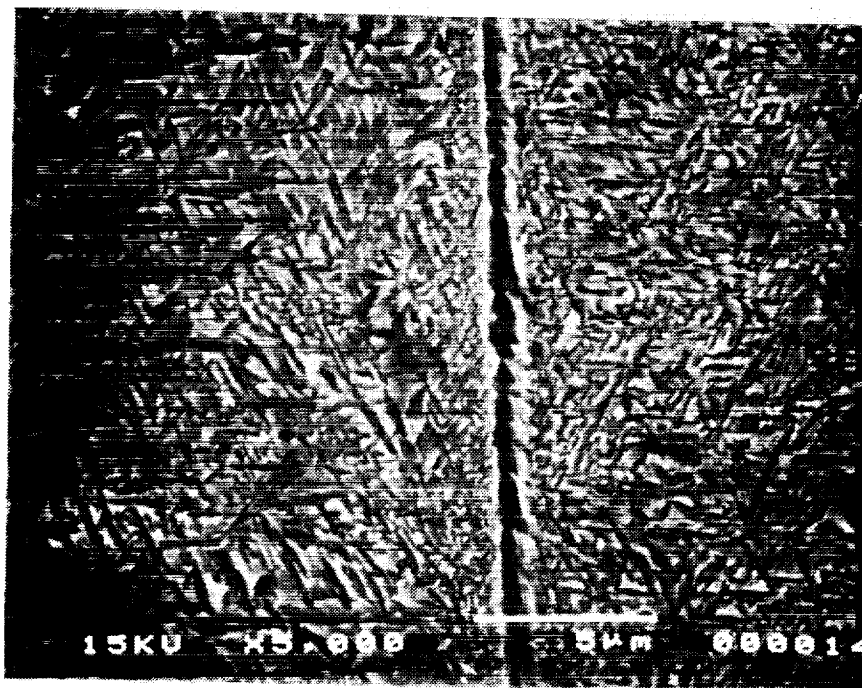
Figure 21b - SEM photograph of heat treated 13 ply neat Ti-15-3
laminate (side view, 5000x).

45
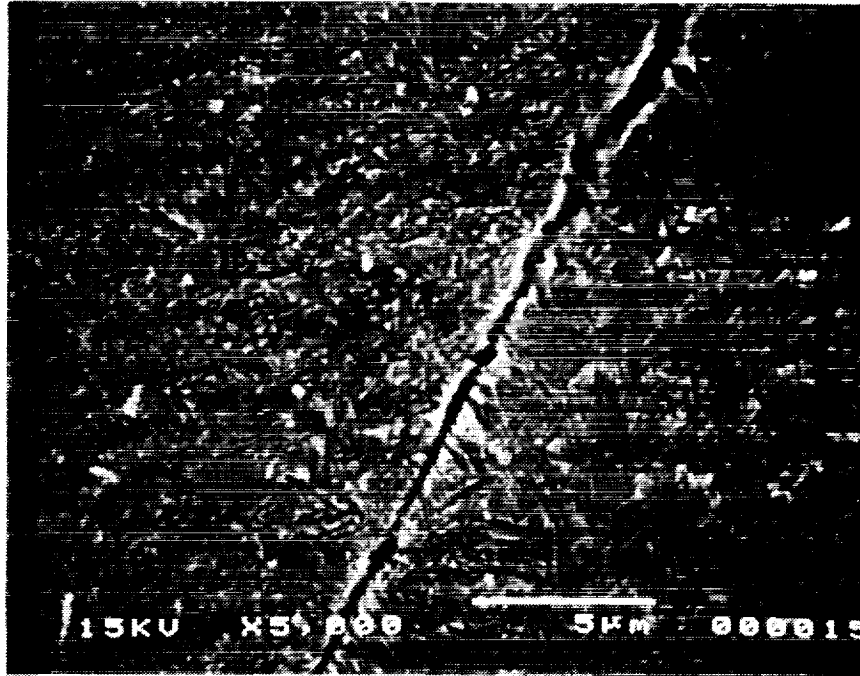
Figure 21c - SEM photograph of heat treated 13 ply neat Ti-15-3 laminate
(axial view, 5000x).
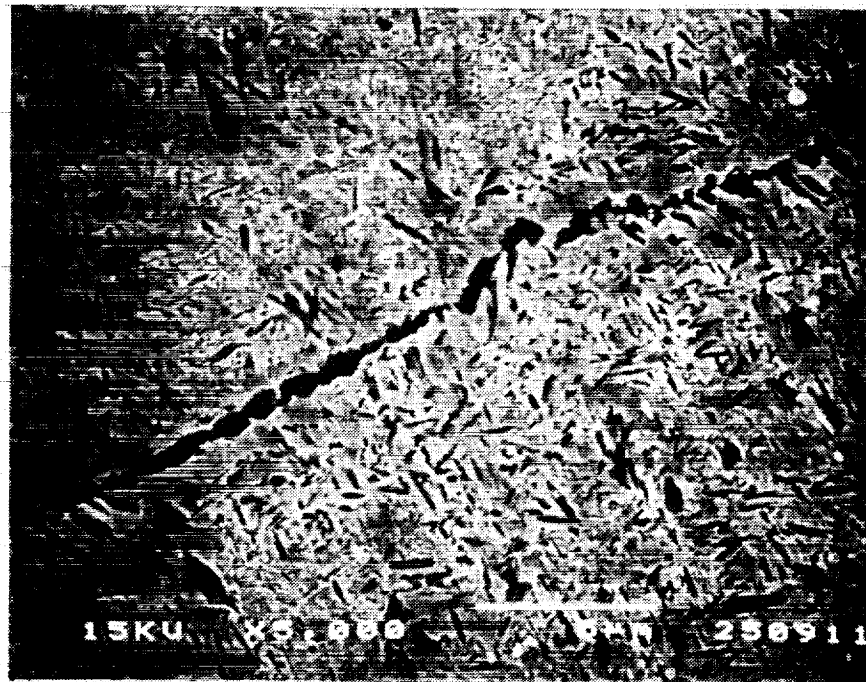
Figure 22a - SEM photograph of heat treated 13 ply neat Ti-15-3
laminate after creep test at 482 C and 48/97 Mpa
(top view, 5000x).
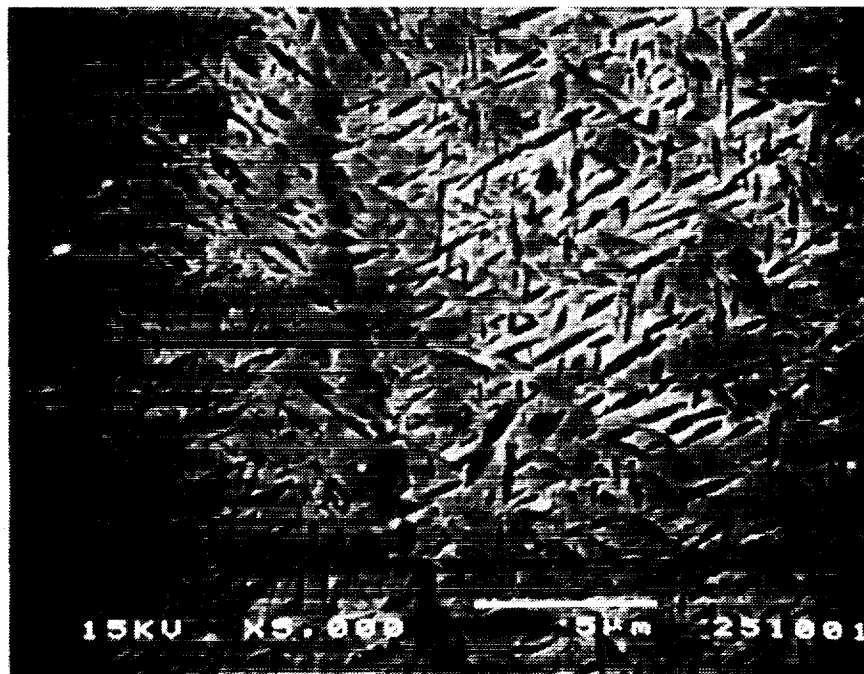
Figure 22b - SEM photograph of heat treated 13 ply neat Ti-15-3 laminate
after creep test at 566 C and 48/97 Mpa
(top view, 5000x).
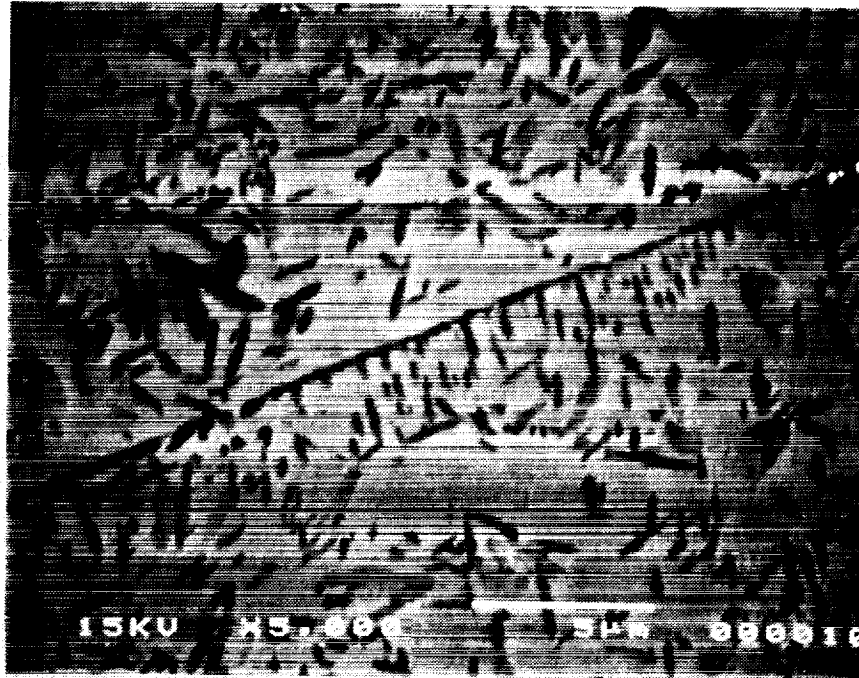
Figure 22c - SEM photograph of heat treated 13 ply neat Ti-15-3
laminate after creep test at 649 C and 48/97 Mpa
(top view, 5000x).

Figure 23a - SEM photograph of heat treated 13 ply neat Ti-15-3
laminate after creep test at 482 C and 34.5 Mpa (top view, 5000x).
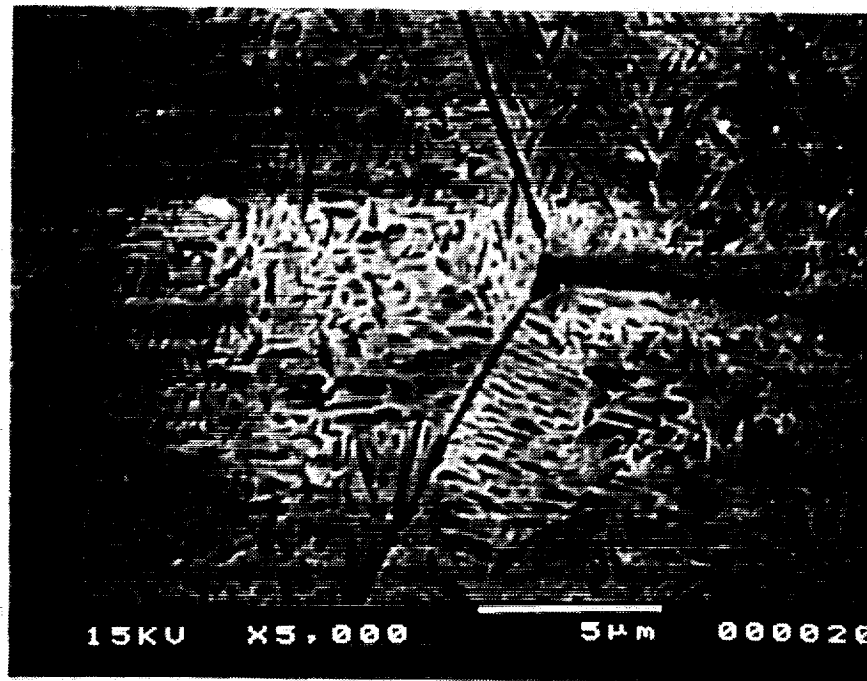
Figure 23b - SEM photograph of heat treated 13 ply neat Ti-15-3 laminate
after creep test at 649 C and 34.5 Mpa (top view, 5000x).

49

Figure 23c - SEM photograph of heat treated 13 ply neat Ti-15-3 laminate
after creep test at 482 C and 172.4 Mpa
(top view, 5000x).
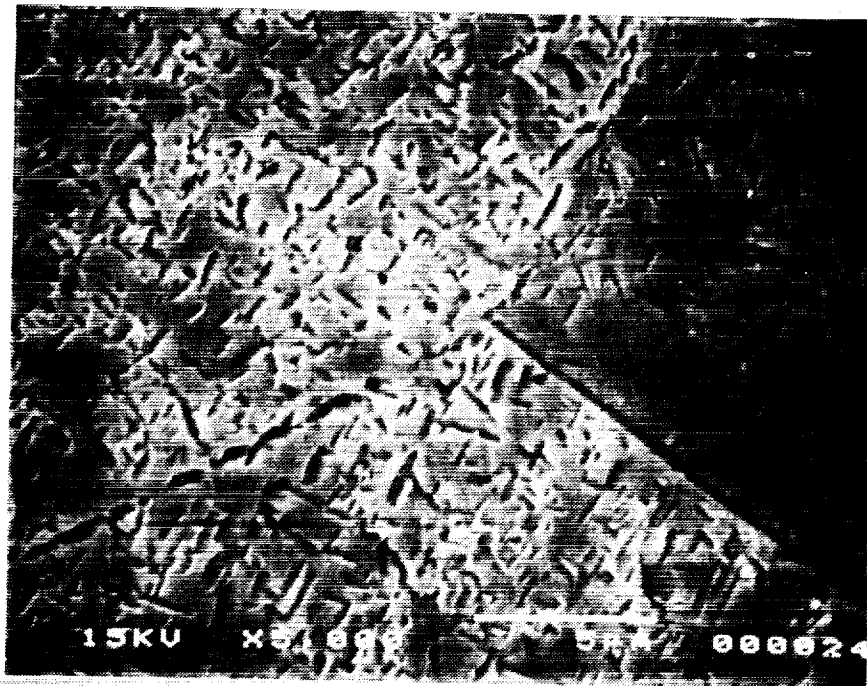
Figure 23d - SEM photograph of heat treated 13 ply neat Ti-15-3
laminate after creep test at 649 C and 172.4 Mpa
(top view, 5000x).

SUMMARY

An ongoing project at the University of Washington is to develop a combined experimental-analytic methodology for predicting the thermoviscoplastic behavior of multi-angle metal matrix composites (MMC's). The particular MMC being investigated in the study consists of a titanium Ti-15-3 matrix reinforced with continuous silicon carbide fibers. A requirement of the study is to identify a constitutive model which can adequately predict the thermoviscoplastic behavior of Ti-15-3 at elevated temperatures. Towards this end the models previously proposed by Bodner and Partom [3-5], Miller [6-9], Walker [10], and Eisenberg [11,12] are being evaluated to determine if one (or more) of these models can be used effectively.

The subject of this report is the experimental data base which has been generated in support of the above analysis. Four distinct types of material characterization tests have been conducted using "fiberless" Ti-15-3 laminates: creep tests, constant strain rate tests, constant stress rate tests and cyclic constant strain rate tests. The tests have been performed at three different elevated temperatures (482°C, 566°C, and 649°C). In addition, several "complex" tests were conducted using both fiberless Ti-15-3 specimens as well as unidirectional and cross-ply composite specimens. The general features of the data collected during each test have been described in the body of this report, and plots of all data collected are presented in the Appendices.

The authors believe that the data base described herein will be of broad interest to the MMC technical community. The data is presented in this report in the form of graphs and tables. However, if desired a copy of the original data files on computer diskettes can also be obtained. The interested reader should contact the first listed author (Dr. M. E. Tuttle, University of Washington) for instructions on obtaining a copy of the data on computer diskettes.

51

ACKNOWLEDGEMENTS

REFERENCES

1. Rogacki, J. and Tuttle, M. "Experimental Measurement of the Viscoplastic Behavior of SiC/Ti Metal Matrix Composites at Elevated Temperatures," Presented at the 1989 SEM Fall Conference, Nov. 6-8, Kansas City, MO.

2. Rogacki, J. and Tuttle, M. "Thermoviscoplastic Behavior of SCS_6/Ti Metal Matrix Composites," Presented at the 1990 SEM Spring Conference, June 6-8, Albuquerque, NM.

3. Bodner, S.R. and Partom, Y. "Constitutive Equations for Elastic-Viscoplastic Strain-Hardening Materials," *J. Appl. Mech.* Vol 42, pp. 385-389 (1975).

4. Bodner, S.R., Partom, I., and Partom, Y. "Uniaxial Cyclic Loading of Elastic-Viscoplastic Materials," *J. Appl. Mech.* Vol. 46, pp. 805-810 (1979).

5. Imbrie, P.K., Haisler, W.E., and Allen, D.H. "Evaluation of the Numerical Stability of Material Parameter Variations for Several Unified Constitutive Models," Aerospace Engineering Department, Texas A&M University, College Station, TX, #MM4998-85-6, May 1985.

6. Miller, A. "An Inelastic Constitutive Model for Monotonic, Cyclic, and Creep Deformation: Part I—Equations Development and Analytical Procedures," *ASME J. Eng Matls. and Tech.* pp. 97-105 (April 1976).

7. Miller, A. "An Inelastic Constitutive Model for Monotonic, Cyclic, and Creep Deformation: Part II—Application to Type 304 Stainless Steel," *ASME J. Eng Matls. and Tech.* pp. 106-113 (April 1976).

8. Hartmann, G. and Kollman, F.G. "A Computational Comparison of the Inelastic Constitutive Models of Hart and Miller," *Acta Mechanica* Vol. 69, pp. 139-165 (1987).

9. Beek, J.M., Allen, D.H., and Milly, T.M. "A Qualitative Comparison of Current Models for Nonlinear Rate-Dependent Materials Behavior of Crystalline Solids," Mechanics and Materials Center, Texas A&M University, College Station, TX, #MM 4246T-83-14, Nov. 1983.

10. Walker, K.P. "Research and Development Program for Nonlinear Structural Modeling With Advanced Time-Temperature Dependent Constitutive Relationships," NASA Tech Report #CR-165533, NASA Lewis Research Center, Cleveland, OH, 1981.

11. Eisenberg, M.A. and Yen, C.-F. "A Theory of Multiaxial Anisotropic Viscoplasticity," *J. App. Mech.* Vol 48, pp. 276-284 (1981).

12. Eisenberg, M.A. and Yen, C.-F. "Application of a Theory of Viscoplasticity to Uniaxial Cyclic Loading," *J. Eng. Matls. Tech.* Vol. 105, pp. 106-112 (1983).

13. Rosenberg, H.W. "Ti-15-3: A New Cold-Formable Sheet Titanium Alloy," *J. of Metals* Vol. 35, No. 11, pp. 30-34 (1986).

14. "Passage II: Numerics and Graphics for the Apple Macintosh II Computer", Passage Software, Inc, Fort Collins, CO .

15. Johnson, W.S., Lubowinski, S.J., Highsmith, A.J., Brewer, W.D., and Hoogstraten, C.A. "Mechanical Characterization of SCS_6/Ti-15-3 Metal Matrix Composites at Room Temperature," NASP Tech. Mem. 1014, (April 1988).

APPENDIX A

PLOTS OF DATA COLLECTED DURING CREEP TESTS
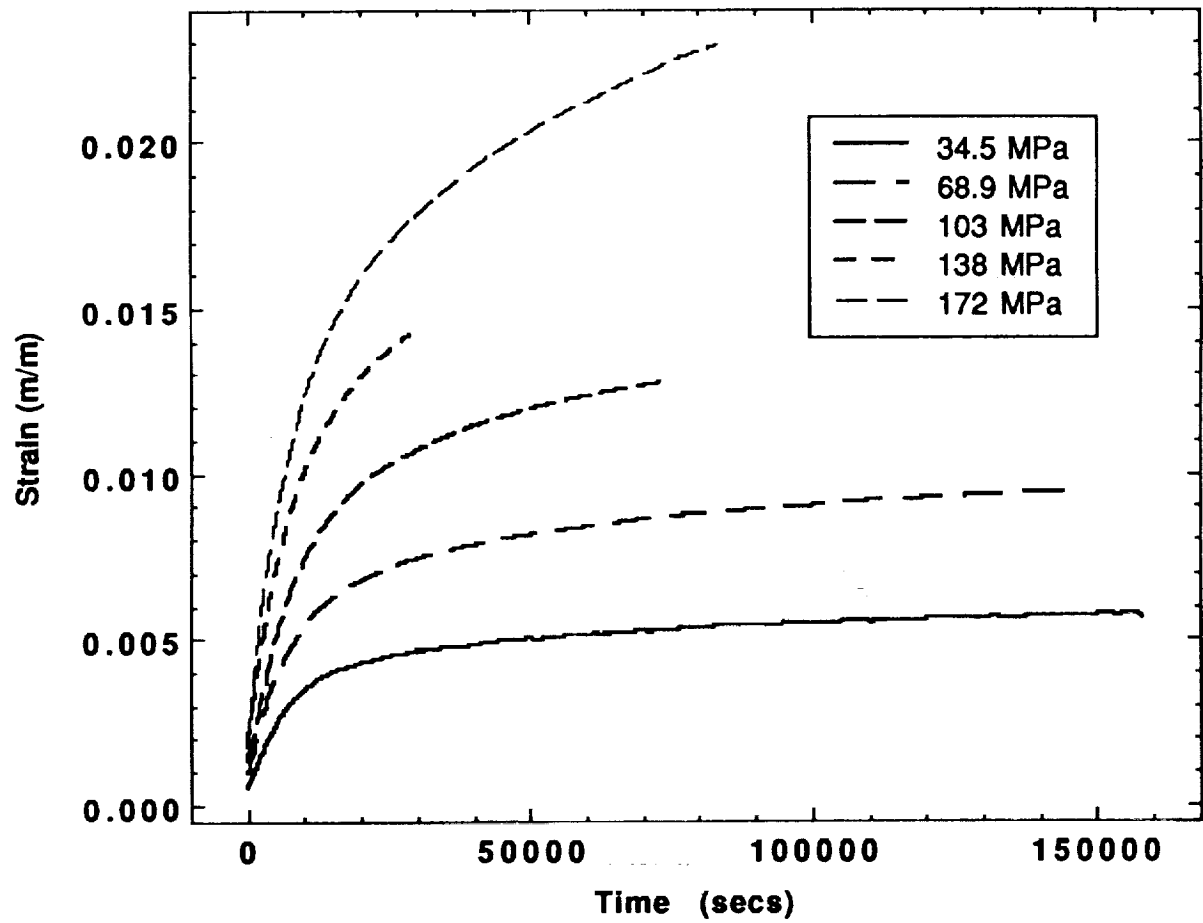
Figure A1: Creep Strains Measured at 482°C
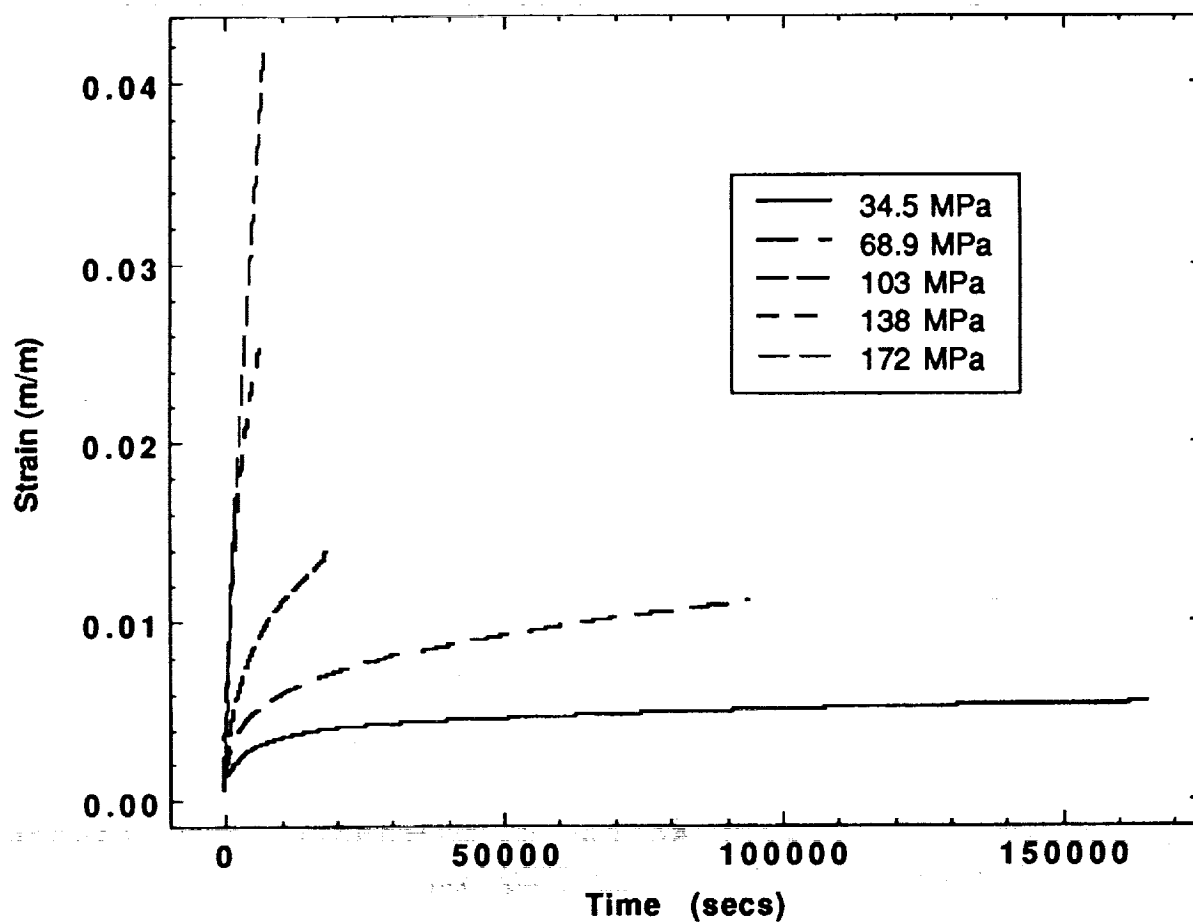
Figure A2: Creep Strains Measured at 566°C
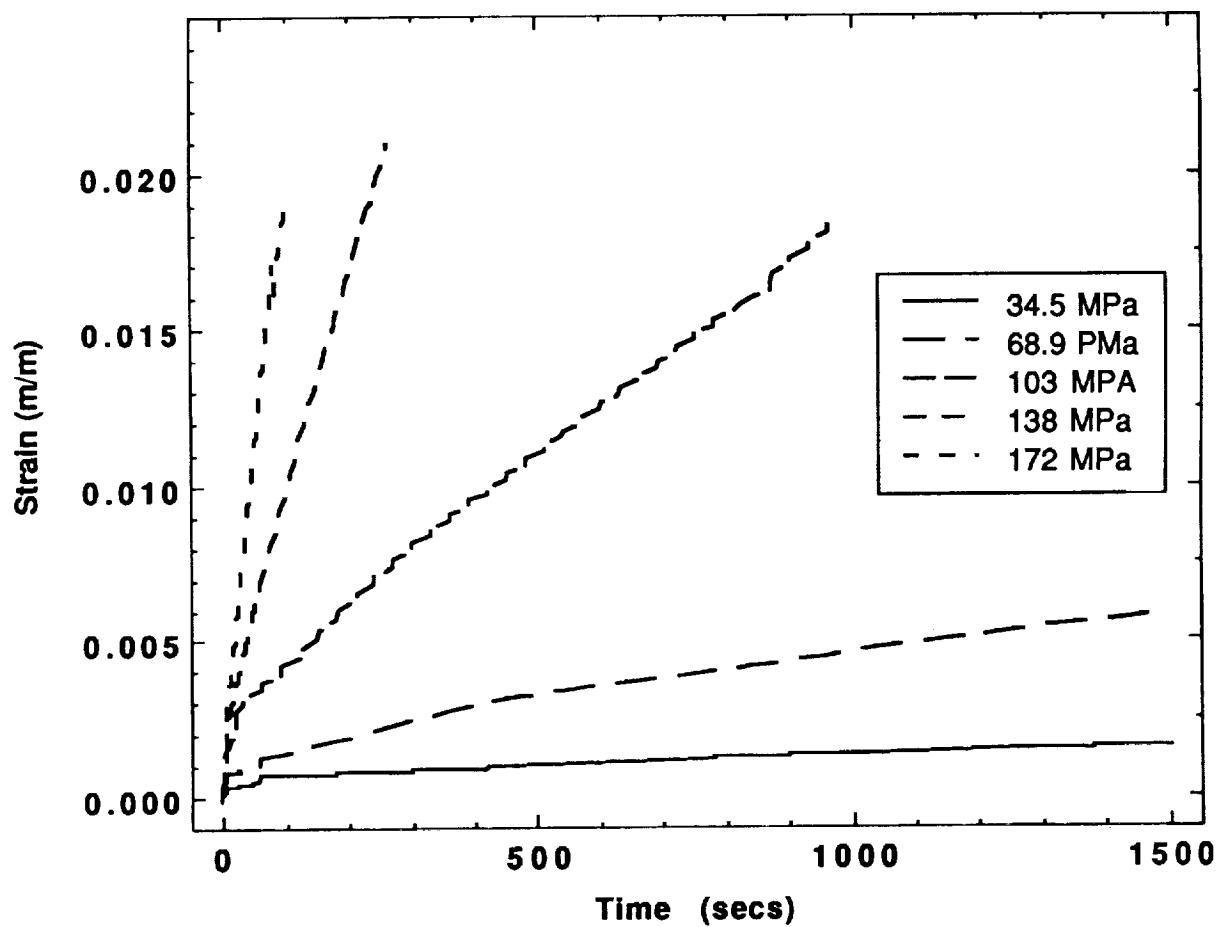
Figure A3: Creep Strains Measured at 649°C
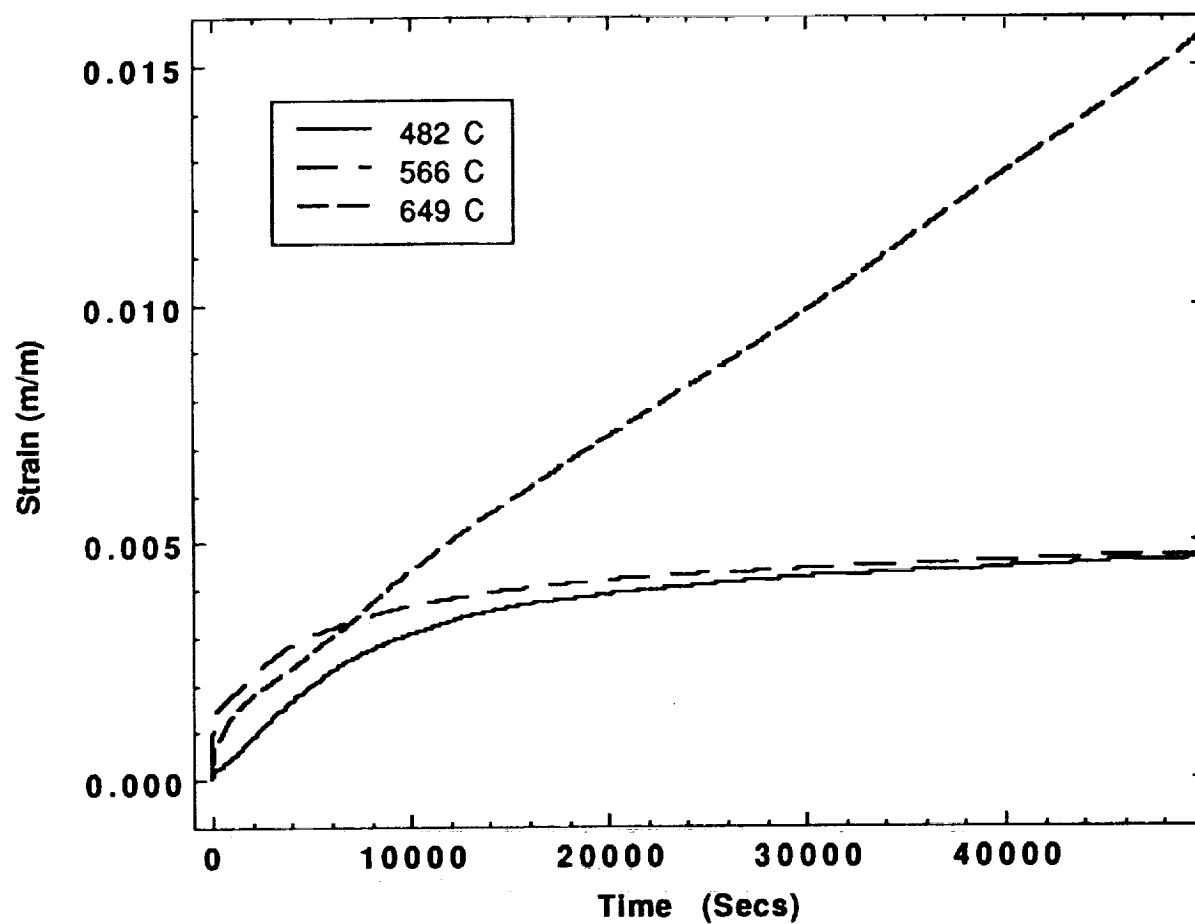
Figure A4: Creep Strains Measured at 34.5 MPa
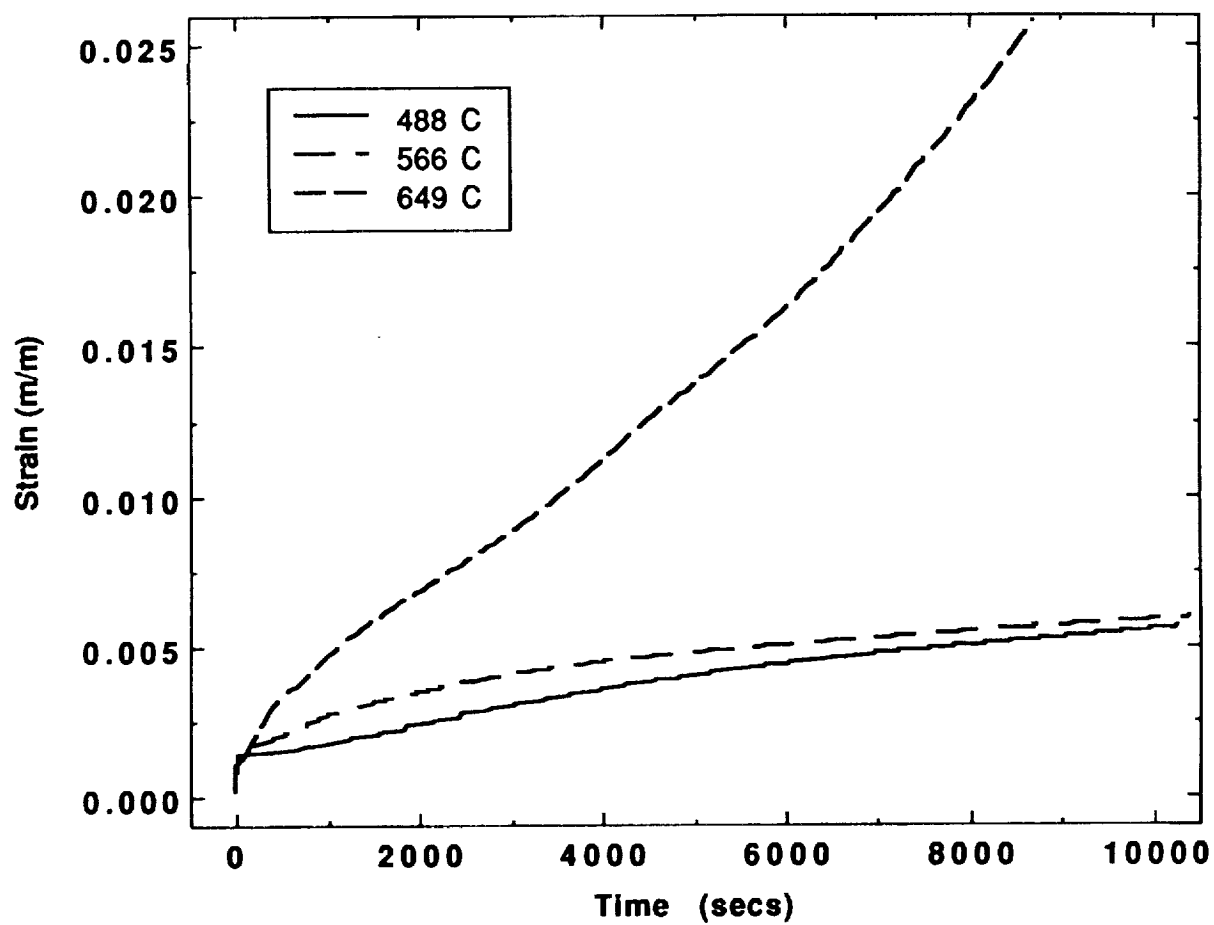
Figure A5: Creep Strains Measured at 68.9 MPa
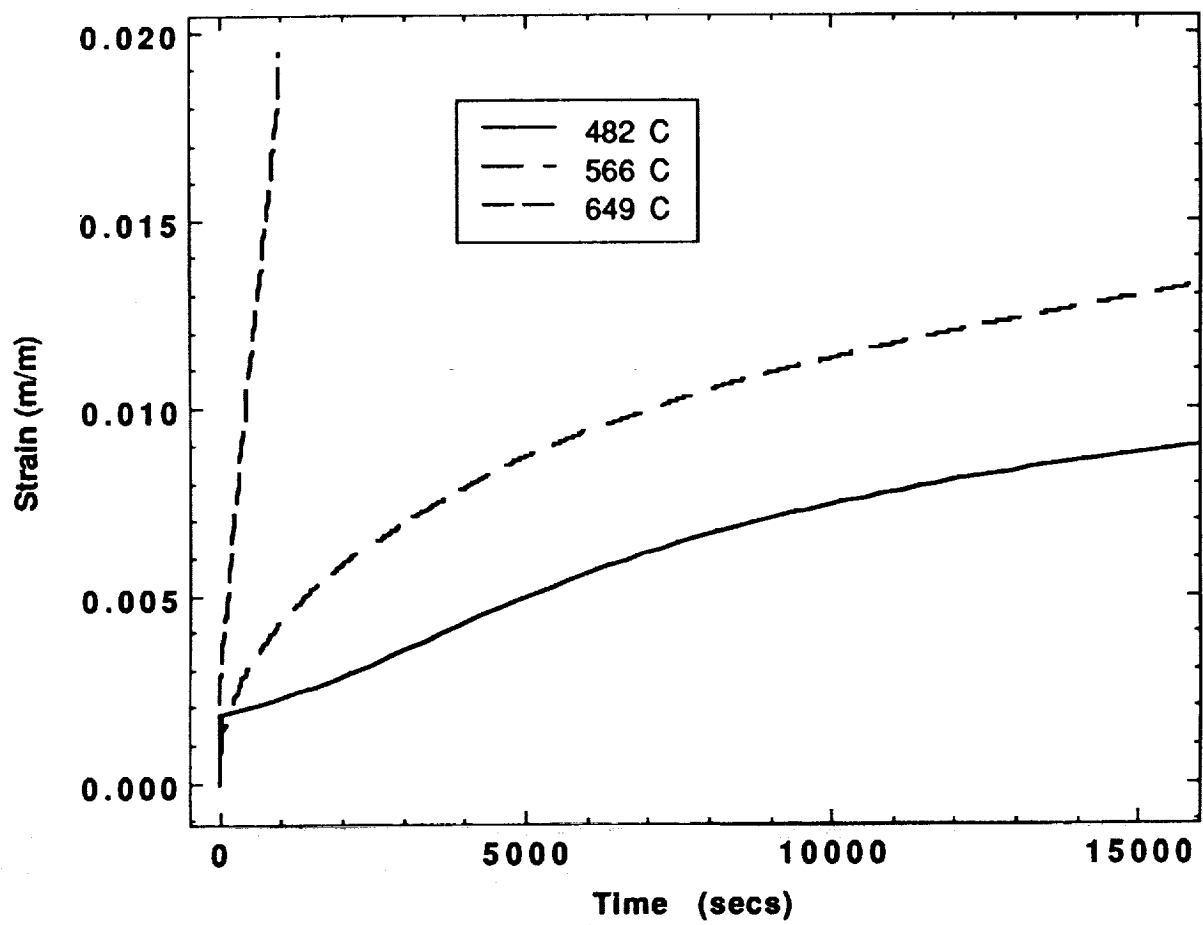
Figure A6: Creep Strains Measured at 103 MPa
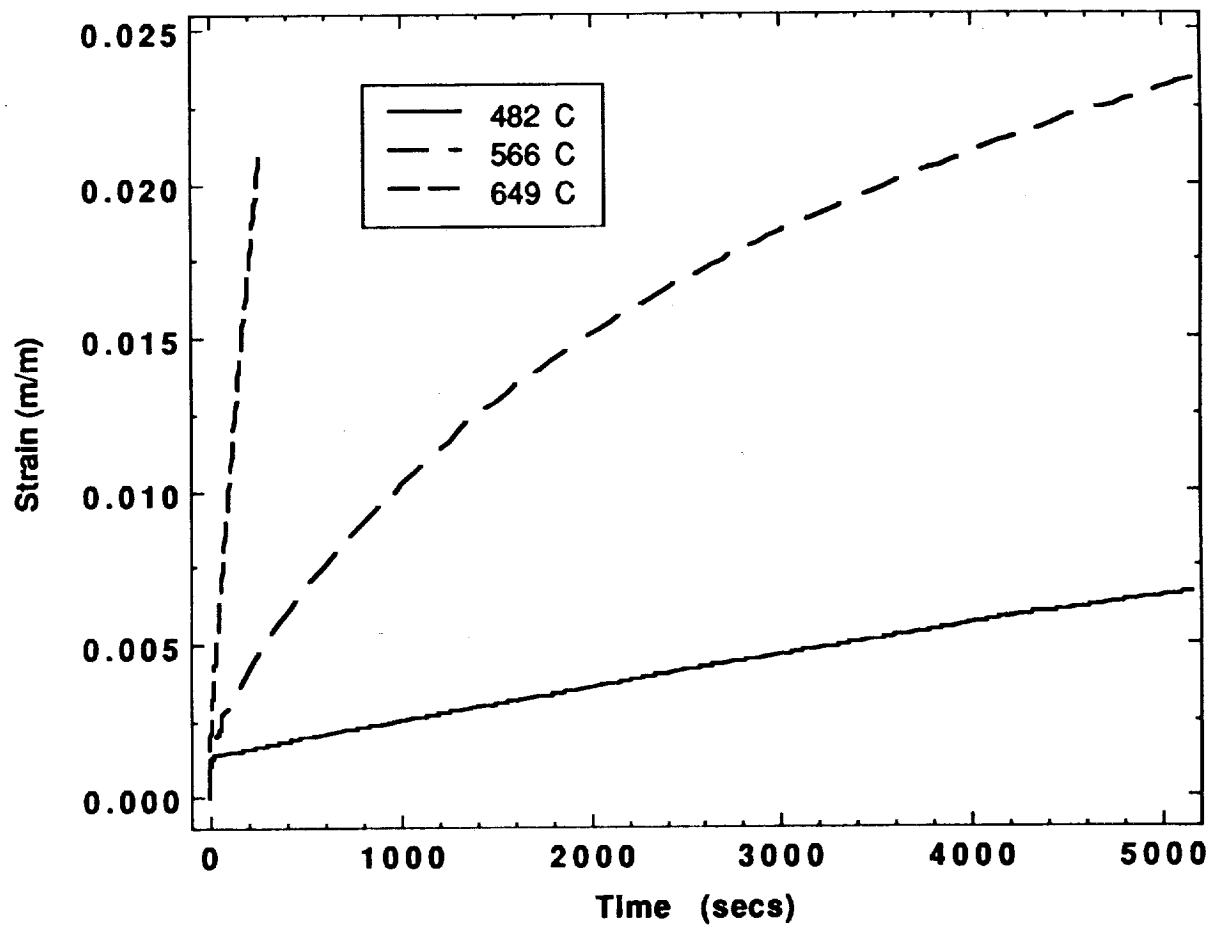
Figure A7: Creep Strains Measured at 138 MPa
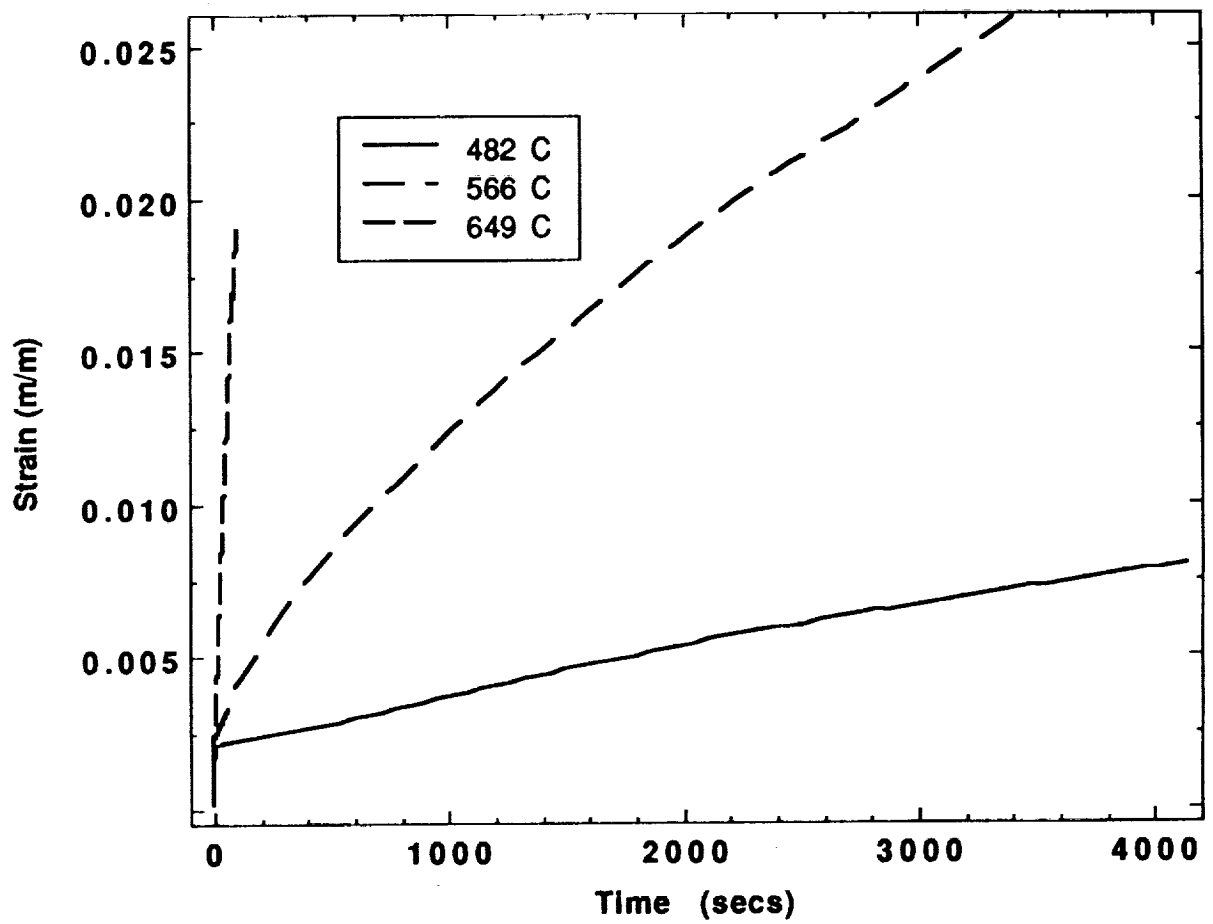
Figure A8: Creep Strains Measured at 172 MPa

APPENDIX B

PLOTS OF DATA COLLECTED DURING CONSTANT STRAIN RATE TESTS
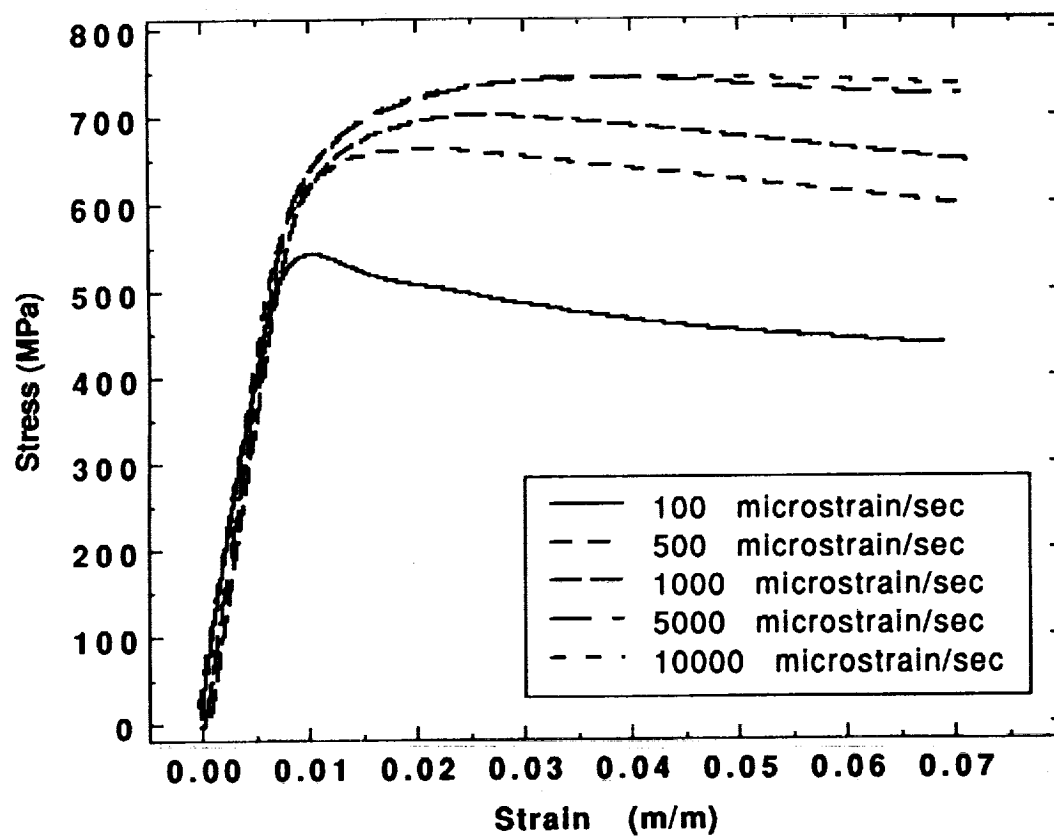
Figure B1: Data Collected During CSR Tests at 482°C
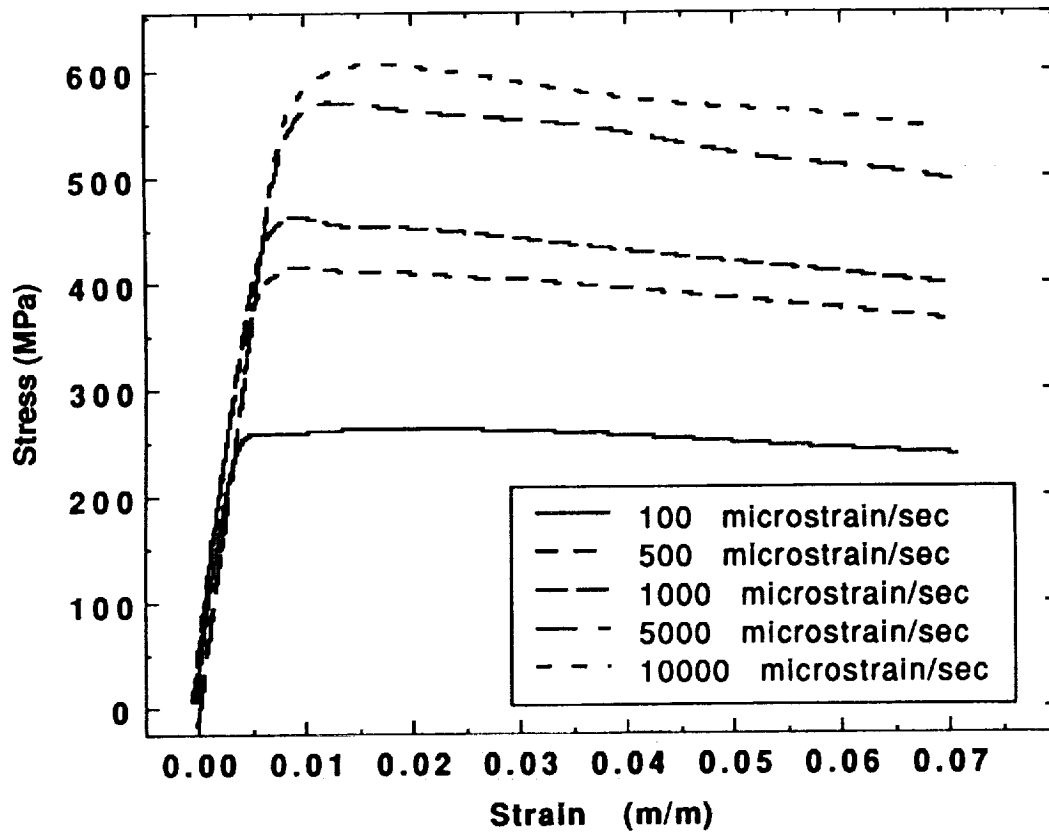
Figure B2: Data Collected During CSR Tests at 566°C
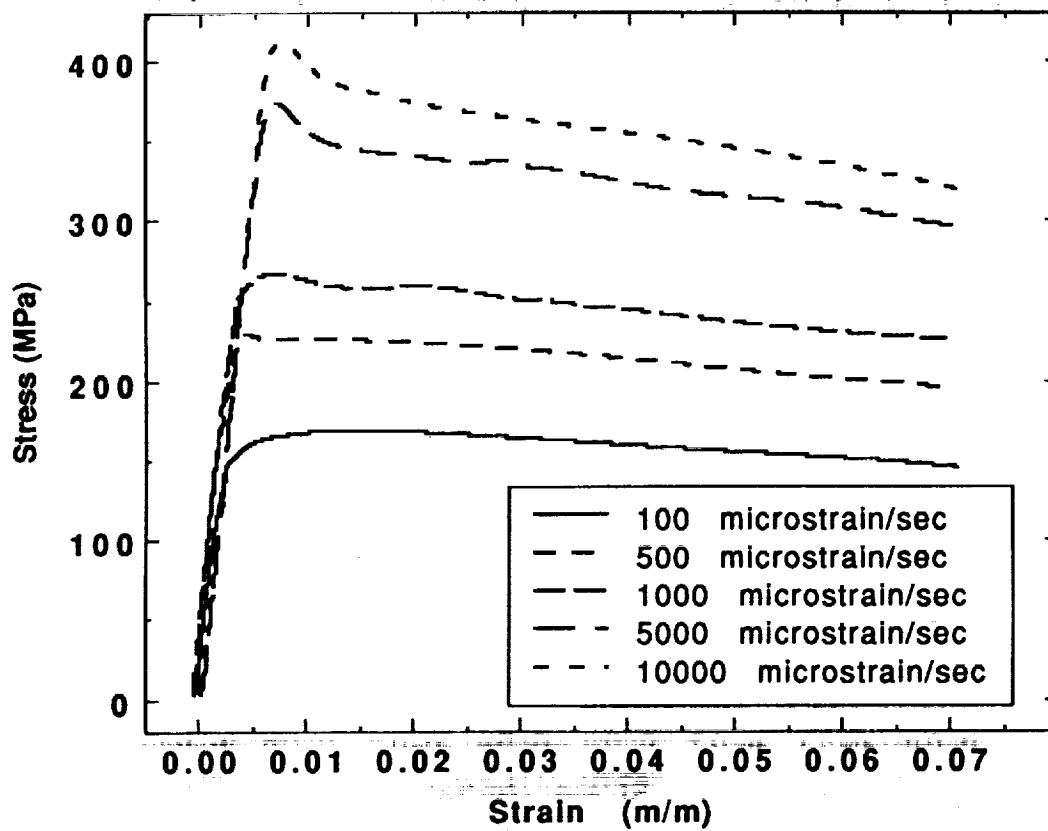
Figure B3: Data Collected During CSR Tests at 649°C
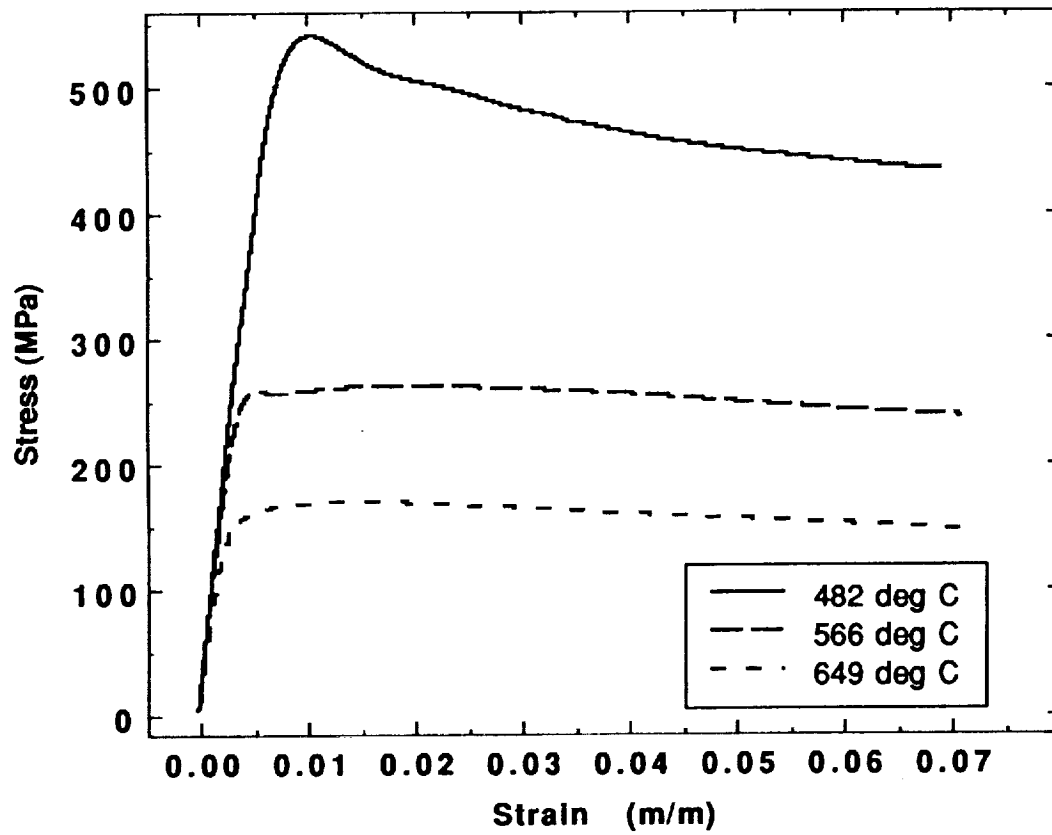
Figure B4: Data Collected During CSR Tests at 100 μm/m/sec
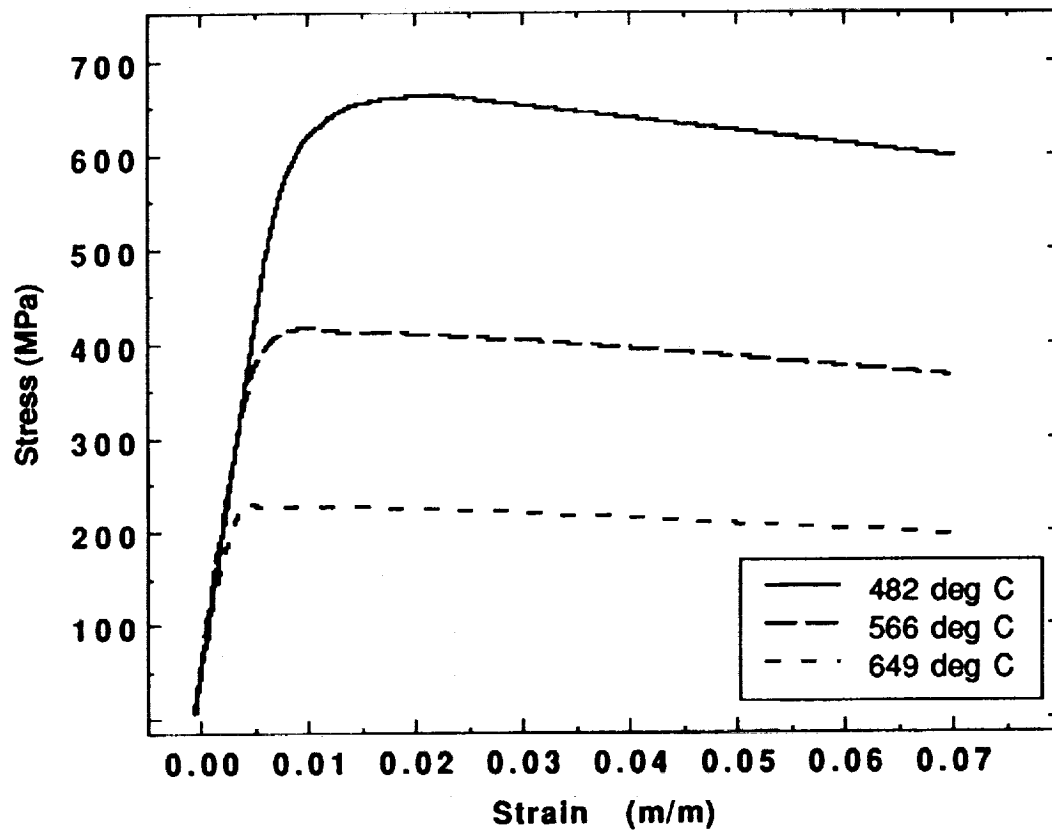
Figure B5: Data Collected During CSR Tests at 500 μm/m/sec
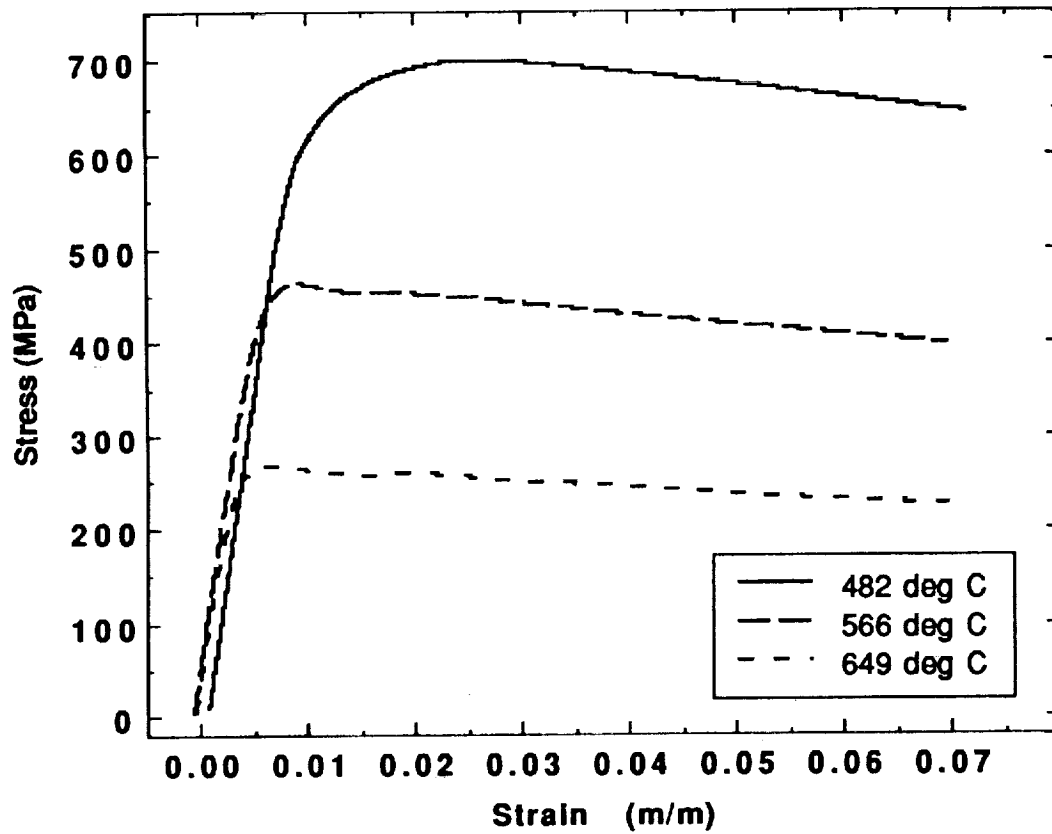
Figure B6: Data Collected During CSR Tests at 1,000 μm/m/sec
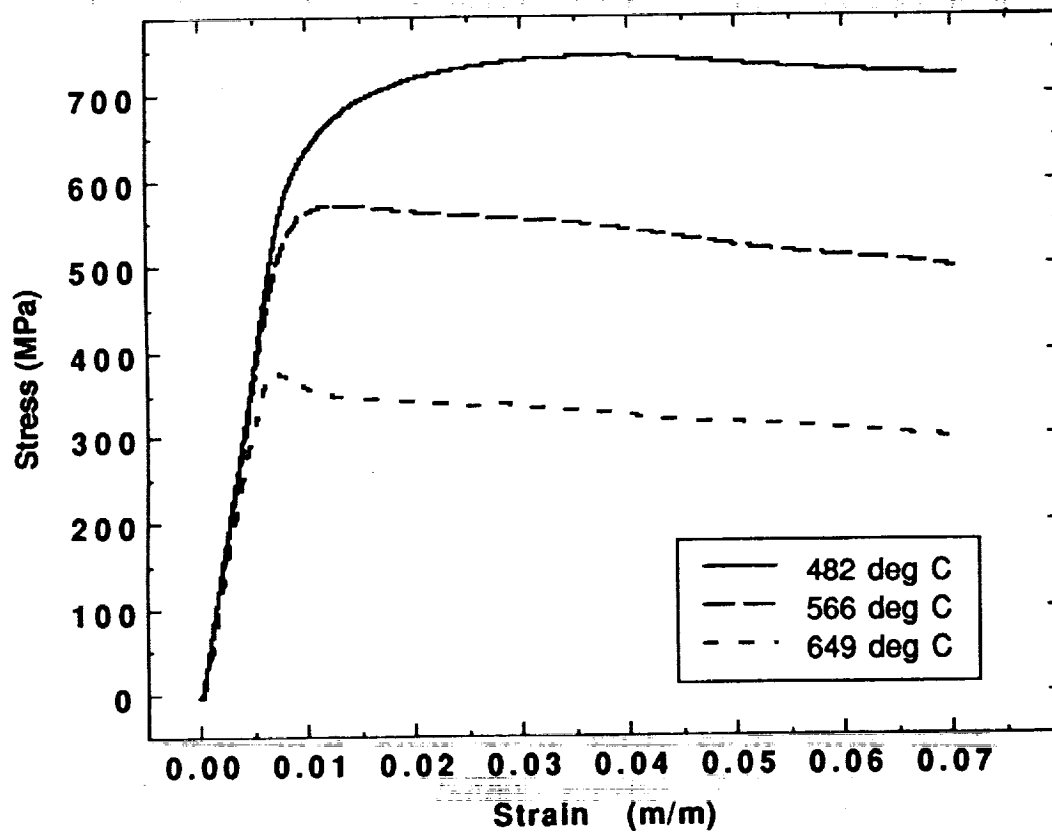
Figure B7: Data Collected During CSR Tests at 5,000 μm/m/sec
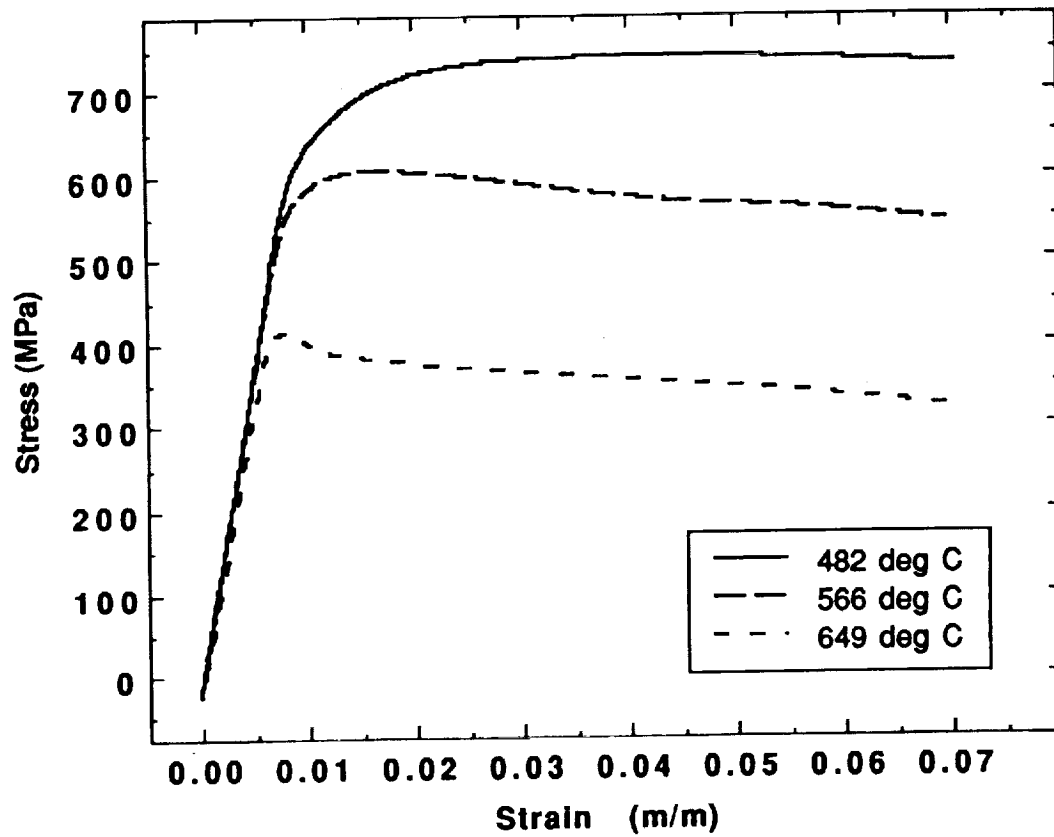
Figure B8: Data Collected During CSR Tests at 10,000 µm/m/sec

APPENDIX C

PLOTS OF DATA COLLECTED DURING CYCLIC CONSTANT STRAIN RATE TESTS
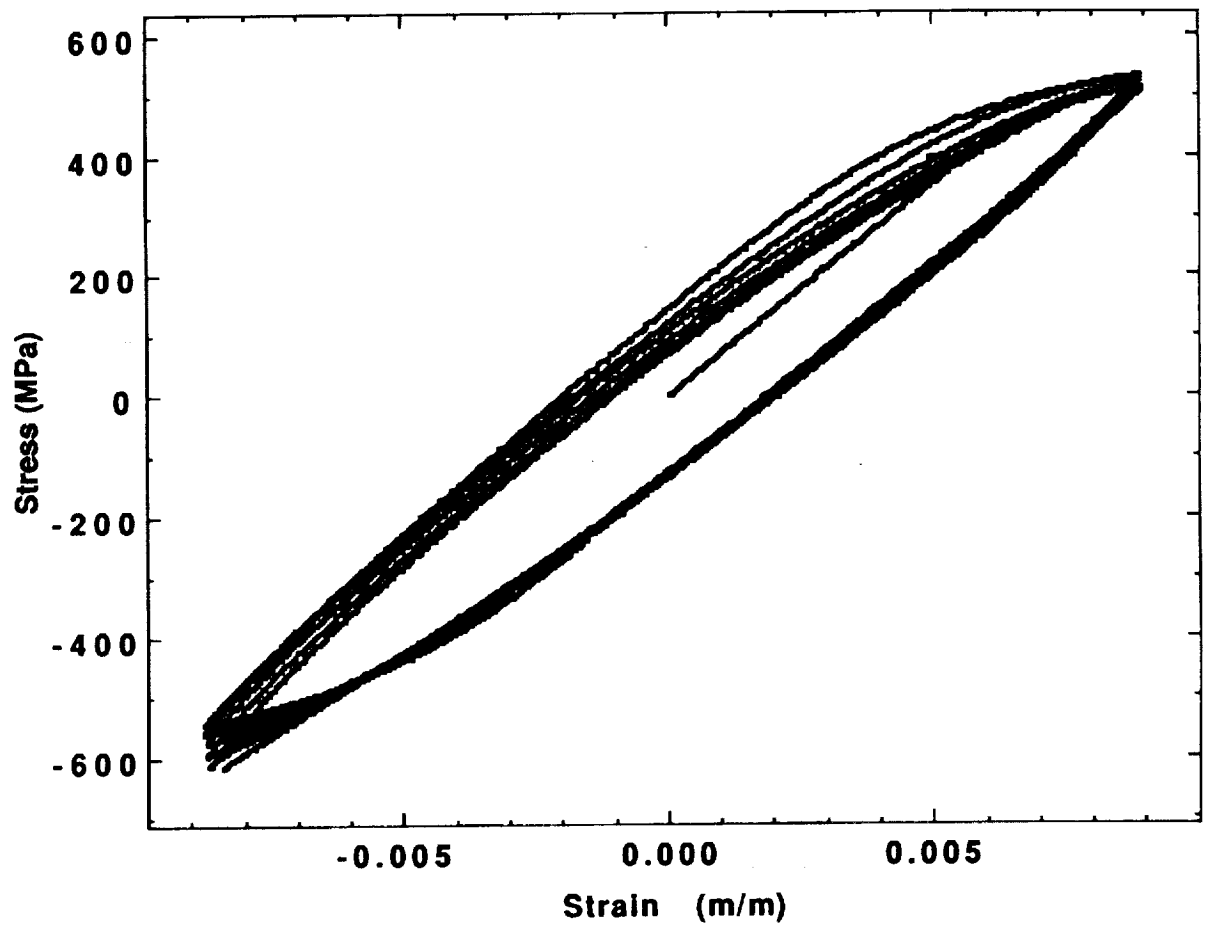
Figure C1: Data Collected During CCSR Test at 482°C and 100 μm/m/sec
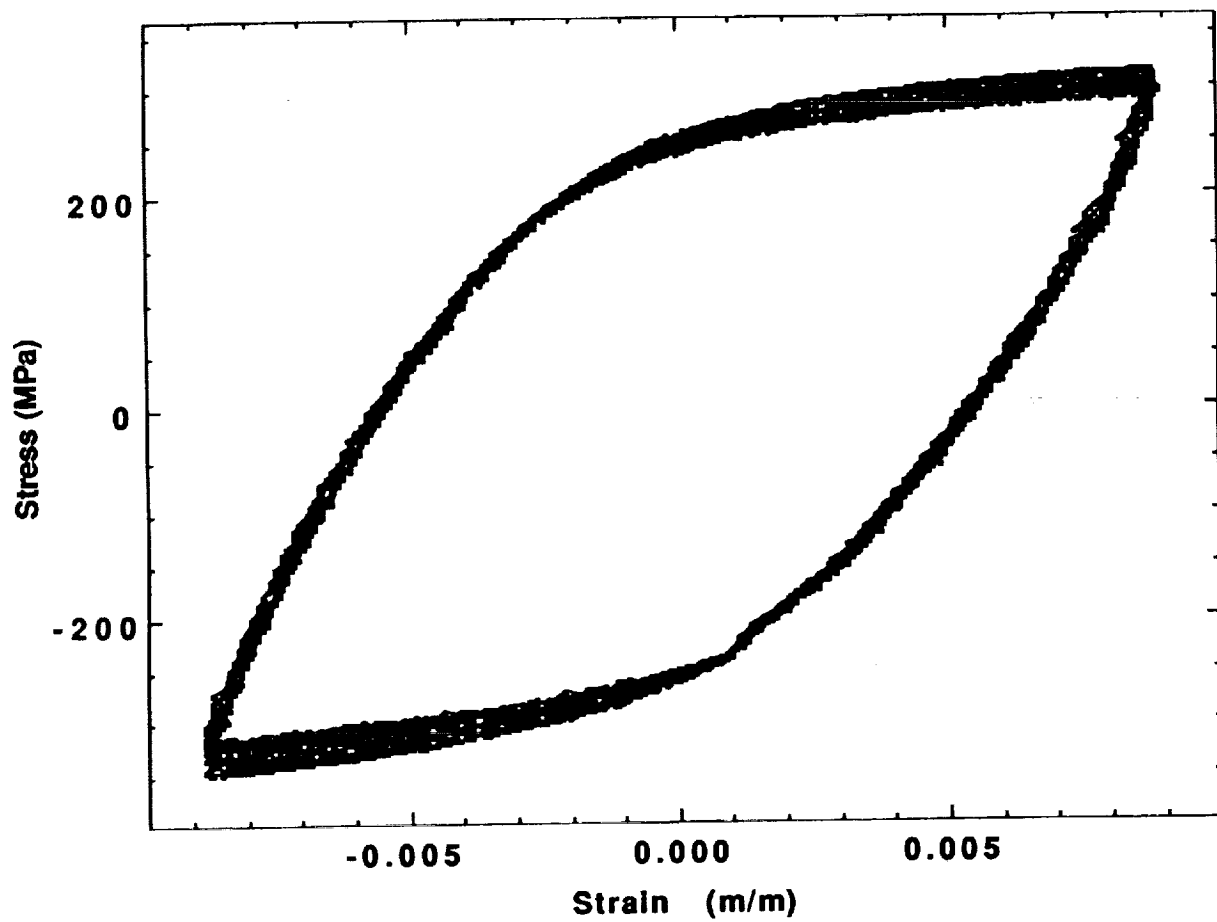
Figure C2: Data Collected During CCSR Test at 566°C and 100 µm/m/sec
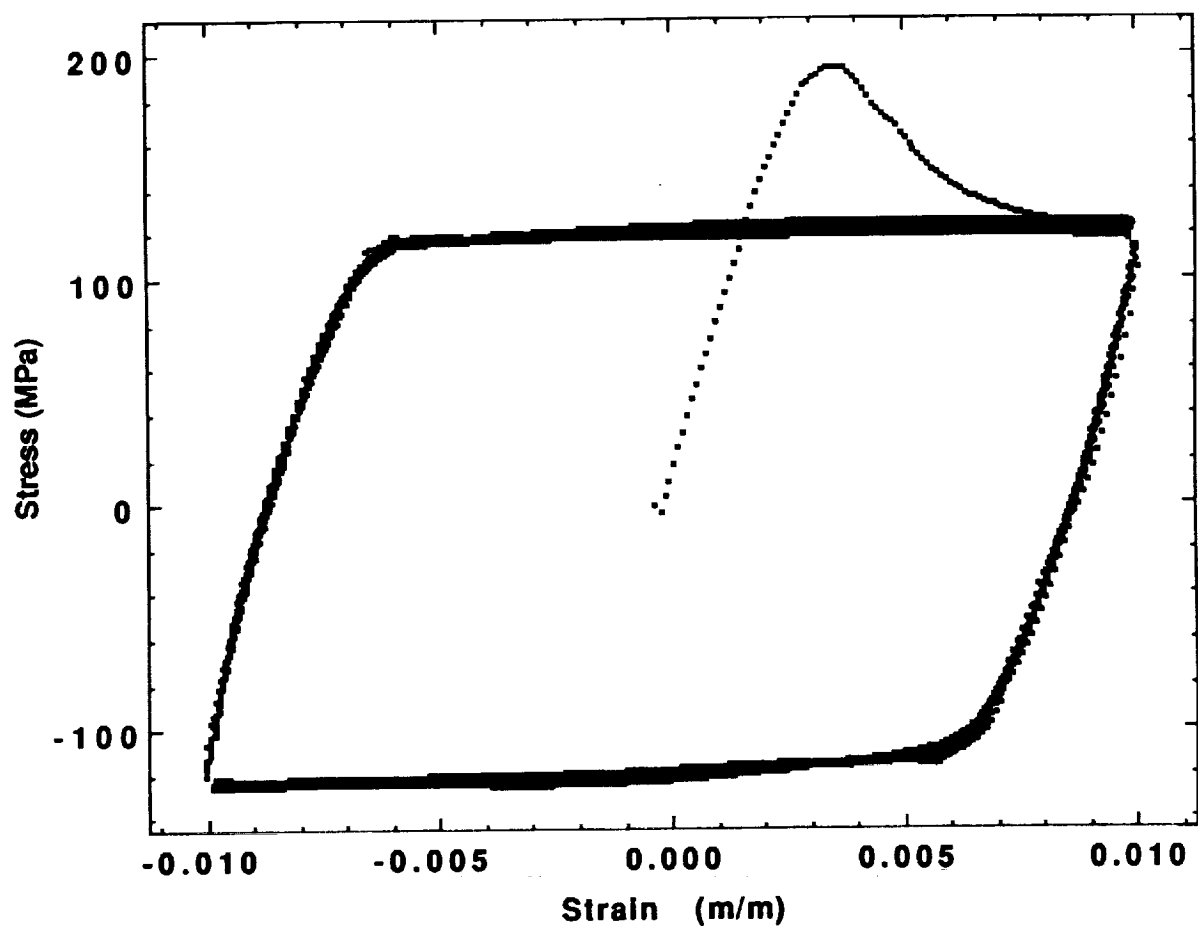
Figure C3: Data Collected During CCSR Test at 649°C and 100 µm/m/sec
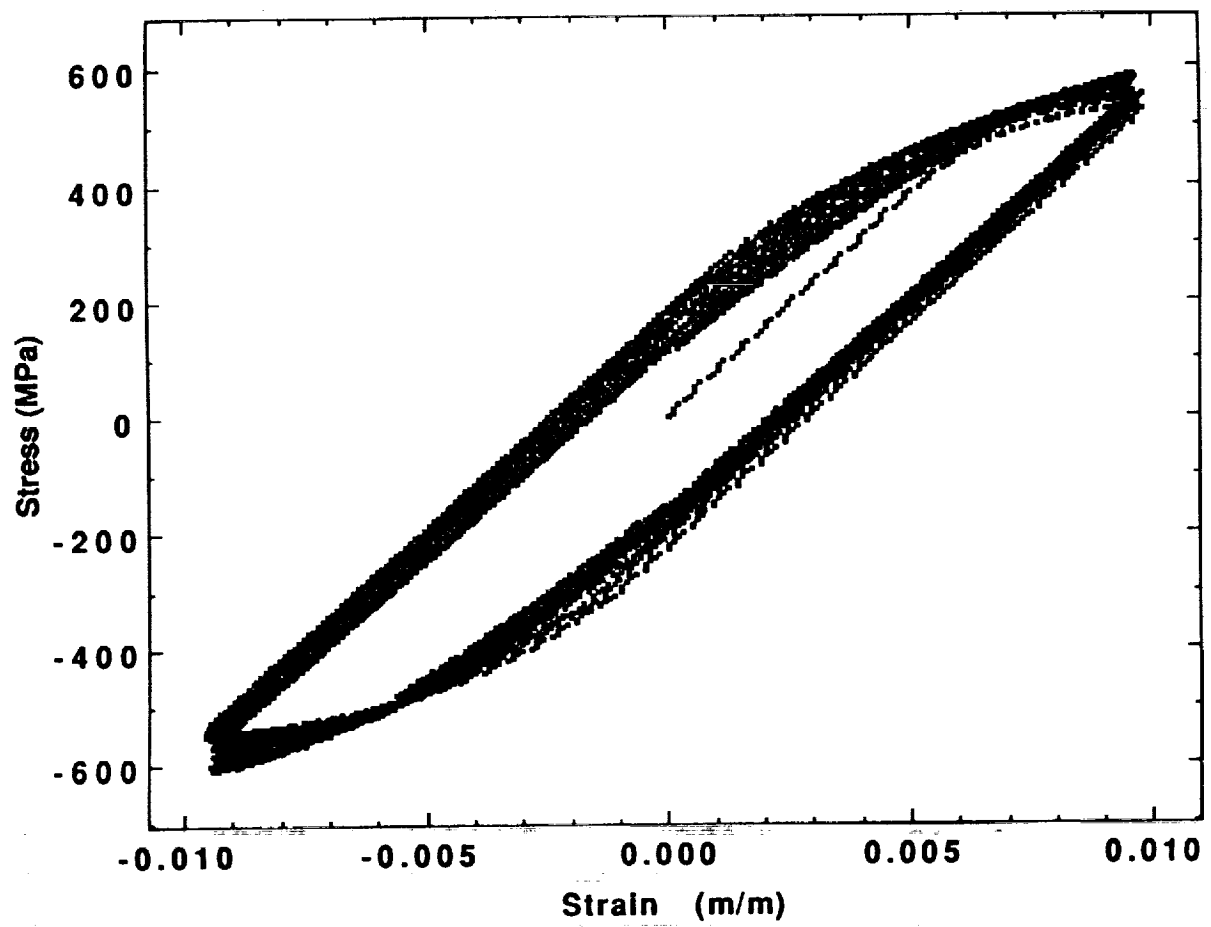
Figure C4: Data Collected During CCSR Test at 482°C and 500 μm/m/sec

76
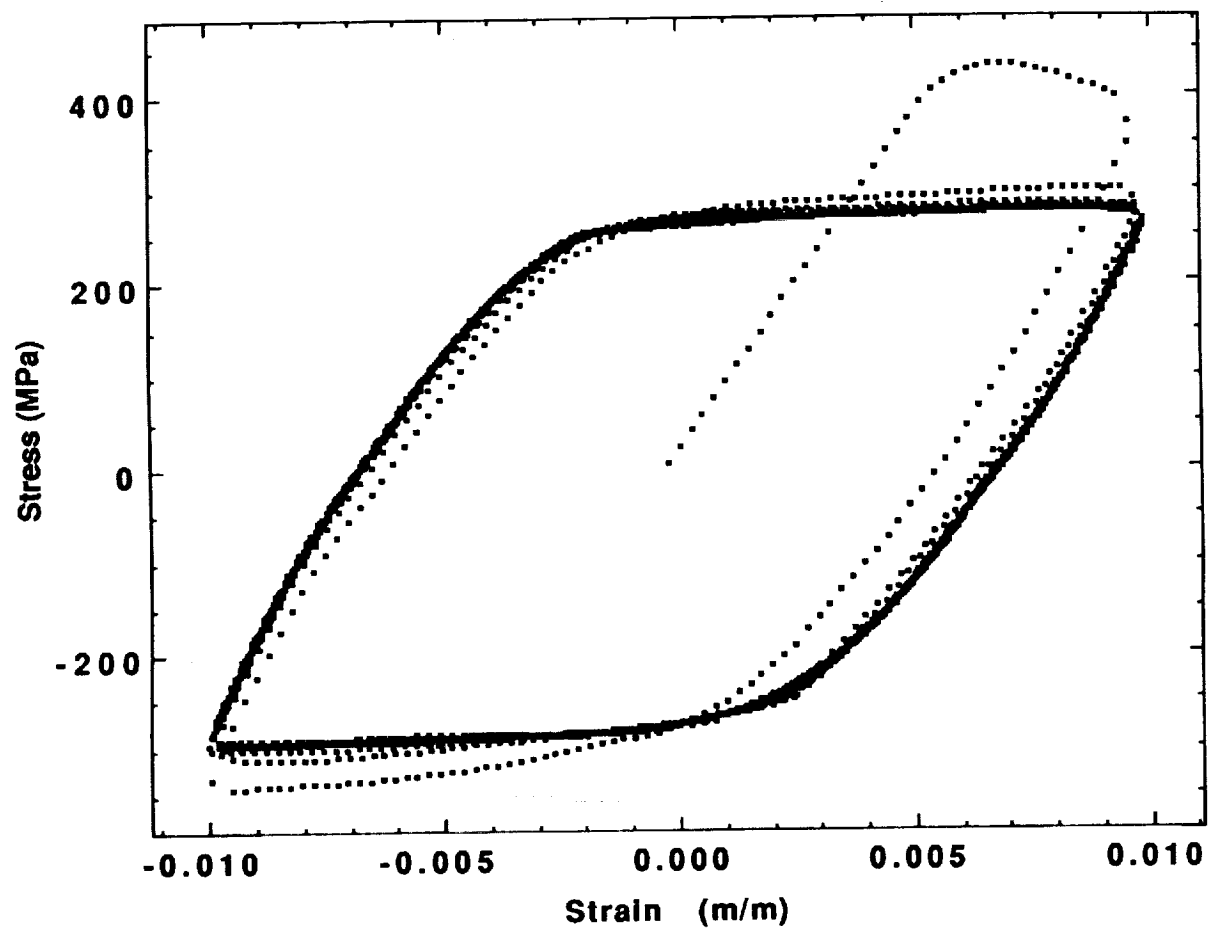
Figure C5: Data Collected During CCSR Test at 566°C and 500 μm/m/sec
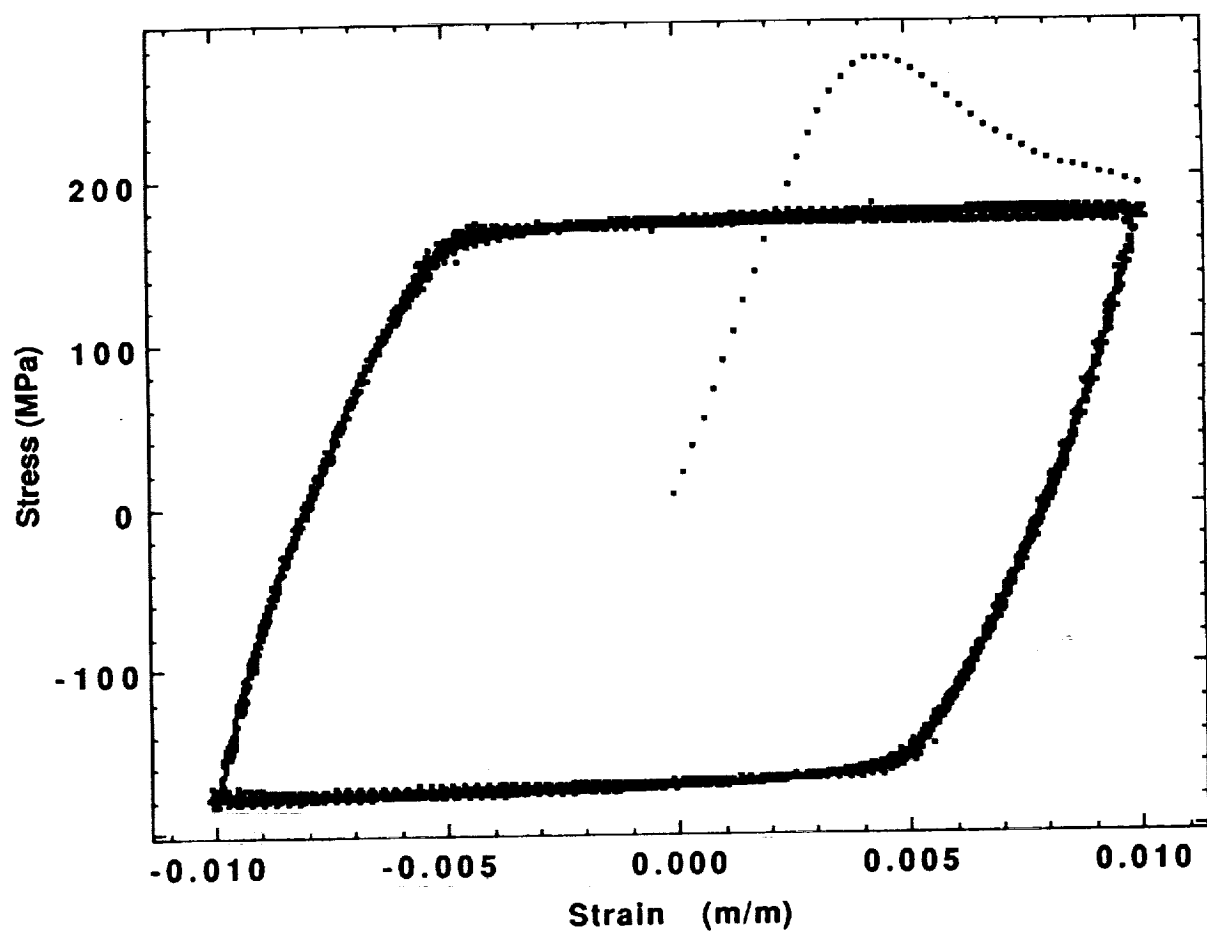
Figure C6: Data Collected During CCSR Test at 649°C and 500 μm/m/sec
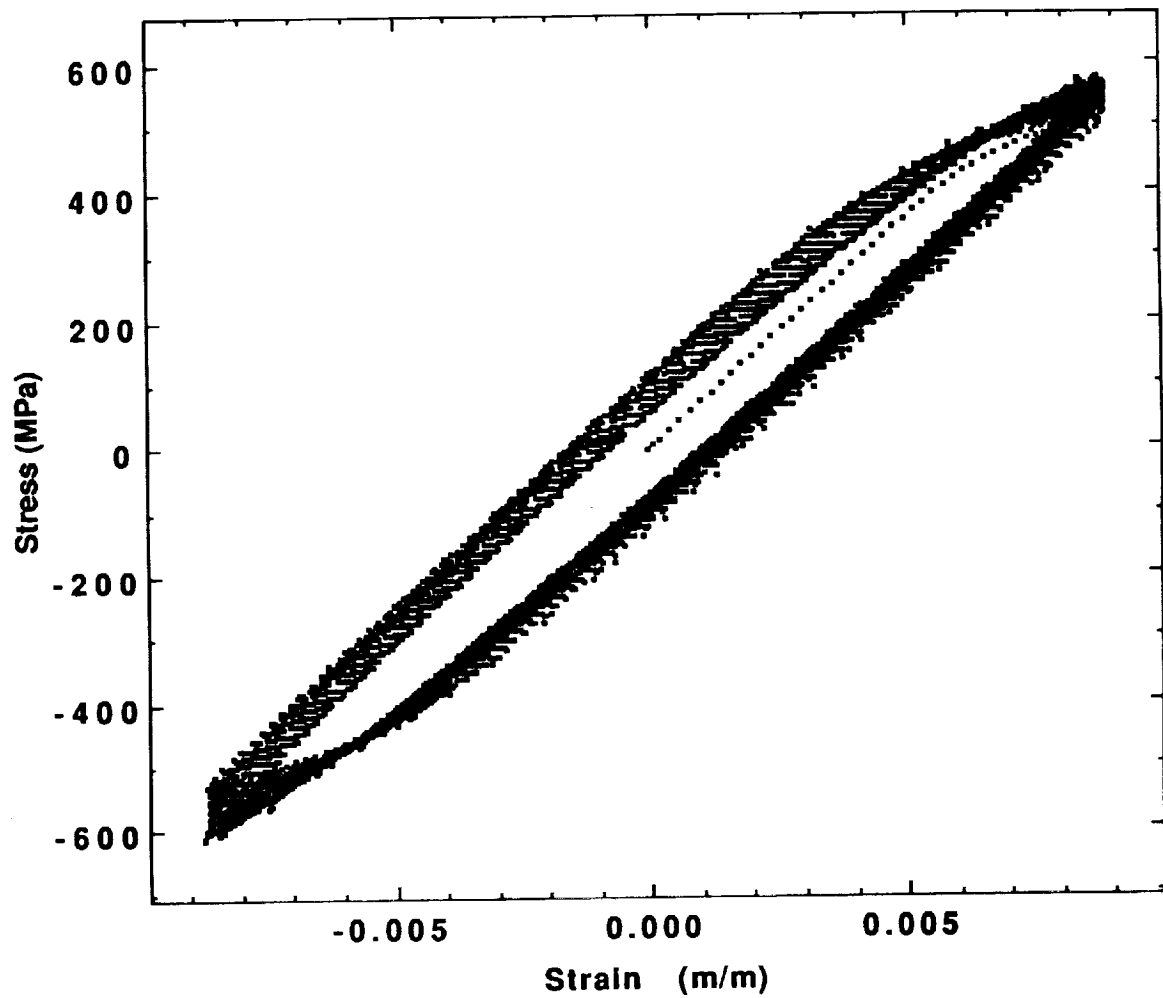
Figure C7a: Data Collected During Modified CCSR Test at 482°C and 1000 µm/m/sec; CCSR Cycle #1
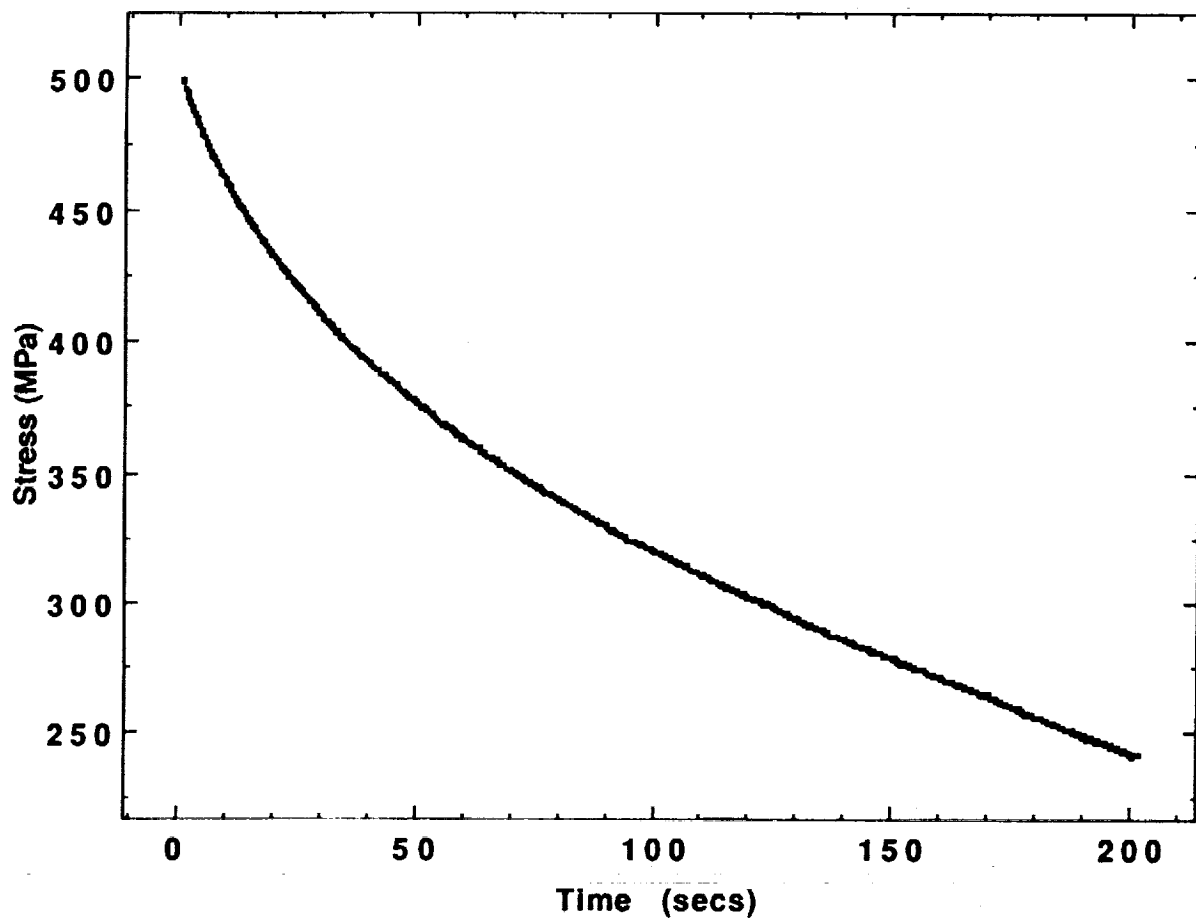
Figure C7b: Data Collected During Modified CCSR Test at 482°C and 1000 μm/m/sec; Stress Relaxation #1, Strain = 0.8%.
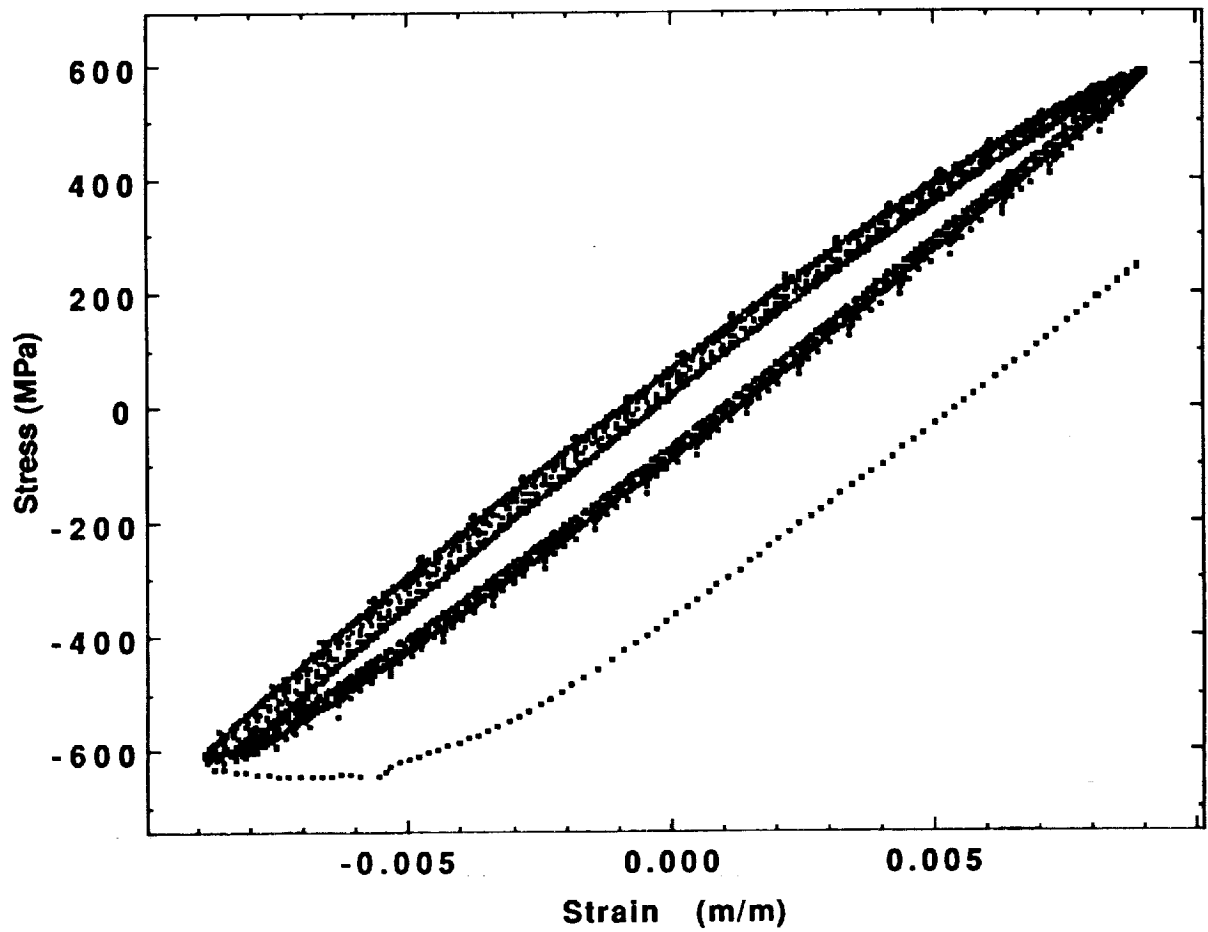
Figure C7c: Data Collected During Modified CCSR Test at 482°C and 1000 μm/m/sec; CCSR Cycle #2
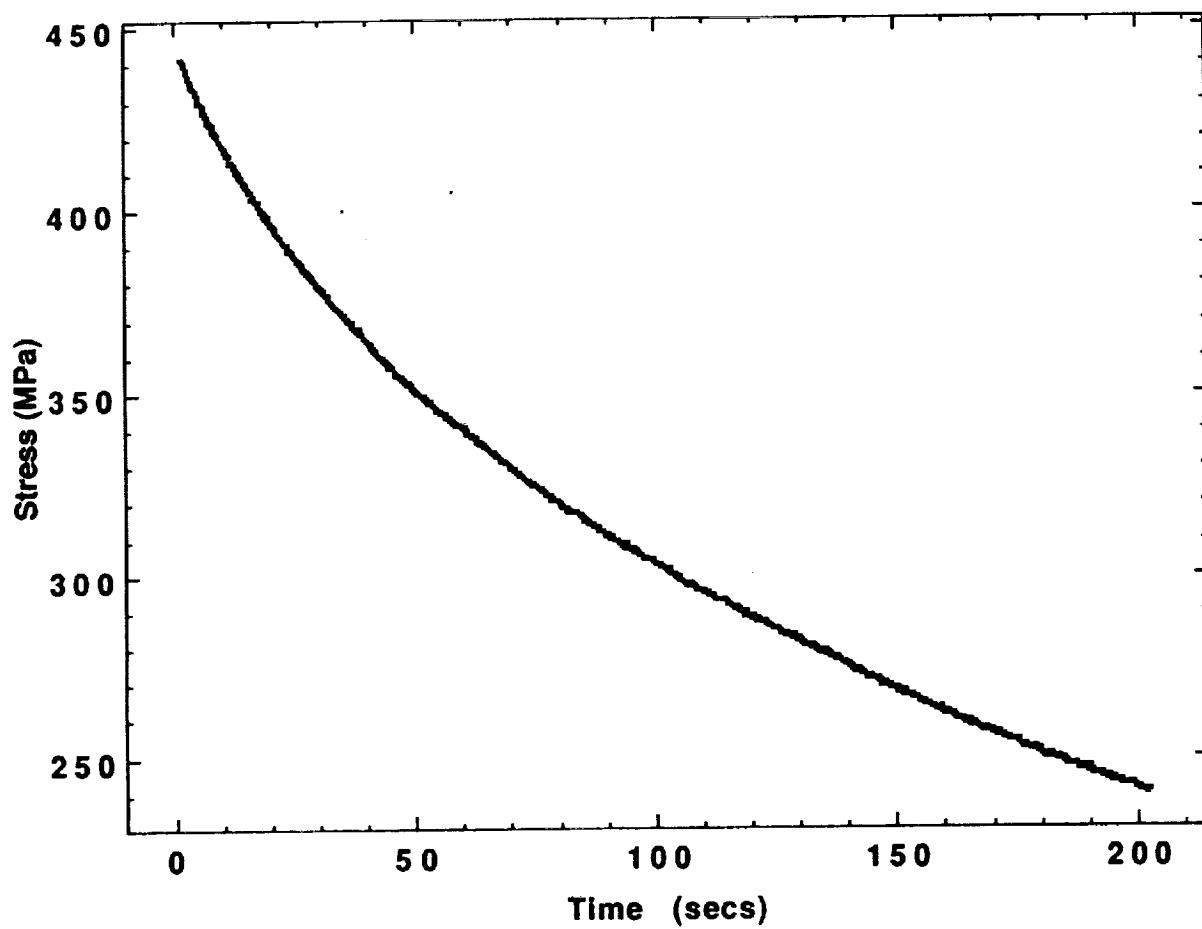
Figure C7d: Data Collected During Modified CCSR Test at 482°C and 1000 µm/m/sec; Stress Relaxation #2, Strain = 0.7%.
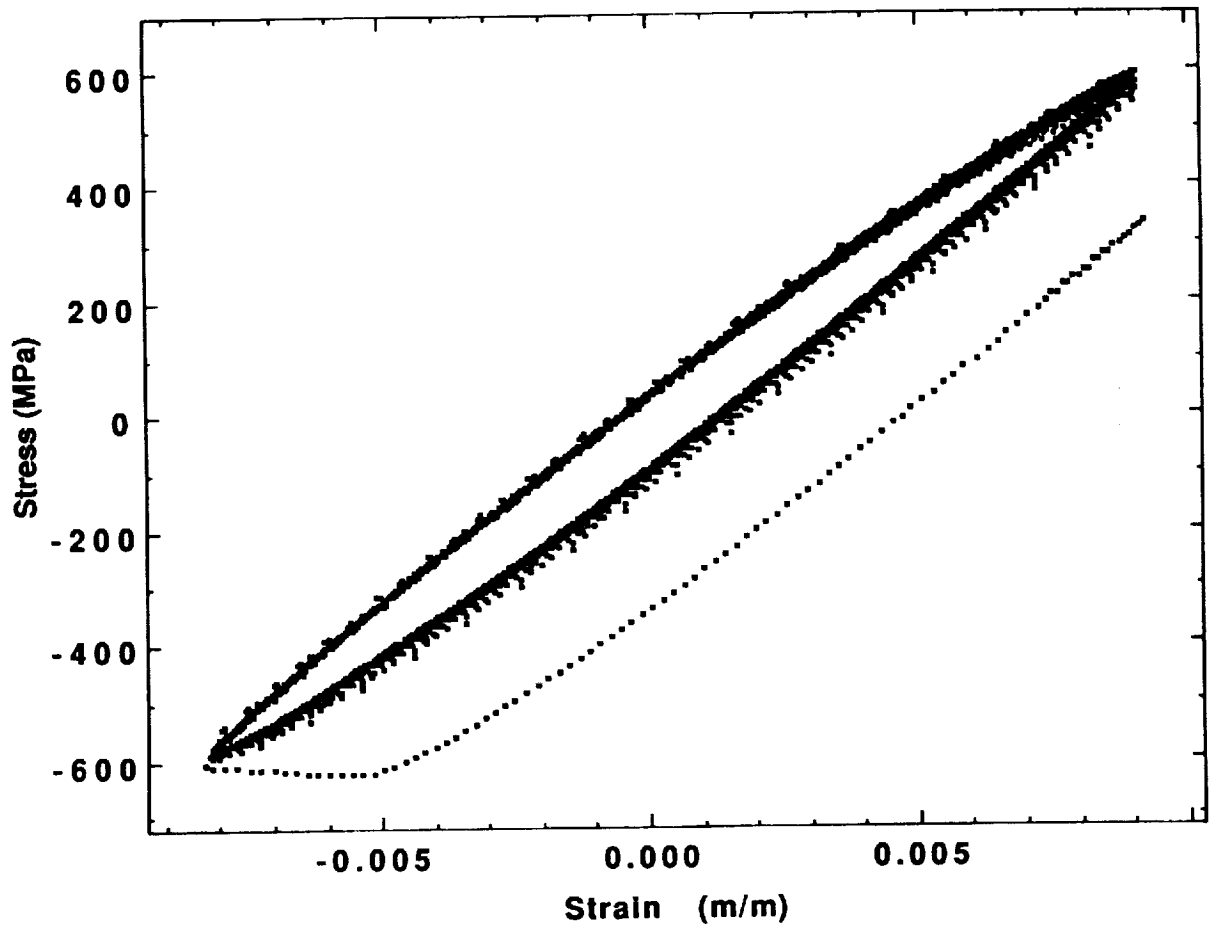
Figure C7e: Data Collected During Modified CCSR Test at 482°C and 1000 µm/m/sec; CCSR Cycle #3
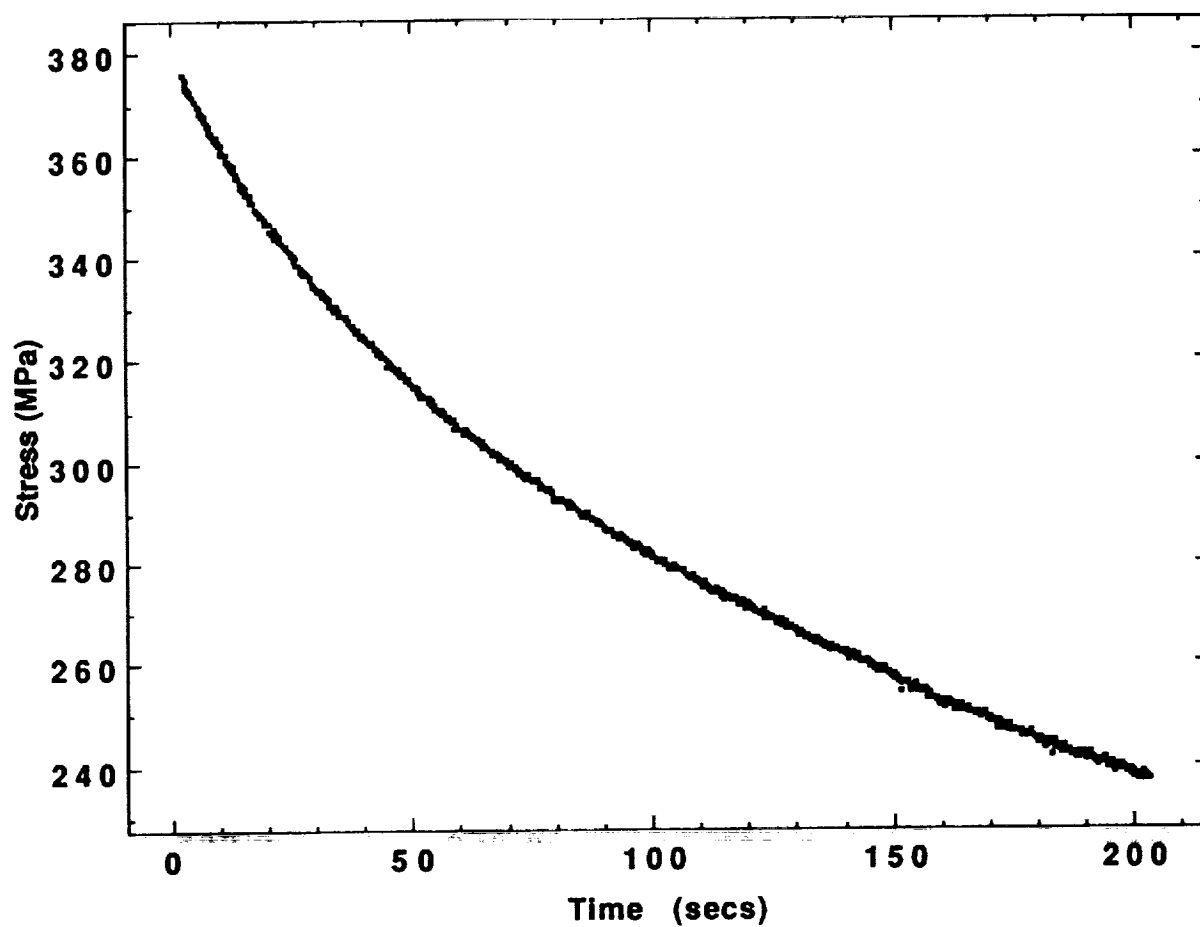
Figure C7f: Data Collected During Modified CCSR Test at 482°C and 1000 μm/m/sec; Stress Relaxation #3, Strain = 0.6%.
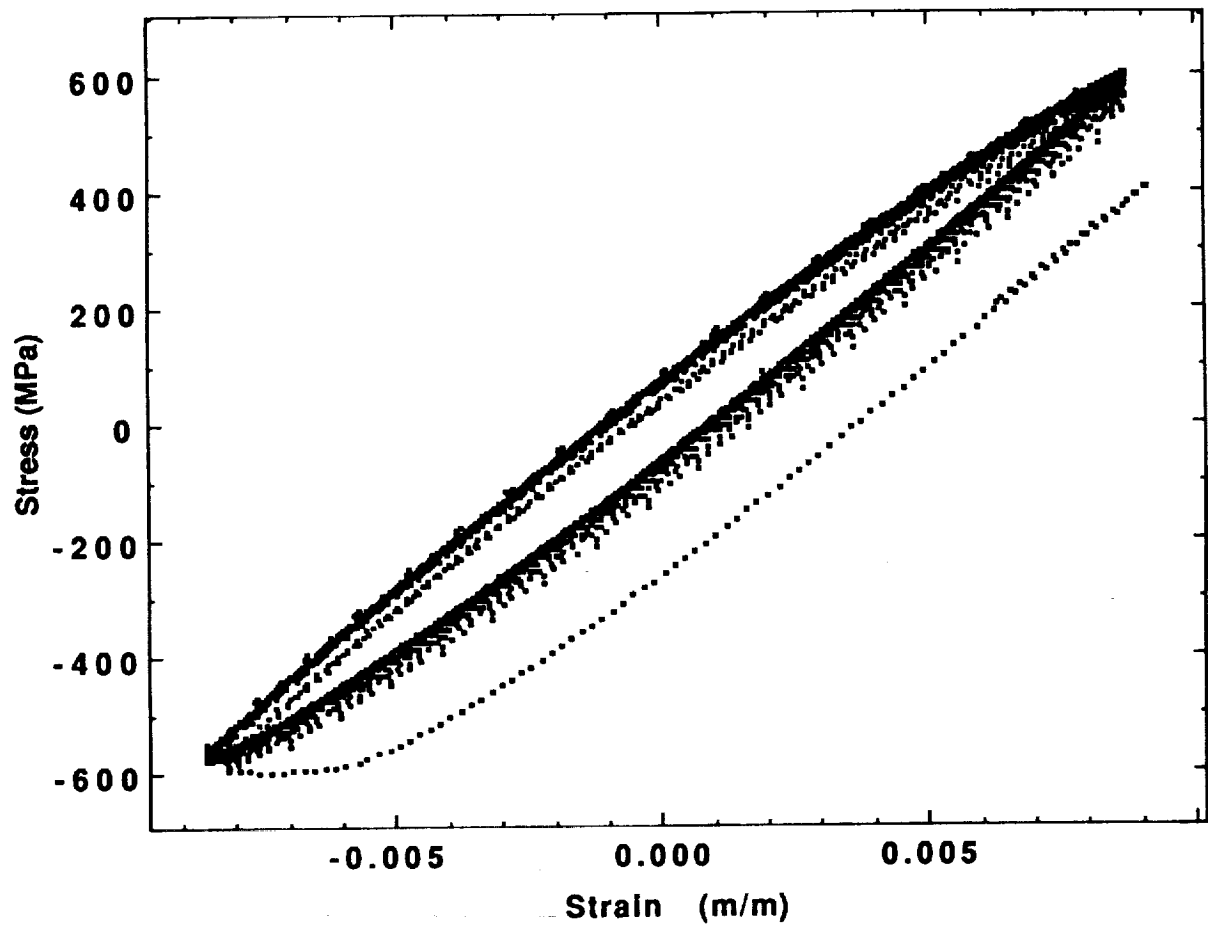
Figure C7g: Data Collected During Modified CCSR Test at 482°C and 1000 μm/m/sec; CCSR Cycle #4
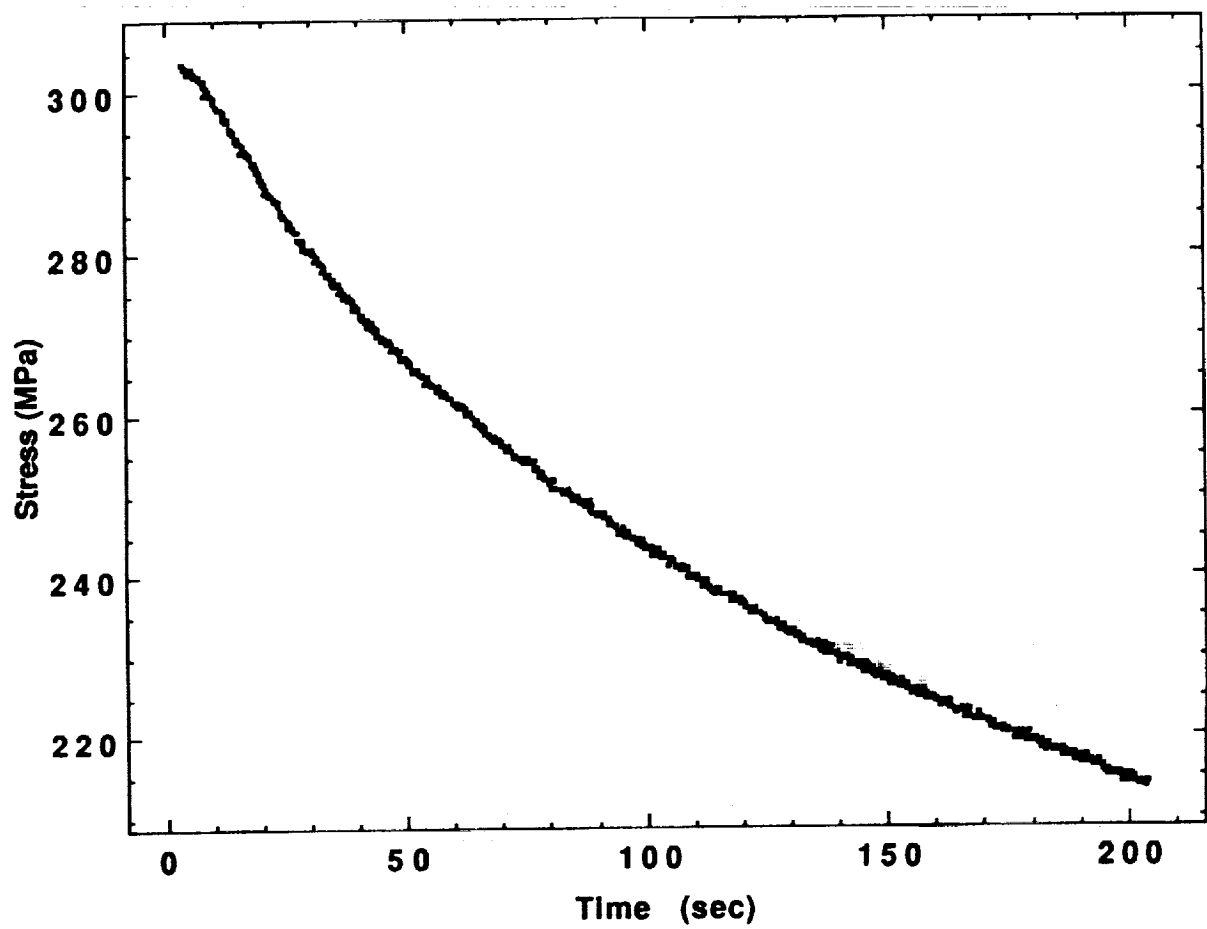
Figure C7h: Data Collected During Modified CCSR Test at 482°C and 1000 μm/m/sec; Stress Relaxation #4, Strain = 0.5%.
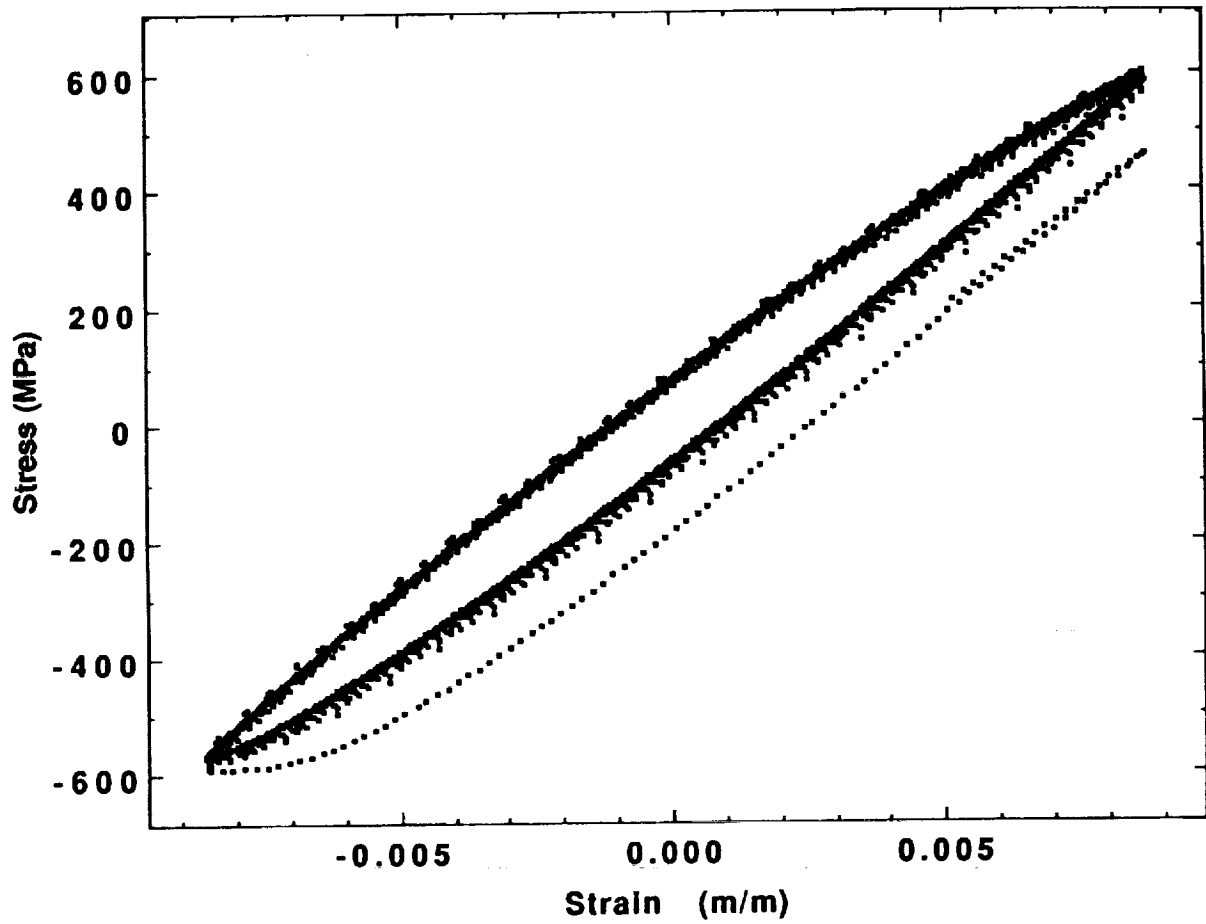
Figure C7i: Data Collected During Modified CCSR Test at 482°C and 1000 μm/m/sec; CCSR Cycle #5
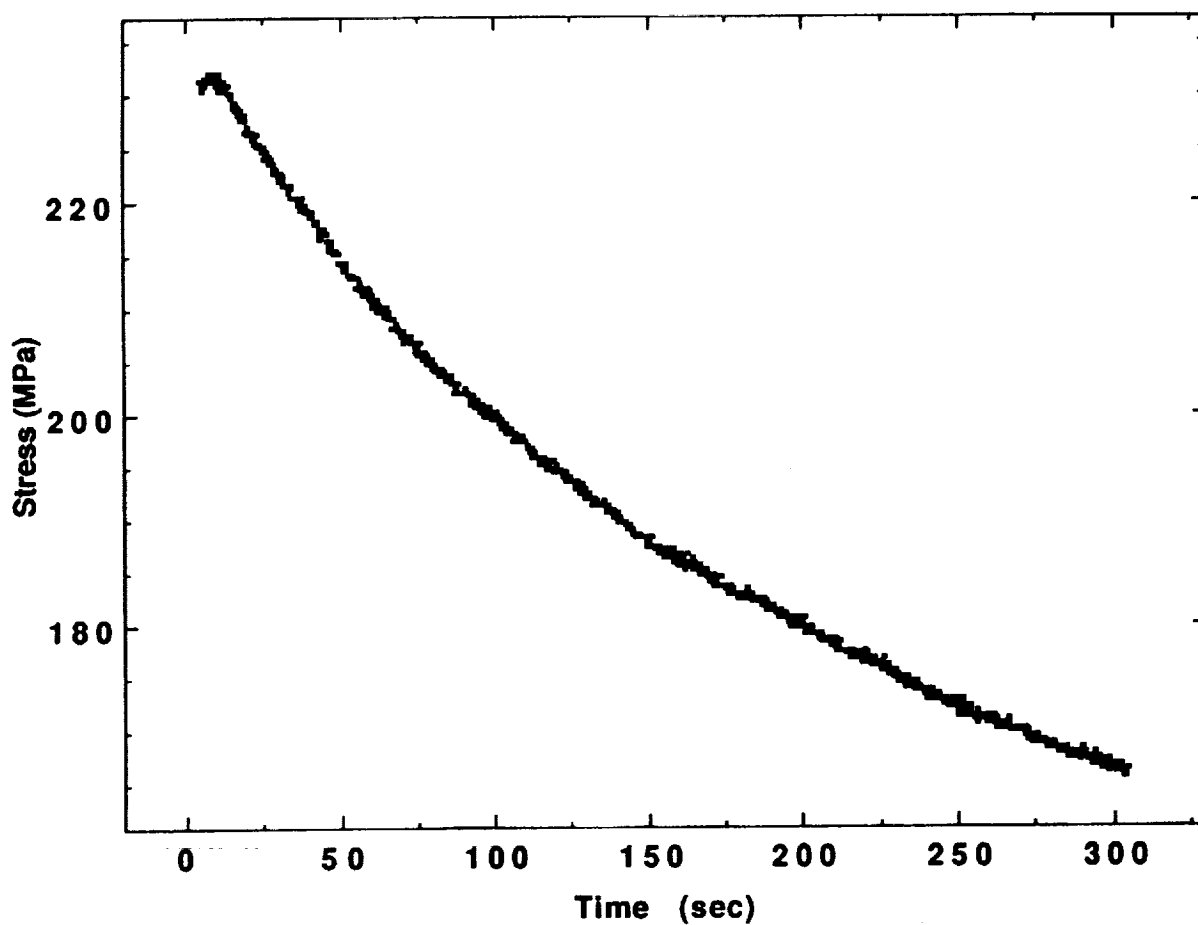
Figure C7j: Data Collected During Modified CCSR Test at 482°C and 1000 µm/m/sec; Stress Relaxation #5, Strain = 0.4%.
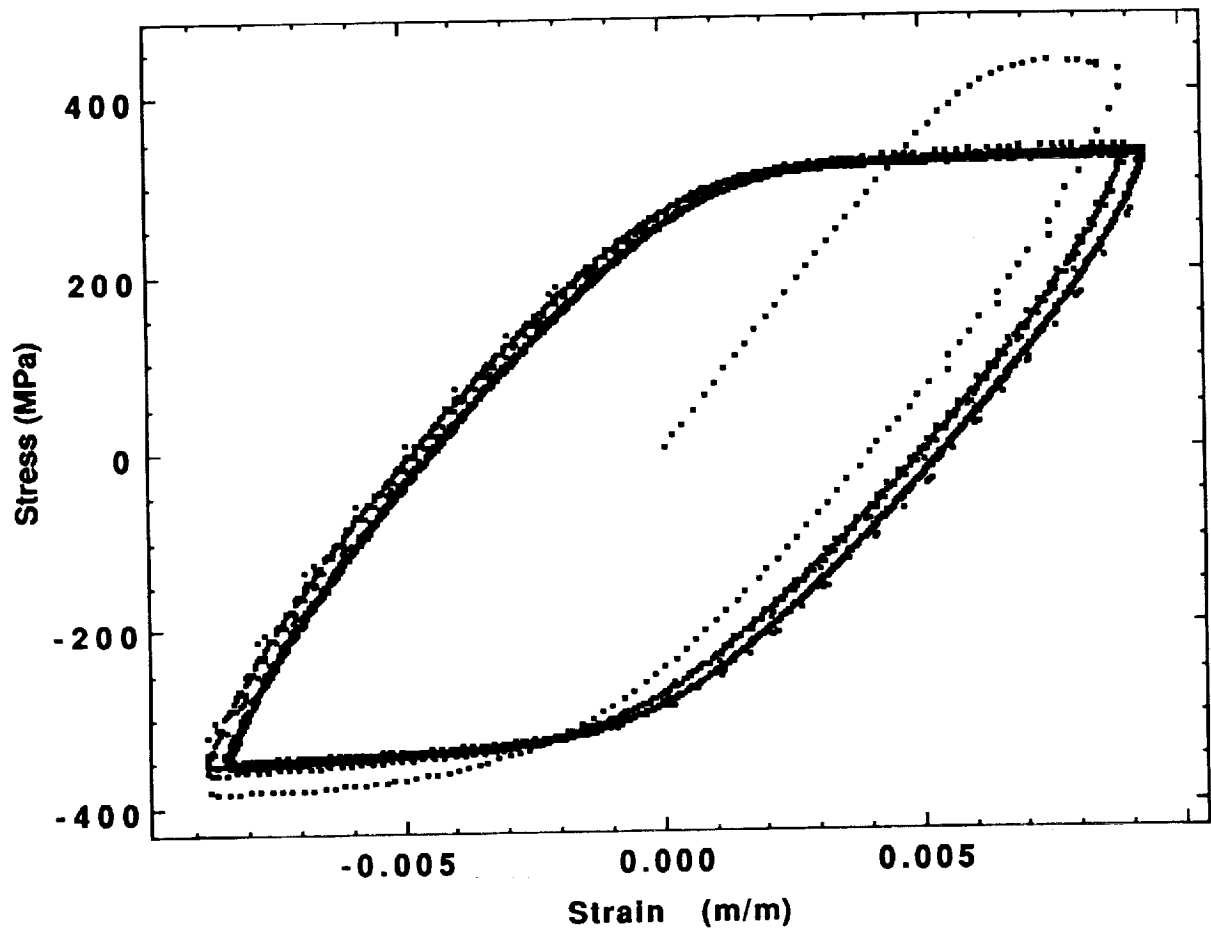
Figure C8a: Data Collected During Modified CCSR Test at 566°C and 1000 μm/m/sec; CCSR Cycle #1 (Note: Data During Cycle #3 Was Lost; Data Plotted Was Obtained During Cycles 1-2 and 4-30)
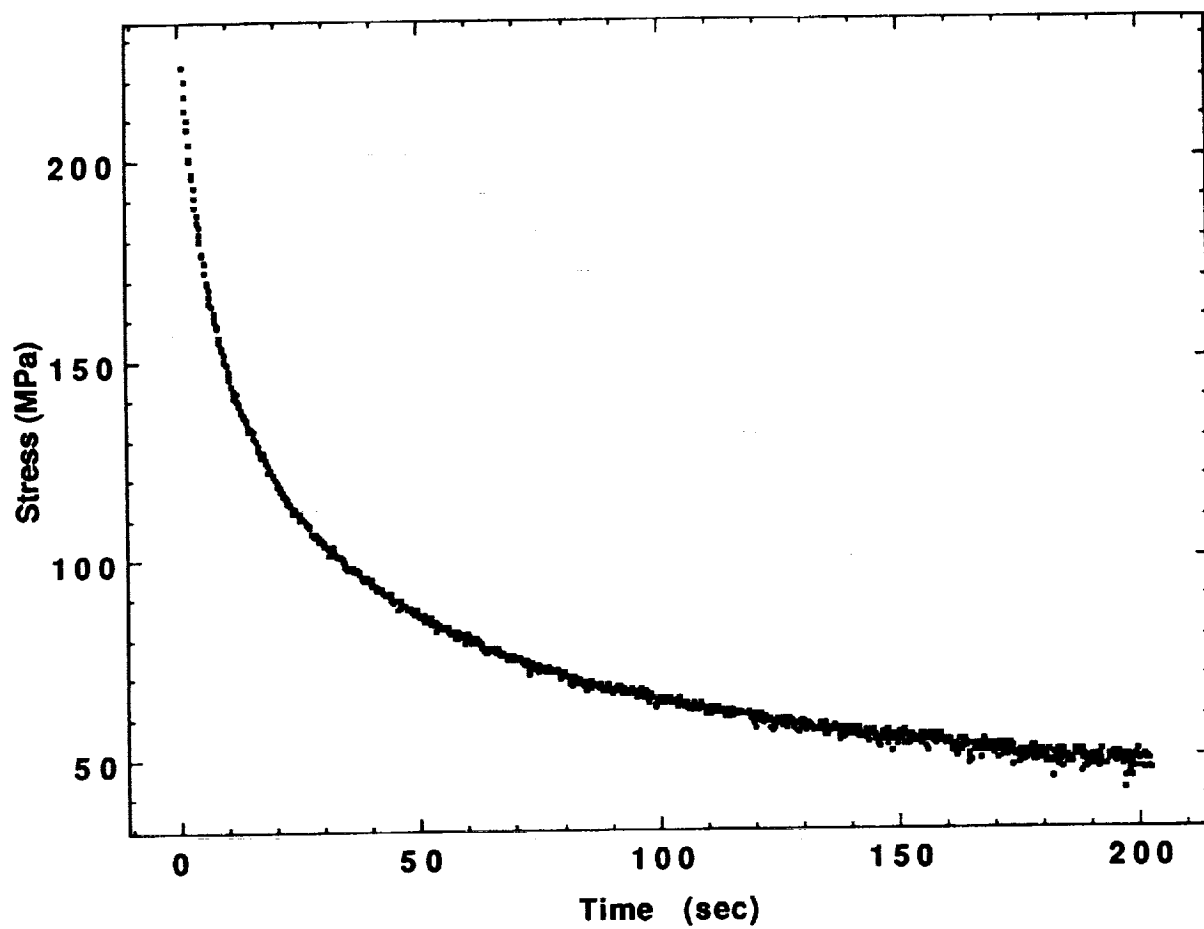
Figure C8b: Data Collected During Modified CCSR Test at 566°C and 1000
μm/m/sec; Stress Relaxation #1, Strain = 0.8%.
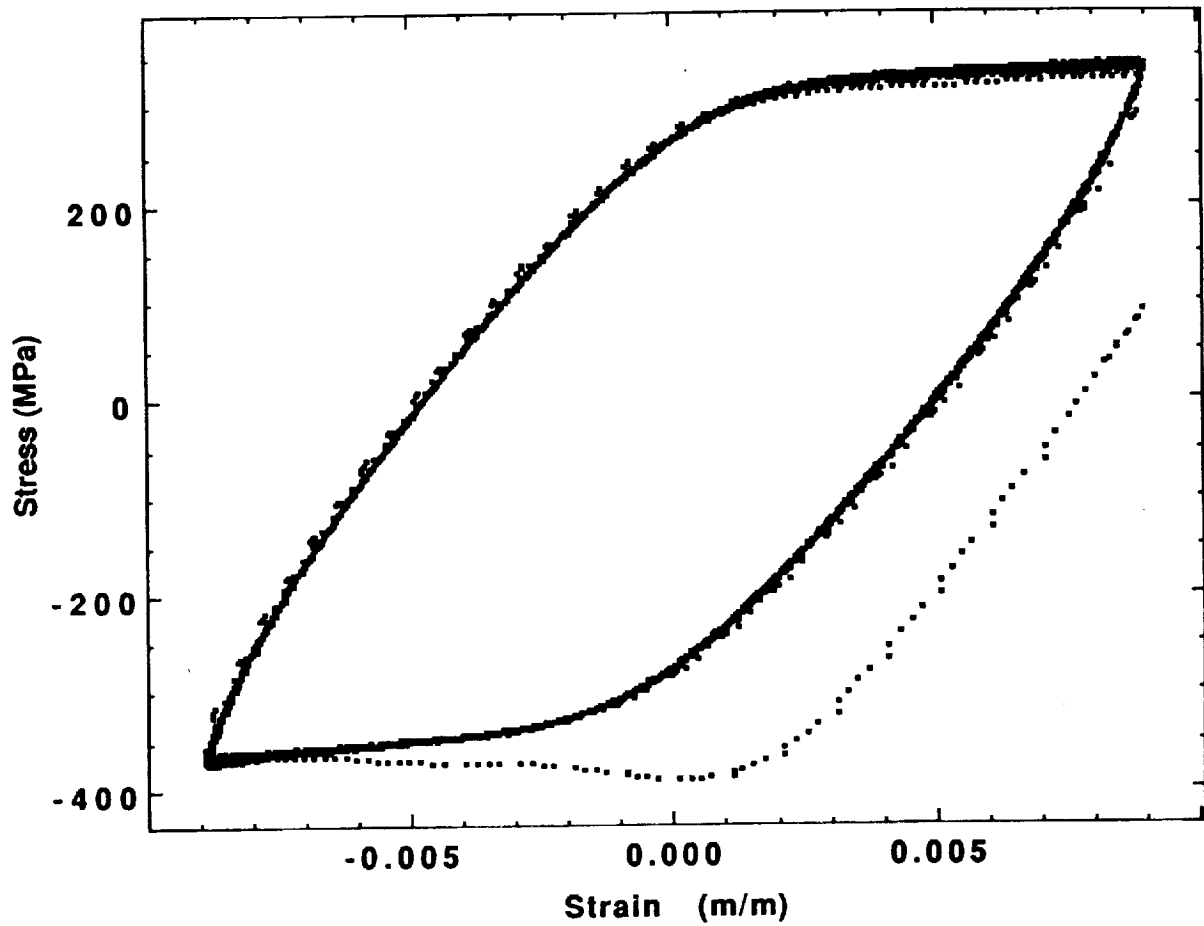
Figure C8c: Data Collected During Modified CCSR Test at 566°C and 1000 μm/m/sec; CCSR Cycle #2
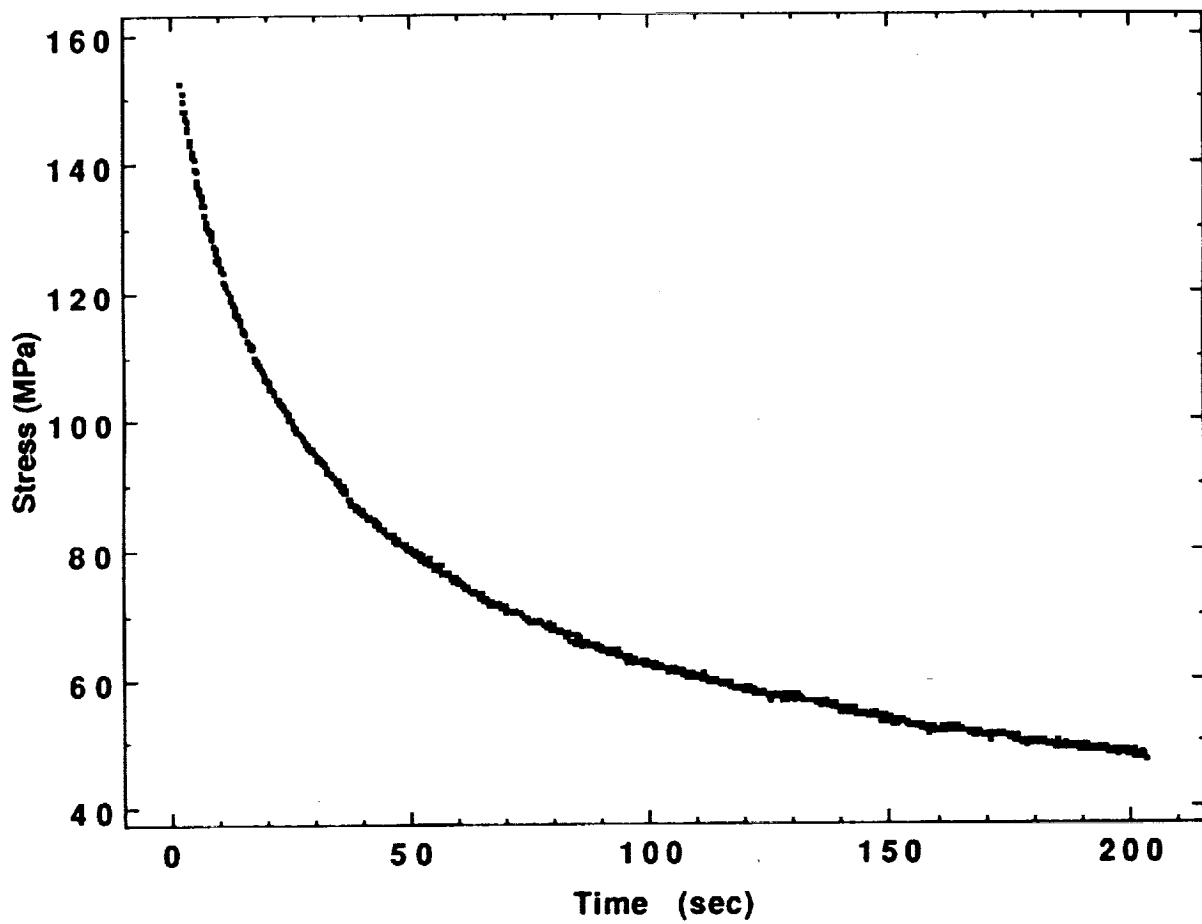
Figure C8d: Data Collected During Modified CCSR Test at 566°C and 1000 µm/m/sec; Stress Relaxation #2, Strain = 0.7%.
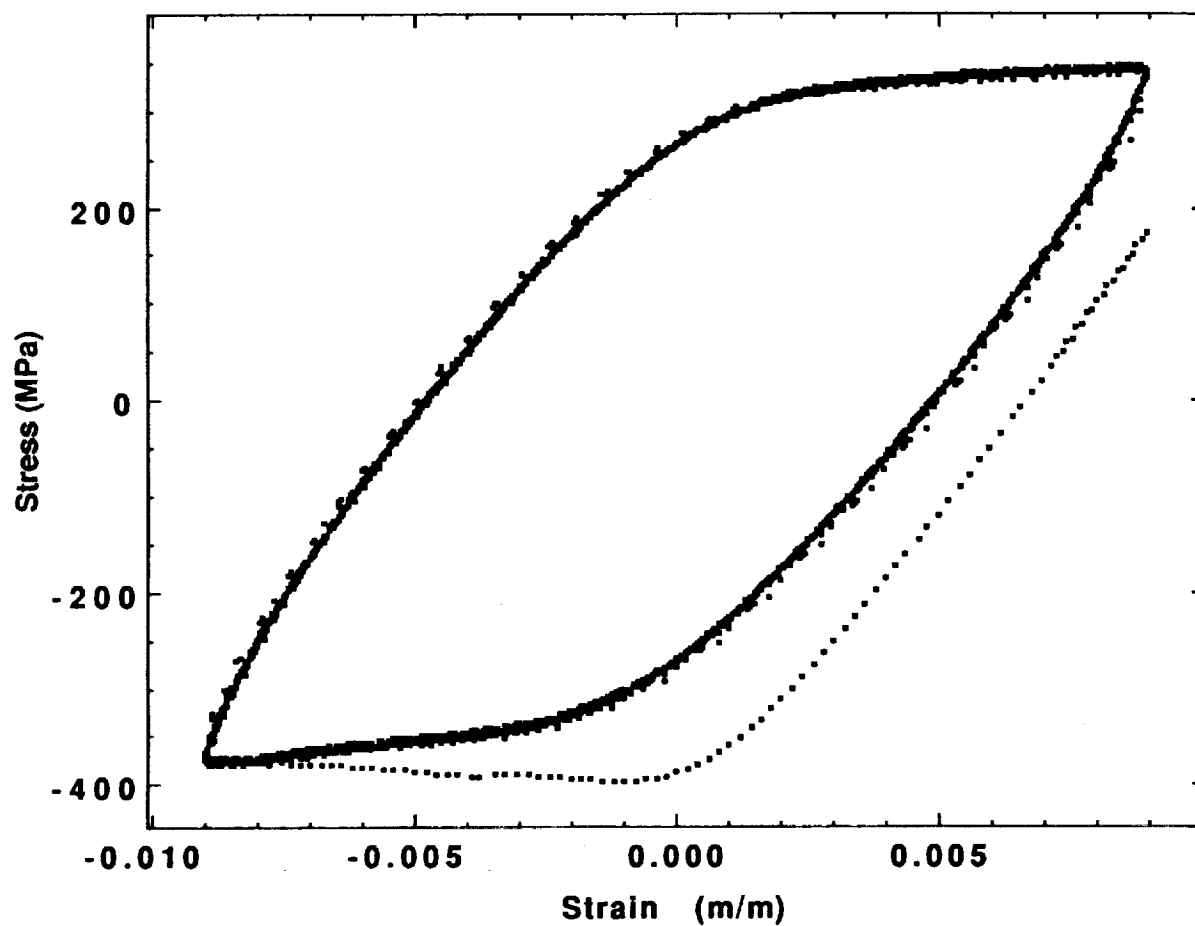
Figure C8e: Data Collected During Modified CCSR Test at 566°C and 1000 μm/m/sec; CCSR Cycle #3
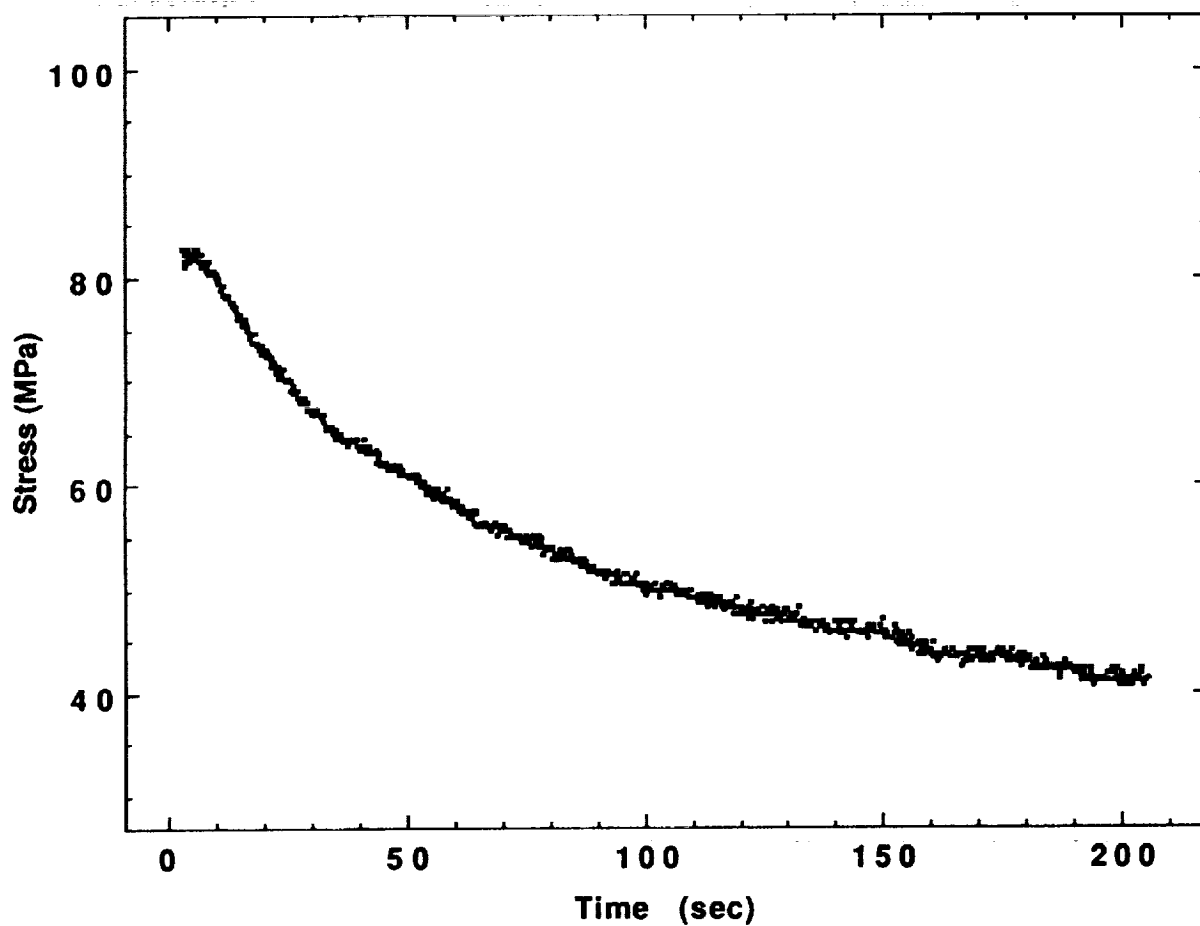
Figure C8f: Data Collected During Modified CCSR Test at 566°C and 1000 μm/m/sec; Stress Relaxation #3, Strain = 0.6%.
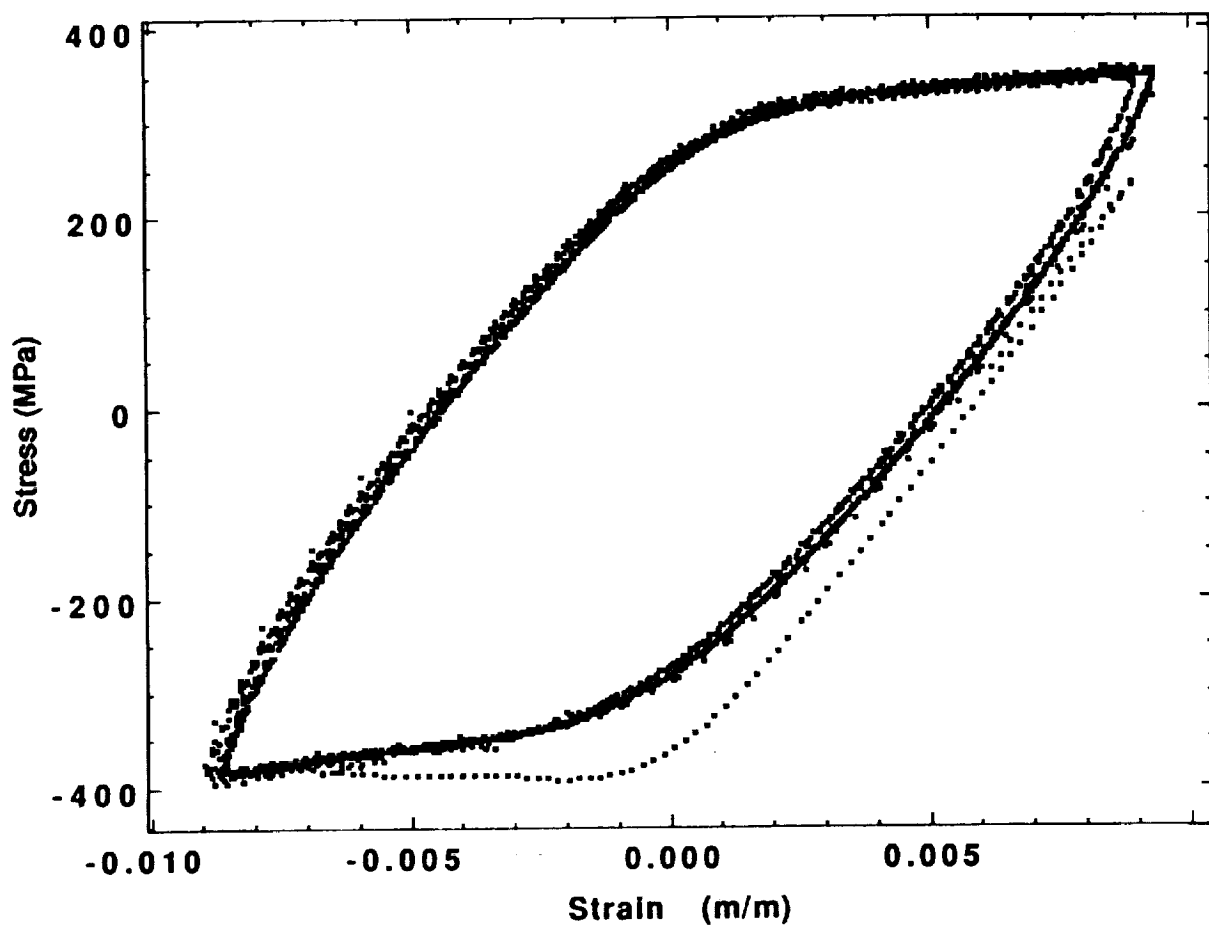
Figure C8g: Data Collected During Modified CCSR Test at 566°C and 1000 μm/m/sec; CCSR Cycle #4
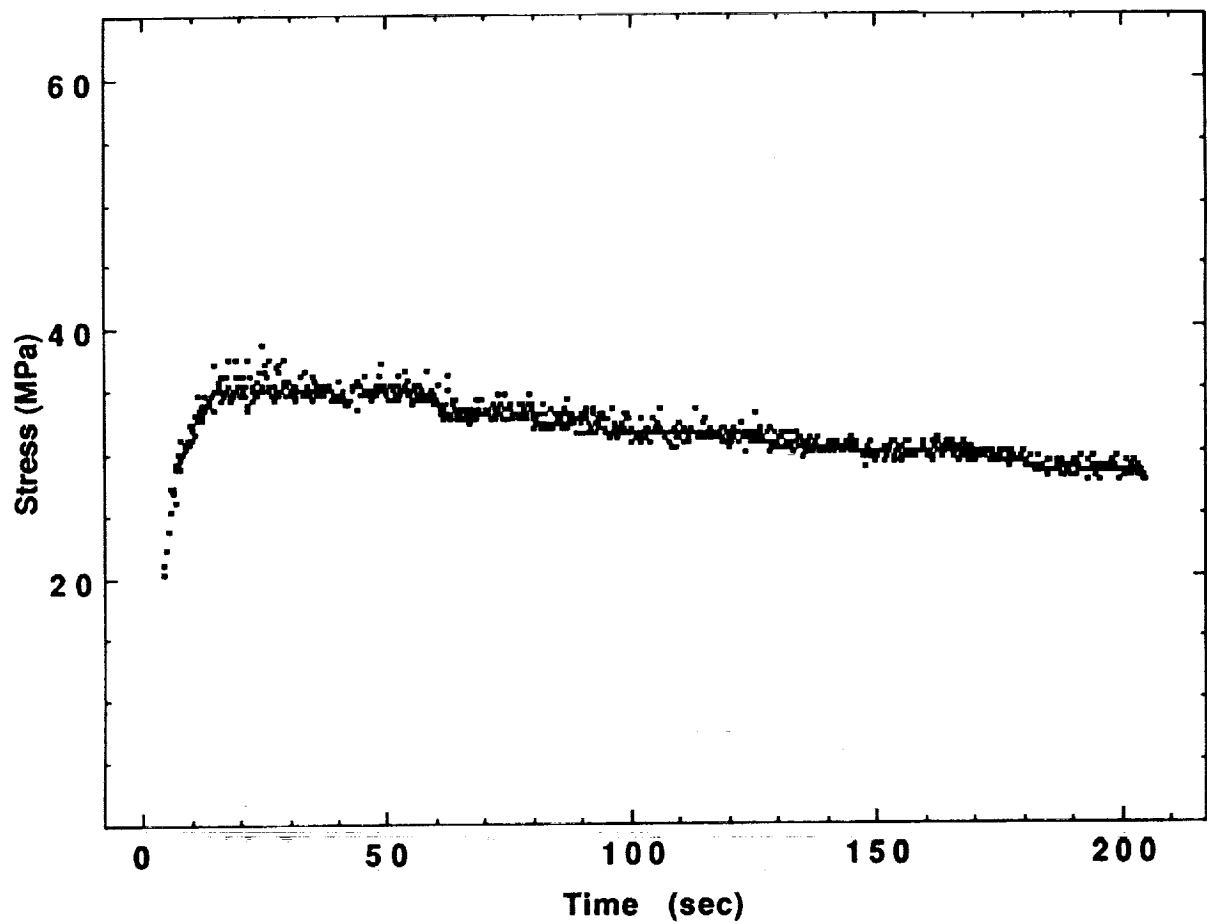
Figure C8h: Data Collected During Modified CCSR Test at 566°C and 1000 μm/m/sec; Stress Relaxation #4, Strain = 0.5%.

C-2
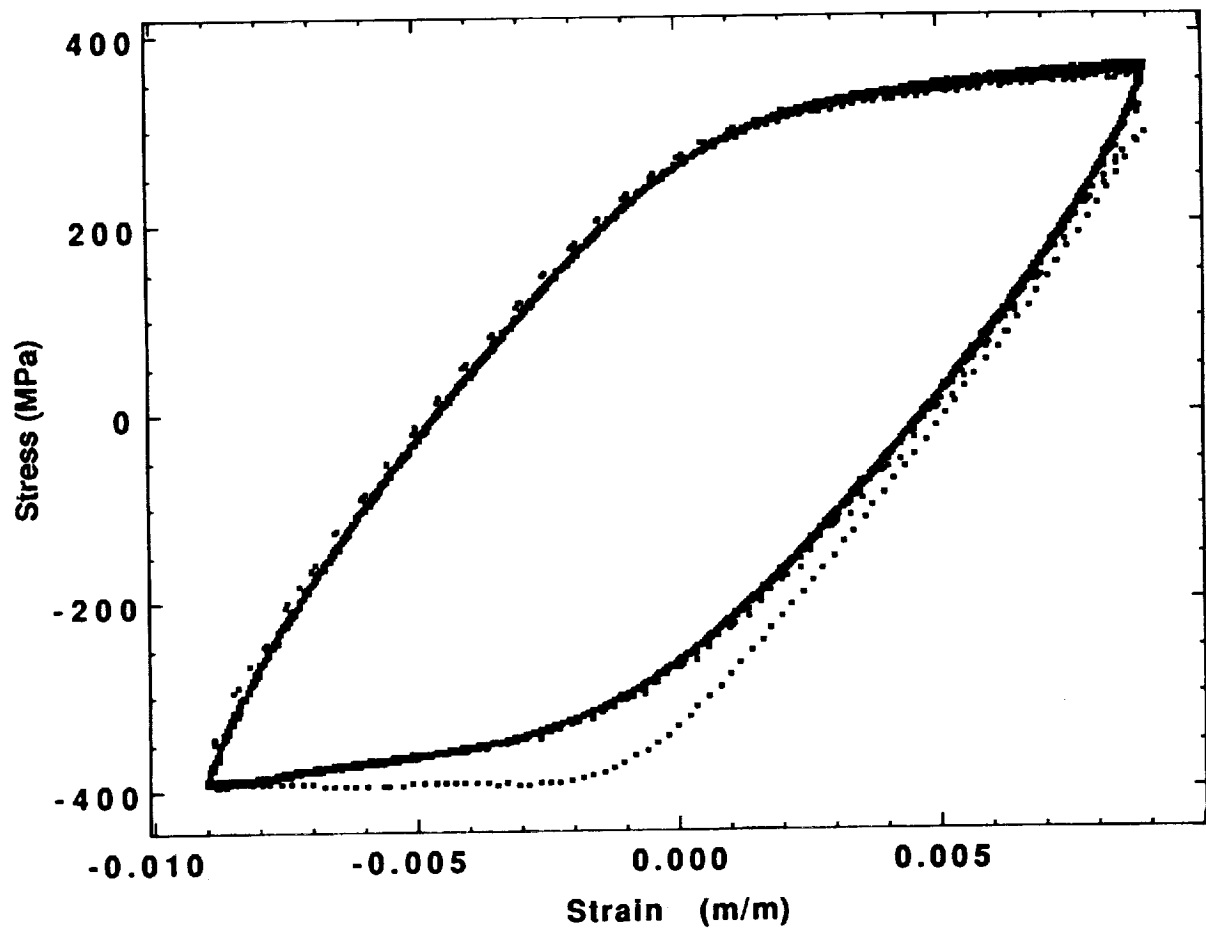
Figure C8i: Data Collected During Modified CCSR Test at 566°C and 1000 μm/m/sec; CCSR Cycle #5
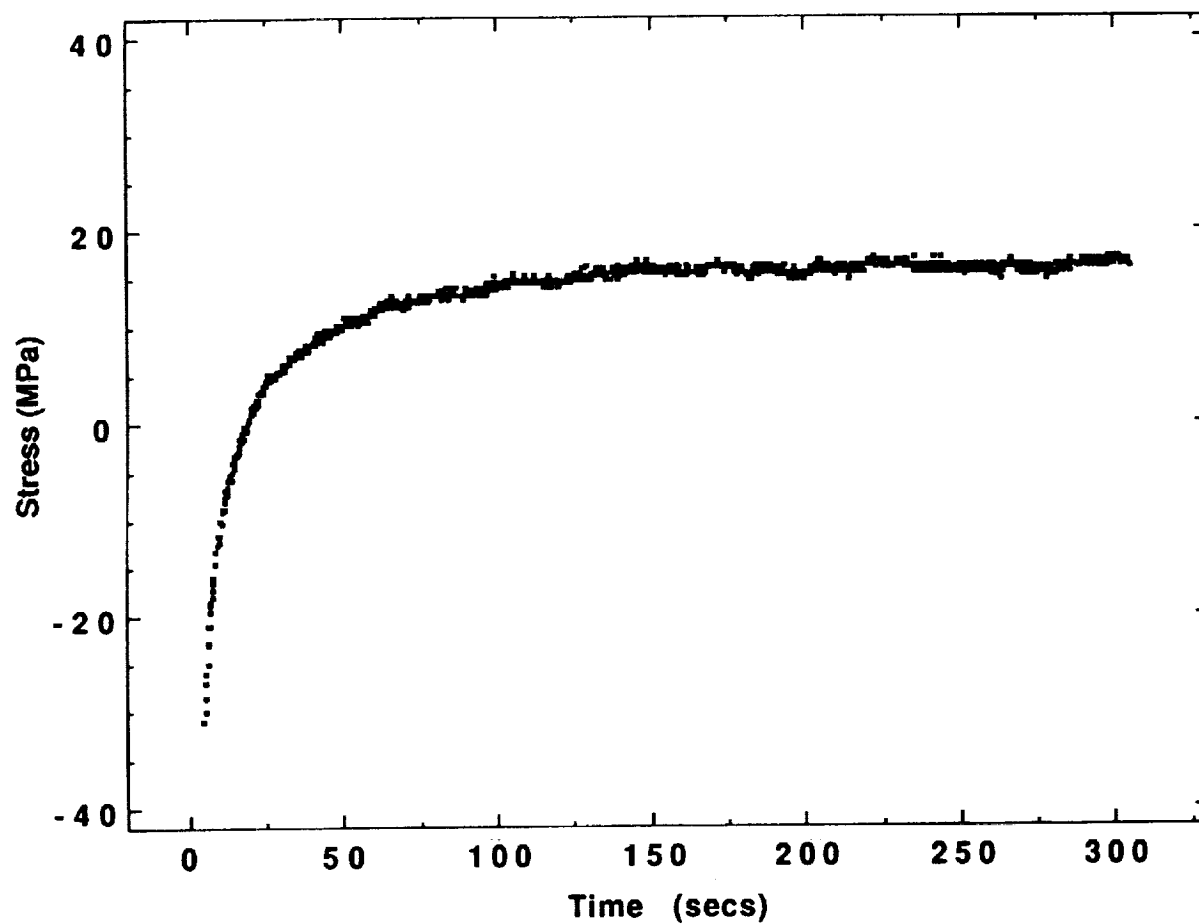
Figure C8j: Data Collected During Modified CCSR Test at 566°C and 1000 μm/m/sec; Stress Relaxation #5, Strain = 0.4%.
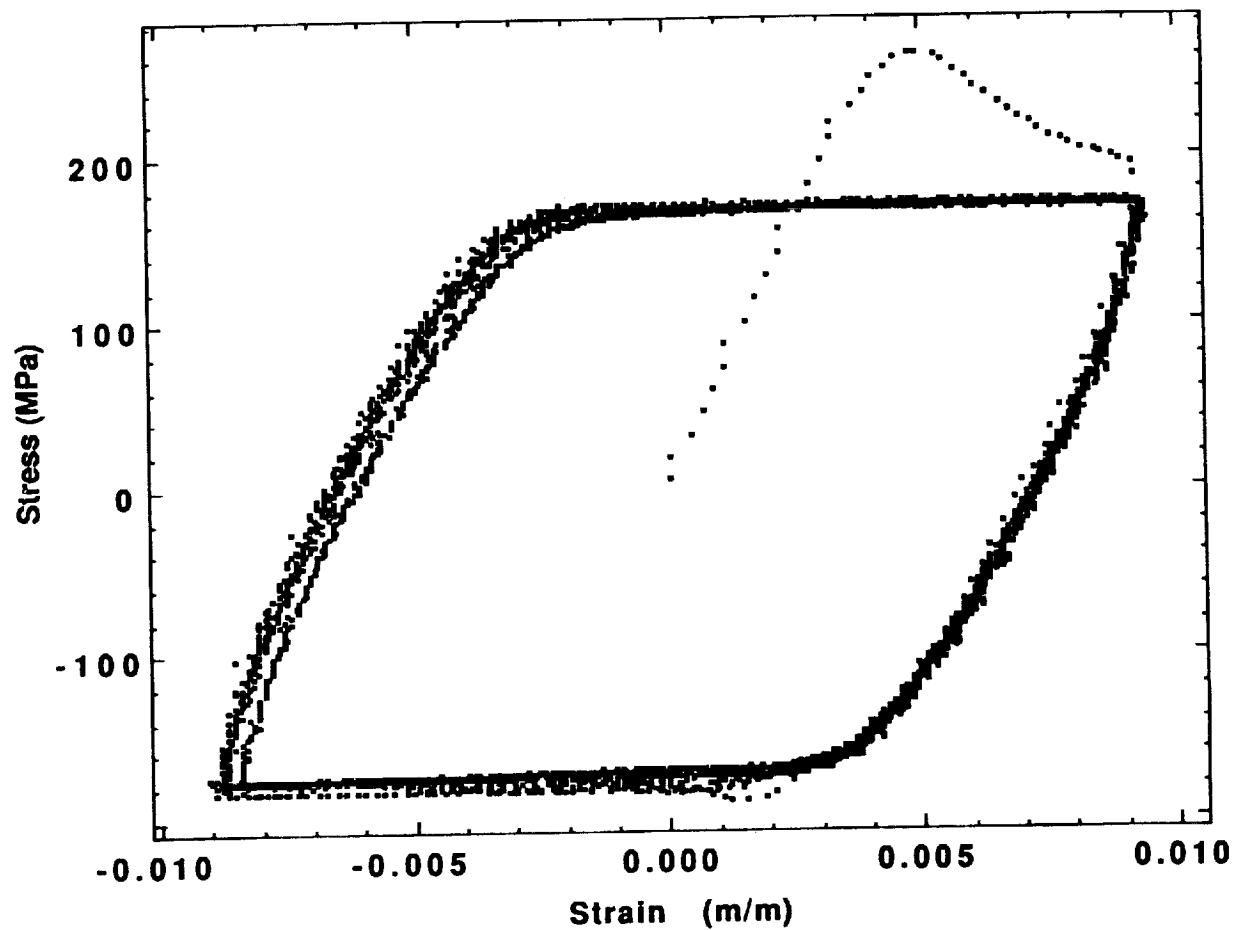
Figure C9a: Data Collected During Modified CCSR Test at 649°C and 1000
μm/m/sec; CCSR Cycle #1
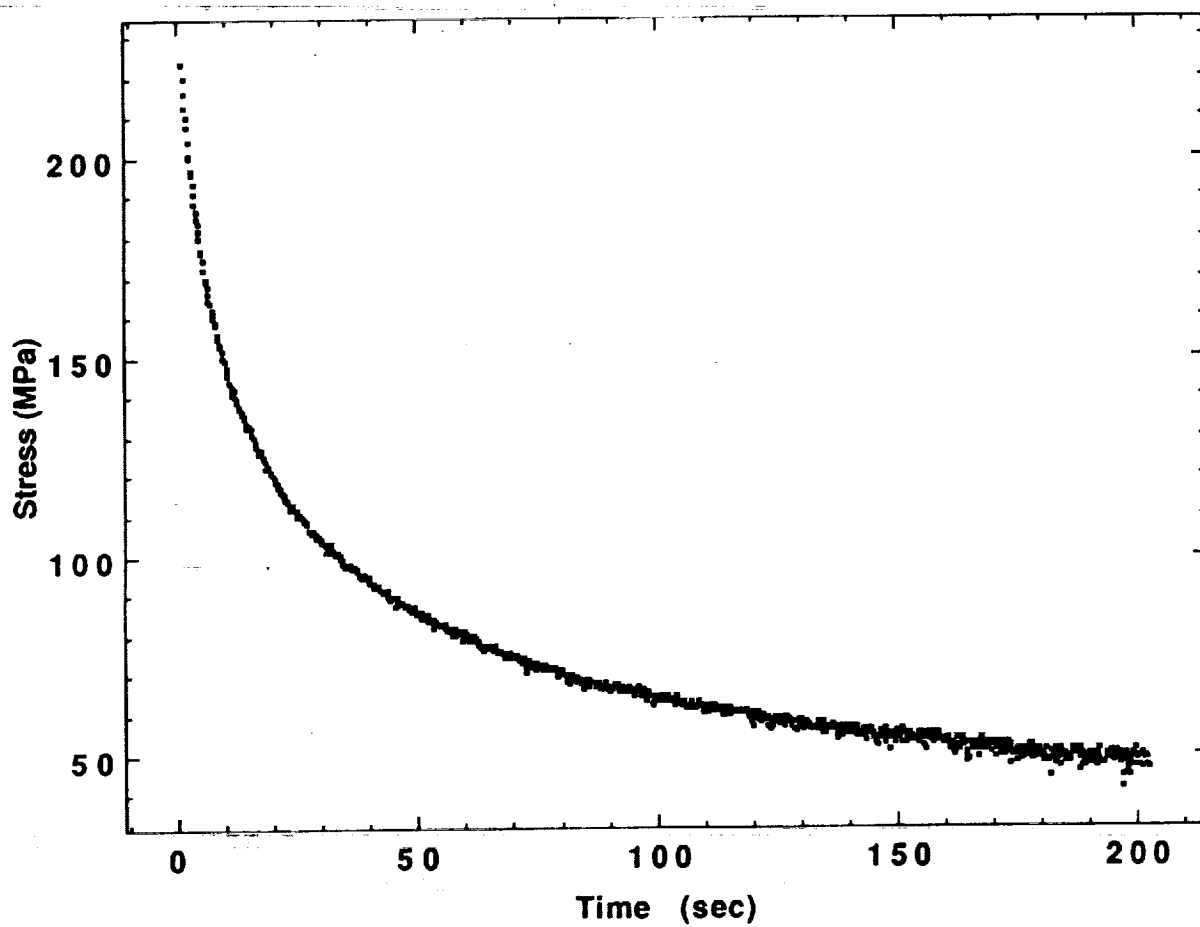
Figure C9b: Data Collected During Modified CCSR Test at 649°C and 1000 μm/m/sec; Stress Relaxation #1, Strain = 0.85%.
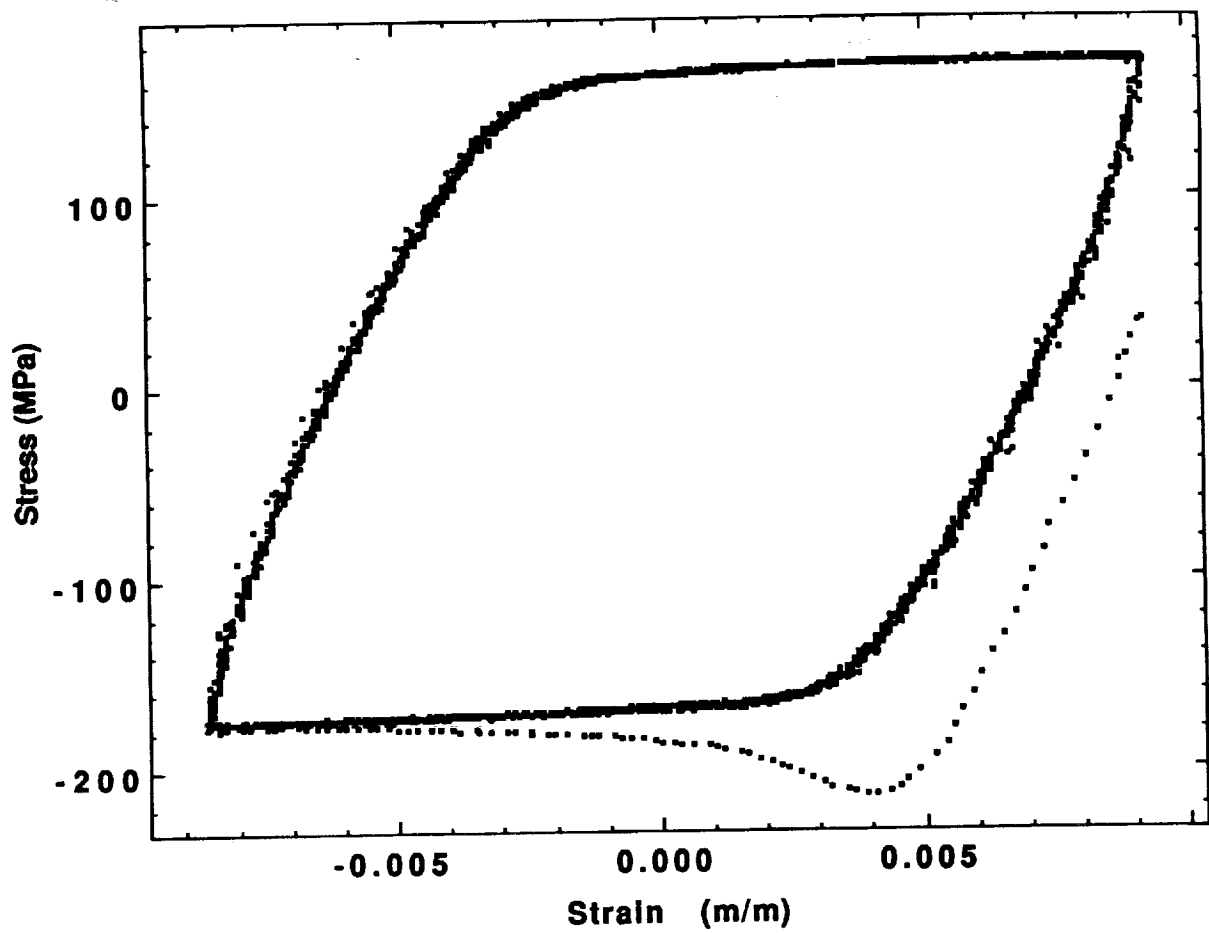
Figure C9c: Data Collected During Modified CCSR Test at 649°C and 1000 µm/m/sec; CCSR Cycle #2
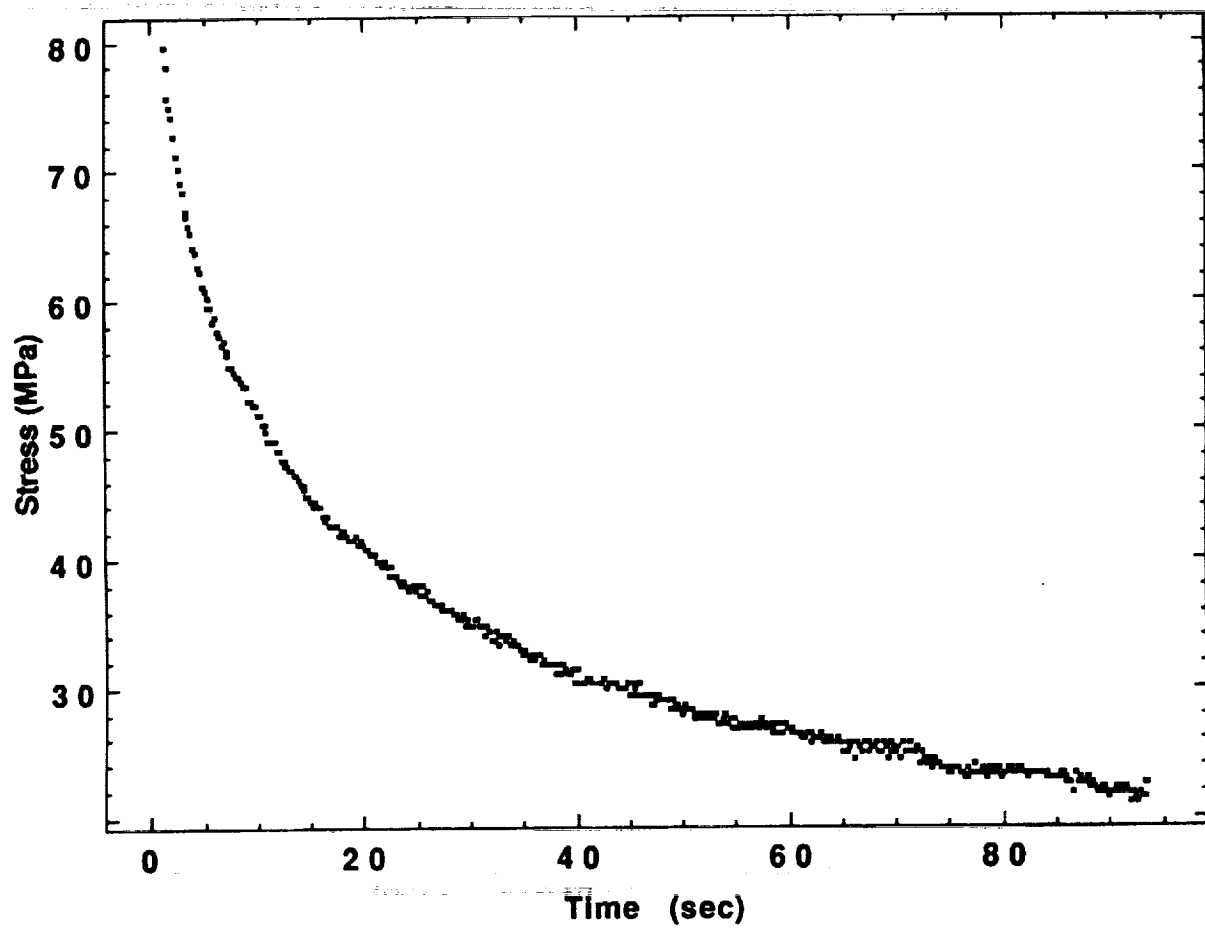
Figure C9d: Data Collected During Modified CCSR Test at 649°C and 1000
μm/m/sec; Stress Relaxation #2, Strain = 0.80%.
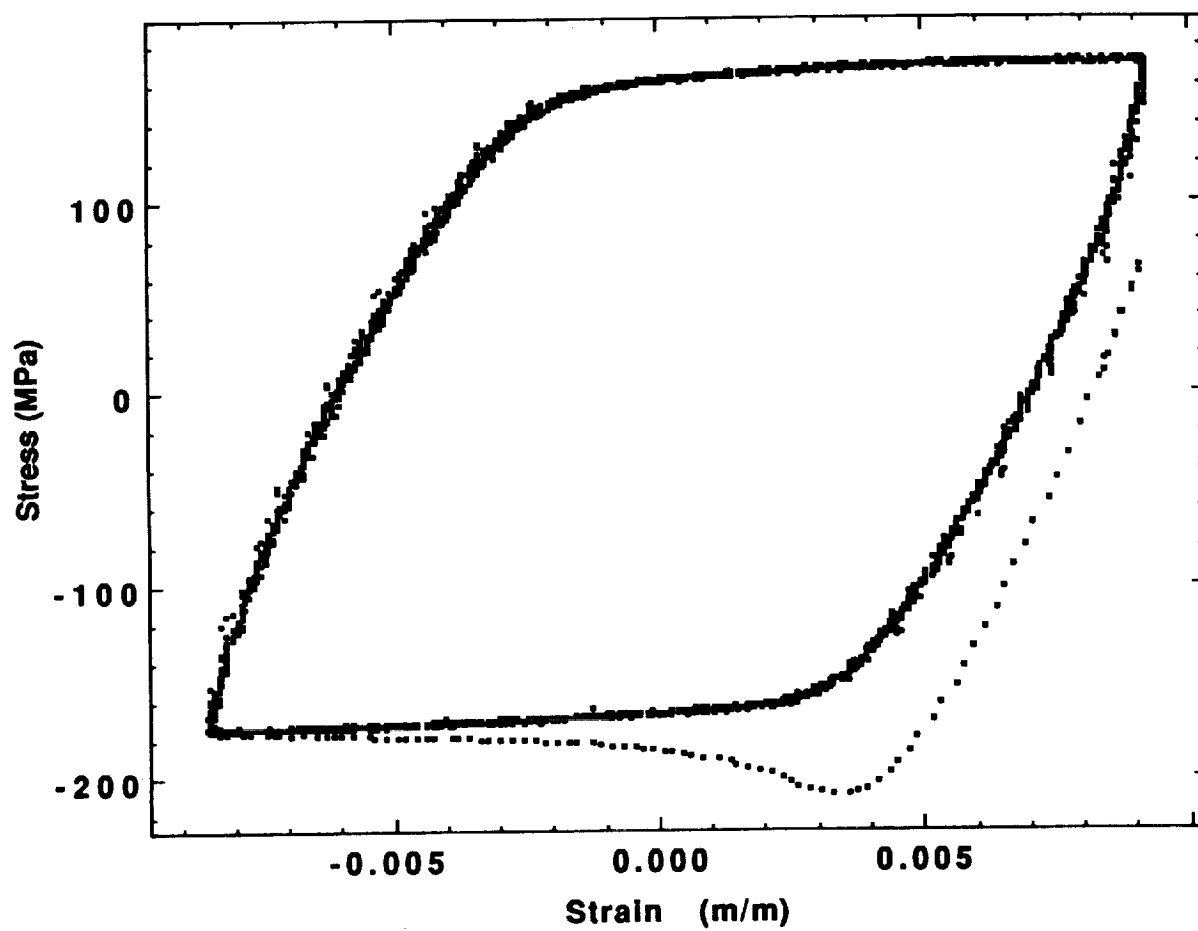
Figure C9e: Data Collected During Modified CCSR Test at 649°C and 1000 μm/m/sec; CCSR Cycle #3
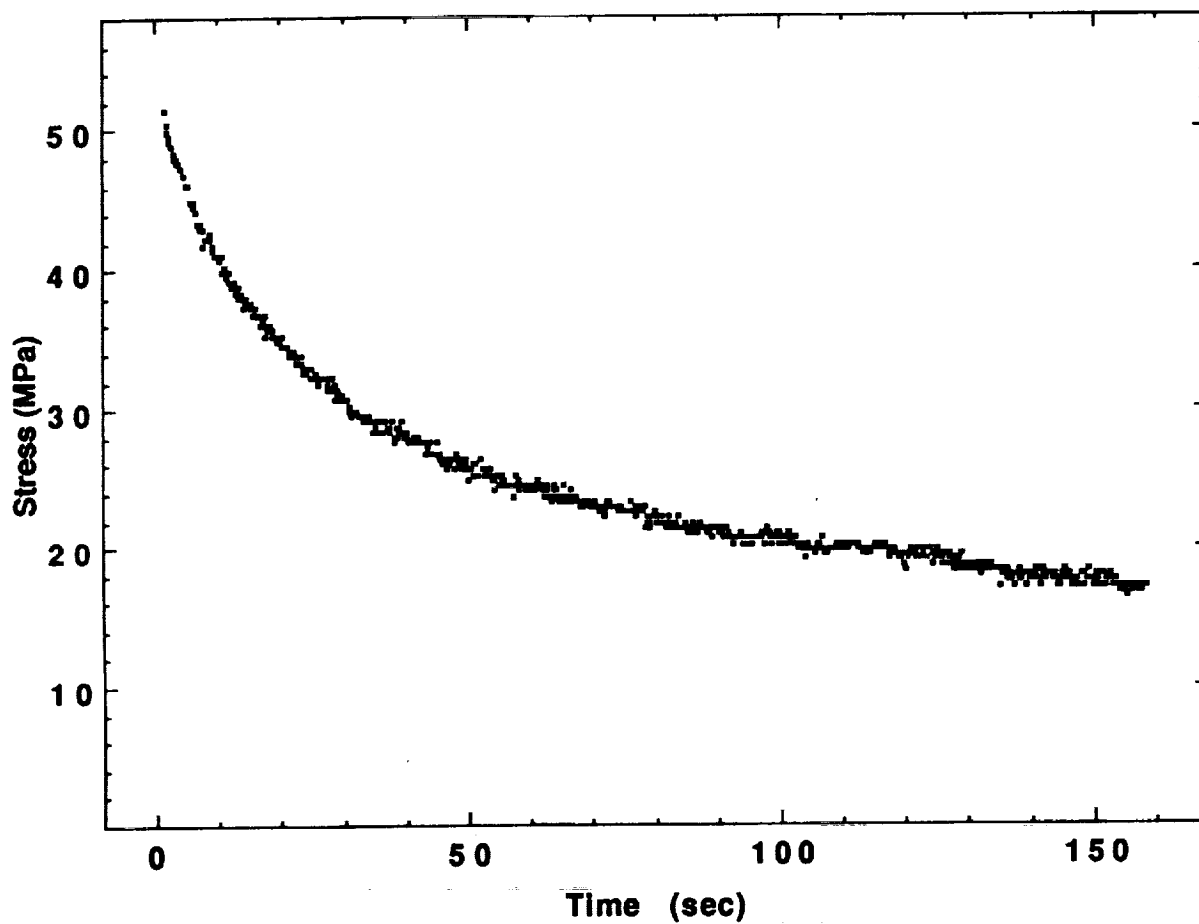
Figure C9f: Data Collected During Modified CCSR Test at 649°C and 1000 μm/m/sec; Stress Relaxation #3, Strain = 0.75%.
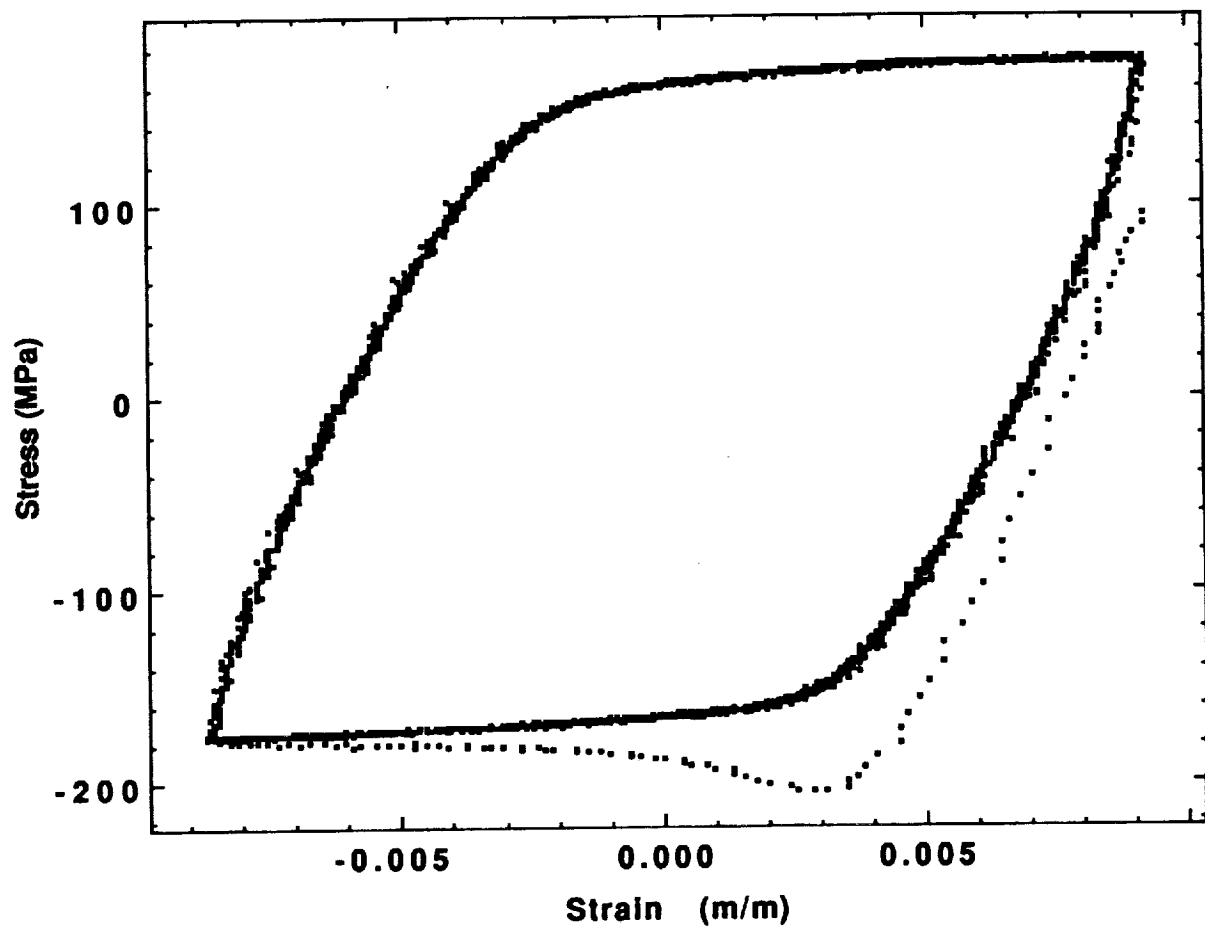
Figure C9g: Data Collected During Modified CCSR Test at 649°C and 1000 μm/m/sec; CCSR Cycle #4
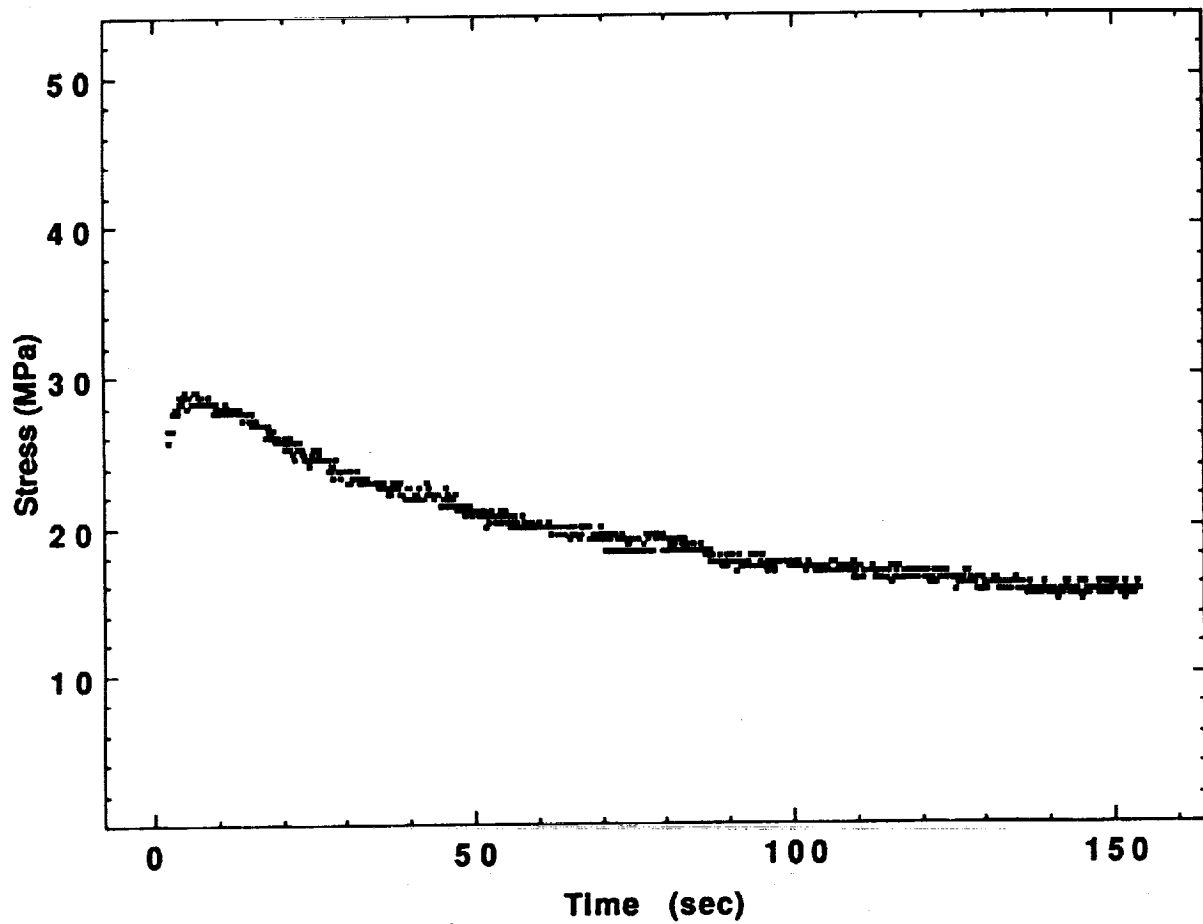
Figure C9h: Data Collected During Modified CCSR Test at 649°C and 1000 μm/m/sec; Stress Relaxation #4, Strain = 0.70%.
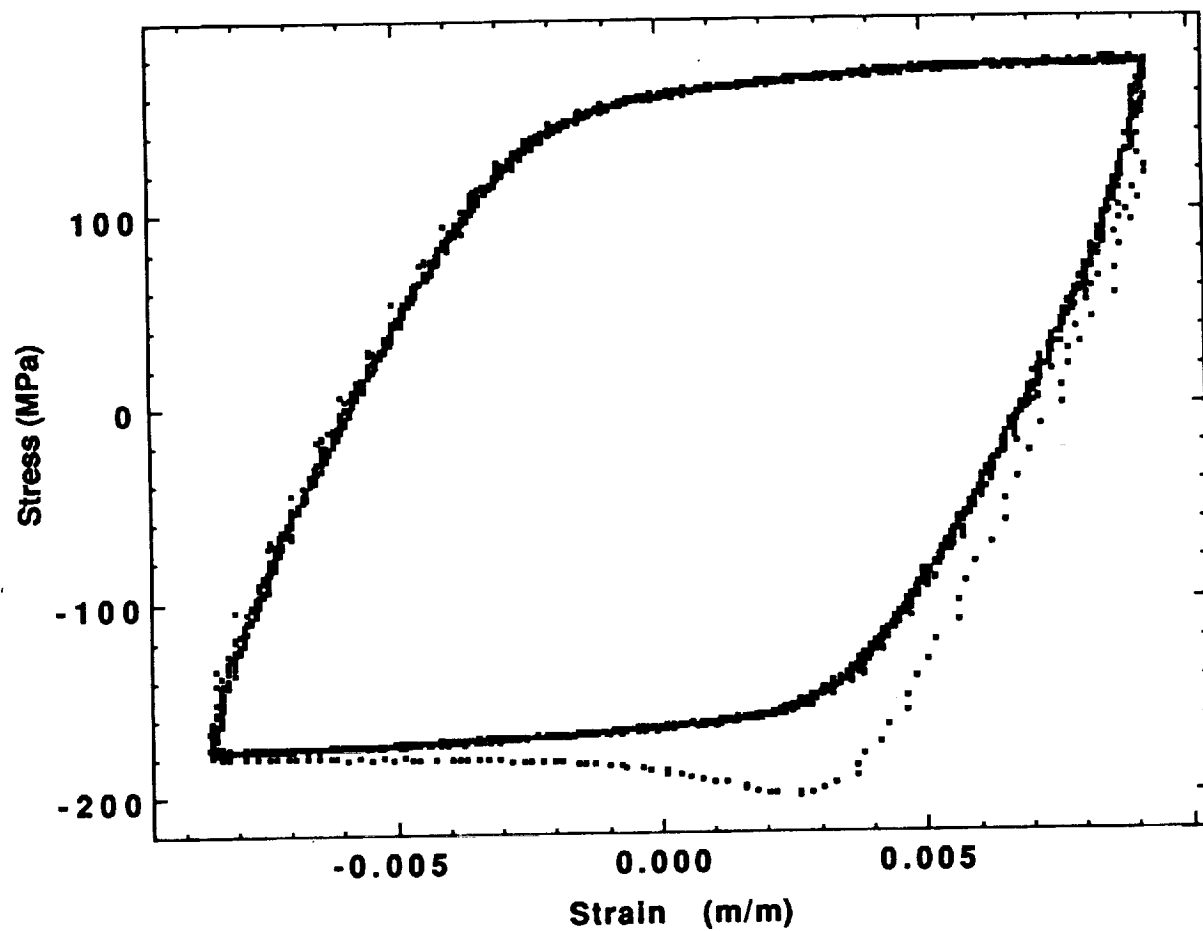
Figure C9i: Data Collected During Modified CCSR Test at 649°C and 1000 μm/m/sec; CCSR Cycle #5
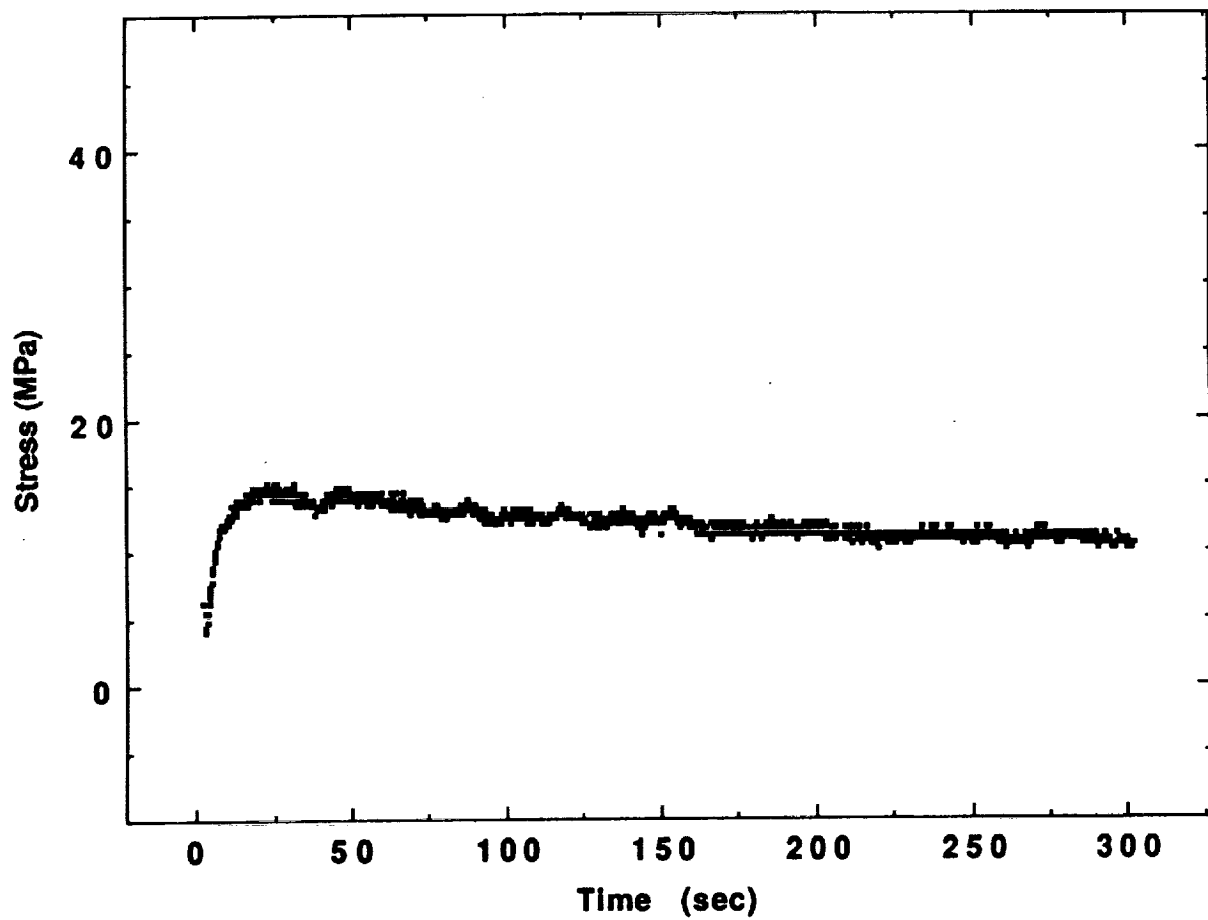
Figure C9j: Data Collected During Modified CCSR Test at 649°C and 1000 μm/m/sec; Stress Relaxation #5, Strain = 0.65%.
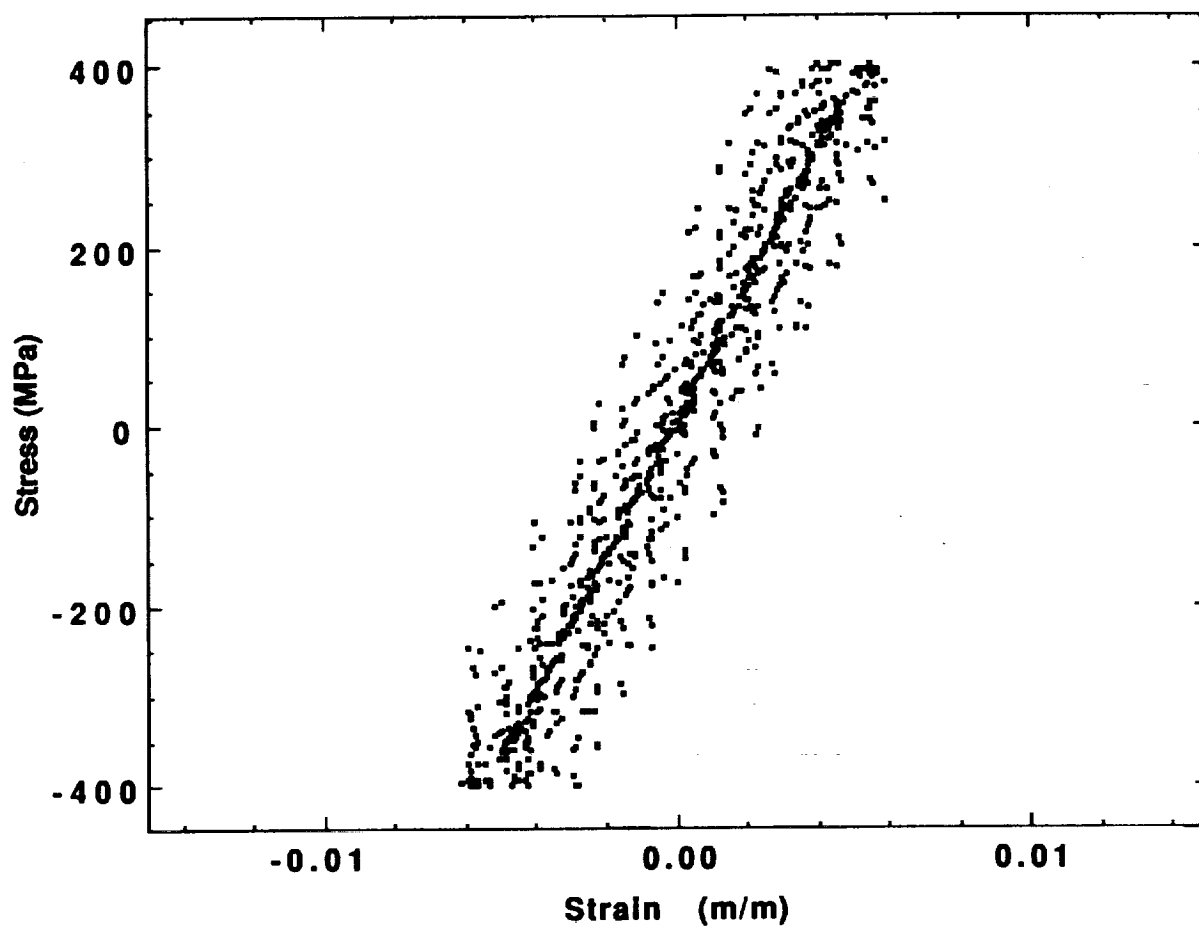
Figure C10a: Data Collected During CCSR Test at 482°C and 5000 μm/m/sec; Strain Range = ±0.6%.
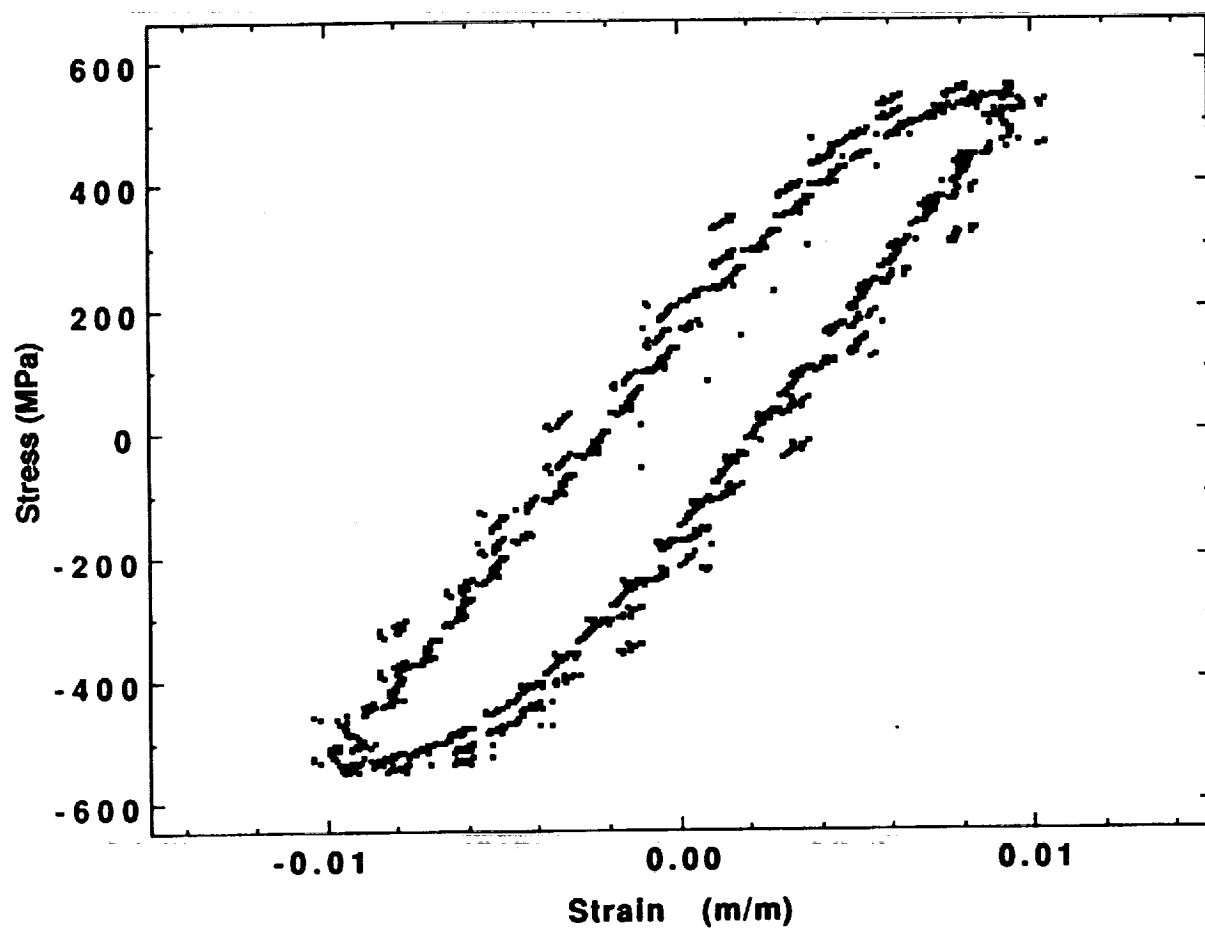
Figure C10b: Data Collected During CCSR Test at 482°C and 5000 μm/m/sec; Strain Range = ±1.0%.
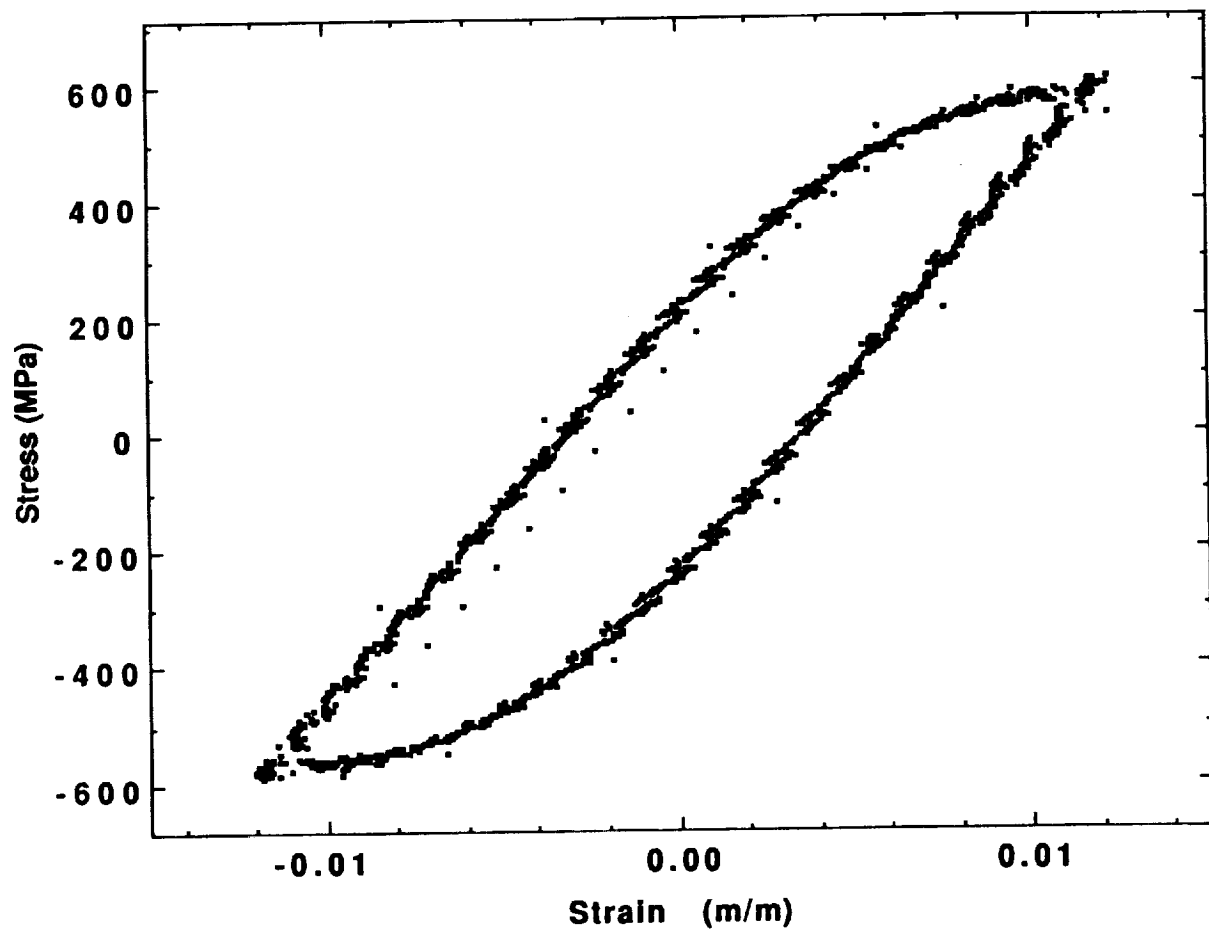
Figure C10c: Data Collected During CCSR Test at 482°C and 5000 µm/m/sec; Strain Range = ±1.2%.
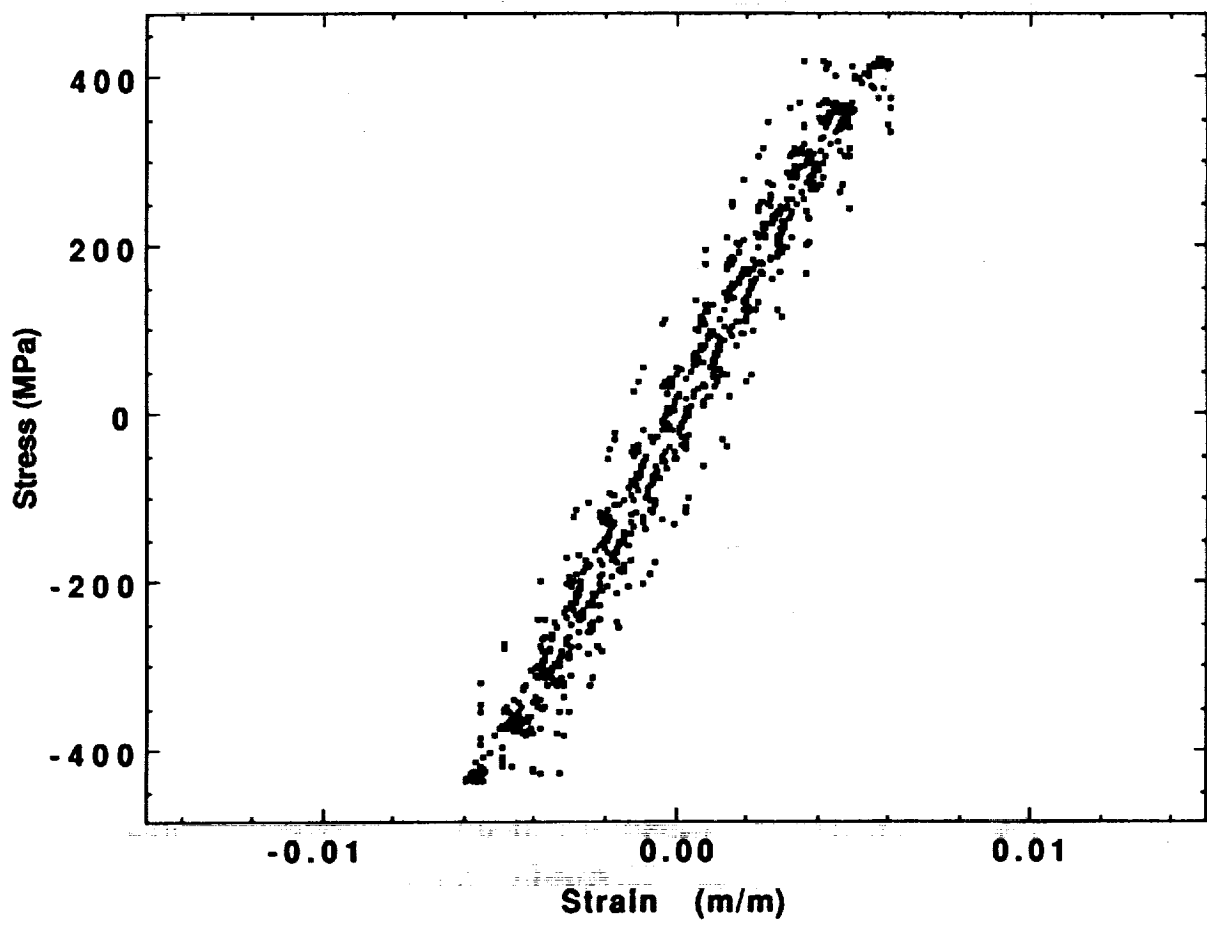
Figure C11a: Data Collected During CCSR Test at 566°C and 5000 μm/m/sec; Strain Range = ±0.6%.
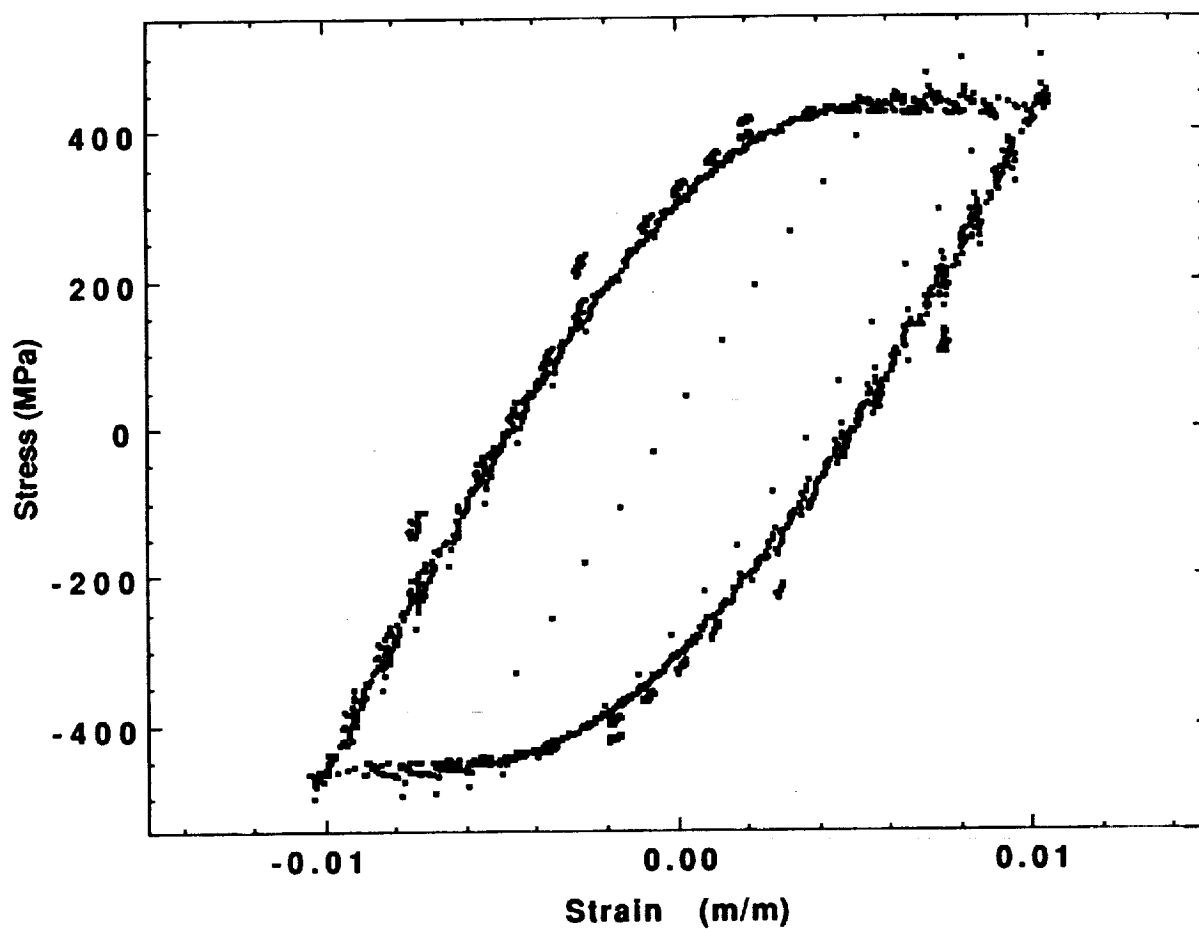
Figure C11b: Data Collected During CCSR Test at 566°C and 5000 µm/m/sec; Strain Range = ±1.0%.
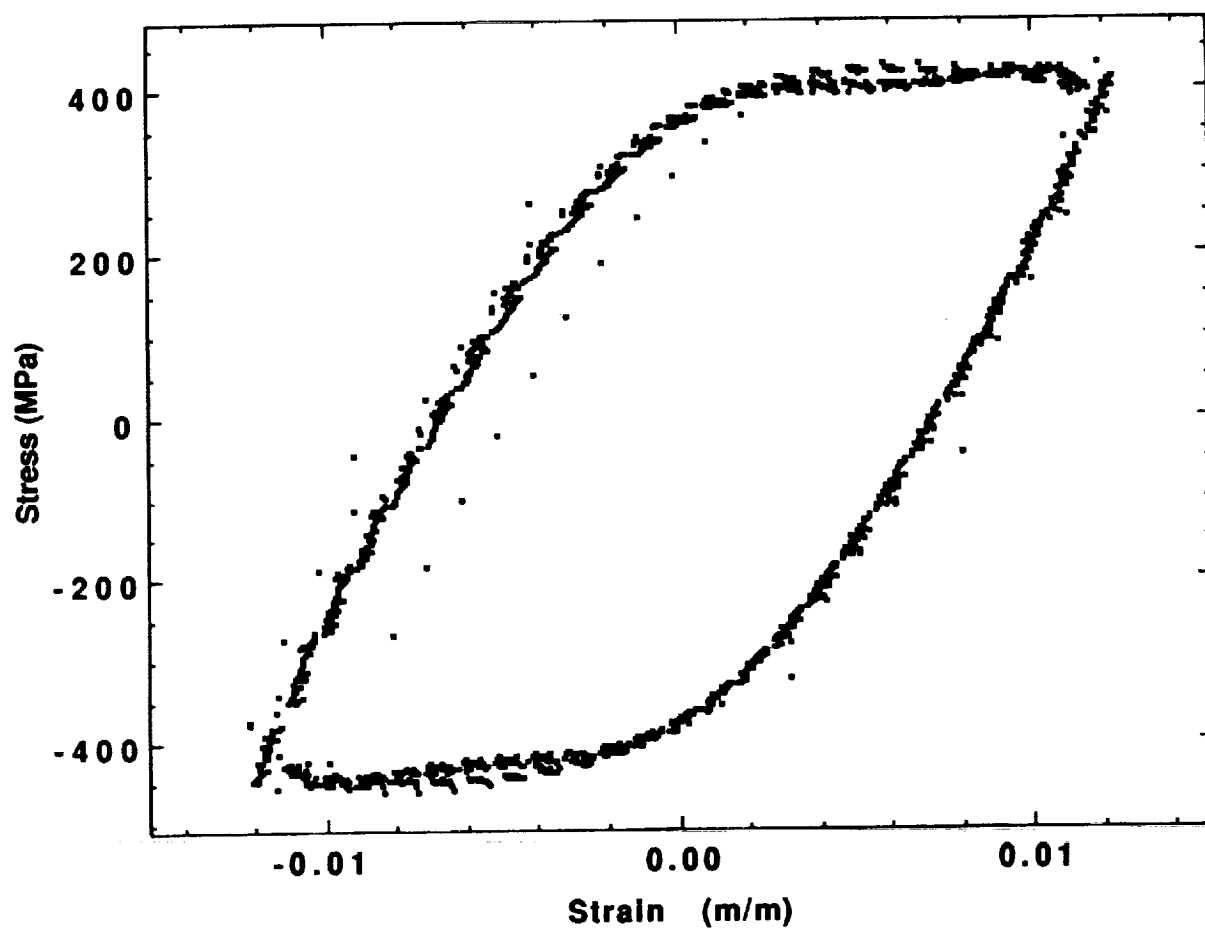
Figure C11c: Data Collected During CCSR Test at 566°C and 5000 μm/m/sec; Strain Range = ±1.2%.
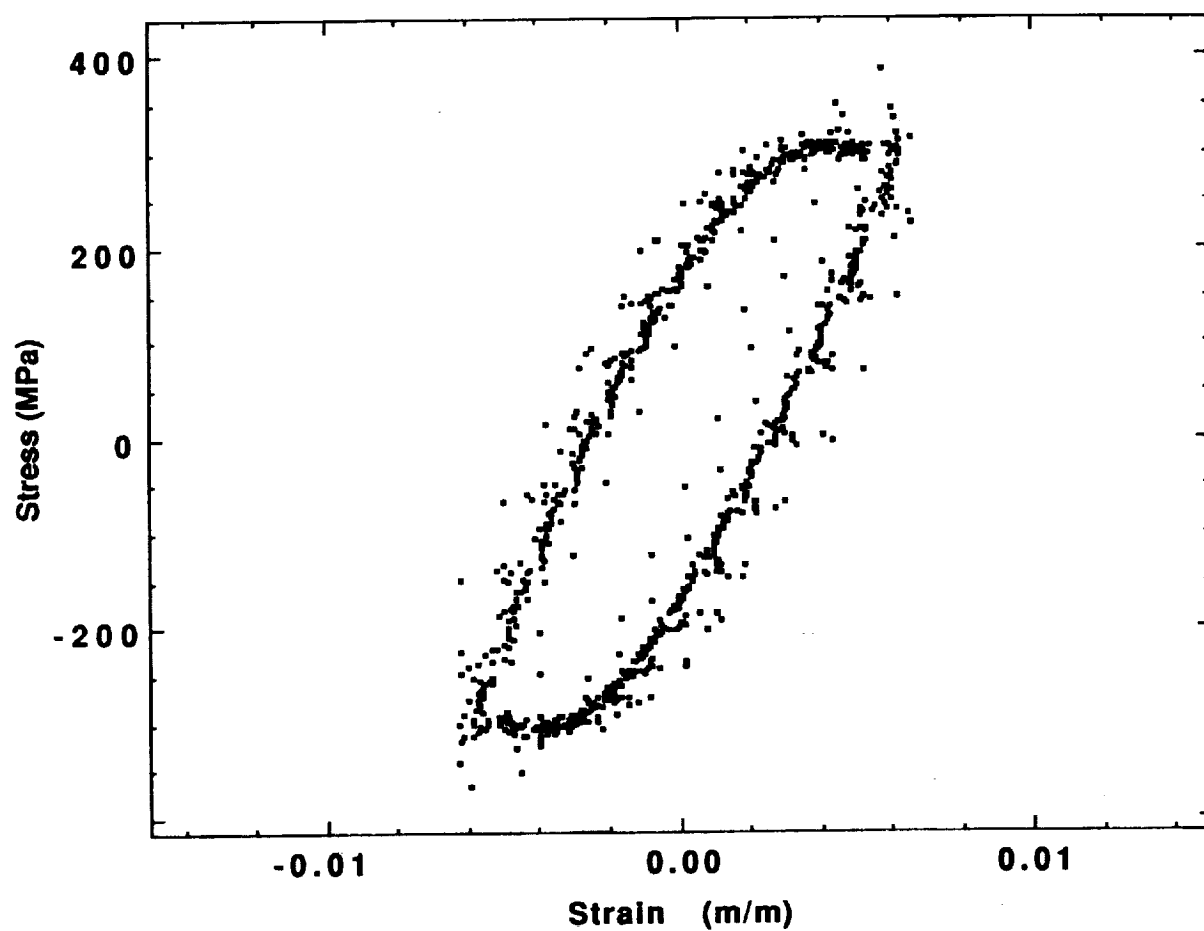
Figure C12a: Data Collected During CCSR Test at 649°C and 5000 μm/m/sec; Strain Range = ±0.6%.
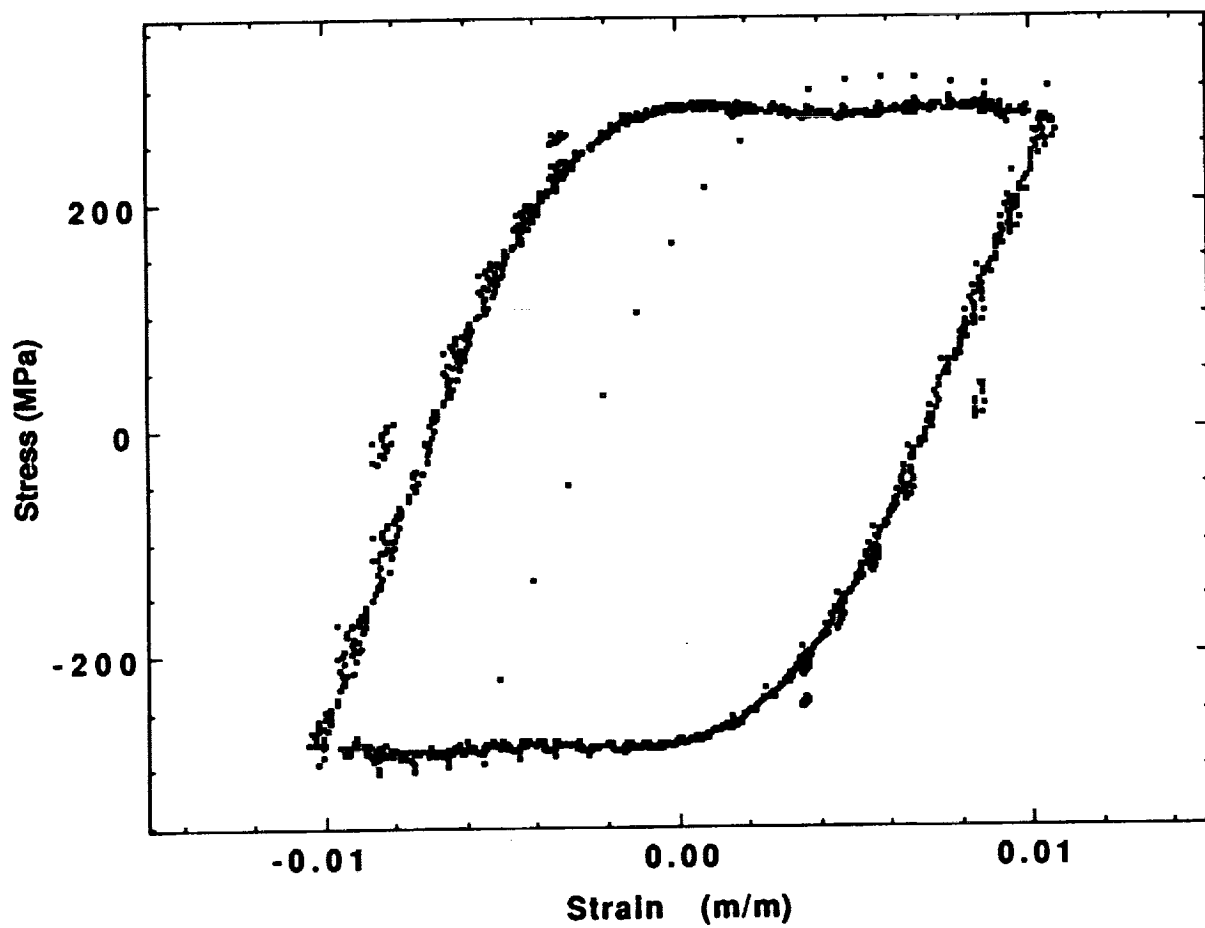
Figure C12b: Data Collected During CCSR Test at 649°C and 5000 μm/m/sec; Strain Range = ±1.0%.
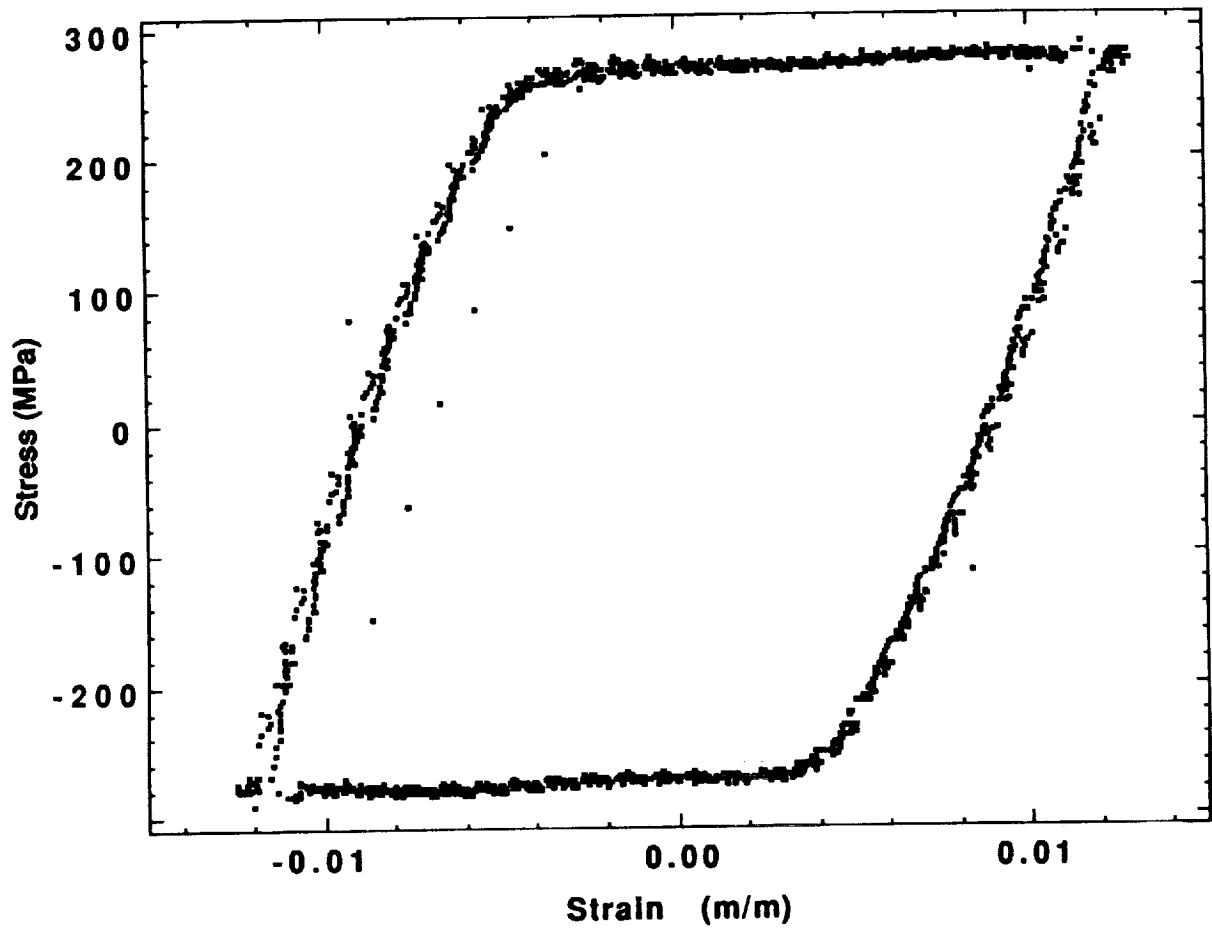
Figure C12c: Data Collected During CCSR Test at 649°C and 5000 μm/m/sec; Strain Range = ±1.2%.
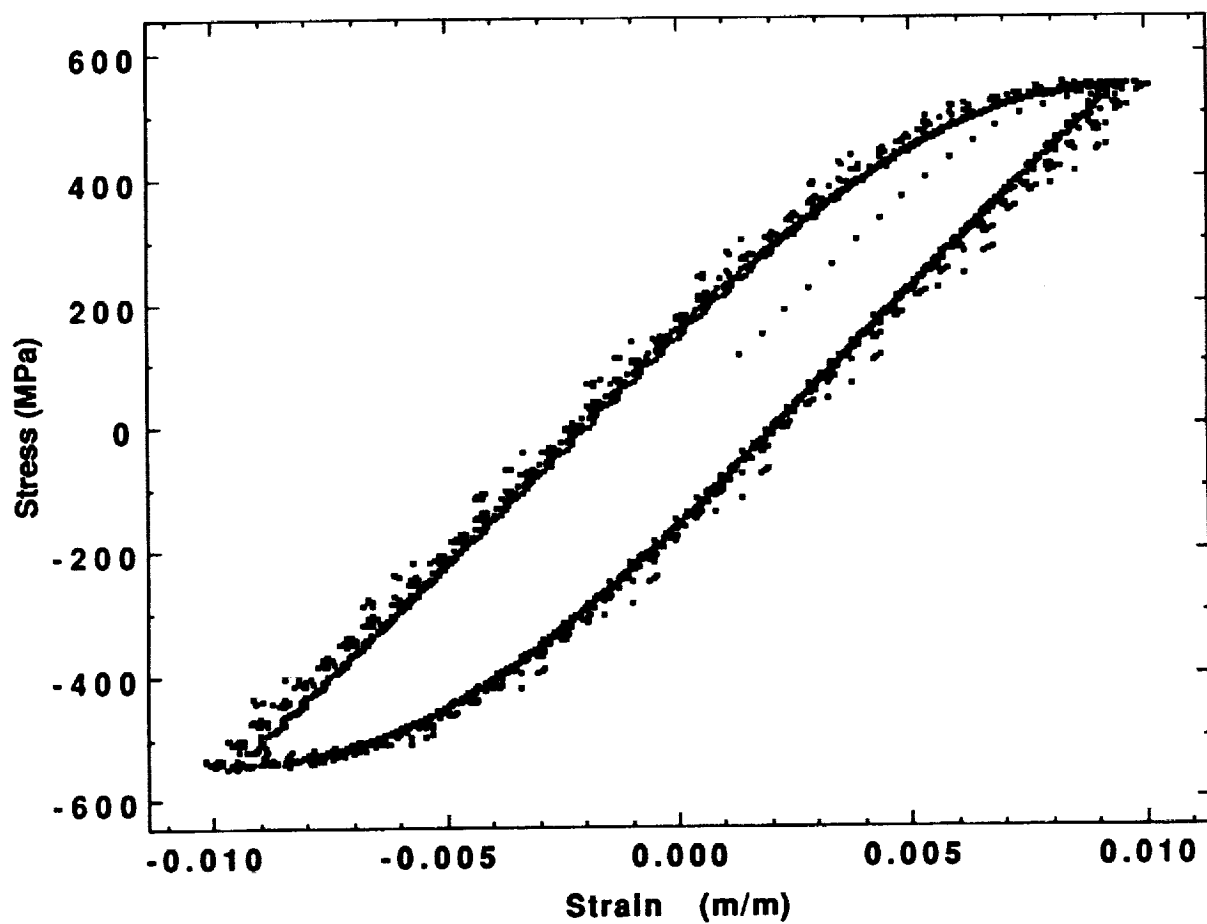
Figure C13: Data Collected During CCSR Test at 482°C and 10000 µm/m/sec
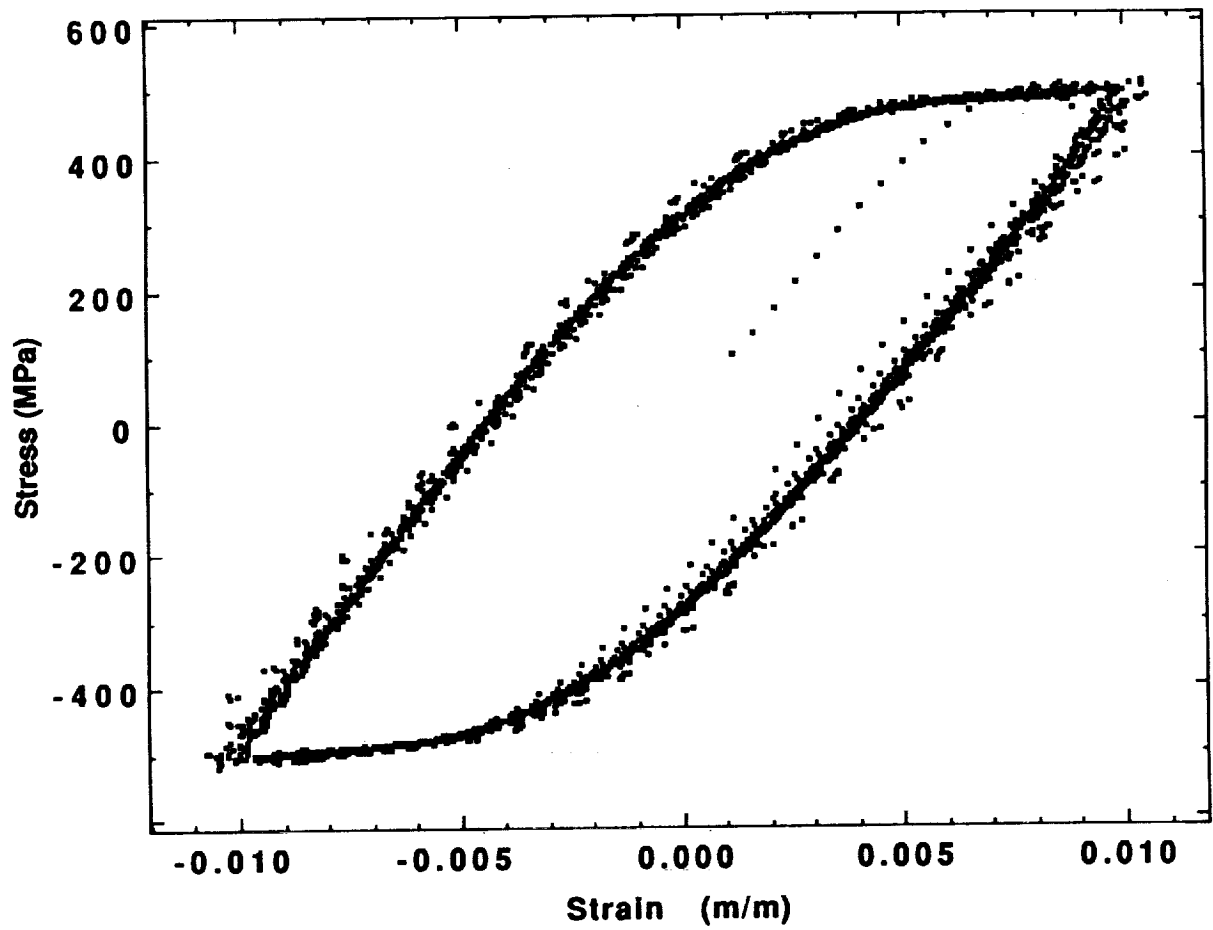
Figure C14: Data Collected During CCSR Test at 566°C and 10000 μm/m/sec
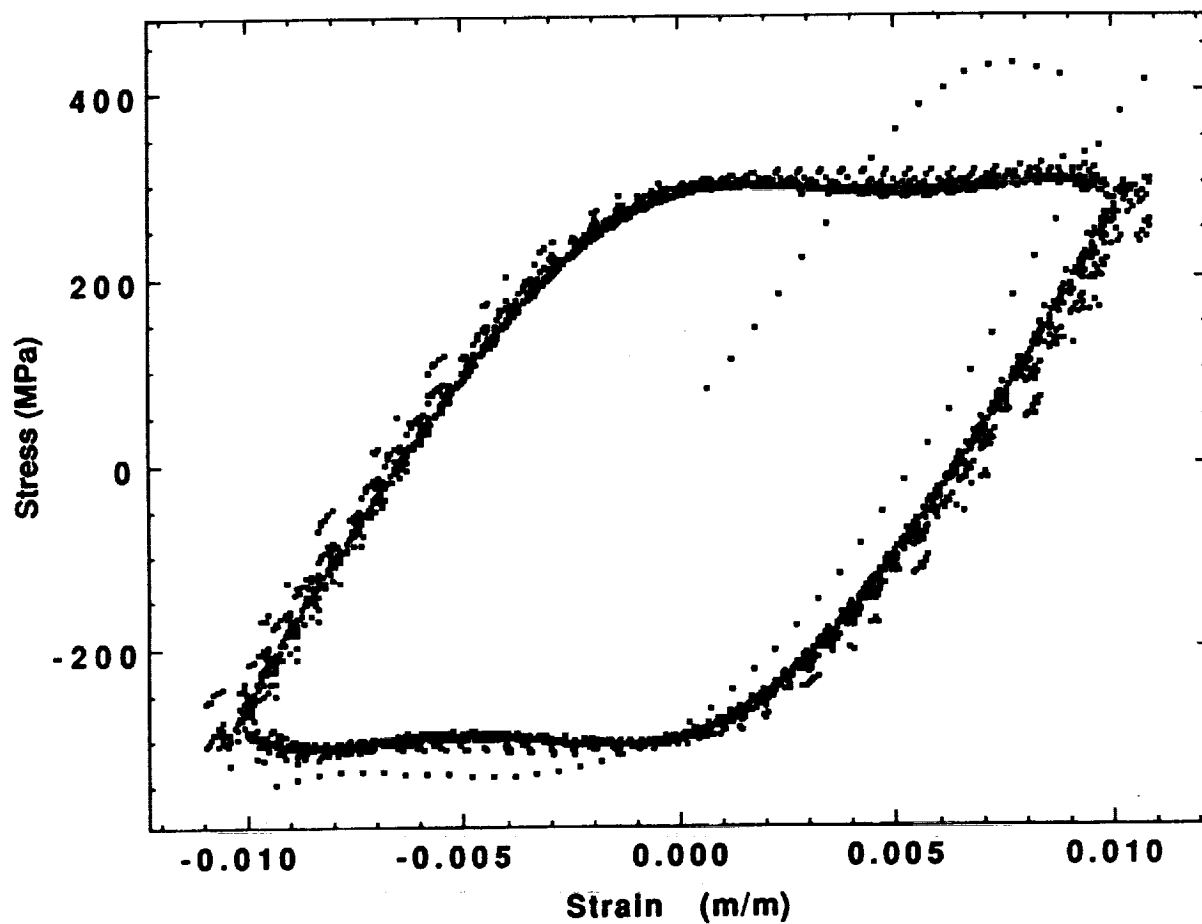
Figure C15: Data Collected During CCSR Test at 649°C and 10000 μm/m/sec

APPENDIX D

PLOTS OF DATA COLLECTED DURING CONSTANT STRESS RATE TESTS
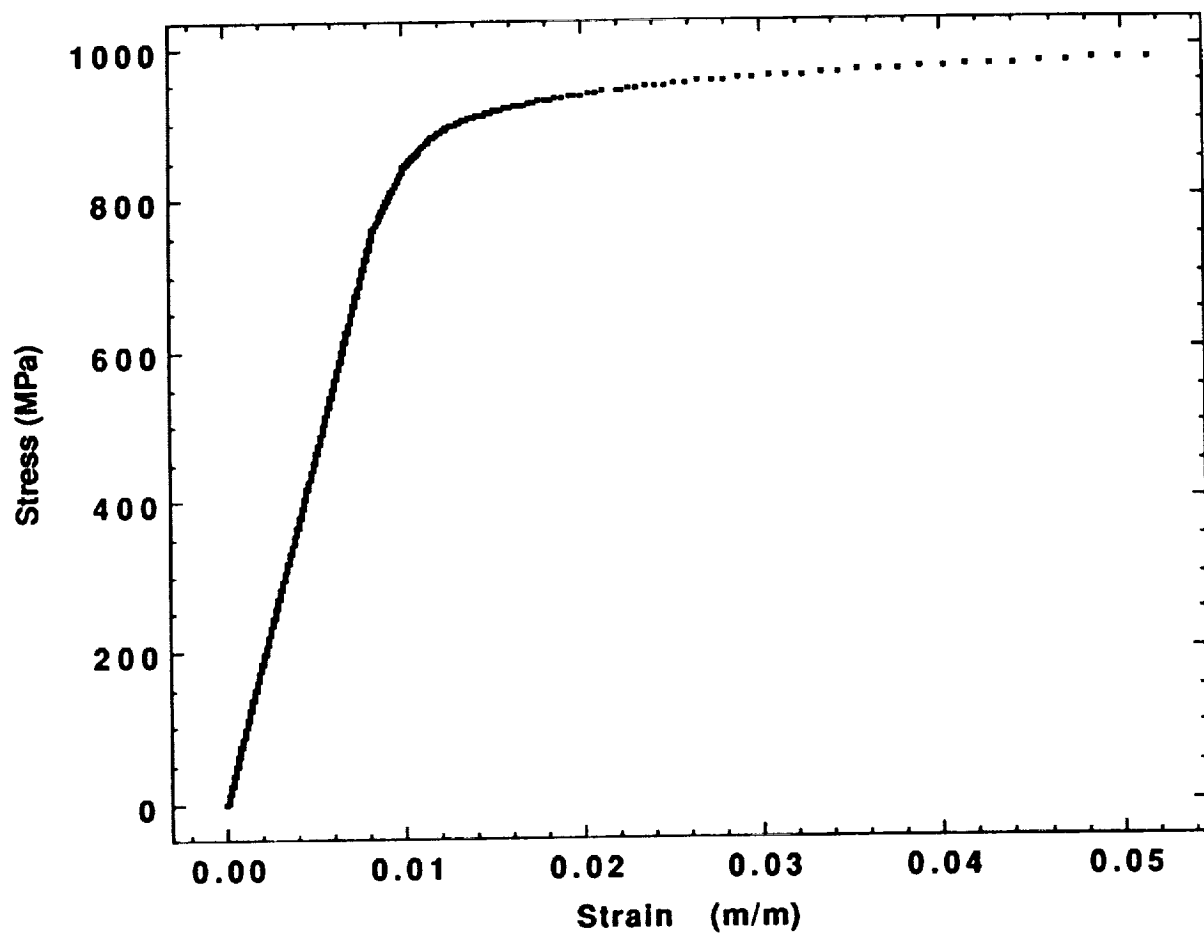
Figure D1: Data Collected During CσR Test at 21°C and 2.6 MPa/sec
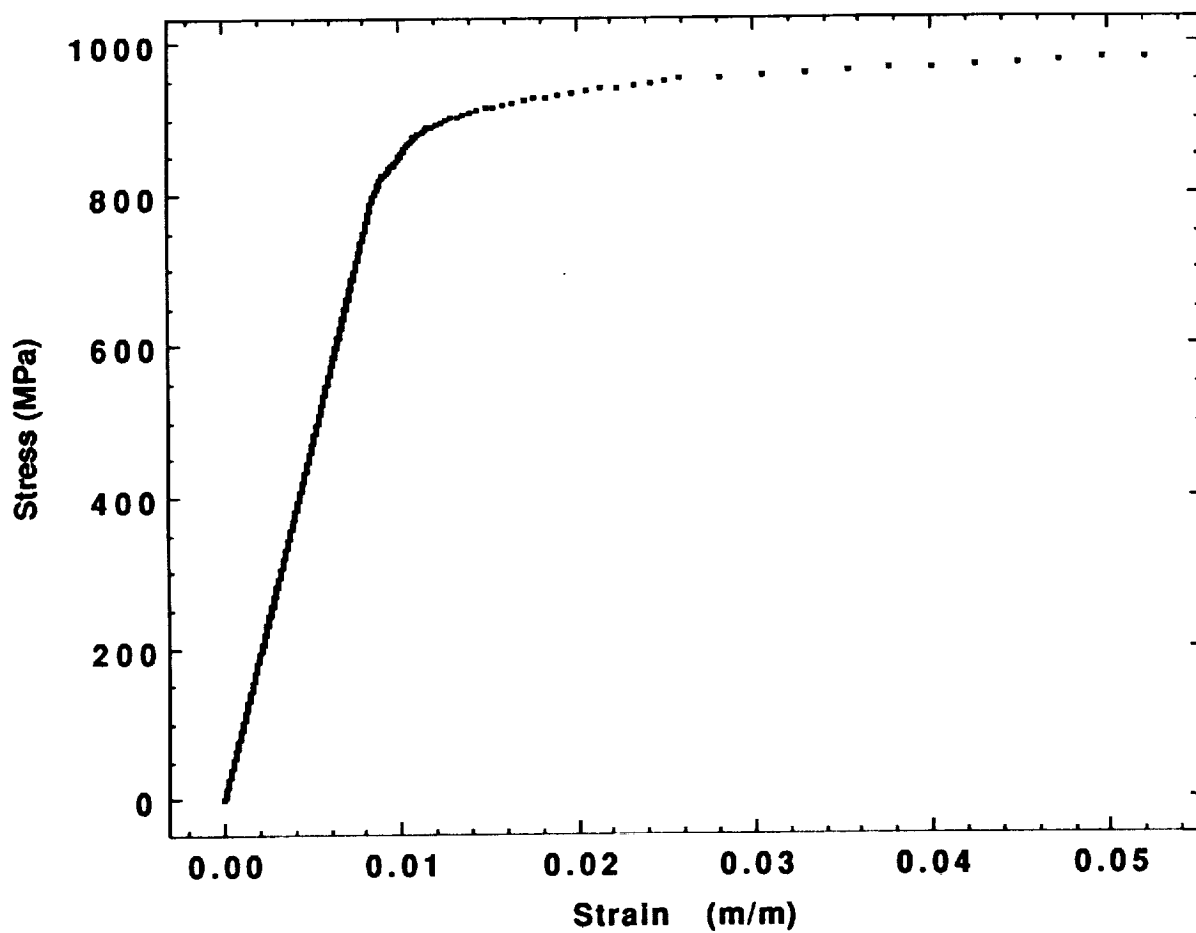
Figure D2: Data Collected During CσR Test at 21°C and 5.2 MPa/sec
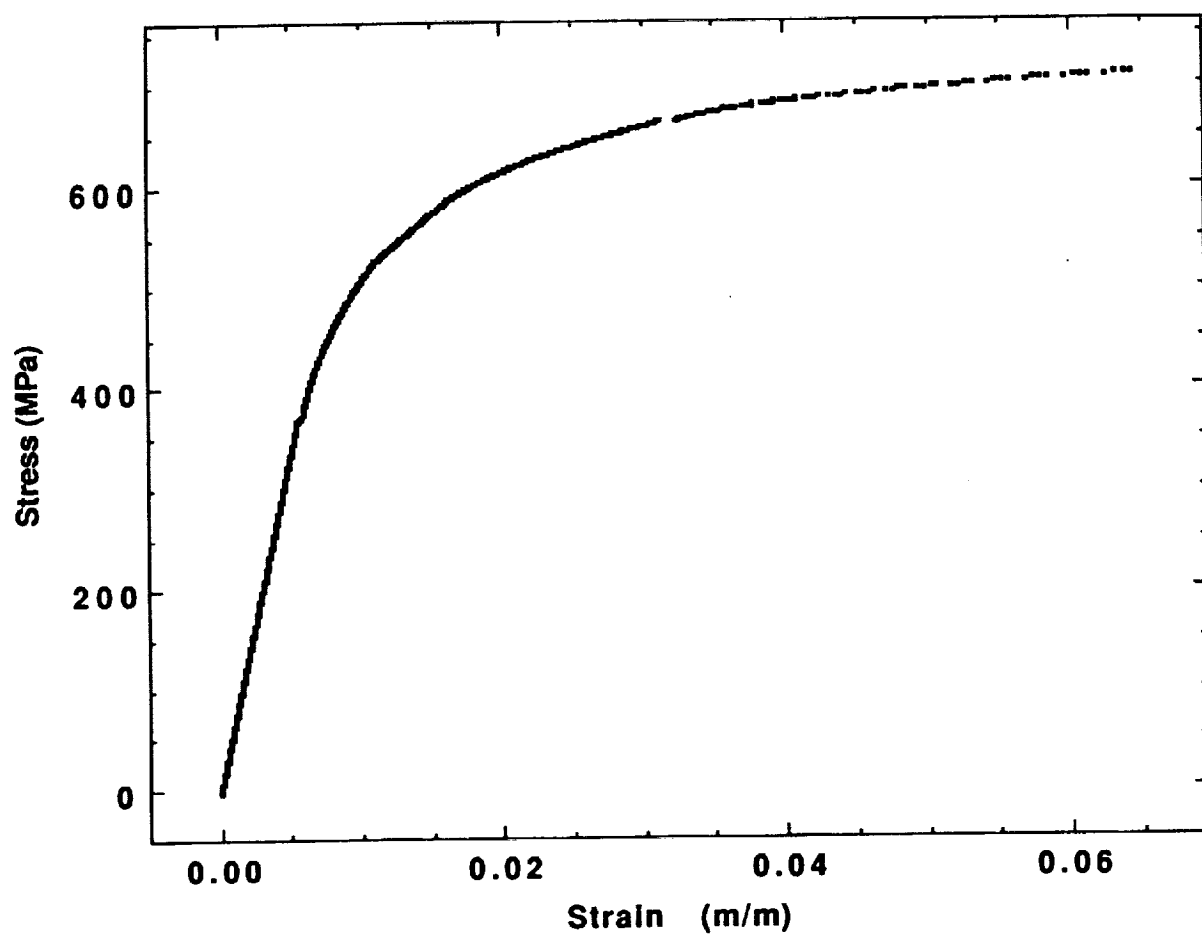
Figure D3: Data Collected During CσR Test at 482°C and 2.6 MPa/sec
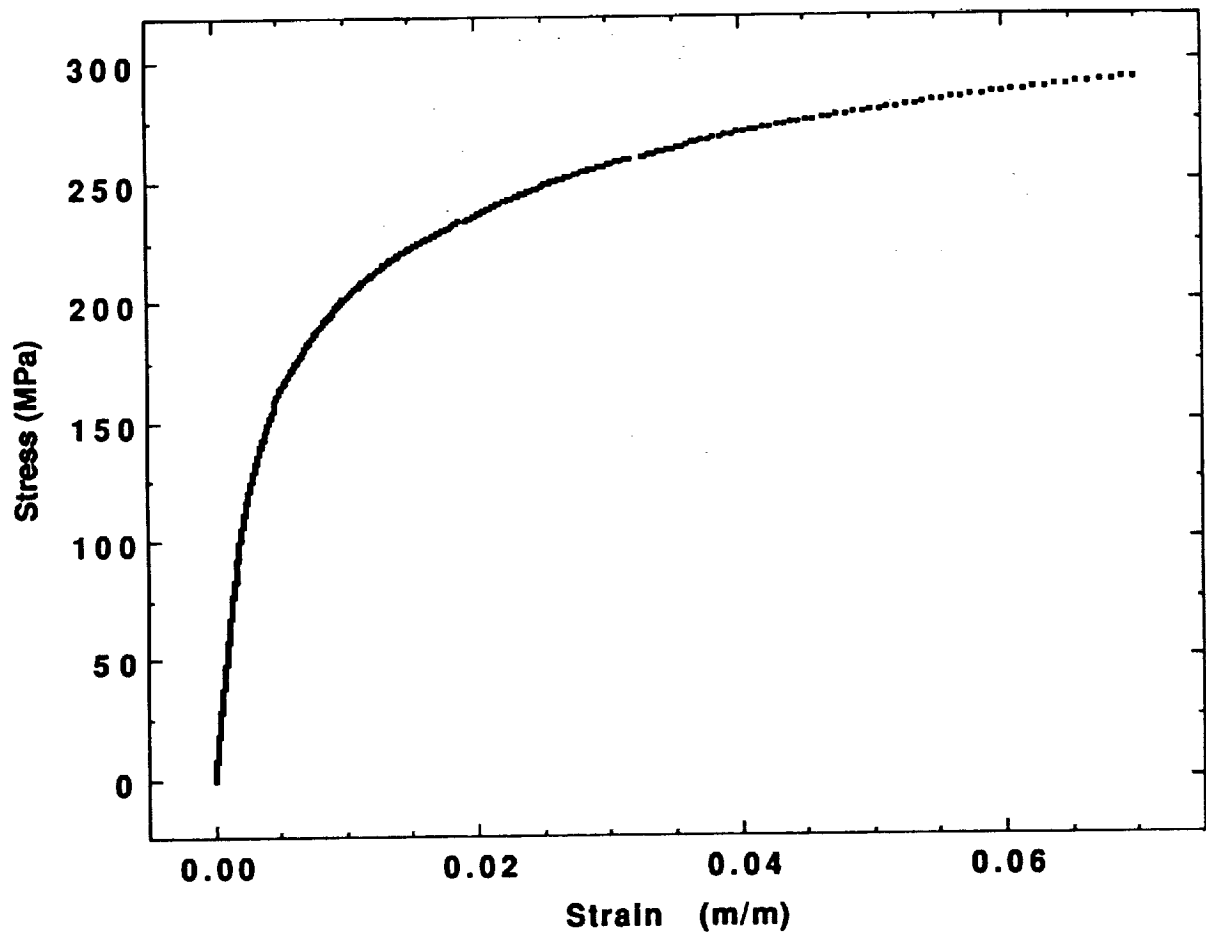
Figure D4: Data Collected During CσR Test at 649°C and 2.6 MPa/sec

APPENDIX E

PLOTS OF DATA COLLECTED DURING "COMPLEX" BENCHMARK TESTS
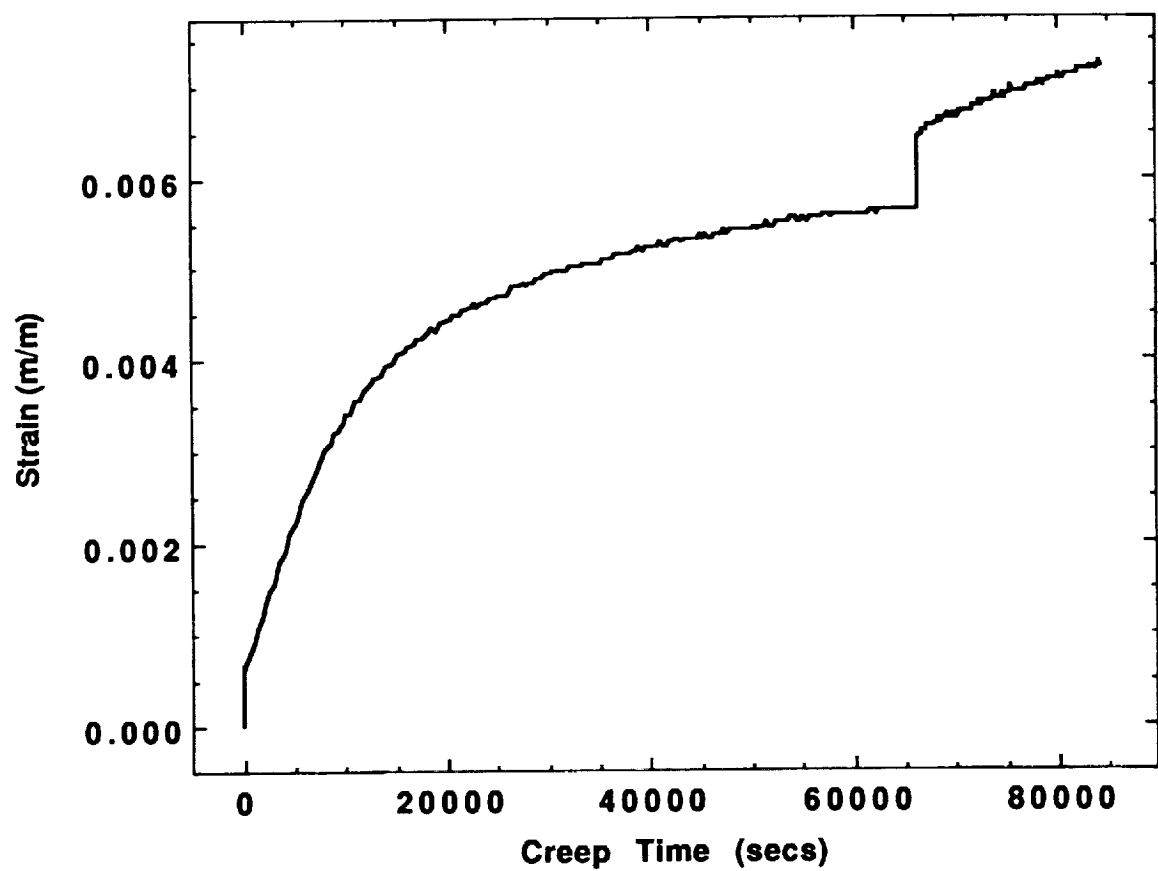
Figure E1: Strains Measured During Multi-Step Creep Test U31 (482°C)
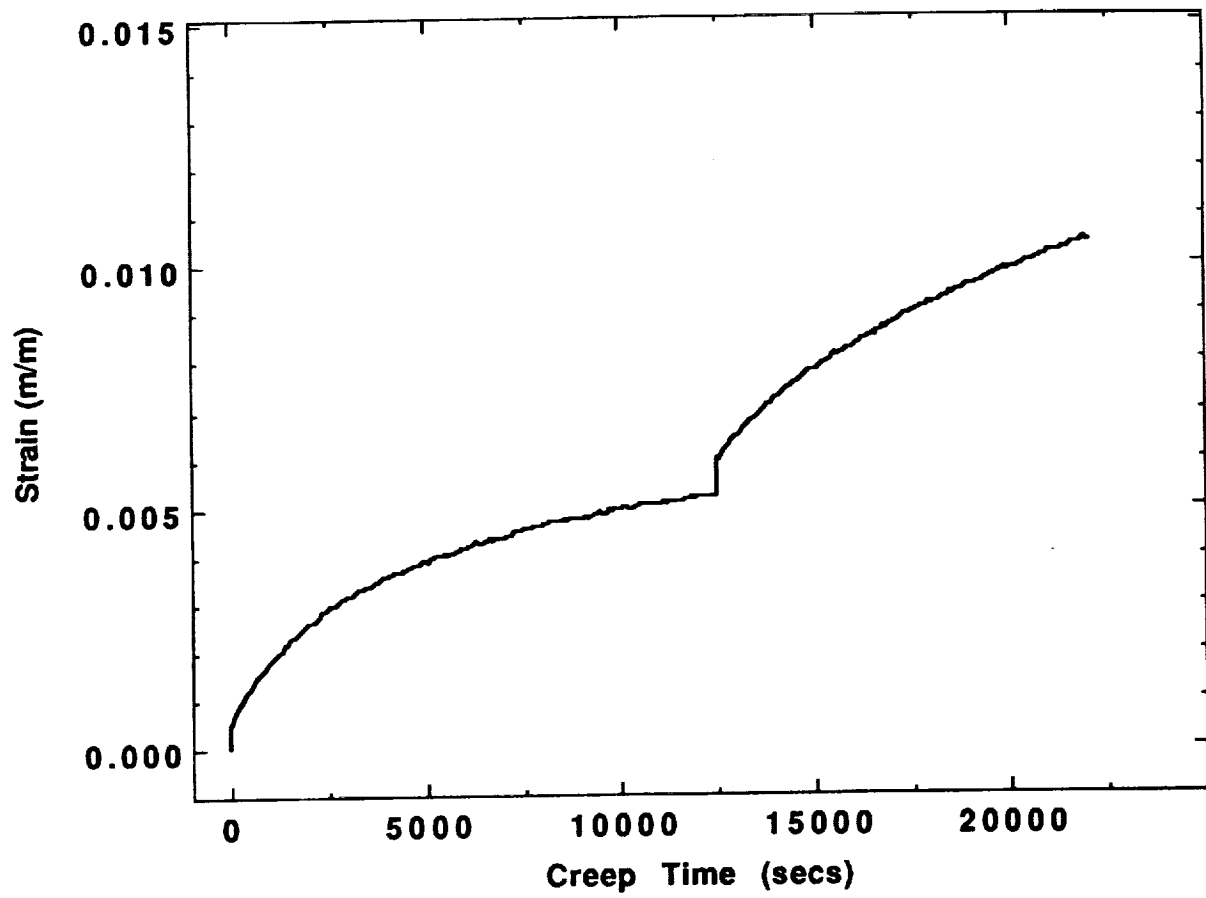
Figure E2: Strains Measured During Multi-Step Creep Test U33 (566°C)
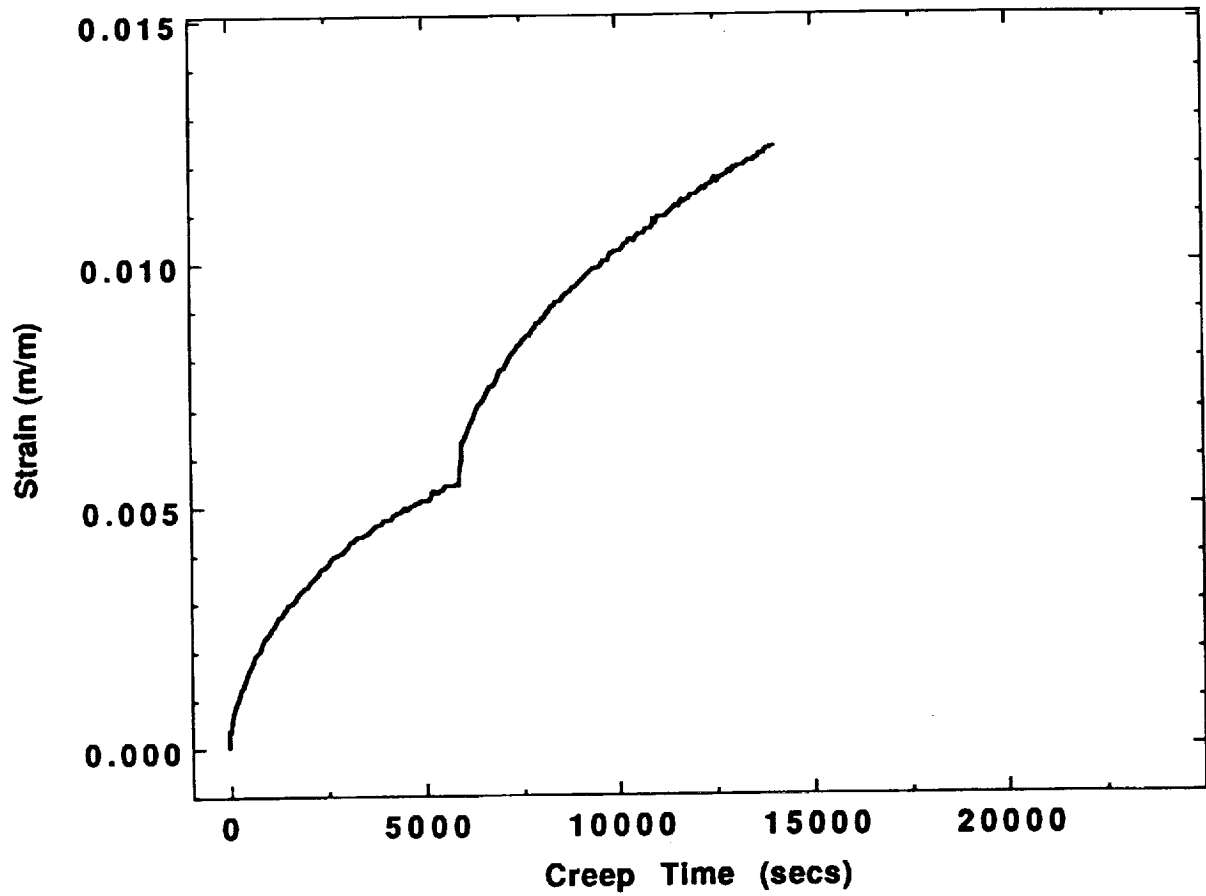
Figure E3: Strains Measured During Multi-Step Creep Test U34 (566°C)
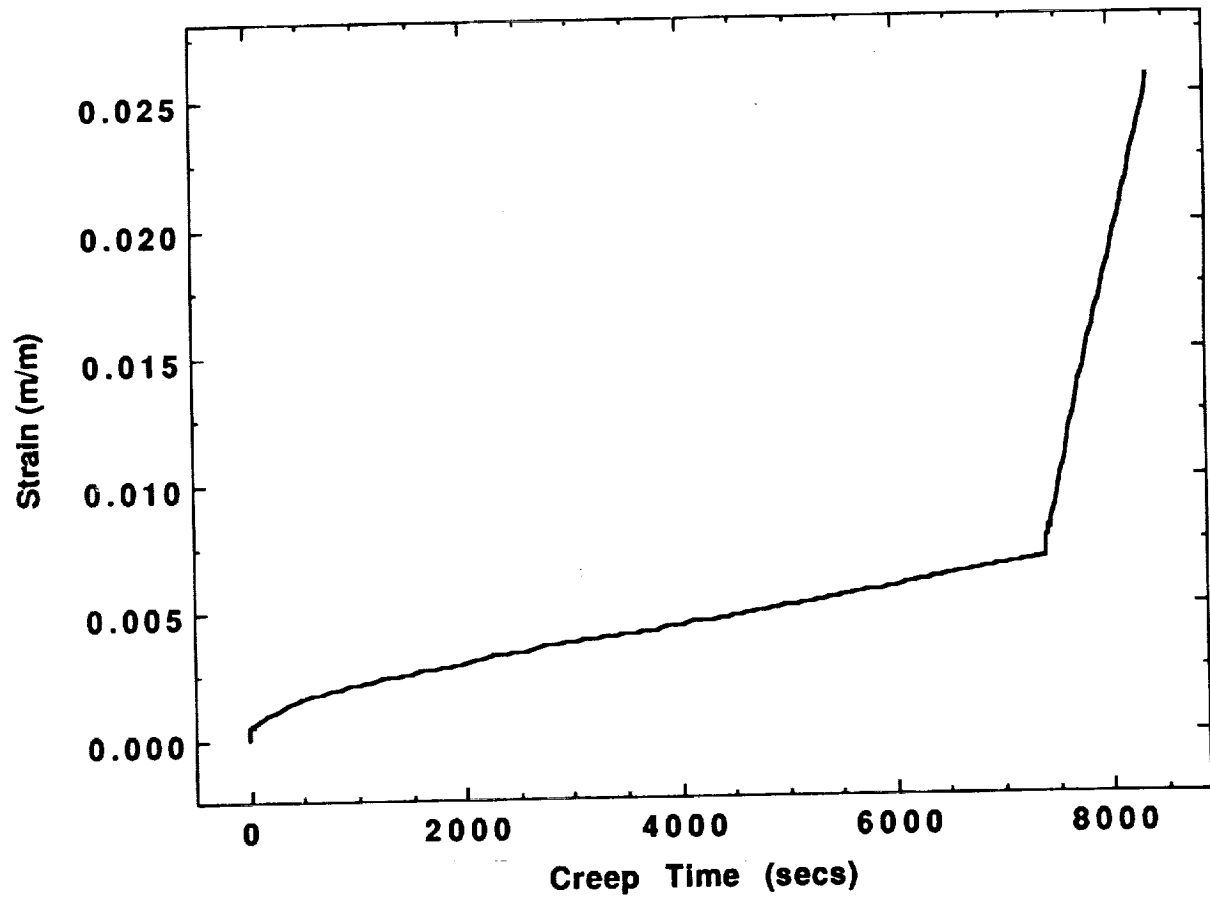
Figure E4: Strains Measured During Multi-Step Creep Test U35 (649°C)
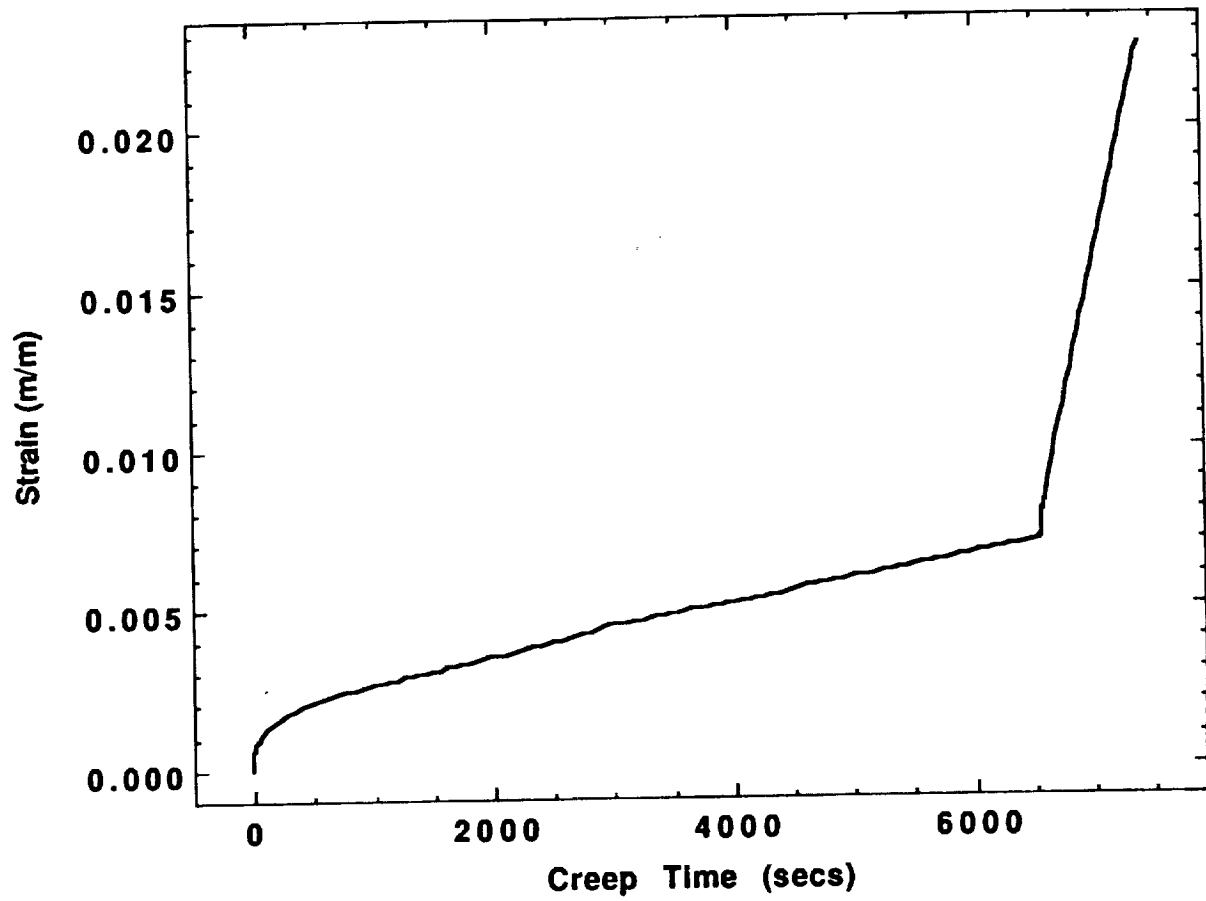
Figure E5: Strains Measured During Multi-Step Creep Test U36 (649°C)
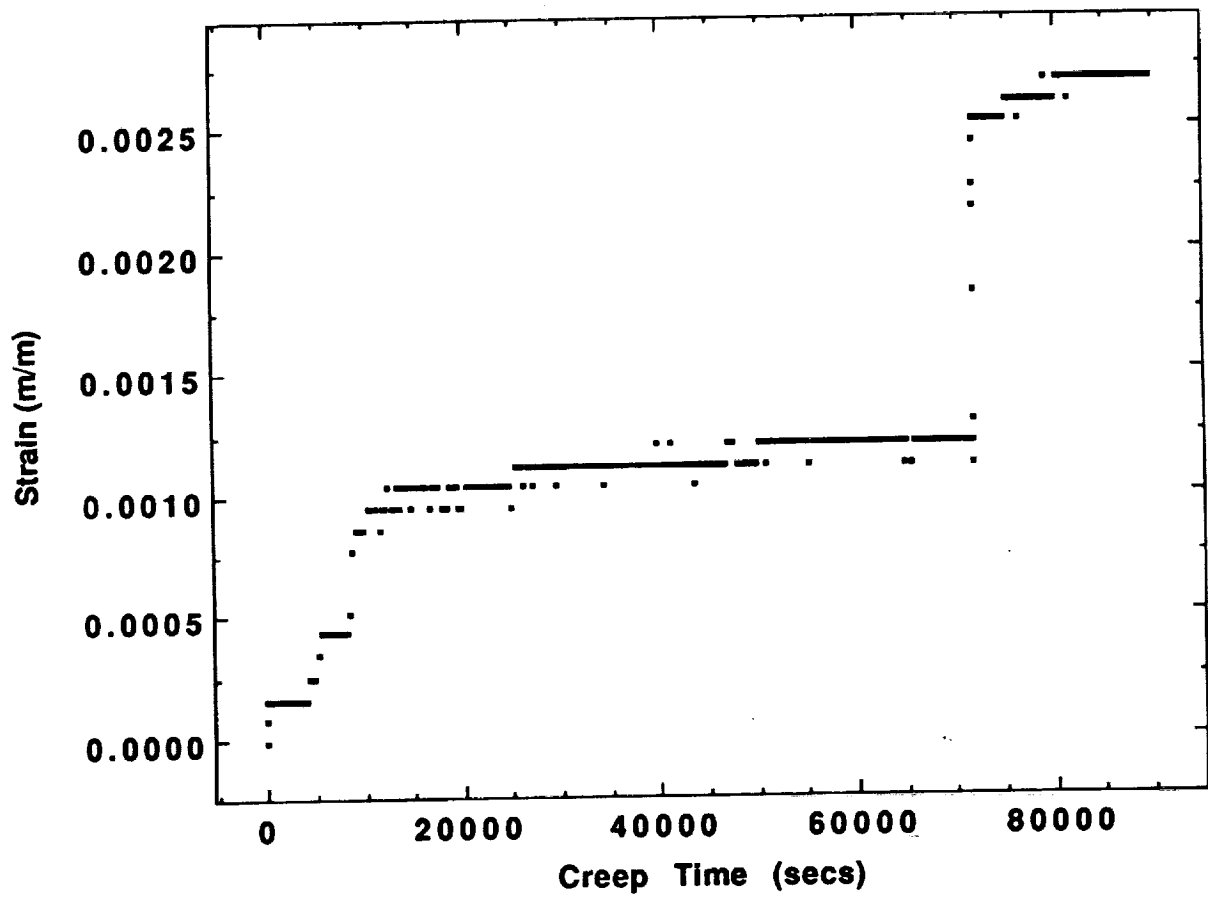
Figure E6: Strains Measured During Multi-Step Creep Test U38 (649°C)
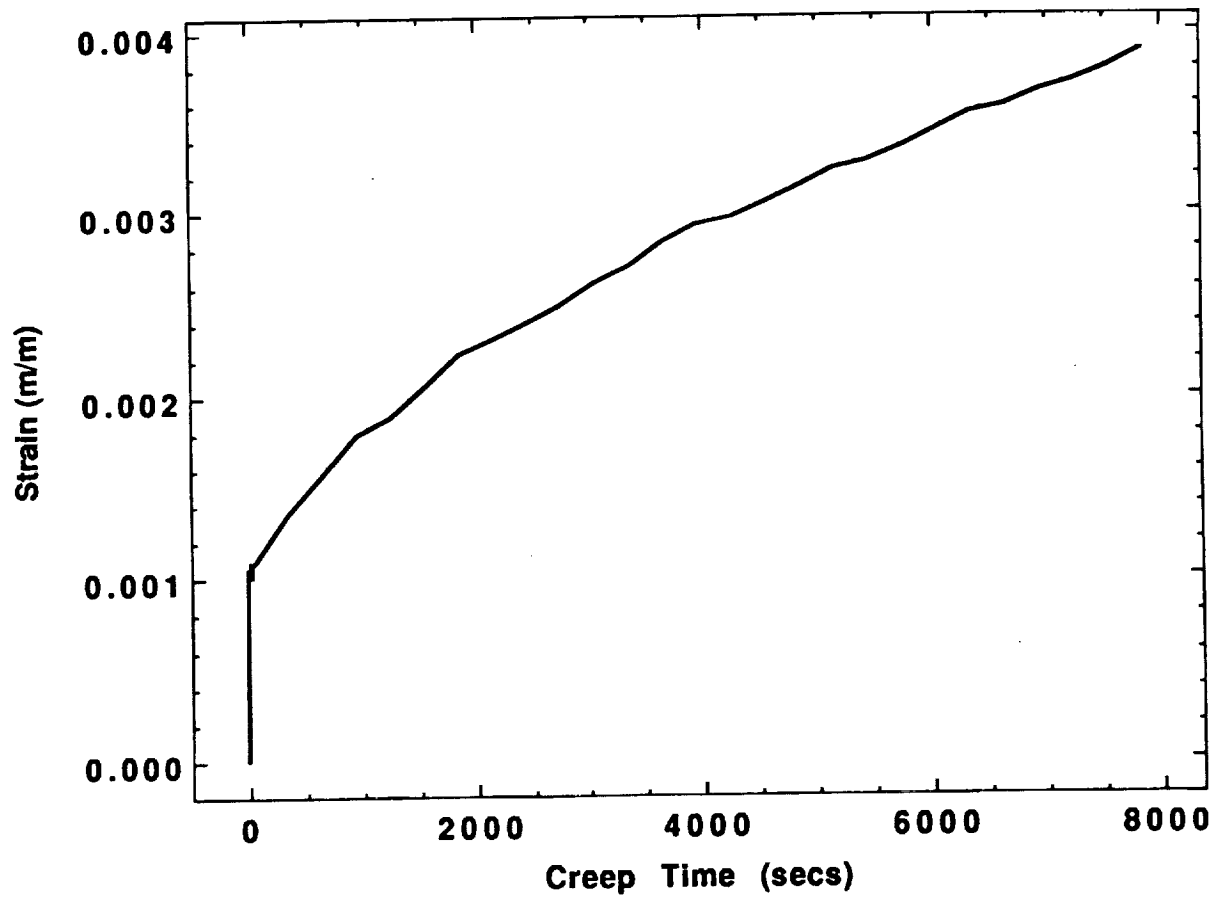
Figure E7: Strains Measured During Creep Test U41 (649°C)
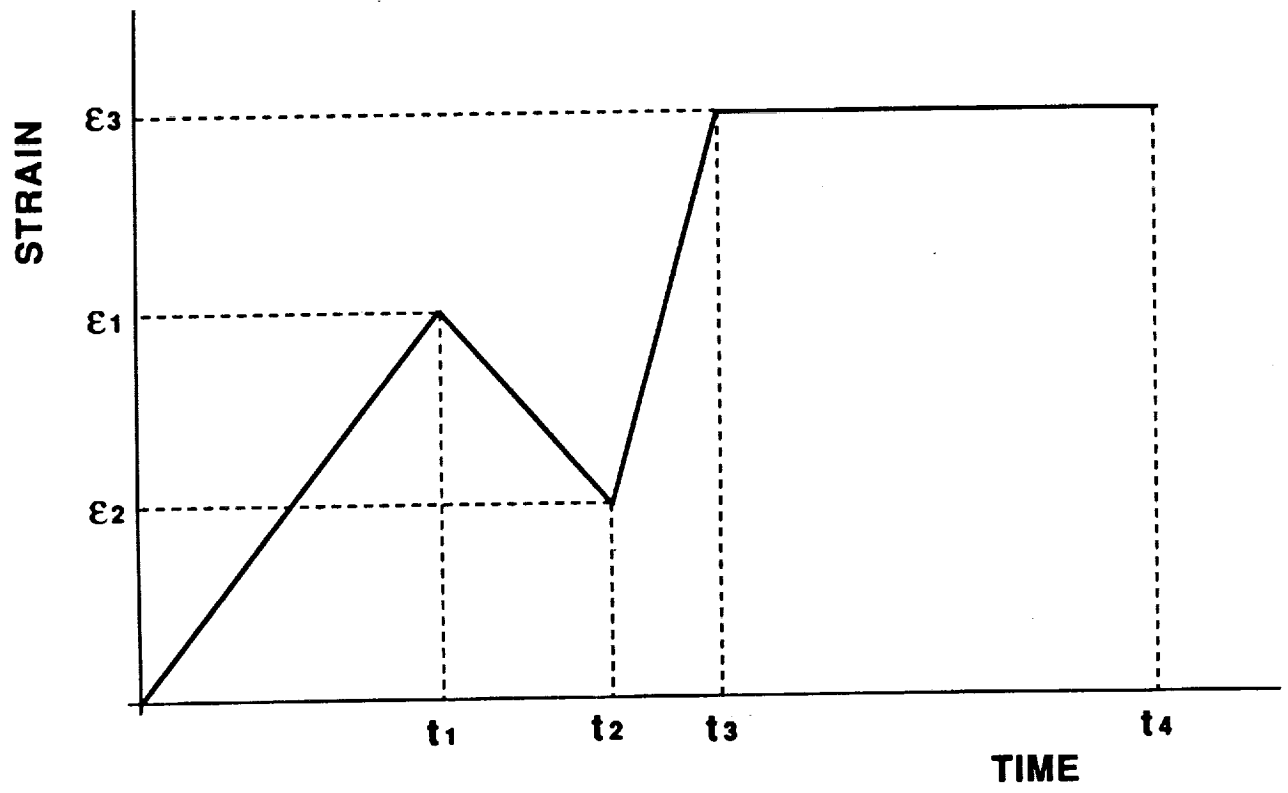
Figure E8: Strain History Applied During Multi-Rate Tests L33 through L36 (Schematic)
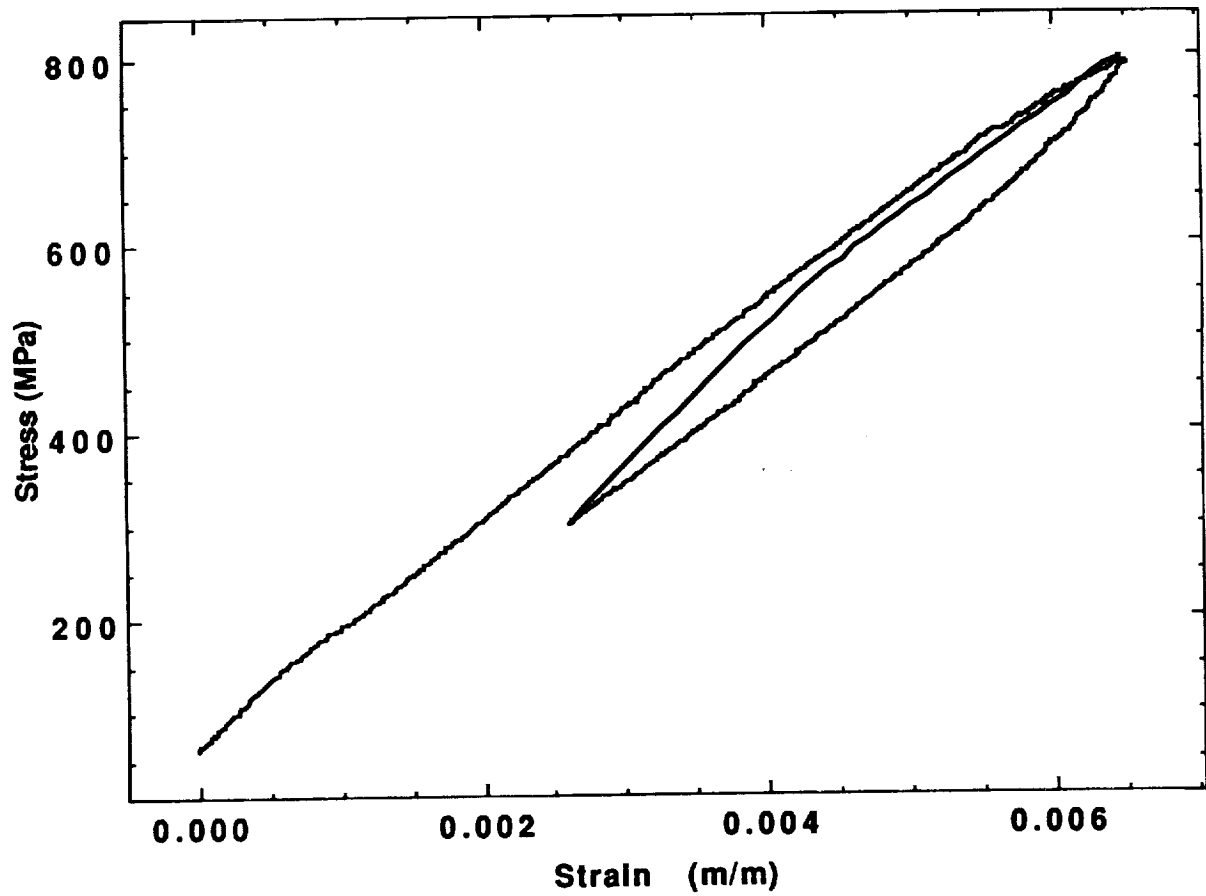
Figure E9(a): Strains Measured During Constant Strain-Rate Portion of Test
L33 (649°C)
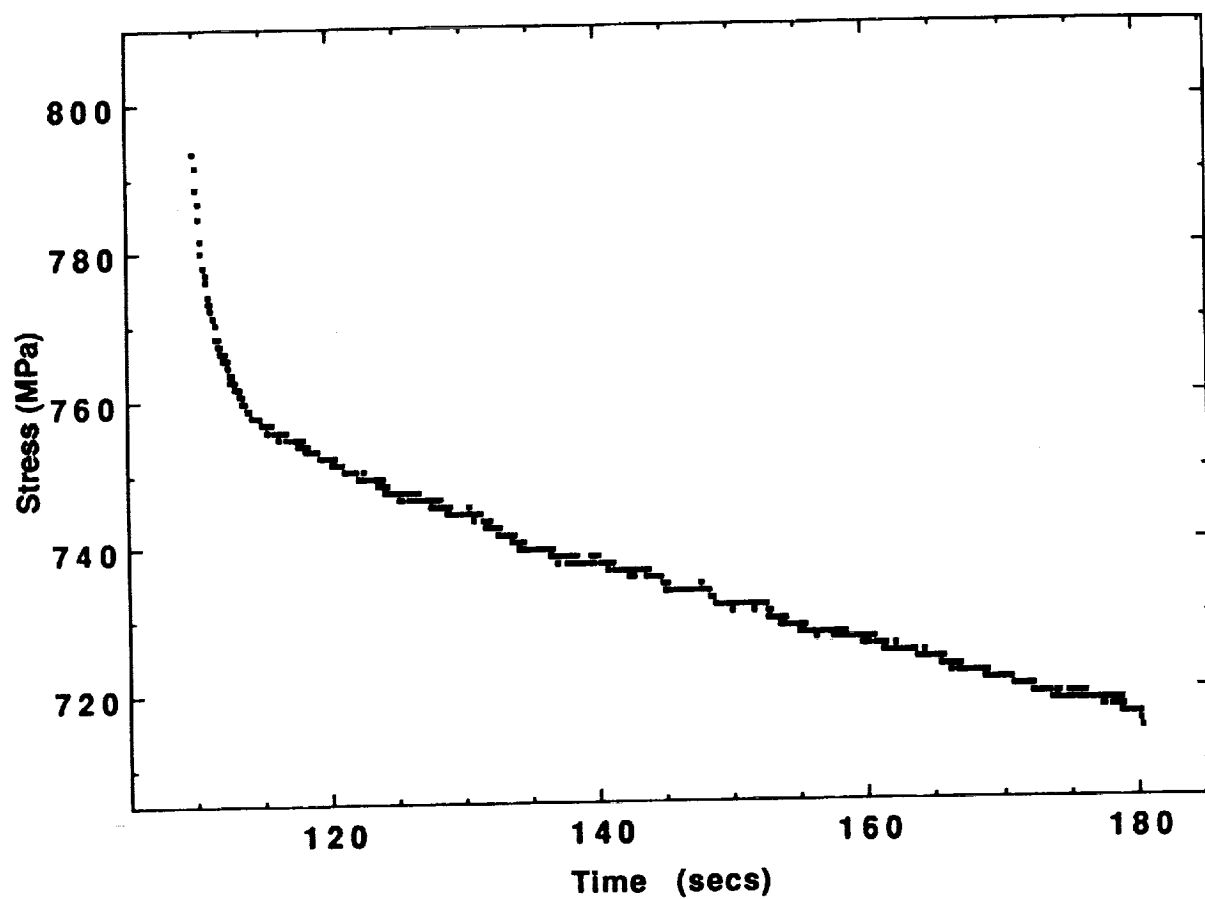
Figure E9(b): Stresses Measured During Stress Relaxation Portion of Test
L33 (Strain = 6488 μm/m; 649°C)
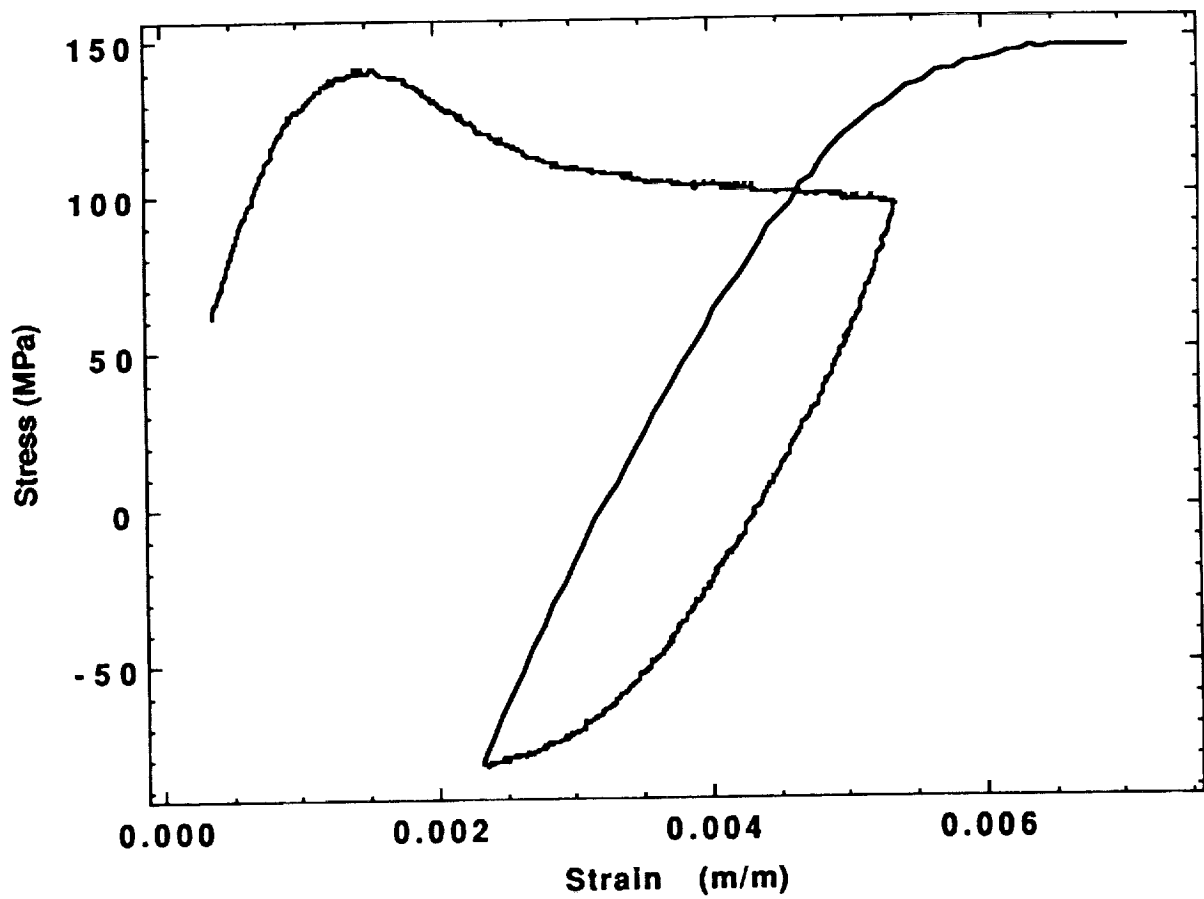
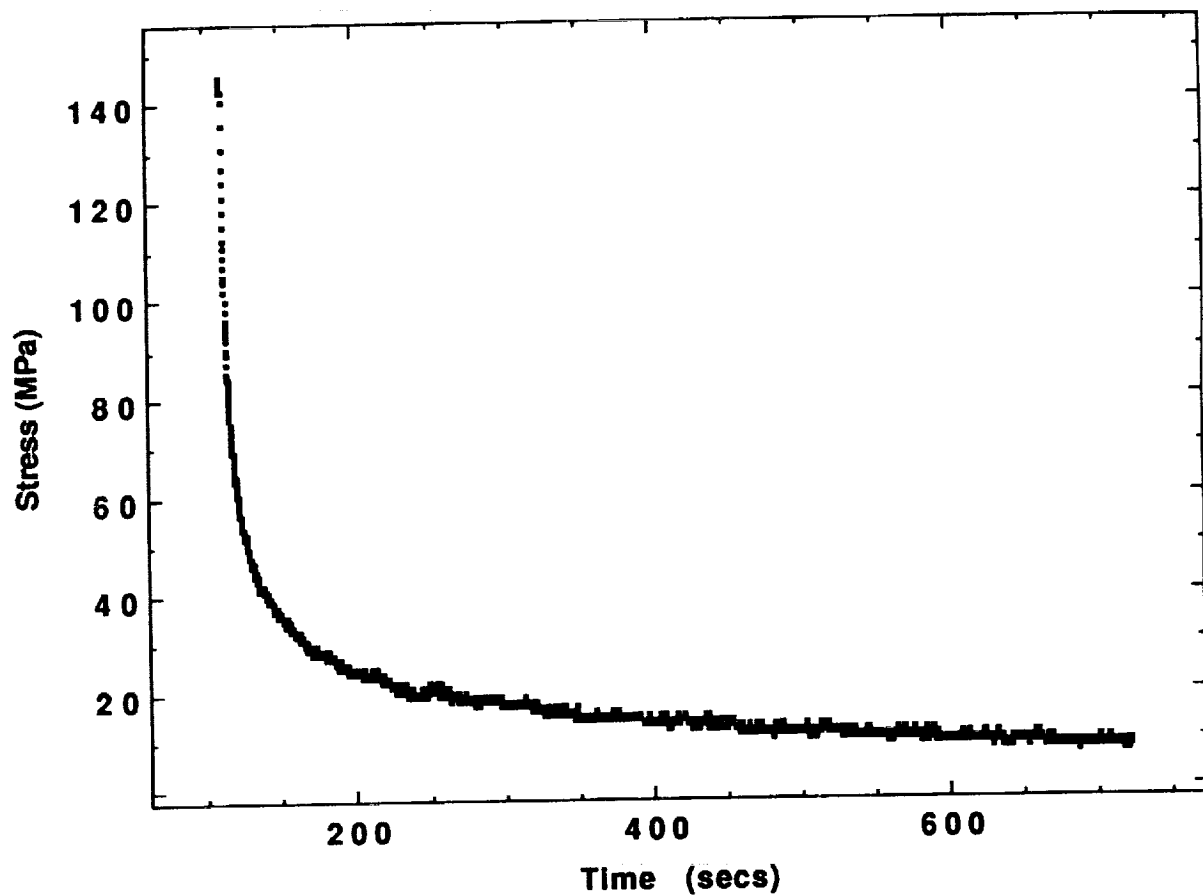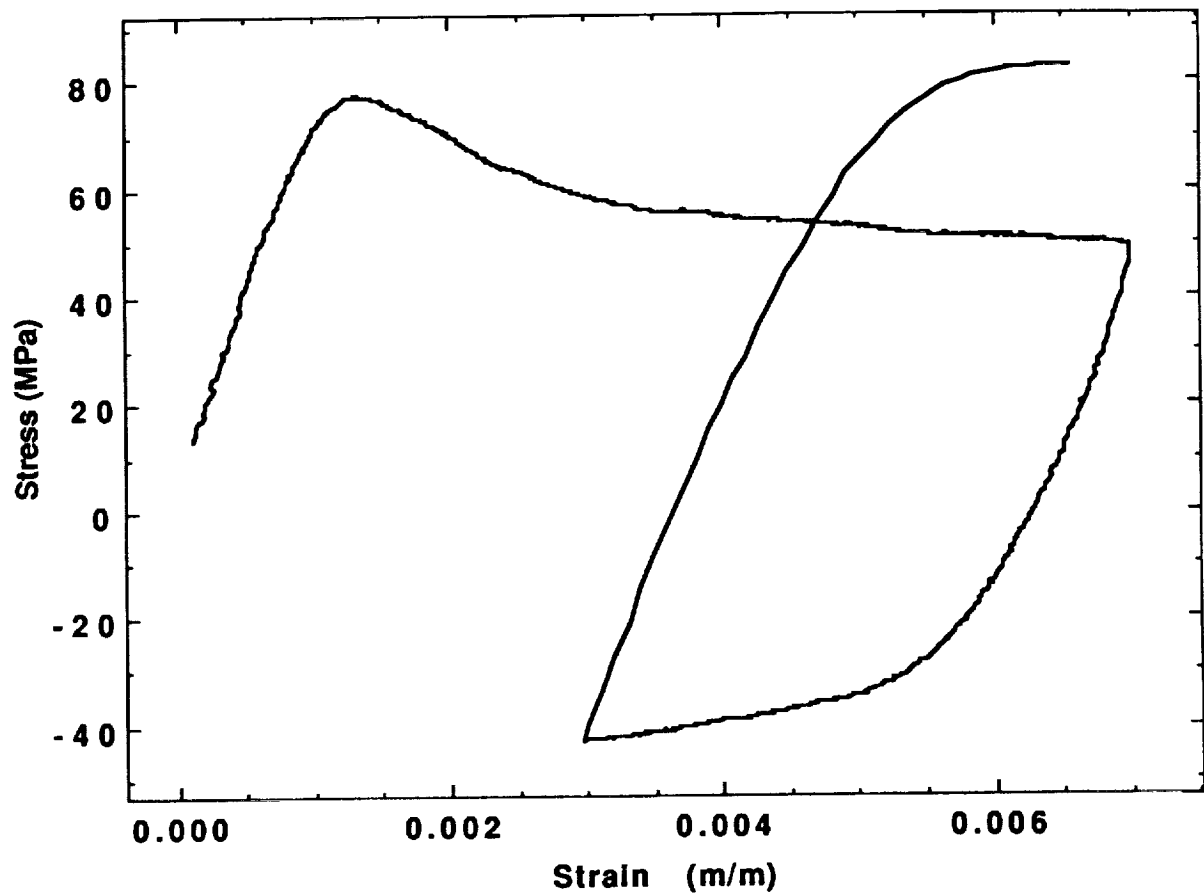Figure E10(a): Strains Measured During Constant Strain-Rate Portion of Test L34 (482°C)

Figure E10(b): Stresses Measured During Stress Relaxation Portion of Test
L34 (Strain = 7067 μm/m; 482°C)

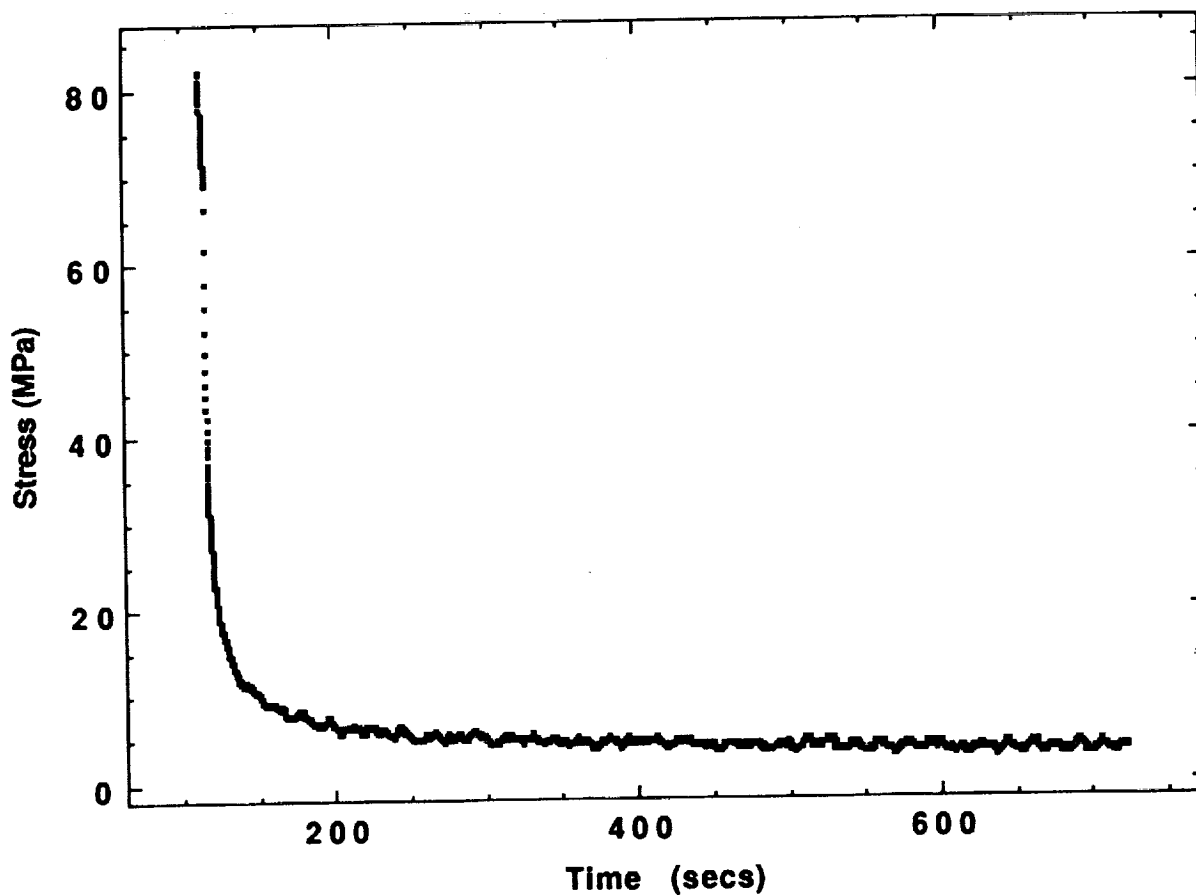Figure E11(a): Strains Measured During Constant Strain-Rate Portion of Test L35 (566°C)

Figure E11(b): Stresses Measured During Stress Relaxation Portion of Test
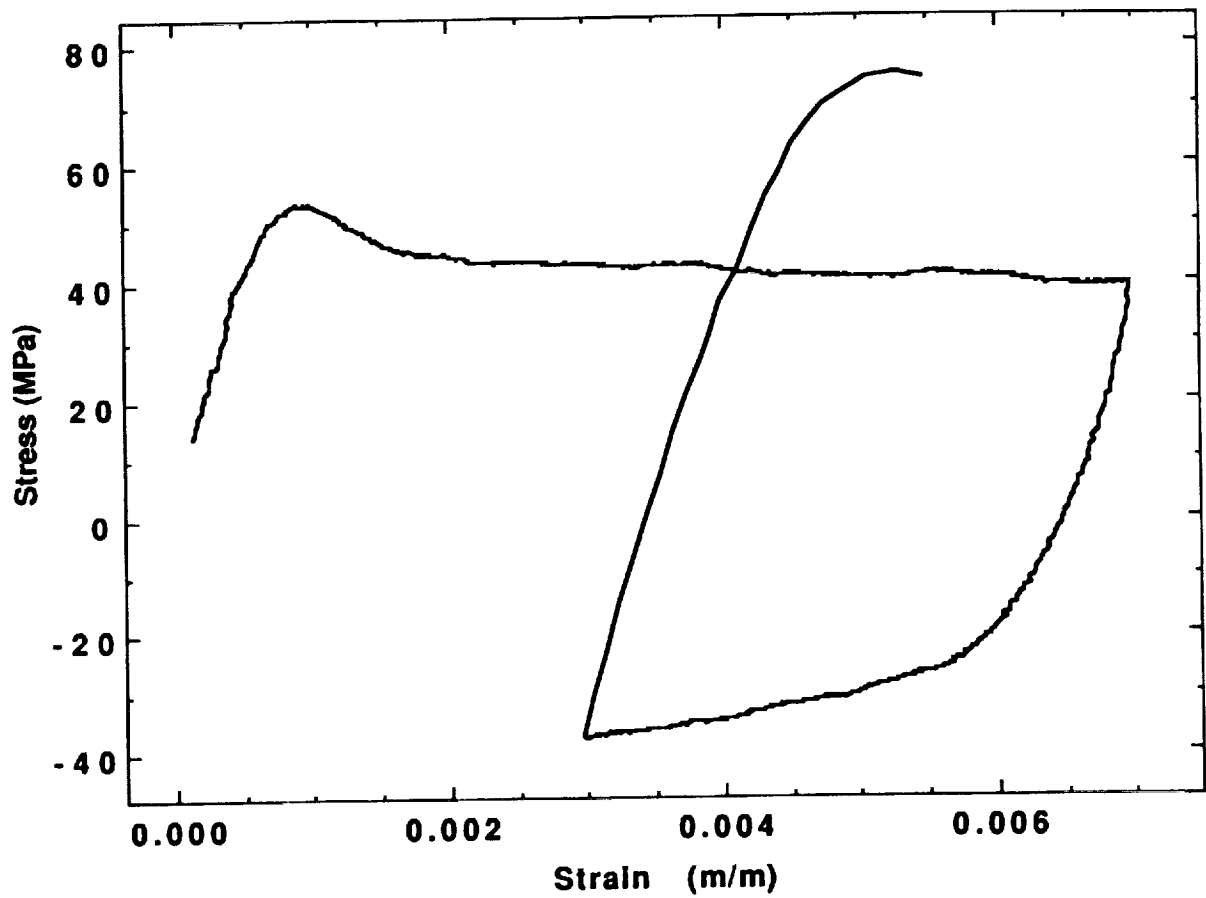L35 (Strain = 6570 μm/m; 566°C)

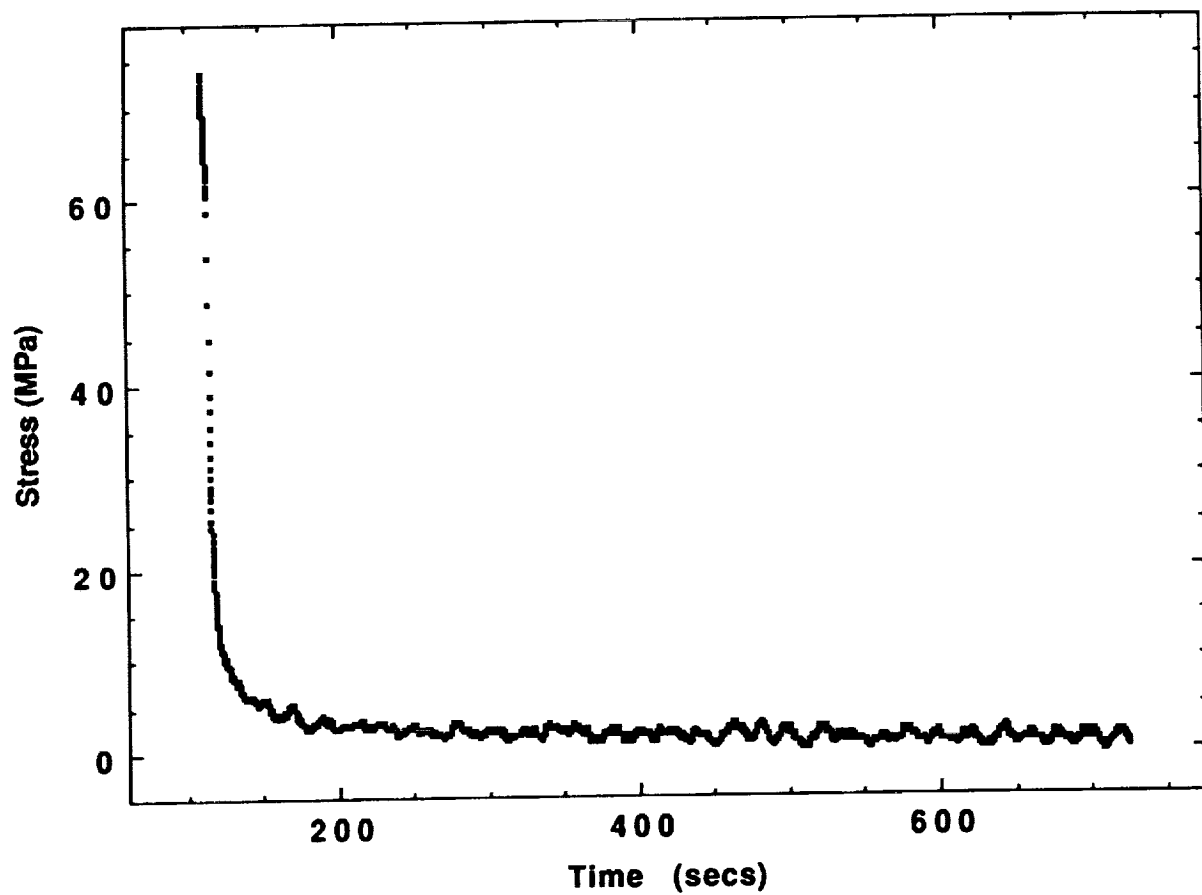Figure E12(a): Strains Measured During Constant Strain-Rate Portion of Test L36 (649°C)

Figure E12(b): Stresses Measured During Stress Relaxation Portion of Test L36 (Strain = 5483 μm/m; 566°C)
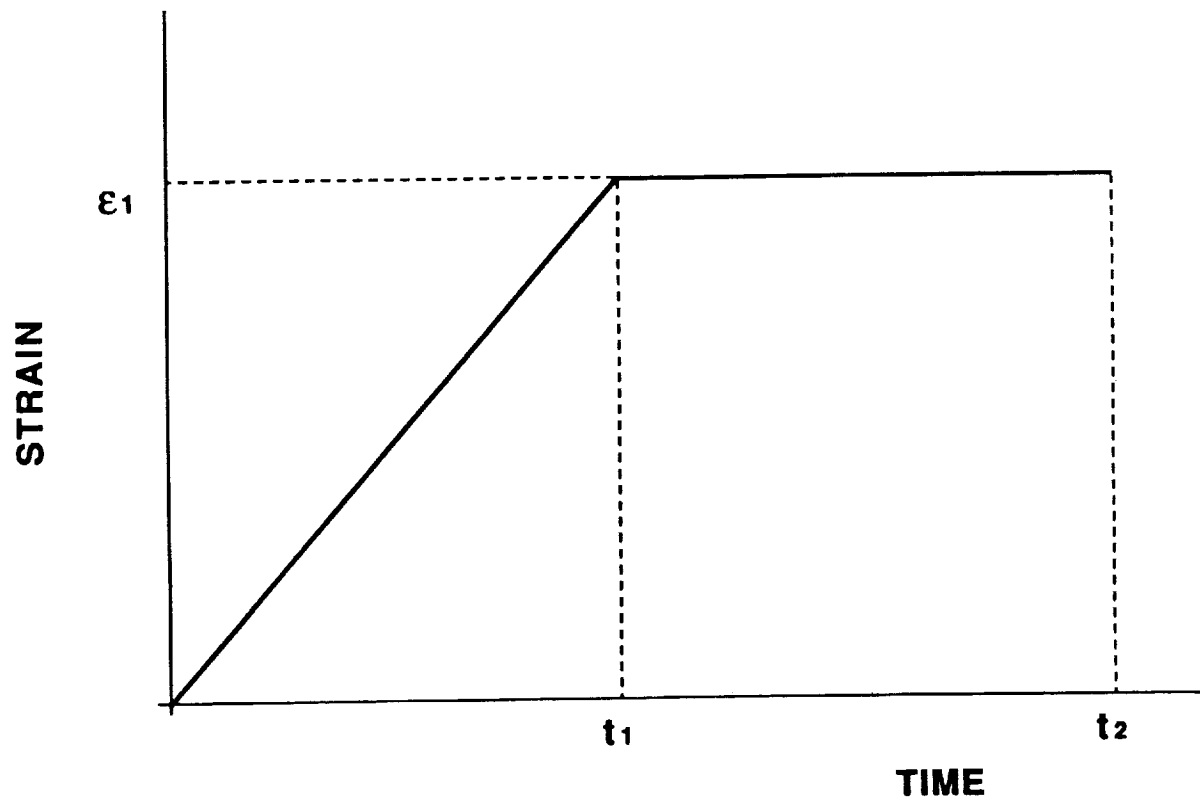
Figure E13: Strain History Applied During Multi-Rate Tests L37 through L39 (Schematic)
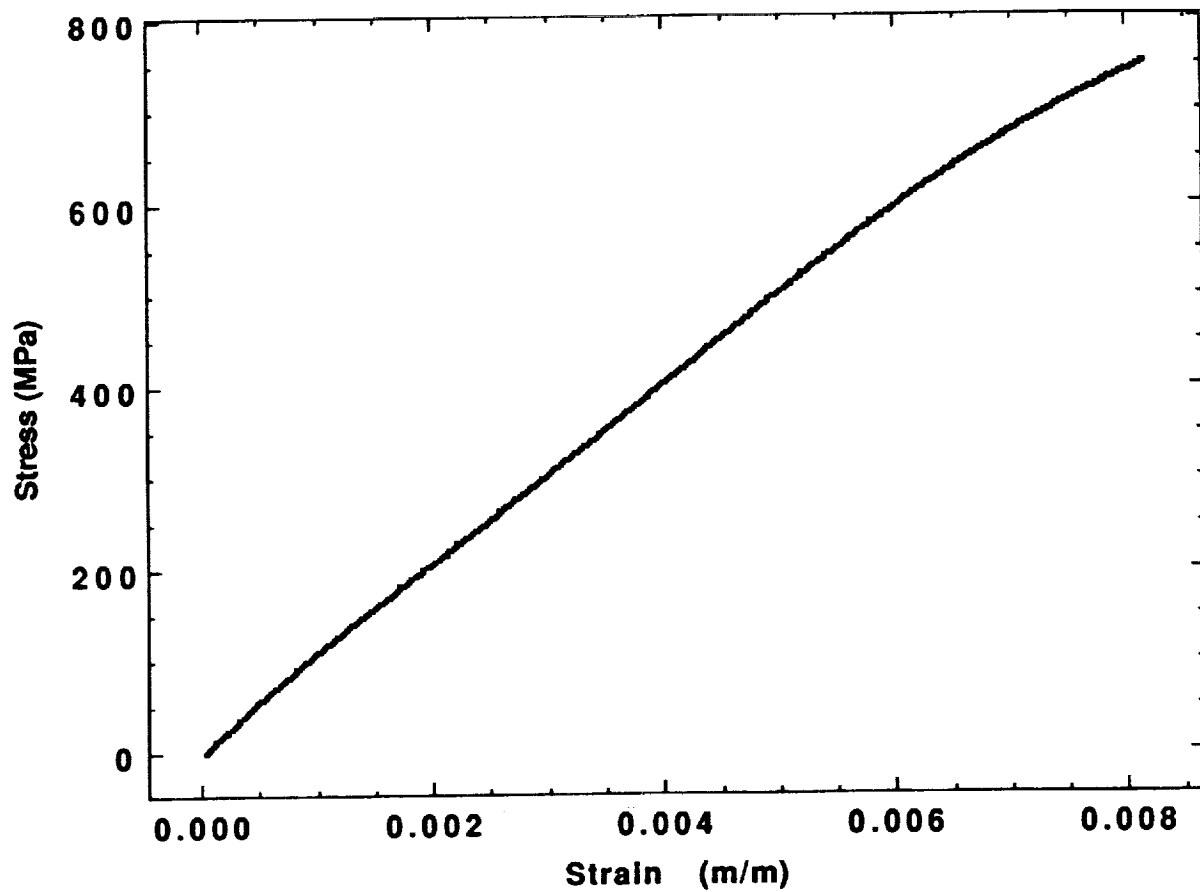
Figure E14: Strains Measured During Constant Strain-Rate Portion of Test L37 (482°C; Note: Specimen Failed Before Stress Relaxation Portion of Test Was Initiated)
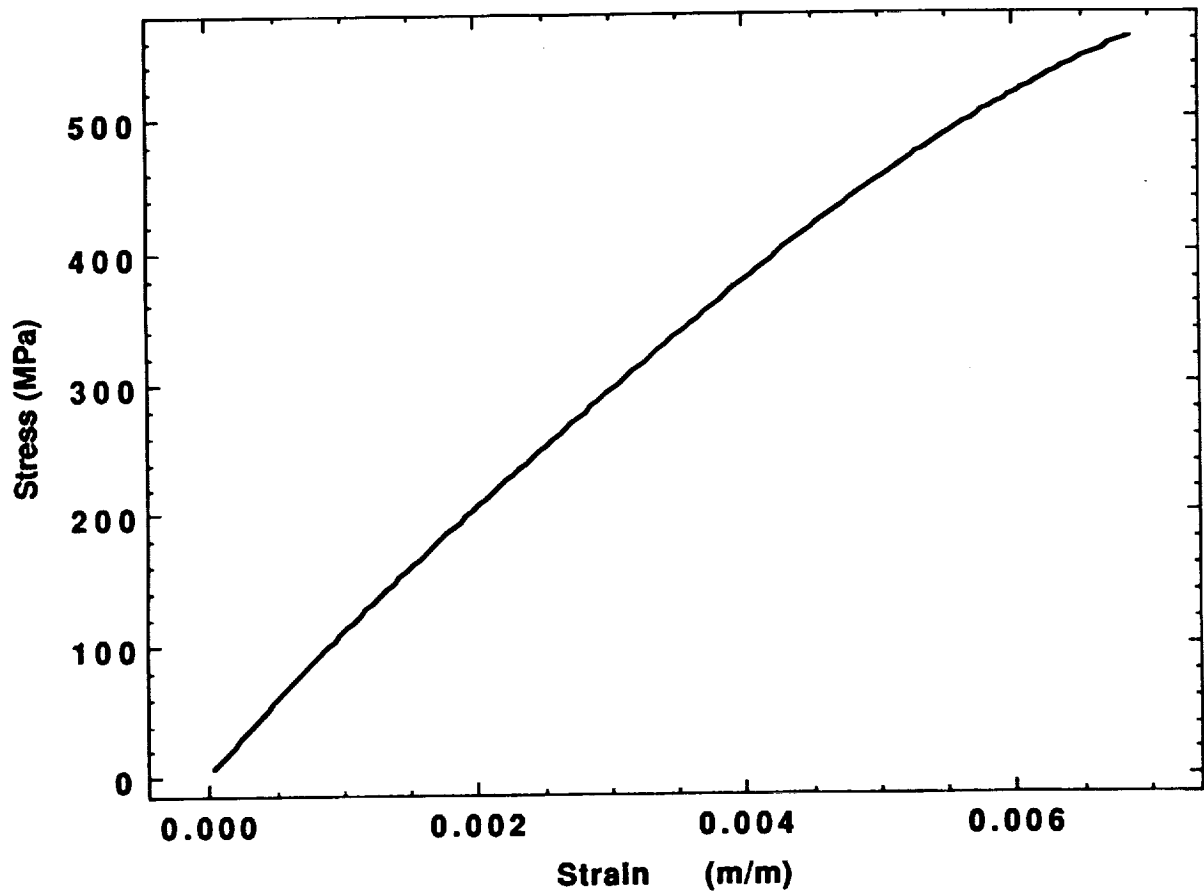
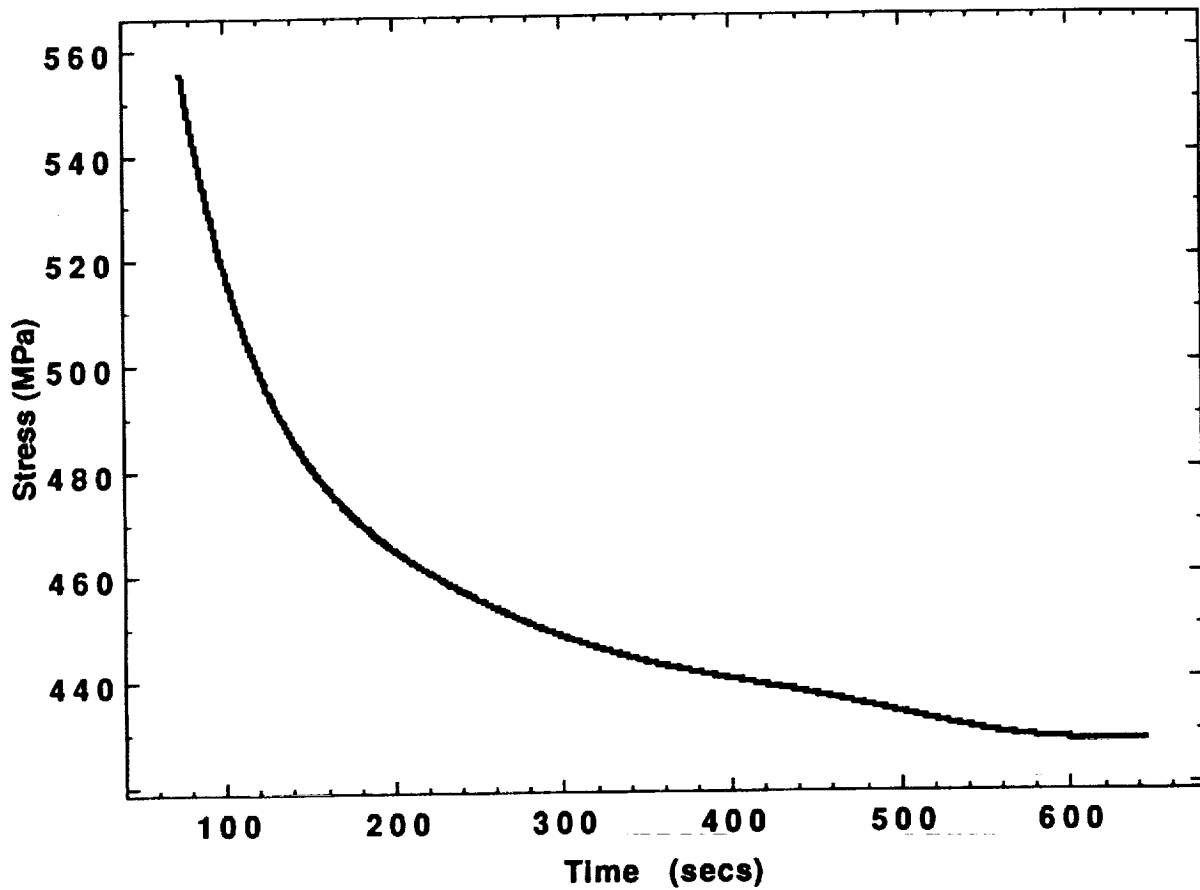Figure E15(a): Strains Measured During Constant Strain-Rate Portion of Test L38 (566°C)

Figure E15(b): Strains Measured During Stress Relaxation Portion of Test
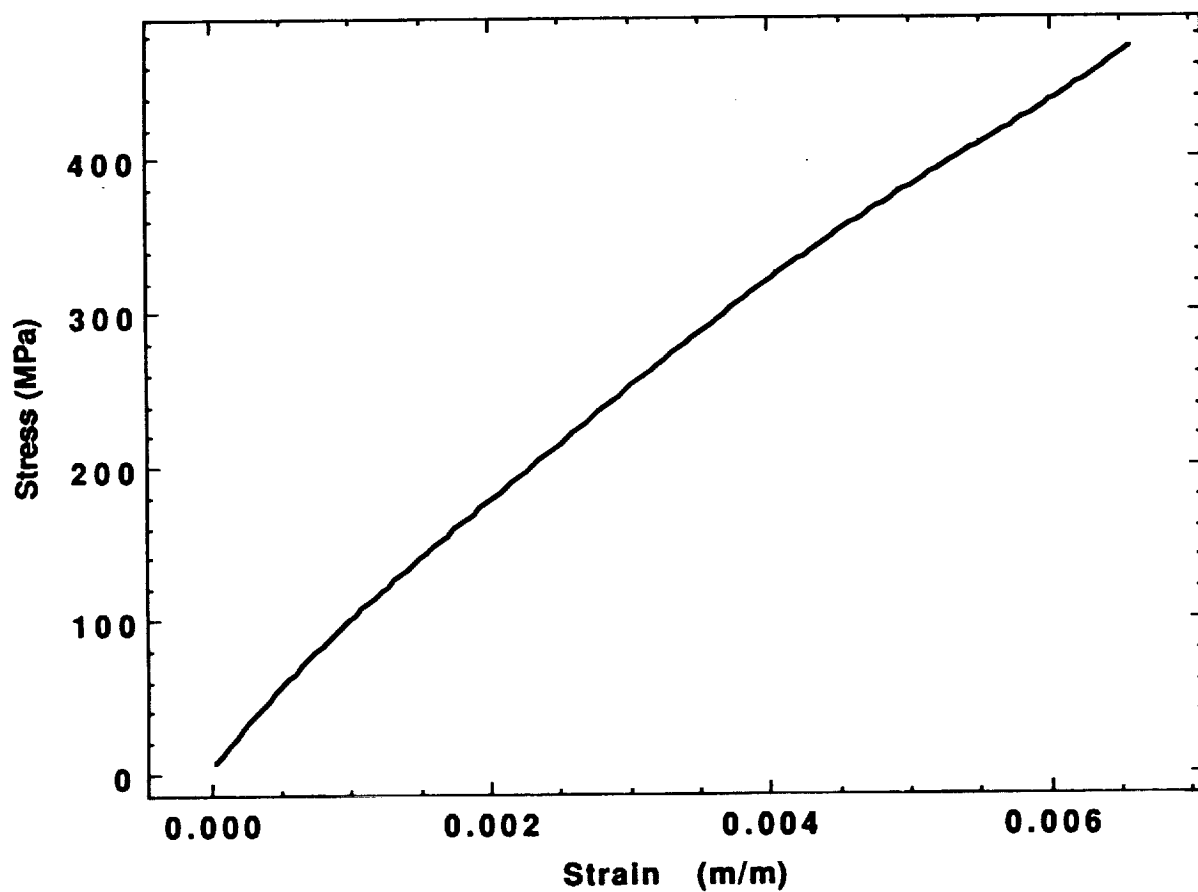L38 (Strain = 6875 µm/m; 566°C)

Figure E16(a): Strains Measured During Constant Strain-Rate Portion of Test L39 (649°C)

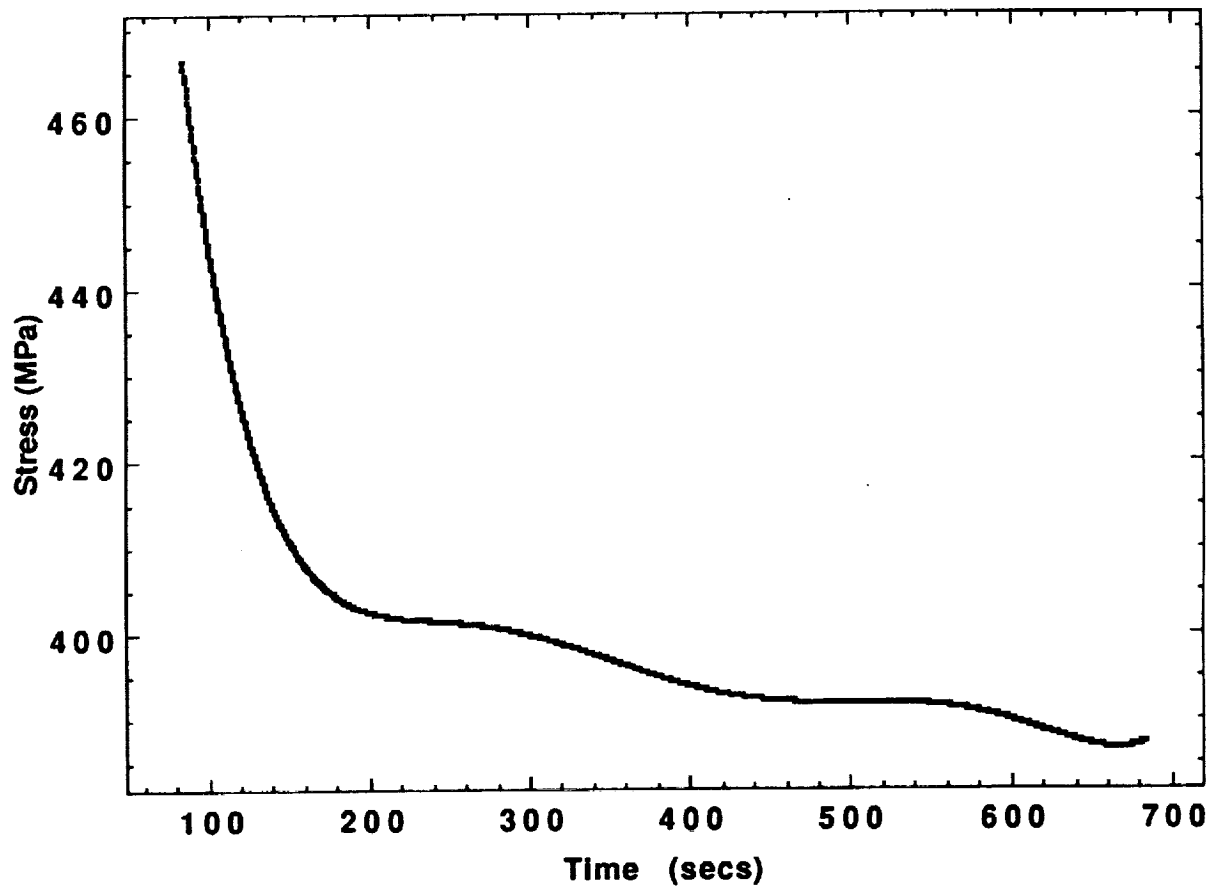Figure E16(b): Strains Measured During Stress Relaxation Portion of Test L38 (Strain = 6579 μm/m; 649°C)

NASA

National Aeronautics and
Space Administration

Report Documentation Page

1. Report No.	2. Government Accession No.	3. Recipient's Catalog No.
NASA CR-187621		

4. Title and Subtitle	5. Report Date
Thermoviscoplastic Response of Ti-15-3 Under Various Loading Conditions	October 1991
	6. Performing Organization Code

7. Author(s)	8. Performing Organization Report No.
M. E. Tuttle and J. Rogacki	
	10. Work Unit No.
	505-63-50-04

9. Performing Organization Name and Address	11. Contract or Grant No.
University of Washington Department of Mechanical Engineering Seattle, WA 98195	NAG1-974
	13. Type of Report and Period Covered

12. Sponsoring Agency Name and Address	Contractor Report
National Aeronautics and Space Administration Langley Research Center Hampton, VA 23665-5225	14. Sponsoring Agency Code

15. Supplementary Notes

Langley Technical Monitor: W. S. Johnson

16. Abstract

Metal matrix composites (MMCs) are candidate matrials for use in high temperature, high loading applications. In particular, an MMC consisting of a titanium alloy reinforced with silicon-carbide fibers is being considered for use on the National Aerospace Plane (NASP). Compared to other metals and metallic alloys, titanium alloys retain relatively high stiffness, strength, and corrosion resistance at elevated temperatures. However, above roughly 316°C (600°F) titanium exhibits a significant thermoviscoplastic (i.e., "creep") response. Since the temperatures encountered in many regions of the NASP are expected to exceed 316°C, the potential thermoviscoplastic behavior of titanium-based MMC's at elevated temperatures must be thoroughly investigated.

17. Key Words (Suggested by Author(s))	18. Distribution Statement
Creep Titanium Cyclic strain Metal matrix composite Microsructure	Unclassified - Unlimited Subject Category - 39

19. Security Classif. (of this report)	20. Security Classif. (of this page)	21. No. of pages	22. Price
Unclassified	Unclassified	150	A07

NASA FORM 1626 OCT 86